RENORMALIZATION GROUP APPROACH TO TWO STRONGLY CORRELATED CONDENSED MATTER MODELS

RENORMALIZATION GROUP APPROACH TO TWO STRONGLY CORRELATED CONDENSED MATTER MODELS

By

M. SEDIGH GHAMARI, B.Sc., M.Sc.

A Thesis
Submitted to the School of Graduate Studies
in Partial Fulfilment of the Requirements
for the Degree
Doctor of Philosophy

McMaster University

DOCTOR OF PHILOSOPHY (2014) McMaster University
(Physics) Hamilton, Ontario

TITLE:	Renormalization Group Approach to Two Strongly Correlated Condensed Matter Models
AUTHOR:	M. Sedigh Ghamari, B.Sc., Sharif University of Technology (2007), M.Sc., Brock University (2009)
THESIS ADVISER:	Dr. Catherine Kallin
NUMER OF PAGES:	xi , 152

Abstract

This thesis presents renormalization group (RG) analyses of two strongly correlated condensed matter systems.

In the first part, the phase diagram of the spin-$\frac{1}{2}$ Heisenberg antiferromagnetic model on a spatially anisotropic triangular lattice is discussed. This model, together with a Dzyaloshinskii-Moriya (DM) interaction, describes the magnetic properties of the layered Mott insulator Cs_2CuCl_4. Employing a real-space RG approach, it is found, in agreement with a previous similar study, that a fragile collinear antiferromagnetic (CAF) state can be stabilized at sufficiently strong anisotropies. The presented RG analysis only indicates the presence of the CAF and spiral states in the phase diagram, with no extended quantum-disordered state at strong anisotropies. Specifically, it reveals a fine-tuning of couplings that entails the persistence of ferromagnetic correlations between second-nearest chains over large length scales even in the CAF phase. This has important implications on how numerical studies on finite-size systems should be interpreted, and reconciles the presence of the CAF state with the observation of only ferromagnetic correlations in numerical studies. The effect of a weak DM interaction within this RG approach is examined. It is concluded that Cs_2CuCl_4 is well within the stability region of the spiral ordering.

In the second part, the fate of a neck-narrowing Lifshitz transition in two-dimensions and in the presence of weak interactions is studied. Such a transition is a topological quantum phase transition, with no change in symmetry. At the critical point of this transition, the density of states at the Fermi energy is logarithmically divergent and a van Hove singularity appears. It is found that, at the critical point, the Wilsonian effective action is intrinsically non-local. This non-locality is attributed to integrating out an emergent soft degree of freedom. Away from the critical point, a local perturbative RG description is presented, and it is shown that weak attractive interactions grow as $\log^2 L$ (L is the physical length). However, this local description is restricted to a finite momentum range that shrinks as the critical point is approached.

Acknowledgements

This thesis marks the end of five fruitful and inspiring years of my life as a PhD student. The thought that it all has come to an end saddens me. But, *c'est la vie*! All that remains for me now is to express my heartfelt gratitude and great appreciation to all those who helped me along the way, those who made what otherwise would have been unbearable and gruelling so pleasant and memorable, those without whom there would not have been a thesis to write.

First and foremost, I would like to extend my sincerest gratitude to my advisor, Prof. Catherine Kallin, and my co-advisor, Prof. Sung-Sik Lee, for their guidance, patience, understanding, encouragement and unwavering support throughout my PhD. I am most indebted to Catherine not only for everything I learned from her but also for all her support when I needed it the most. She gave me the freedom to pursue research topics that I was interested in even though they were removed from her mainstream research. In spite of her busy schedule, she always had time for my questions and random ideas, even in times that it was too demanding for her condition. Her deep insight and vast knowledge in condensed matter physics have been essential and immensely valuable in my path to becoming a physicist. On the same note, I am greatly indebted to Sung-Sik for his great patience, deep insight, constant willingness to help and enthusiasm. Sung-Sik's strong intuition and remarkable clarity of thought is truly unique. He is an exceptional, yet very humble physicist, a deep and careful thinker and a role model to look up to. Also, I wish to profusely thank him for stepping up to the plate during Catherine's medical leave of absence. Catherine and Sung-Sik are great mentors, brilliant physicists to learn from and wonderful individuals to get to know. I certainly consider myself most fortunate and privileged to have had their guidance.

I would like to express my deep gratitude to Prof. John Berlinsky for all his help and guidance throughout my PhD, and for serving on my advisory committee up until the last year of my PhD. John's deep insight and comments on the Heisenberg antiferromagnetic triangular problem were absolutely essential to the successful completion of that work. Also, I greatly thank him for providing me with the opportunity to stay at Perimeter Institute for Theoretical Physics (PI) in the fall of 2012 as his teaching

assistant. My stay at PI proved incredibly valuable and fruitful.

I wish to thanks Profs. Erik Sorensen and Michel Gingras for serving on my thesis committee and for their invaluable comments on this thesis. Erik's collaboration on my first project is greatly acknowledged. That study would not have possibly been as successful without his insight and his careful ED and DMRG results. His meticulousness and precision in numerical analysis is truly exemplary. Also, I thank him for taking John's place on my advisory committee during the last year of my PhD. Dr. Gingras's careful read of the thesis and invaluable comments are greatly acknowledged. It was truly an honor to have such a distinguished physicist as my external examiner. I also wish to thank him for pointing me in the right direction when I was considering to pursue a PhD in condensed matter physics more than five years ago.

My thanks go to all the faculties and the staff in the physics and astronomy department for their support throughout my PhD. Specially, I wish to thank Hua Wu, Tina Stewart, Rosemary McNeice, Cheryl Johnston, Mara Esposto and Liz Penny for all their help. Profs. Cliff Burgess, Bruce Gaulin, Kari Dalnoki-Veress and Itay Yavin are greatly thanked for many valuable interactions.

Without the encouragement and support of many friends I would not have been able to make it this far. Thank you Allan Bayntum, Andreas Deschner, Anna Kostouki, Annie Hou, Dan Irvine, Dave Bazak, Edward Taylor, Jackie Browning, Josh McGraw, Kate Ross, Kristoffer Meinander, Laura Toppozini, Leo van Nierop, Matthew Williams, Mischa Thesberg, Nathan Leigh, Nick Miladinovic, Olesya Peshko, Peter Lunts, Phil Ashby, Prasanna Balasubramanian, Ray Ng, Rory Woods, Sandy Hsu, Sean Williams, Shawn Armstrong, Shouvik Sur, Subhro Bhattacharjee, Tibra Ali, Wen Huang, William Witczak-Krempa and many others at McMaster, Pulse, PI, My Dog Joe, Hamilton Tongo, UofT and University of Waterloo for being such amazing friends!

Last but not the least, I thank my aunts, my father and my uncle for their unwavering love, support and encouragement throughout my life. Words fall short to express my gratitude to you.

To my **family** and **friends**,
without whom I could not not have made it this far.

Contents

List of Figures

List of Tables

Chapter 1

Introduction

Condensed matter physics concerns itself with the study of matter in its condensed form where interactions between microscopic degrees of freedom become important and enormous complexity can arise. This complexity is more prevalent at low temperatures where thermal fluctuations are not strong enough to overwhelm quantum mechanical effects, and a variety of exotic quantum ground states may appear. At first glance, studying such strongly correlated quantum systems might seem hopeless as most of their properties (e.g., ground state energy) crucially depend on the precise details of interactions, number of particles, *etc.* Even if, hypothetically, one ascertains such details, these systems possess such large degrees of freedom ($\sim 10^{23}$ particles) that any first-principle approach becomes unthinkable.[1]

Despite these daunting aspects of strongly-correlated quantum many-body systems, certain commonalities among microscopically distinct systems emerge at macroscopic scales. In practice, only certain macroscopic properties that characterize the *phase* of the system and typically are not sensitive to microscopic details, such as the presence or absence of a net magnetization or critical exponents of various thermodynamic functions near a critical point [2, 3], are primarily of interest. From this perspective, condensed matter systems that manifest the same such macroscopic properties, in spite of having different microscopic details, can be regarded equivalent. In general, any equivalence relation entails a classification. In condensed matter physics the equivalence classes that are defined based on manifesting similar such macroscopic properties are called *universality classes*, and are labeled by the common *phase* of the systems in that universality class [1]. Some well-known examples are paramagnetic, ferromagnetic, antiferromagnetic, Fermi liquid and superconducting universality classes. It is the ultimate goal of condensed matter physics to identify

[1] A simple back-of-the-envelope estimate (see, for example, Chapter 1 in [1]) shows that even storing the quantum state of a magnetic sample of localized spin-$\frac{1}{2}$ particles of the size of a sugar cube, in the crudest approximation, will require more atoms than those in the known universe (the Hilbert space will be $2^{10^{23}} \simeq 10^{3\times 10^{22}}$ dimensional). However, it is believed that a quantum computer will be capable of dealing with these otherwise intractable problems efficiently.

and characterize all possible universality classes, i.e., states of matter.[2]

Another remarkable phenomena in condensed matter physics is *emergence*. The significance of the notion of emergence, not only in condensed matter physics but also in disciplines outside physics, was first pointed out by Anderson in his famous 1972 article "More Is Different" [7]. Emergence,[3] in contrast to *reductionism*,[4] is the view that at each level of complexity qualitatively new behavior may arise. For example, rotationally-invariant particles and interactions form highly anisotropic objects (see Chapter 19 in Weinberg's book [9]), or a system comprised of only electrons confined to a plane and subject to a strong magnetic field can manifest *anyonic* excitations that are neither bosons nor fermions (fractional quantum Hall effect) [10]. Thus, complex condensed matter systems not only exhibit certain well-defined universal properties but also these properties may very well be in stark contrast with what one might naively expect from the attributes of their constituent degrees of freedom.

One cannot help but wonder why complex condensed matter systems manifest universality and emergence, and what the underlying principle of these phenomena is. For a long time it was believed that the answer to these questions as well as the question of what the possible universality classes (i.e., states of matter) are, was *symmetry*, which, together with spatial dimensionality, would exhaust all possible phases. Several groundbreaking works in condensed matter physics, statistical physics and high energy physics culminated in the celebrated Landau-Ginzburg-Wilson theory [11, 12] of phases and phase transitions, which posits that phases of matter can be uniquely labeled by their symmetries. The essence of this theory can be understood in an ordinary magnetic system that undergoes a phase transition from a paramagnetic state to a ferromagnetic state. Such a transition is characterized by the spontaneous breaking of the rotational symmetry in the ferromagnetic phase. The statement that Landau-

[2]The notions of universality and universal classes were originally developed in the context of critical phenomena [4, 5, 6]. However, later on they were extended to zero-temperature quantum phase transitions.

[3]To avoid any confusion, it is important to distinguish between *strong emergence* and *weak emergence* [8]. What is intended here is weak emergence where the facts about the high-level phenomenon (properties of the whole) are unexpected, but, in principle, deducible from the facts in the low-level domain (properties of the constituents and the rules that govern their interactions).

[4]By reductionism we neither mean *constituent reductionism*, which states a complex system is nothing but the sum of its constituents, nor *causal reductionism*, which states that, for instance, the pressure exerted by a gas in a container on the inner surface of the container is caused by its constituent atoms or molecules. In fact, these two types of reductionism underlie physics. What is intended here by reductionism is *conceptual reductionism*, which holds that the concept applicable to the whole system is reducible to the concepts that apply to the individual constituents.

Ginzburg-Wilson theory explains all continuous[5] quantum phase transitions[6] tacitly implies that spontaneous symmetry breaking is the only route to emergence. However, now we know that this theory, despite explaining myriad of phase transitions in nature (symmetry-breaking phase transitions) is not complete [13, 15]. Surprisingly, there are states of matter that are distinct even though they share the same symmetries [16]. Examples include fractional quantum Hall systems and various spin-liquid states [1].

What is meant by "distinct phases" is that the two cannot be transformed into each other without encountering a phase transition.[7] For zero-temperature quantum phase transitions, this is phrased as the possibility of adiabatically connecting the ground states. For instance, Fermi liquids are adiabatically connected to non-interacting electrons, and therefore one can employ perturbation theory to compute various observables in a Fermi liquid [17, 18]. By contrast, the ground state of a superconductor is not adiabatically connected to non-interacting electrons, and thus is a distinct phase from the Fermi-liquid phase [19, 20].[8]

Seeking the underlying principle of universal behavior and emergence leads us to the important and intimately related concepts of *effective description* [21, 22, 23] and *renormalization group* (RG) [5, 6]. Both of these notions, perhaps in slightly different guises, have existed in condensed matter physics long before they were introduced in their modern forms. The appearance of the Heisenberg Hamiltonian as the low-energy description of the Hubbard model at half-filling and in the strong repulsion (large-U) limit is an instance of effective description [24]. The block-spin approach of Kadanoff,

[5] Phase transitions are either continuous or first order. First order phase transitions are conceptually much simpler as they are brought about by one state becoming energetically more favourable than the other, and thus a crossover from one state to another. In contrast, continuous phase transitions can be very subtle. For example in the Kosterlitz-Thouless phase transition no symmetry is broken and it is only the behavior of correlations or, equivalently, susceptibilities that reveal the transition. Interestingly, the Landau-Ginzburg-Wilson (LGW) theory was known to fail to describe Kosterlitz-Thouless phase transitions long before the discovery of deconfined quantum critical points (see Ref. [13] and references therein).

[6] It is worth mentioning that the Landau-Ginzburg-Wilson theory was originally developed in the context of critical phenomena (phase transitions driven by thermal fluctuations). However, when it comes to discussing states of matter one is often interested in quantum phase transitions at zero temperature that are driven by quantum fluctuations and are controlled by some parameter such as density or the strength of interactions. The broad inapplicability of the LGW paradigm to all continuous quantum phase transitions stems from the fact that only certain D-dimensional quantum systems, upon analytically continuing real time to imaginary time, can be regarded as (D+1)-dimensional classical systems at a finite temperature [14].

[7] For example, liquid and gas are not distinct phases [3].

[8] From a mathematical point of view, a phase transition is a non-analyticity [2]. Analyticity is important because it allows us to completely determine the value of an analytic function at any point, as accurately as desired, merely by knowing its local properties (its derivatives) at a single point. Thus, various systems that fall within the same universality class are equivalent in a stronger sense: they are connected and even their non-universal properties, in principle, can be obtained using perturbation theory. This is why universality is such a profound concept in condensed matter physics.

which eventually led to modern RG schemes, is an intuitive instance of RG [25]. In fact, as pointed out by Michael Fisher in Ref. [5], the historical development of the Landau-Ginzburg-Wilson theory encompasses both of these notions. In particular, the concept of order parameter, which was originally introduced by Landau, is, in essence, an effective description.

The central idea in effective descriptions is that it is possible to replace the original microscopic description, which describes the system on all length and energy scales, with an effective theory that describes the system, as accurately as desired, only below a certain energy scale or, equivalently, beyond a certain length scale [21, 22, 26]. In other words, it is possible to accurately determine the long-distance behavior of the system from a coarse-grained version of it. Often the effective description is in a continuum form, in which case the term *effective field theory* is used [21, 23]. Such effective field theories are accompanied by a characteristic energy scale (an energy cutoff). This characteristic scale indicates how "coarse grained" the effective description is.[9] Naturally, one expects to be able to determine a more coarse-grained effective description not only from the original microscopic description but also from any other less coarse-grained effective description of the system [29]. This is indeed what is at the heart of any RG approach, which, in fact, defines a semigroup not a group [5, 30]. RG is a framework for systematically and gradually determining more coarse-grained effective theories of a given model. More technically, RG describes how the effective field theory of a system evolves as the energy cutoff is lowered, or, equivalently, as we probe the system at length scales larger than its shortest length scale. RG not only is a powerful concept, but is also a versatile framework to deal with problems that seem intractable when approached by other methods such as perturbation theory. In fact, the popularity of RG in condensed matter physics primarily stems from its practical utility.

Let us see how universality and emergence can be understood from the perspective of effective field theories and RG. The statement of universality, in the language of effective field theories, becomes the statement that systems within the same universality class ultimately share the same low-energy effective theory. Similarly, emergence, in this language, becomes the statement that the degrees of freedom in the low-energy theory may not be the same as those in the original microscopic description. Still this does not explain why most microscopic details are usually irrelevant to low-energy descriptions. The answer to this question becomes obvious once universality is stated in the RG language. Universality classes are characterized by *fixed points* [1, 31], i.e., effective field theories in the space of possible theories that are invariant under the action of RG. A fixed point is, in fact, the ultimate common low-energy effective field

[9] In condensed matter, the shortest length scale of the effective theory of a model, which defines the energy cutoff of the theory, always has to be larger than the lattice spacing or any microscopic scale of the original microscopic model. Nevertheless, as a mere curiosity, one might wonder whether it is possible to take the energy cutoff to infinity and obtain a well-defined genuine continuum limit. Such well-defined continuum limit quantum field theories are called renormalizable theories in high energy physics (see, for example, the entry by Weinberg in [27] and the paper by Polchinski [28]).

theory of all the systems in its universality class. Thus, universality classes are characterized by their fixed points. RG not only describes fixed points, but also explains how low-energy theories *flow* to and away from fixed points as the length scale at which the system is examined is increased or as the energy cutoff is lowered.

We finally can have an explanation as to why there are so few universality classes in comparison to the number of systems they encompass. In other words, why the microscopic details that distinguish different systems within the same universality class are impertinent to their shared macroscopic (large-distance) properties. This is because, as explained in more detail in next sections, such microscopic details correspond to *irrelevant terms* in the RG sense, which, by definition, are terms that get suppressed in the course of RG.

In this thesis we present the application of renormalization group techniques to two strongly correlated condensed matter systems. The notions of effective field theories and RG are central to the analyses presented in the following chapters, and, thus, merit a more thorough and detailed description. In the following two sections we briefly outline these important concepts. First, we briefly describe effective field theories, and then describe how RG naturally arises from the notions of universality and effective field theories.

1.1 Low-Energy Effective Field Theories

The notion of low-energy effective field theories is of great importance in both condensed matter and high energy physics as both disciplines heavily rely on quantum field theory to describe systems composed of many particles [21, 22, 27]. The central premise of low-energy effective field theories is that in a quantum field theory the high-energy (short-distance) modes play a limited role in the low-energy (large-distance) observables [23]. This is the statement that it is possible to entirely capture the effect of high-energy modes on low-energy dynamics by including terms that solely involve low-energy modes.

Determining the low-energy effective theory of a many-body quantum system is done most conveniently and systematically when the system is expressed as a quantum field theory [1]. The quantum field theory of a lattice model can be obtained from the continuum limit of its path integral formulation [32, 33], which provides an equivalent description at length scales larger than a shortest length.[10] This shortest scale corresponds to a largest energy in the continuum limit, referred to as the UV energy cutoff (Λ_0) of the quantum field theory. Dispensing with some subtleties of the continuum limit of the path integral formulation of some lattice models,[11] we start from the quantum field theory of the model and explain how its low-energy effective theory below the energy scale $\Lambda \ll \Lambda_0$ is determined.

[10] In fact, this continuum theory itself is already an effective description of the original lattice model.

[11] See Refs. [34] and [35].

Before proceeding to how this is done in practice, let us first see what the benefit of having a low-energy effective theory is when the original field theory already describes the physics at all energy scales below Λ_0, including the low-energy observables that one is interested in. In principle, the main advantage of a low-energy effective theory is that it provides a more economical description [23], as the low-energy description only involves low-energy modes. Having a low-energy effective field theory becomes particularly advantageous in practice where we are severely limited by our computational capabilities:[12] often, the original quantum field theory is too complicated or even intractable when it comes to computing low-energy observables. A good example of this is the quantum Ginzburg-Landau theory for a s-wave superconductor. The quantum Ginzburg-Landau theory is a bosonic theory that accurately describes the low-energy (energies smaller than the superconducting gap) properties of the superconducting state while the underlying microscopic model is an interacting fermionic theory [36, 37].

The low-energy (*Wilsonian*) effective action of a quantum field theory is obtained from the original action by integrating out high-energy modes [23, 38]. Here we illustrate how this is done in the context of a real scalar theory. This scalar theory can be regarded as the continuum limit description of a system that consists Ising spins on a D-dimensional lattice [6]. The main object of interest in any quantum field theory is the *partition functional* $\mathcal{Z}[J]$ [31], from which all observables of the theory can be obtained. The partition function $\mathcal{Z}[J]$ is given by the following path integral:

$$\mathcal{Z}[J] = \int_{E<\Lambda_0} \mathcal{D}\Phi \; e^{-\mathcal{S}[\Phi]+\int J(\mathbf{r},\tau)\Phi(\mathbf{r},\tau)\mathrm{d}\mathbf{r}\,\mathrm{d}\tau} \,. \tag{1.1}$$

Here Φ is the scalar field variable, $\mathcal{S}[\Phi]$ is the action, J is an external current and the cutoff Λ_0 suppresses the contribution of high-energy modes.

In general, regardless of what formulation one uses to describe a quantum field theory, whether a Hamiltonian formulation or a path-integral description, only physical observables of the theory (the content of the theory) are of interest and meaningful. These observables are the expectation values of time-ordered products of the field variables at various space-time points:

$$C(\mathbf{r}_1,\tau_1\,;\,\mathbf{r}_2,\tau_2\,;\,\cdots\mathbf{r}_n,\tau_n) = \langle \mathrm{T}\,\Phi(\mathbf{r}_1,\tau_1)\Phi(\mathbf{r}_2,\tau_2)\cdots\Phi(\mathbf{r}_n,\tau_n)\rangle \,. \tag{1.2}$$

Various linear response functions are related to these correlation functions [1]. The external current J in Eq. (1.1) allows us to conveniently obtain these observables from the partition function $\mathcal{Z}[J]$ much the same way one obtains magnetization or specific heat in statistical mechanics by taking the derivative of the partition function with

[12] We can always cast the problem in terms of a path integral, but, except in a very few cases, we do not have a general prescription for dealing with such mathematical objects. This is perhaps best expressed in the words of A.M. Polyakov: "There are no tables for path integral".

respect to the appropriate variables:

$$\langle \mathrm{T}\, \Phi(\mathbf{r}_1,\tau_1)\Phi(\mathbf{r}_2,\tau_2)\cdots\Phi(\mathbf{r}_n,\tau_n)\rangle = \frac{\delta}{\delta J(\mathbf{r}_1,\tau_1)}\frac{\delta}{\delta J(\mathbf{r}_2,\tau_2)}\cdots\frac{\delta}{\delta J(\mathbf{r}_n,\tau_n)}\mathcal{Z}[J]\Big|_{J=0}, \tag{1.3}$$

where, $\frac{\delta}{\delta J(\mathbf{r},\tau)}$ indicates taking the functional derivative with respect to the external current J at the point $(\mathbf{r},t)$.

Let us assume that the scalar theory in Eq. (1.1) is perturbative, i.e., $\mathcal{S}$ is of the following form:

$$\mathcal{S} = \mathcal{S}_0 + \lambda\mathcal{S}_{\text{int}}\,, \tag{1.4}$$

where $\mathcal{S}_0$ is a free action, which describes non-interacting bosonic degrees of freedom, and the parameter $\lambda \ll 1$.[13] Here, $\mathcal{S}_{\text{int}}$ introduces interactions and, in general, is a sum of various products of the field variables and their derivatives (e.g., $\int \mathrm{d}\mathbf{r}\mathrm{d}\tau\, \Phi^4(\mathbf{r},\tau)$). The perturbativity assumption ($\lambda \ll 1$) is necessary for being able to systematically carry out the path integral perturbatively within a so-called loop expansion approximation [31, 39, 40].

Let us see why the Wilsonian effective action is obtained from integrating out high-energy modes. The external current $J(\mathbf{r},\tau)$ in the path integral in Eq. (1.1]) plays a similar role to a local external magnetic field in the partition function of the Ising model whose derivative at zero field yields the local magnetization. Using this intuition, we notice an important advantage of this path-integral formulation. The energy cutoff Λ_0 of the theory suppresses field configurations that oscillate rapidly. Suppose there is another energy scale $\Lambda \ll \Lambda_0$ associated with the external current that corresponds to a length scale that denotes how rapidly the external current $J(\mathbf{r},\tau)$ varies (its shortest wavelength) [31, 39]. When performing the path integral in Eq. (1.1), there will be modes integrated over that oscillate much faster than the scale corresponding to the energy scale Λ but still slower than the scale corresponding to the energy cutoff Λ_0. These high-energy field configurations ($\Phi_>$), therefore, result in a vanishing $\int J(\mathbf{r},\tau)\Phi_>(\mathbf{r},\tau)\mathrm{d}\mathbf{r}\mathrm{d}\tau$, i.e., do not couple to the external current. This is because, by assumption, $J(\mathbf{r},\tau)$ is almost stationary over scales shorter than the length scale corresponding to the energy scale Λ, while $\Phi_>$ still rapidly oscillates (since $\Lambda \ll \Lambda_0$). Thus, we can ignore the direct contribution of these rapidly oscillating modes $\Phi_>$ to the observables that are being measured via this external current, i.e., the low-energy observables.

Usually, when the model possesses translational symmetry, it is more convenient to work in momentum space. This is because, typically, the unperturbed action $\mathcal{S}_0$ becomes trivial once expressed in terms of $\Phi(\mathbf{q},\omega)$ in momentum space. Upon Fourier transformation, rapidly oscillating modes in space-time are mapped onto large-momentum field variables. Then the energy dispersion relation in $\mathcal{S}_0$ makes the correspondence between rapidly oscillating and high-energy models explicit [6, 29]. In

[13] In fact, $\mathcal{S}_0$ does not necessarily have to be a free action. All we need is a theory that we know its full content (all n-point functions). We will see a neat example of this in Chapter 2.

the remainder of this chapter we work in momentum space.

Let us explain why the fact that high-energy modes do not directly contribute to low-energy observables does not mean that they can be simply ignored. In other words, why the same path integral with Λ instead of Λ_0 in general does not reproduce the same low-energy observables as those in the original theory Eq. (1.1). This is because of the possibility of virtual processes in quantum mechanical systems. This is best exemplified in the derivation of the Heisenberg Hamiltonian from the Hubbard model at half-filling and in the limit $U \to \infty$. In this limit, double occupancy is energetically prohibited yet virtual processes that involve double occupancy result in effective spin exchange terms, with the Heisenberg Hamiltonian being the leading term [24, 41]. Similarly, in a quantum field theory, although high-energy modes do not directly contribute to the low-energy observables, they, nevertheless, result in *quantum corrections* to the low-energy effective action. This is why the correct low-energy effective action is obtained by integrating out high-energy modes in the original action:

$$\mathcal{Z}[J] = \int_{E<\Lambda} \mathcal{D}\Phi \; e^{-\mathcal{S}_{\text{eff}}[\Phi] + \int \frac{\mathrm{d}\mathbf{q}}{(2\pi)^D} \frac{\mathrm{d}\omega}{2\pi} J(\mathbf{q},\omega)\Phi(-\mathbf{q},-\omega)}, \tag{1.5}$$

where,

$$e^{-\mathcal{S}_{\text{eff}}[\Phi]} = \int_{\Lambda<E<\Lambda_0} \mathcal{D}\Phi \; e^{-\mathcal{S}[\Phi]}. \tag{1.6}$$

So far we have shown that low-energy (at energies below the energy scale $\Lambda < \Lambda_0$) observables of a quantum field theory with the energy cutoff Λ_0 can be obtained not only from the original theory but also from a low-energy effective theory with the Wilsonian effective action given in Eq. (1.6). Thus, the effective Wilsonian action of the theory is parameterized by Λ, and coincides with the original action when $\Lambda = \Lambda_0$ [23, 38]. Assuming locality,[14] the Lagrangian density[15] of the Wilsonian action can be written as a linear combination of *local operators* (products of the field variables with derivatives) compatible with the symmetries and conserved quantum numbers of the original theory. Therefore, the Wilsonian effective action can be viewed as a point in an infinite-dimensional linear space, for which these local operators furnish a complete basis.Then, the coefficients of local terms in the action (the coupling constants) are the coordinates of the point that represents the low-energy effective theory in this space of possible theories. Thus, determining $\mathcal{S}_{\text{eff}}$ at any energy scale below Λ_0 reduces to determining the couplings of local operators as a function of Λ with initial values given by the bare couplings (the couplings in bare action $\mathcal{S}$) at $\Lambda = \Lambda_0$.

It might seem that we have not made much progress as we still have to perform

[14] A quantum field is local if its Lagrangian density solely involvs the product of field operators and their derivatives at the same space-time points.

[15] The action of a quantum field theory is usually expressed as an integral in the space-time or in the momentum space. The integrand of this integral is the Lagrangian density of the quantum field theory.

a path integral in Eq. (1.6) to determine the Wilsonian effective action of the theory. Furthermore, integrating out high-energy modes usually generates an infinite number of terms. The power of low-energy effective field theories lies in the fact that most of these generated terms are ultimately unimportant (hence dubbed as irrelevant) and can be ignored [42]. As for the loop integrals encountered in computing the effective action in Eq. (1.6), these loop integrals are explicitly UV and IR finite, and, therefore, do not suffer from any divergences. Ignoring irrelevant terms often results in a quantitative error of order $\mathcal{O}(\frac{\Lambda}{\Lambda_0})^{(h-h_{\text{u.c.}})}$, where $h_{\text{u.c.}}$ is the *upper critical dimension* of the theory and h is the scaling dimension of the irrelevant term [29, 31, 43].[16] This justifies restricting the analysis to terms that are not irrelevant, i.e., the subspace spanned by local operators with scaling dimensions not greater than the upper critical dimension of the theory ($h \leq h_{\text{u.c.}}$).[17]

As pointed out above, since in integrating out high-energy modes Λ_0 and Λ serve, respectively, as UV and IR cutoffs, loop integrals can be carried out unambiguously. However, in practice, we have to truncate the loop expansion when integrating out high-energy modes in Eq. (1.6), and it is not clear at what order in the expansion this can be done without introducing any bias. Thus, we still lack a systematic prescription for determining the Wilsonian effective action even in local perturbative field theories [33]. This point becomes particularly crucial in cases where there are competing terms in the interaction action that affect each other as high-energy modes are integrated out. We will see a good example of this in the RG analysis of Chapter 2. RG solves this problem by incrementally integrating out high-energy modes [33].

1.2 Renormalization Group

In this section we illustrate how RG naturally arises from the notions of universality and low-energy effective field theories [1, 3, 26, 44, 45, 46]. In condensed matter physics we are ultimately interested in universality classes and their best representatives, which are their fixed-point theories. Let us first clarify what constitutes a good representative for a universality class, which explains why fixed-point theories are privileged. As pointed out earlier, any member of a universality class serves as a representative for that universality class. What distinguish various systems within the same universality class are non-universal properties. Non-universal properties stem from terms in the action of the quantum field theory of the system that are ultimately unimportant in describing the universal (i.e., large-distance or, equivalently, low-energy) properties of that universality class. Thus, based on Occam's razor principle, the best representative for a universality class is the theory that contains no

[16] This is because the coupling of irrelevant terms (as well as relevant terms – $h < h_{\text{u.c.}}$) are dimensionful and their values depend on the energy scale they are measured at.

[17] Often we do not know the full scaling dimension of an operator. However, when the theory is perturbative it is possible to use the scaling dimension of operators with respect to $\mathcal{S}_0$, i.e., we can ignore the *anomalous scaling dimension* [43] of field variables.

non-universal terms, as such a theory provides the most straightforward description of its universality class. Recall that universality becomes manifest at macroscopic scales, and non-universal properties typically disappear when one probes the system over sufficiently large length scales. This suggests that the ideal representative theory for a universality class should be *scale invariant*.

The statement that a quantum field theory is scale invariant implies that the observables of the theory do not involve any intrinsic scale. However, there is at least one intrinsic scale in the path-integral formulation of the theory, namely the energy cutoff. Therefore, somehow the dependence on the energy cutoff in the observables should disappear. In what follows we demonstrate this for a fixed-point scalar field theory. Then we illustrate how RG can be used to track the flow of the low-energy effective field theory of a system to or away from a fixed point.

Since the fixed-point theory is scale invariant, all of its observables including its two-point function $C(\mathbf{q},\omega)$ should scale [45, 47]:

$$C(s^{-1}\,\mathbf{q}, s^{-z}\,\Omega) \;=\; s^{2\eta}\; C(\mathbf{q},\Omega) \;\;, \tag{1.7}$$

where z is the *dynamical exponent* [45], η is the scaling dimension of the field variables and $s \gtrsim 1$ is a scaling parameter.[18] To deduce the criterion for being a fixed-point action from the above scaling relation, we start with the path-integral representation of the two-point function on the left hand side of Eq. (1.7):

$$C(s^{-1}\,\mathbf{q}, s^{-z}\,\Omega) \;=\; \frac{1}{\mathcal{Z}} \int_{\Lambda} \mathcal{D}\Phi \; e^{-\mathcal{S}_{\text{F.P.}}[\Phi(\mathbf{k},\omega)]} \; \Phi(s^{-1}\,\mathbf{q}, s^{-z}\,\Omega)\, \Phi(-s^{-1}\,\mathbf{q}, -s^{-z}\,\Omega)\,. \tag{1.8}$$

Here, we use $\mathcal{S}_{\text{F.P.}}[\Phi(\mathbf{k},\omega)]$ as a shorthand for $\int \mathrm{d}\mathbf{k}\mathrm{d}\omega\, \mathcal{L}_{\text{F.P.}}[\Phi(\mathbf{k},\omega)]$. Let us rewrite the action in terms of integrals over the new variables $\tilde{\mathbf{k}} = s\mathbf{k}$ and $\tilde{\omega} = s^z\omega$. We get:

$$\begin{aligned} &C(s^{-1}\,\mathbf{q}, s^{-z}\,\Omega) \;= \\ &\frac{1}{\mathcal{Z}} \int_{\Lambda'} \mathcal{D}\Phi \; e^{-\mathcal{S}_{\text{F.P.}}[s^{-\eta}\Phi(s^{-1}\,\tilde{\mathbf{k}}, s^{-z}\,\tilde{\omega})]} \; \Phi(s^{-1}\,\mathbf{q}, s^{-z}\,\Omega)\, \Phi(-s^{-1}\,\mathbf{q}, -s^{-z}\,\Omega)\,, \end{aligned} \tag{1.9}$$

where, again, $\mathcal{S}_{\text{F.P.}}[s^{-\eta}\Phi(s^{-1}\,\tilde{\mathbf{k}}, s^{-z}\,\tilde{\omega})]$ is a shorthand for $\int \mathrm{d}\tilde{\mathbf{k}}\mathrm{d}\tilde{\omega}\, \mathcal{L}_{\text{F.P.}}[s^{-\eta}\Phi(\tilde{\mathbf{k}},\tilde{\omega})]$. The extra factor $s^{-\eta}$, which originates from the Jacobian and the change of the Lagrangian density under the change of the integration variables, has been grouped with the field variable Φ so that it can be absorbed into the field variables subsequently. Note that, due to this change of variables, the energy cutoff appears larger ($\Lambda \to \Lambda' = s\Lambda$). Next, we "relabel" the field variables of the path integral in Eq. (1.9) as follows:

$$\Phi(\mathbf{k},\omega) \;\; \to \;\; \Phi(s\mathbf{k}, s^z\Omega)\,. \tag{1.10}$$

[18] In RG schemes the scaling is infinitesimal so that integrating out high-energy modes is incremental.

We get:

$$C(s^{-1}\,\mathbf{q}, s^{-z}\,\Omega) \;=\; \frac{1}{\mathcal{Z}} \int_{\Lambda'} \mathcal{D}\Phi \; e^{-\mathcal{S}_{\text{F.P.}}[s^{-\eta}\Phi(\tilde{\mathbf{k}},\tilde{\omega})]} \; \Phi(\mathbf{q},\Omega)\, \Phi(-\mathbf{q},-\Omega)\,. \tag{1.11}$$

Scaling the field variables by s^{η},

$$\Phi(\mathbf{k},\omega) = s^{\eta}\tilde{\Phi}(\mathbf{k},\omega)\,, \tag{1.12}$$

we obtain:

$$C(s^{-1}\,\mathbf{q}, s^{-z}\,\Omega) \;=\; \frac{s^{2\eta}}{\mathcal{Z}} \int_{\Lambda'} \mathcal{D}\tilde{\Phi} \; e^{-\mathcal{S}_{\text{F.P.}}[\tilde{\Phi}(\mathbf{k},\omega)]} \; \tilde{\Phi}(\mathbf{q},\Omega)\, \tilde{\Phi}(-\mathbf{q},-\Omega)\,. \tag{1.13}$$

Eq. (1.13) is different from the path integral representation of $C(\mathbf{q},\Omega)$ in that the cutoff is at $\Lambda' = s\Lambda > \Lambda$. Since, by assumption, the observables that we are interested in correspond to energies much smaller than the energy cutoff Λ, we can integrate out modes that lie at high energies (between Λ and $\Lambda' = s\Lambda$) to obtain an effective Wilsonian action:

$$e^{-\mathcal{S}_{\text{eff}}} \;\equiv\; \int_{\Lambda<E<\Lambda'} \mathcal{D}\tilde{\Phi} \; e^{-\mathcal{S}_{\text{F.P.}}[\tilde{\Phi}(\tilde{\mathbf{k}},\tilde{\omega})]}\,. \tag{1.14}$$

Using this effective Wilsonian action, we should be able to reproduce exactly the same low-energy observables:

$$C(s^{-1}\,\mathbf{q}, s^{-z}\,\Omega) \;=\; \frac{s^{2\eta}}{\mathcal{Z}} \int_{\Lambda} \mathcal{D}\tilde{\Phi} \; e^{-\mathcal{S}_{\text{eff}}[\tilde{\Phi}(\tilde{\mathbf{k}},\tilde{\omega})]} \; \tilde{\Phi}(\mathbf{q},\Omega)\, \tilde{\Phi}(-\mathbf{q},-\Omega)\,, \tag{1.15}$$

We see that the scaling relation that characterizes the fixed point translates into a statement about the effective Wilsonian action of the theory. Often, up to an unimportant constant, $\mathcal{S}_{\text{eff}} = \mathcal{S}_{\text{F.P.}}$ [29, 45].

Suppose that instead of the fixed-point theory with the action $\mathcal{S}_{\text{F.P.}}$, we have a different theory described by the action $\mathcal{S}$ within the universality class of $\mathcal{S}_{\text{F.P.}}$. This implies that,

$$\mathcal{S} \;=\; \mathcal{S}_{\text{F.P.}} \;+\; \sum_i g_i \mathcal{O}_i\,, \tag{1.16}$$

where g_i is the coupling constant of the irrelevant term $\mathcal{O}_i$. The set of irrelevant coupling constants $\{g_i\}$ under the above RG procedure will flow to zero. Due to the presence of these irrelevant terms in $\mathcal{S}$, the scaling relation in Eq. (1.7) does not hold. This can be made explicit by repeating the above steps but this time for $\mathcal{S}$ instead of $\mathcal{S}_{\text{F.P.}}$. This time, Eq. (1.14) becomes:

$$C(s^{-1}\,\mathbf{q}, s^{-z}\,\Omega, \{g_i\}) \;=\; \frac{s^{2\eta}}{\mathcal{Z}} \int_{\Lambda'} \mathcal{D}\tilde{\Phi} \; e^{-\mathcal{S}'[\tilde{\Phi}(\mathbf{k},\omega)]} \; \tilde{\Phi}(\mathbf{q},\Omega)\, \tilde{\Phi}(-\mathbf{q},-\Omega)\,. \tag{1.17}$$

where, $\mathcal{S}'$ may not be the same as $\mathcal{S}$ due to the tree-level running (classical scaling) of the couplings and $\{g_i\}$ are the couplings of the irrelevant terms in $\mathcal{S}$ at the scale Λ. Integrating out modes between Λ and $s\Lambda$, we find:

$$\begin{aligned} C(s^{-1}\,\mathbf{q}, s^{-z}\,\Omega, \{g_i\}) &= \frac{s^{2\eta}}{\mathcal{Z}} \int_{\Lambda} \mathcal{D}\tilde{\Phi}\; e^{-\mathcal{S}_{\rm eff}[\tilde{\Phi}(\mathbf{k},\omega)]}\; \tilde{\Phi}(\mathbf{q},\Omega)\, \tilde{\Phi}(-\mathbf{q},-\Omega) \\ &= s^{2\eta}\, C(\mathbf{q},\Omega,\{g_i'\})\,, \end{aligned} \tag{1.18}$$

where,

$$e^{-\mathcal{S}_{\rm eff}} \equiv \int_{\Lambda<E<\Lambda'} \mathcal{D}\tilde{\Phi}\; e^{-\mathcal{S}'[\tilde{\Phi}(\tilde{\mathbf{k}},\tilde{\omega})]}\,, \tag{1.19}$$

and $g_i' = s^{(h_{\rm u.c.}-h_i)} g_i + \delta g_i(s)$ (here $\delta g_i(s)$ is the quantum correction to g_i from integrating out high-energy modes).

Most of the time we do not know to what universality class a given theory belongs. In principle, RG is capable of addressing this question. However, carrying this out can be very difficult and often impractical, unless a systematic approximation is made. The main difficulty arises from integrating out high-energy modes to obtain an effective action as in Eq. (1.19) where we do not have a generic prescription for performing the path integral even when the energy cutoff is lowered incrementally ($\Lambda' = e^{{\rm d}\ell}\Lambda$).

When the theory is perturbative, i.e., $\mathcal{S} = \mathcal{S}_0 + \lambda\,\mathcal{S}_{\rm int}$ with $|\lambda| \ll 1$, one can employ perturbation theory to integrate out high-energy modes perturbatively. This is done by expanding the full action, $\mathcal{S}$, in λ:

$$\begin{aligned} e^{-\mathcal{S}_{\rm eff}} &= \int_{\Lambda<E<\Lambda'} \mathcal{D}\tilde{\Phi}\; e^{-\,\mathcal{S}_0[\tilde{\Phi}(\tilde{\mathbf{k}},\tilde{\omega})]\,-\,\lambda\mathcal{S}'_{\rm int}[\tilde{\Phi}(\tilde{\mathbf{k}},\tilde{\omega})]} \\ &\approx \int_{\Lambda<E<\Lambda'} \mathcal{D}\tilde{\Phi}\; e^{-\mathcal{S}_0[\tilde{\Phi}(\tilde{\mathbf{k}},\tilde{\omega})]} \Bigg[1 \,-\, \lambda\; \mathcal{S}'_{\rm int}[\tilde{\Phi}(\tilde{\mathbf{k}},\tilde{\omega})] + \\ &\qquad\qquad \frac{\lambda^2}{2}\Big(\mathcal{S}'_{\rm int}[\tilde{\Phi}(\tilde{\mathbf{k}},\tilde{\omega})]\Big)^2 \,+\, \mathcal{O}(\lambda^3)\Bigg]\,, \end{aligned} \tag{1.20}$$

where, again, $\mathcal{S}'_{\rm int}$ can be different from $\mathcal{S}_{\rm int}$ due to the tree-level running of the couplings (after scaling the field operators). Therefore, as long as the theory is perturbative, integrating out high-energy modes does not pose any serious problem and can be performed perturbatively.

Often $\mathcal{S}_0$, the unperturbed theory, itself is a fixed point theory and we want to systematically determine how $\mathcal{S}_{\rm int}$ evolves in the course of RG. This requires determining the flow of not only the coupling constants originally present in $\mathcal{S}_{\rm int}$ but also those that are generated in the course of RG. However, there are potentially an infinite number of coupling constants. Therefore, we need to find a way to consistently restrict the analysis to a more manageable set of couplings to be able to make any progress.

As in the discussion of effective field theories in the previous section, suppose local operators provide a complete basis for any possible term that can be generated in this perturbative theory (the assumption of locality). Then the question of how $\mathcal{S}_{\text{int}}$ evolves in the course of RG becomes how the coupling constants of the local terms, $\{g_i\}$, flow as the cutoff Λ is lowered. For an infinitesimal scaling $s = e^{\mathrm{d}\ell}$ this procedure gives differential equations (β-functions) that govern the flow of the coupling constants. The initial conditions are provided by the coupling constants in $\mathcal{S}_{\text{int}}$ in the beginning.

The β-functions for a given coupling constant with the initial condition $g \propto \lambda \ll 1$ and the scaling dimension h (with respect to $\mathcal{S}_0$) is of the form $\partial_\ell g_i = (h_{\text{u.c.}} - h_i)g_i + \mathcal{O}(\lambda)^2$ ($\ell = \log L$ is the "RG time" – here L is the physical length). Thus, as long as $\lambda \ll 1$, the β-functions are dominated by the *tree-level* scaling dimensions, i.e., $(h_{\text{u.c.}} - h_i)$.[19] Therefore, most of the time,[20] it is justified to ignore irrelevant terms, i.e., terms with $h > h_{\text{u.c.}}$, and only focus on tree-level marginal and relevant terms (those with scaling dimensions $h \leq h_{\text{u.c.}}$).

The above outlined RG procedure is common to a class of RG schemes referred to as *local perturbative RG* schemes. This is because of the two main assumptions that were made in arriving at the β-functions: locality and perturbativity. In cases where any (or both) of these assumptions fails, one has to resort to other RG schemes such as *functional (exact) RG* schemes [29, 48]. In functional RG schemes the evolution of $\mathcal{S}_{\text{int}}$ is usually described in terms of an infinite hierarchy of integro-differential equations for n-point *one-particle irreducible (1PI)* vertices. Such integro-differential equations are very formal and cannot be carried out exactly [49, 48, 33]. Nonetheless, functional RG schemes are useful as they, together with various (often case-specific) approximations that make computations possible, can provide alternative approaches to local perturbative RG schemes. For examples of such approximate functional RG approaches see [50, 51, 52].

1.3 This Thesis

This thesis presents how renormalization group ideas can be fruitfully utilized in addressing two strongly correlated problems in two dimensions: the spin-$\frac{1}{2}$ Heisenberg antiferromagnetic model on an anisotropic triangular lattice, and the effect of weak interactions on a neck-narrowing Lifshitz transition. These two problems are not only of considerable interest for their relevance to real materials, but also are of interest from a theoretical point of view. The RG analyses presented in this thesis, besides addressing the physics of these two problems, provide instances of somewhat novel RG scenarios.

[19] The term tree-level is used because the $(h_{\text{u.c.}} - h_i)$ term in the β-function appears at $\mathcal{O}(\lambda)$ (tree level) in the expansion in Eq. (1.20).

[20] One should be mindful of dangerously irrelevant terms, i.e., irrelevant terms that might affect the flow of marginal or relevant terms in a significant way.

The spin-$\frac{1}{2}$ Heisenberg antiferromagnetic model on an anisotropic triangular lattice (Fig. [1.1]) is discussed in Chapter 2. The phase diagram of this model has been the subject of extensive analytical and numerical studies, and is relevant to certain Mott insulator materials such as Cs_2CuCl_4 and Cs_2CuBr_4. The intense interest in this model originated from the possible existence of a two-dimensional spin-liquid state in its phase diagram, as this model is a low-dimensional geometrically frustrated quantum antiferromagnet. This was further fueled by the experimental observation of a featureless continuum in the inelastic neutron scattering spectrum of Cs_2CuCl_4 [53]. This observation was taken as evidence for deconfined two-dimensional spinons and led to the suggestion that, while Cs_2CuCl_4 itself exhibits an incommensurate spiral ground state, it, nevertheless, may be in close proximity to a quantum phase transition to a two-dimensional spin-liquid state [54]. Inspired by this proposal, numerous studies suggested the presence of spin-liquid state(s) in the phase diagram of this model at strong and even moderate anisotropies [55] as shown in Fig. [1.2a]. In contrast, Starykh and Balents [56], based on a one-dimensional real-space RG approach, argued that this model exhibits a collinear antiferromagnetic (CAF) state at strong anisotropies, with a crossover to an incommensurate spiral state at some point (Fig. [1.2a]).

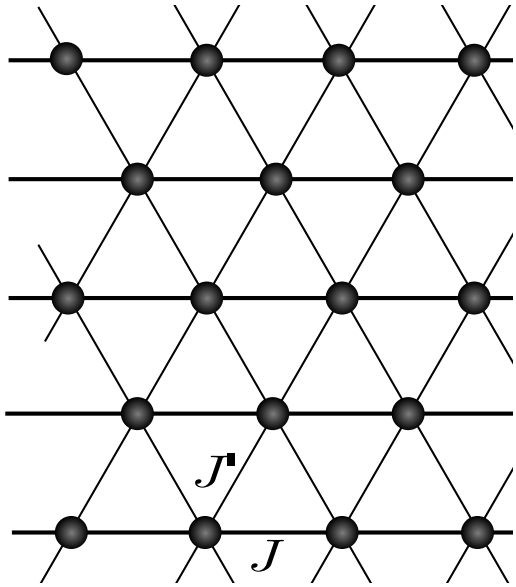

Figure 1.1: Spatially anisotropic triangular lattice. Spin-$\frac{1}{2}$'s reside on the sites of the lattice. Spatial anisotropy stems from the fact that the strength of the coupling between spins along the horizontal bonds, J, is different (here larger) than that of the diagonal bonds, J'.

In a collinear antiferromagnetic spin texture (see Fig. [2.7b]), unlike in a spiral spin configuration (see Fig. [2.7a]), second-nearest chains are coupled antiferromag-

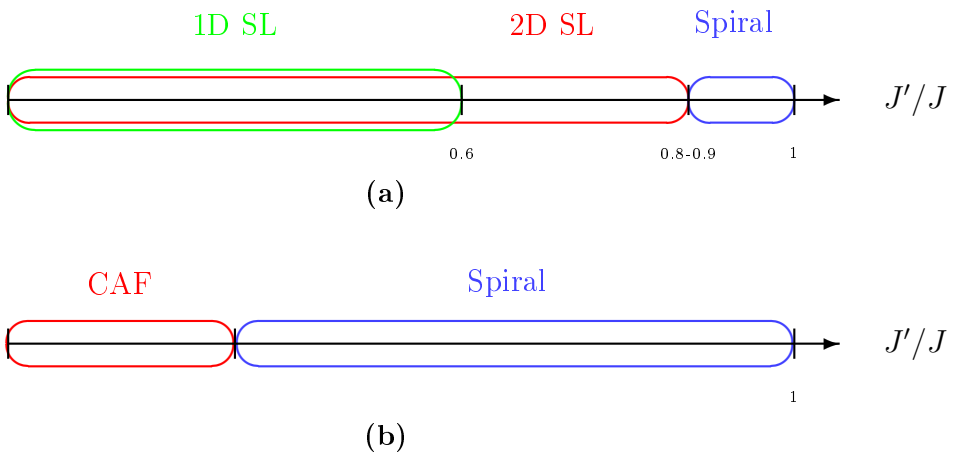

Figure 1.2: Proposed phase diagrams for the spin-$\frac{1}{2}$ HAF model on a spatially anisotropic triangular lattice. (a) studies that advocated for the presence of quantum-disordered states in the phase diagram. (b) studies that did not indicate any extended quantum-disordered state in the phase diagram.

netically. However, this does not necessarily mean that second-nearest chains are coupled antiferromagnetically on all length scales when the system is in the CAF phase: the antiferromagnetic coupling between second-nearest chains in the CAF phase may manifest itself only at large length scales, while on short length scales spins on second-nearest chains can even exhibit ferromagnetic correlations. Whether or not this is the case can be easily determined from the RG flow of the couplings. The RG analysis of Starykh and Balents [56] suggests that second-nearest chains are antiferromagnetically coupled on all length scales. However, high-precision numerical studies on finite-size systems only indicate ferromagnetic correlations between spins on second-nearest chains, which is very puzzling. Using the same real-space one-dimensional RG approach of Starykh and Balents, we examine a more comprehensive set of β-functions, and find, due to a subtle fine-tuning of couplings, the presence of ferromagnetic correlations over large length scales is compatible with such a collinear antiferromagnetic state. Also, we examine the effect of a weak Dzyaloshinskii-Moriya interaction term, which is relevant to materials such as Cs_2CuCl_4 and Cs_2CuBr_4 within this RG approach. The presented RG analysis does not indicate any extended quantum-disordered state in the phase diagram of this model at strong anisotropies. Given the experimentally determined parameters in the Hamiltonian of Cs_2CuCl_4, we conclude that this material is well within the stability region of the spiral state.

The RG analysis for a neck-narrowing Lifshitz transition in two-dimensions and in the presence of weak interactions is presented in Chapter 3. At the critical point of the neck-narrowing Lifshitz transition studied here, the Fermi surface contains a van Hove singular point. The interest in this problem stems from the fact that van Hove singularities or proximity to such singular points are ubiquitous in real materials.

Examples of such Fermi surfaces include the diamond Fermi surface of the Hubbard model on a square lattice at half filling and Graphene at $\frac{3}{8}$ or $\frac{5}{8}$ filling, which contains three distinct van Hove singularities and has received a great deal of attention in recent years. Neck-narrowing transitions are, in fact, topological quantum phase transitions where, across the transition, only the topology of the Fermi surface changes, with no change in symmetry. It is, thus, of great importance to understand the effect of interactions on such transitions.

We study a model described by the dispersion $\varepsilon_{\mathbf{k}} = k_x^2 - k_y^2$, together with a momentum cutoff that plays the role of the size of the Fermi surface. The neck-narrowing transition in this model is controlled by the chemical potential, with the critical point at $\mu_c = 0$. Slightly away from the critical point, the Fermi surface has a narrow neck, which vanishes as the critical point is approached. We find that, at the critical point, the Wilsonian effective action is intrinsically non-local. This intrinsic non-locality of the effective action is attributed to integrating out a soft degree of freedom. Away from the critical point, locality in the Wilsonian effective action can be restored only in the presence of a momentum cutoff that keeps the size of the Fermi surface finite. However, this local description is available only within a finite momentum range that shrinks in the course of RG. Within this analytic range, we find that attractive interactions grow as $\log^2 L$.

Chapter 2

Spin-$\frac{1}{2}$ Heisenberg Antiferromagnetic Model on a Spatially Anisotropic Triangular Lattice

This chapter presents an RG analysis of the spin-$\frac{1}{2}$ Heisenberg antiferromagnetic (HAF) model on a spatially anisotropic triangular lattice in the strong anisotropy limit. In the strong anisotropy limit, this model is quasi-one-dimensional, and becomes amenable to a real-space RG scheme [57] appropriate for spin-$\frac{1}{2}$ Heisenberg antiferromagnetic chains. Treating the coupling between the chains as a weak perturbation to decoupled spin-$\frac{1}{2}$ chains, we analyze the nature of the dominant interchain coupling at large length scales. Clearly, this perturbative RG approach is feasible only up to a length scale where a renormalized interchain coupling becomes comparable to the intrachain coupling. Once this scale is reached, we use the output of this RG, i.e., the renormalized interchain couplings, to predict the fate of the system based on what is known about certain two-dimensional quantum magnets.

The main focus of the analysis presented in this chapter is on the nearest-neighbor Heisenberg model. Nevertheless, the effect of a weak Dzyaloshinskii-Moriya [58] interaction, which is relevant to materials such as Cs_2CuCl_4 and Cs_2CuBr_4, is briefly discussed within this one-dimensional RG approach at the end. The phase diagram of this model in the presence of a magnetic field is a rich and interesting topic at its own right that will not be discussed here. The analysis presented in this chapter is largely based on Refs. [59, 55]. The DMRG and ED results presented here were obtained by Prof. Erik Sorensen. The RG analysis and the analysis of the DMRG and ED results were all performed by the author of this thesis.

The main results of this chapter are as follows. In contrast to many numerical and theoretical studies that suggest the presence of spin-liquid states over a large parameter range in the phase diagram of this model (see Eq. (2.1)), the presented RG analysis does not indicate any extended quantum-disordered state in the phase dia-

gram at strong anisotropies. The dominant coupling between the chains is a relevant second-nearest-chain Néel coupling that, depending on its sign, either results in ferromagnetically or antiferromagnetically coupled second-nearest chains. Ferromagnetic coupling between second-nearest chains is compatible with spiral ordering, whereas antiferromagnetic coupling, via the order-by-disorder mechanism, entails a collinear antiferromagnetic (CAF) state. Most notably, the β-functions reveal a subtle fine-tuning, because of which the relevant second-nearest chain Néel coupling term does not grow as fast as a relevant coupling is expected to grow. In particular, because of this fine-tuning, even in the CAF state, ferromagnetic correlations persist over large length scales. It is found that the spiral state dominates the phase diagram, and a fragile CAF state can be stabilized only at sufficiently strong anisotropies and when the Dzyaloshinskii-Moriya interaction is extremely weak. It is pointed out that this fine-tuning has important implications on how the results of numerical studies on finite-size systems should be interpreted. Finally, it is concluded that Cs_2CuCl_4 is well within the stability region of the spiral order.

2.1 Introduction

The spin-$\frac{1}{2}$ Heisenberg triangular antiferromagnet is the simplest and perhaps most well-known instance of *geometric frustration* in quantum magnetism. The interest in this model dates back to the early 70s when Anderson [60] suggested that the ground state of this model is likely a *resonating valence bond* (RVB) state, i.e., a spin-liquid state. However, later on, using finite-temperature series expansions, Monte Carlo simulations and exact diagonalization on finite-size systems, it became clear that the ground state of this model exhibits a long-range ordered state: the 120° phase (see Fig. [2.3a]), which is the classical ground state of this model [61, 62, 63, 64]. Nevertheless, Anderson's RVB state, as an instance of quantum-disordered states of matter at zero temperature that do not break any symmetries of the Hamiltonian, introduced the notion of spin liquids in condensed matter physics.[1]

The interest in frustrated quantum magnets has been predominantly driven by the pursuit of spin-liquid ground states in two and higher dimensions [66]. Low-spin two-dimensional frustrated quantum magnets, in particular, have been explored more extensively due mainly to the fact that mean-field effects that favour ordered states are typically weaker in lower dimensions [67, 68]. In general, frustration and low-dimensionality are antagonist to long-range ordered states. Frustration results in energetically less favourable classical ground states[2] that experience stronger quantum fluctuations and are typically degenerate. In lower dimensions, quantum fluctuations

[1] The interest in such quantum disordered states that break none of the symmetries of the Hamiltonian goes back to a very interesting debate between Nevill Mott and John Slater, the account of which can be found in Anderson's book [65].

[2] Spin configurations that minimize the Hamiltonian in which spins are treated as classical vectors of fixed length.

around ordered states could be potent enough to "melt" the long-range magnetic order, and result in a quantum-disordered state. The extreme case of this melting of long-range magnetic order due to strong quantum fluctuations occurs in one dimension, where antiferromagnetic chains either exhibit a spin-liquid ground state or a *valence-bond solid* [69, 67, 24, 57]. This is why low-dimensional frustrated quantum magnets are generally believed to be more prone to realize quantum-disordered ground states, and perhaps spin-liquid states [66, 70].

On the theoretical side, there already exist several artificial two-dimensional models that were specifically designed to manifest spin-liquid ground states [71, 72, 73, 74, 75, 76, 77, 78]. However, most of these models are too abstract, and, thus, are of interest mostly from a theoretical perspective.[3] On the experimental side, the organic Mott insulator κ-(BEDT-TTF)$_2$Cu$_2$(CN)$_3$ [82, 83], which is close to its Mott transition point (is a weak Mott insulator), is suspected to possess a spin-liquid ground state [70]. However, this material, being a weak Mott insulator, involves substantial ring-exchange terms, and cannot be described by a model of short-range Heisenberg exchanges. Another promising experimental candidate is Herbertsmithite [70, 84], which is a mineral with a kagome lattice structure and the chemical structure ZnCu$_3$(OH)$_6$Cl$_2$. We also seem to have strong numerical evidence that the ground state of the spin-$\frac{1}{2}$ HAF model on the kagome lattice is a spin liquid [85].

The spin-$\frac{1}{2}$ HAF model on the kagome lattice had long been suspected to possess a spin-liquid ground state as its classical ground state is highly degenerate (has a thermodynamic degeneracy) [72, 86]. The fact that classical ground state of a model has a thermodynamic degeneracy suggests that its quantum ground state is most likely a quantum disordered state, i.e., either a spin-liquid state or a valence-bond solid [85, 87]. This reasoning proves illuminating in rationalizing the result of the RG analysis on the spin-$\frac{1}{2}$ HAF model on a spatially anisotropic triangular lattice, whose classical ground state is only two-fold degenerate.

Numerical studies on the spin-$\frac{1}{2}$ Heisenberg triangular antiferromagnet indicate significantly renormalized magnetic moments, attesting to strong quantum fluctuations [63, 64]. This suggests that the addition of a moderate perturbation may drive the ground state of this model a spin liquid. Hence, the persistence of interest in this model as a potential candidate for realizing a spin-liquid state. Various extensions of the spin-$\frac{1}{2}$ Heisenberg triangular antiferromagnet have been considered. In particular, easy-plane anisotropy [88, 89], the addition of ring-exchange terms [90, 91, 92, 93, 94], which is relevant to organic Mott insulators κ-(BEDT-TTF)$_2$Cu$_2$(CN)$_3$ and κ-(BEDT-TTF)$_2$Cu$_2$[N(CN)$_2$]Cl, and spatial anisotropy. Here we focus on the spatial anisotropy, which is largely motivated by its relevance to the layered inorganic Mott insulators Cs$_2$CuCl$_4$ and Cs$_2$CuBr$_4$. In the remainder of this chapter, we use the term "Heisenberg Hamiltonian" to refer to the nearest-neighbor isotropic Heisenberg Hamiltonian.

[3] Recently there have been several studies on so-called *Heisenberg-Kitaev* models. See, for example, Refs. [79, 80, 81] and references therein.

2.1.1 Motivation from Experiments

Cs_2CuCl_4, an inorganic layered magnetic salt, is a perfect realization of the spin-$\frac{1}{2}$ HAF model on an anisotropic triangular lattice (see Figs. [2.1,2.2]) [95, 96, 97]. As shown in Fig. [2.2], the Cu^{2+} ions, which carry spin-$\frac{1}{2}$ and are responsible for the magnetic properties of this material, are organized in a staggered stack of triangular layers. The spin Hamiltonian of this material was accurately determined experimentally by applying a strong magnetic field, which polarizes the spins and results in a ferromagnetic texture, and studying the spectrum of its magnons using neutron scattering [98]. It was found that the triangular layers in Cs_2CuCl_4 are weakly magnetically coupled with the interlayer exchange $J'' = 0.045(5)\, J$. Within the triangular layers, the interchain exchange $J' = 0.34(3)\, J$ and the intrachain exchange $J = 0.374(5)\,\text{meV}$. Also there is a weak Dzyaloshinskii-Moriya interaction [58] present in this material, with a $\mathbf{D}$-vector of the magnitude $|\mathbf{D}| = 0.053(5)\, J$ and perpendicular to the triangular layers. Cs_2CuCl_4 exhibits an incommensurate long-range ordered state below the Néel temperature $T_N = 0.62(1)\,\text{K}$. Since it seems that the role of the interlayer couplings is solely to stabilize the ordered state below T_N, the ground state of this material is expected to be accurately described by the following two-dimensional Hamiltonian [54]:

$$\begin{aligned}\mathcal{H} = & J \sum_{x,y} \mathbf{S}_{x,y} \cdot \mathbf{S}_{x+1,y} + J' \sum_{x,y} \mathbf{S}_{x,y} \cdot \mathbf{S}_{x,y+1} + \mathbf{S}_{i,y} \cdot \mathbf{S}_{x\mp1,y+1} + \\ & \pm \sum_{x,y} \mathbf{D} \cdot \left[\mathbf{S}_{x,y} \times \left(\mathbf{S}_{x,y+1} \mp \mathbf{S}_{x\mp1,y+1} \right) \right], \end{aligned} \tag{2.1}$$

where x labels sites on the chains, y labels the chains and the $\mathbf{D}$-vector is along the $\mathbf{a}$-direction (perpendicular to the triangular layers – see Figs. [2.1,2.2]). The choice of sign in the above lattice Hamiltonian depends on y: when y is even the top sign should be used and when odd the bottom sign. This is due to the staggered labelling convention we use for sites on the chains as shown in Fig. [2.9]. For a similar reason, the sign of the $\mathbf{D}$-vector alternates between even and odd layers due to the adjacent layers being shifted with respect to each another as shown in Fig. [2.2].

As mentioned above, experiments indicate that Cs_2CuCl_4 develops incommensurate spiral order (see Fig. [2.3b]) below the Néel temperature $T_N = 0.62(1)\, K$. Such a state is characterized by a $\mathbf{Q}$-vector. For Cs_2CuCl_4, it was found that $\mathbf{Q} = (0.5+\epsilon_0)\mathbf{b}^*$ ($\mathbf{b}^*$ is the reciprocal vector corresponding to the lattice vector $\mathbf{b}$), where $\epsilon_0/\epsilon_{\text{classical}} = 0.56(2)$ [53]. This significantly renormalized ϵ_0 compared to that of its classical ground state ($\mathbf{Q}_{\text{classical}} = \pi + 2\sin^{-1}(J'/2J)$ thus $\epsilon_{\text{classical}} = \frac{1}{\pi}\sin^{-1}(J'/2J)$) indicates strong quantum fluctuations. This significantly renormalized ϵ_0, nevertheless, seems to be in agreement with zero-temperature linked-cluster series expansion studies [99, 100]. Note that, in Cs_2CuCl_4 spins in the spiral state lie in the $\mathbf{bc}$-plane, as depicted in Fig. [2.3b], due to the weak DM interaction.

Low-energy excitations in magnetic systems that exhibit long-range order are *spin-waves* or *magnons*, which are the Goldstone bosons associated with the spontaneously

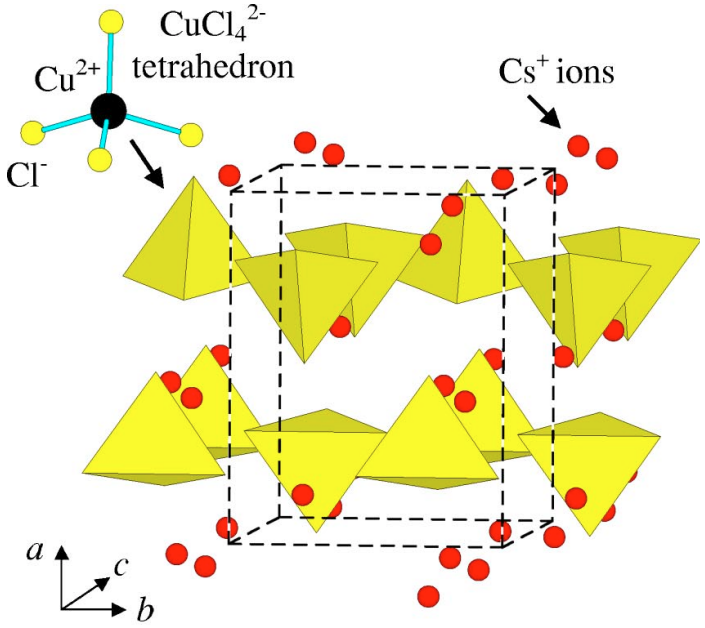

Figure 2.1: Crystal structure of Cs_2CuCl_4. Cu^{2+} ions with spin-$\frac{1}{2}$ are responsible for the magnetic properties of this material. The lattice parameters (at 0.3 K) are as follows: $a = 9.65$ Å, $b = 7.48$ Å and $c = 12.26$ Å. (Reproduced from [54]).

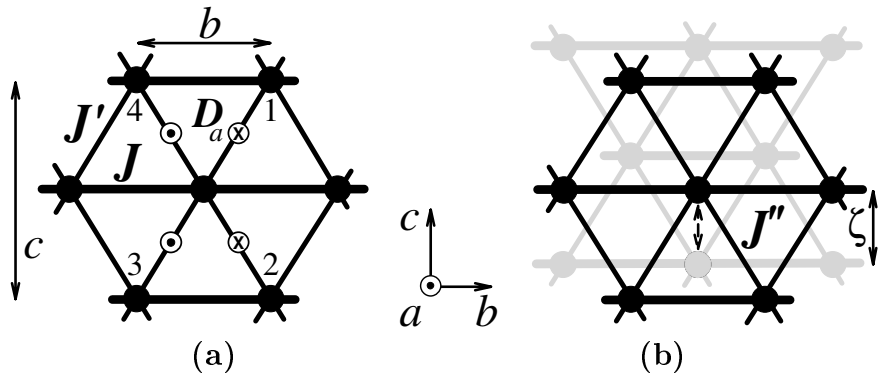

Figure 2.2: (a) Intra- and interchain couplings within a single layer of Cs_2CuCl_4, together with the Dzyaloshinskii-Moriya (DM) interaction. (b) The orientation of two adjacent layers in Cs_2CuCl_4. The D-vector of the DM interaction is perpendicular to the triangular layers (along the **a** direction). The sing of the coupling of the DM interaction in relation to the central spin in the above figure is indicated with $\otimes$ and $\odot$. (Reproduced from [98]).

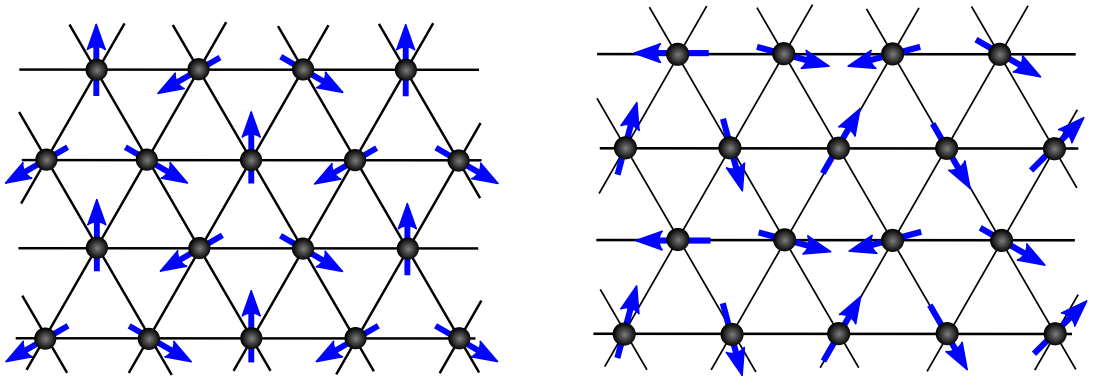

Figure 2.3: Commensurate (a) and incommensurate (b) spiral spin textures.

broken rotational symmetry of the Hamiltonian [45]. Thus, one expects sharp peaks in the magnetic dynamical structure factor of such quantum magnets, which can be determined in inelastic neutron scattering experiments [68]. For Cs_2CuCl_4, inelastic neutron scattering studies found broad peaks instead of sharp peaks with tails that persist to fairly high energies [53, 54]. Such broad peaks are reminiscent of spinon excitations in one-dimensional Heisenberg antiferromagnetic chains [101, 102, 103, 104, 105], with the exception that experiments indicated that the observed continua disperse in both spatial directions within the **bc**-plane, while being non-dispersive along the **a**-direction (perpendicular to the the triangular layers). This feature was found to persist even above the transition temperature T_N, as shown in Fig. [2.5]. These observations were taken as evidence for Cs_2CuCl_4 being in close proximity to a quantum phase transition from an incommensurate spiral state to a two-dimensional spin-liquid state [54]. This proposal rekindled interest in the phase diagram of the spin-$\frac{1}{2}$ HAF model on a spatially anisotropic triangular lattice, and triggered a surge of numerical and theoretical studies to explain the experimental observations.

2.1.2 Previous Theoretical and Numerical Studies

The problem of spatially anisotropic HAF model on a triangular lattice has been extensively studied using various analytical and numerical approaches. However, due to discrepancies between the results from different studies, there seems to be no consensus on the phase diagram of this model except in the vicinity of the isotropic point ($J' \simeq J$). Nonetheless, as explained below, careful unbiased numerical [106, 100] and analytical [59, 56] studies in recent years strongly suggest the presence of incommensurate spiral ordering over most of the phase diagram with possibly a CAF state at sufficiently large anisotropies.

Motivated by the proposal in Ref. [54] that Cs_2CuCl_4 might be in close proximity

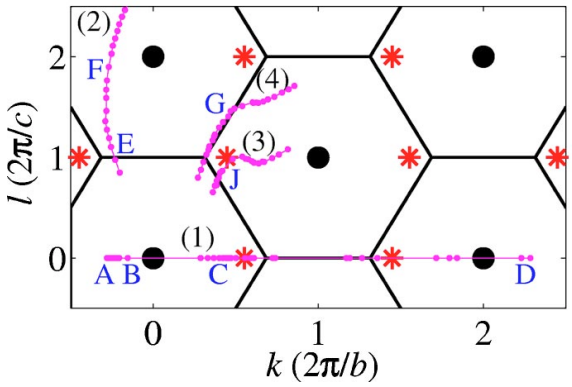

Figure 2.4: Directions along which the dispersion of the magnetic excitations were measured in the reciprocal space. The magenta dots along the curves (1)-(4) are the measurement points. (Reproduced from [98]).

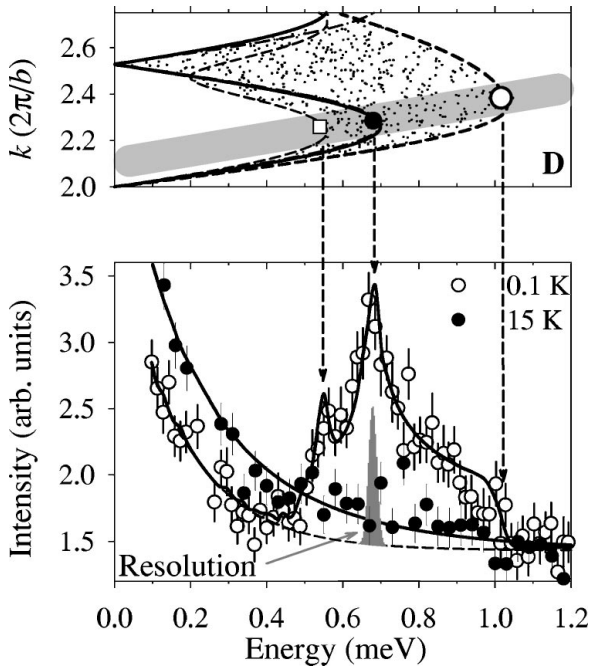

Figure 2.5: Magnetic excitations above (filled circles) and below (empty circles) T_N. The solid and dashed curves are fits to the data points. The resolution of the measurments are indicated by the gray peak. (Reproduced from [98]).

to a quantum phase transition to a spin-liquid state, several studies [88, 89, 107, 108, 109, 110, 111, 112, 113] suggested that the incommensurate spiral state near the isotropic point ($J'/J \lesssim 1$) is destroyed by quantum fluctuations and is replaced by a quantum-disordered state as J'/J is reduced (see Fig. [2.6]). Some of these studies estimated the transition point to a quantum-disordered state to be as large as $J'/J \approx 0.9$. A brief summary of these studies is provided below.

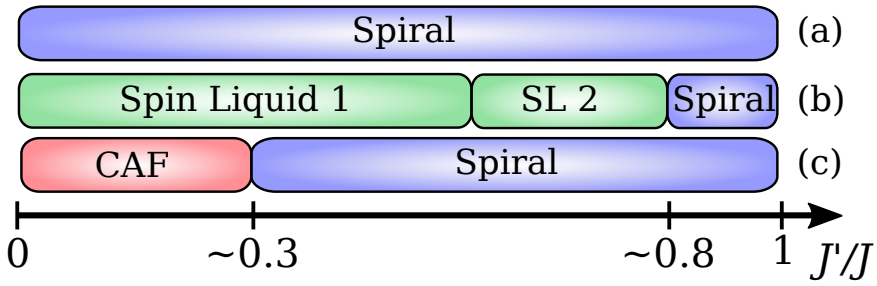

Figure 2.6: A comparison of various suggested phase diagrams for the spin-$\frac{1}{2}$ HAF model on an anisotropic triangular lattice. (a) Incommensurate spiral order with renormalized **Q**-vector throughout the phase diagram suggested in Ref. [100]. (b) The phase diagram suggested by Refs. [109, 110, 111, 112, 113] with two spin-liquid states indicated by 1 and 2. (c) The phase diagram based on the RG studies [56, 59] where a collinear antiferromagnetic (CAF) state appears at strong anisotropies.

Chung *et al.* [107], examined the large-N limit of the Heisenberg and Hubbard models on an anisotropic triangular lattice. For the Heisenberg model, they used a bosonic representation for spins. This bosonic representation is then generalized to a $Sp(N)$ (symplectic) form, which they treated in the large-N limit using a saddle-point approximation. This approach had been developed earlier in Refs. [114, 115] for non-bipartite lattices instead of the $SU(N)$ extension that is appropriate for bipartite lattices. The case $N = 1$ is expected to reduce to the original spin-$\frac{1}{2}$ Heisenberg model, as $Sp(1) \cong SU(2)$. From their saddle-point analysis, they concluded the presence of two phases in the phase diagram in the interval $0 \leq J'/J \leq 1$ for the $N = 1$ (spin-$\frac{1}{2}$) case: an incommensurate long-range ordered state that terminates at $J'/J \simeq 0.128$, followed by a phase where the chains are decoupled.

Isakov *et al.*, [108] studied the quantum phase transition between an incommensurate spiral state and a $\mathbb{Z}_2$ spin-liquid state with bosonic spin-$\frac{1}{2}$ spinons and gapped $\mathbb{Z}_2$ vortices (visons). Since the visons are gapped throughout this quantum phase transition, a direct continuous phase transition from the spin-liquid state to the spiral state is possible via the condensation of the bosonic spinons. The critical point of such a transition is in the universality class of the classical $\mathcal{O}(4)$ model in three dimensions. They obtained a large anomalous exponent ($\eta \approx 1.37$) for the spin-spin correlation function, $\langle \mathbf{S}(-\mathbf{q},\omega) \cdot \mathbf{S}(\mathbf{q},\omega) \rangle \sim \frac{1}{(\omega^2 - k^2)^{1-\eta/2}}$ ($\mathbf{k} = \mathbf{q} - \mathbf{Q}_{\text{spiral}}$), at the critical point.

They argued that their findings are qualitatively consistent with the experimental observation of broad tails in the inelastic neutron scattering spectrum of Cs_2CuCl_4.

Another possible scenario for the destruction of the spiral state and the appearance of a quantum disordered state is a quantum phase transition to a valence-bond solid. This possibility, although for a square lattice with next-nearest-neighbor antiferromagnetic couplings, which is also frustrated, was examined by Bhattacharjee [116]. Such a quantum phase transition would be a "Landau-forbidden" quantum phase transition, as the two phases on both sides of the phase transition break different symmetries of the Hamiltonian (a spiral state breaks the rotational symmetry, while a valence-bond-solid state breaks the lattice transnational symmetry). In contrast to the aforementioned quantum phase transition from a spiral state to a $\mathbf{Z}_2$ spin-liquid state examined by Isakov *et al.* [108], in this quantum phase transition to a valence-bond-solid state, visons are not gapped and play an important role.

Alicea *et al.*, [88, 89] studied this problem using a fermionized vortex approach. This approach applies to both isotropic (XXX) and anisotropic Heisenberg (XXZ) models. The Heisenberg Hamiltonian is regarded as a quantum rotor model ($S^+ \to e^{i\hat{\phi}}$ and $S^z \to \hat{n} - \frac{1}{2}$) with an on-site repulsion term that imposes the hard-core constraint ($\hat{n} = 0, 1$) at each site by energetically penalizing higher occupations (a softened hard-core constraint). Then, using the well-known duality between the XY model and an Abelian $U(1)$ superconductor in two dimensions [117], this quantum rotor model on an anisotropic triangular lattice is mapped to an Abelian $U(1)$ gauge field on the dual lattice (a honeycomb lattice). Finally, using a Chern-Simons flux attachment procedure, the vortices are fermionized (regarded as fermions with flux quanta attached to them). Within a mean-field approach similar to those used in the study of fractional quantum Hall systems, the flux quanta are smeared and treated as a background magnetic field. Solving the resultant free-fermion problem, they found a critical spin-liquid state.

Weng *et al.* [109] examined this problem using exact diagonalization (ED), and density matrix renormalization group (DMRG) on small systems (6×6, 4×4 and 6×4 using ED, and 6×18 and 8×18 using DMRG). They concluded that a spin-liquid state exists in the strong anisotropy limit that persists up to $J'/J \simeq 0.78$.

Yunoki *et al.* [110], using a variational wave-function approach, with Monte Carlo simulations for determining optimal variational parameters, found two spin-liquid states in the phase diagram of this model: a gapless spin liquid at large anisotropies ($J'/J \lesssim 0.65$) and a gapped spin liquid in the parameter range $0.65 \lesssim J'/J \lesssim 0.8$.

Hauke *et al.* [111] studied the ground state of this model using the modified spin-wave theory in Ref. [118], where it is assumed that the sublattice magnetization is zero, together with an ordering vector optimization step. They arrived at a phase diagram very similar to that of Yunoki *et al.* [110].

Heidarian *et al.* [112], using a variational Monte Carlo approach together with the Lanczos (ED) method on a 6×6 cluster, arrived at the same conclusion as Yunoki *et al.* and Hauke *et al.*: a 1D spin liquid for $J'/J \lesssim 0.6$, a 2D spin liquid for

$0.6 \lesssim J'/J \lesssim 0.85$ and finally the long-range ordered state for $0.85 \lesssim J'/J \leq 1$.

Reuther *et al.* [113] used a functional renormalization group approach to compute the magnetic susceptibility and suggested a first-order phase transition at $J'/J \simeq 0.9$ to a quantum-disordered state.

In spite of the above studies that all suggest that the long-range magnetic order is destroyed by quantum fluctuations (see Fig. [2.6]), several other numerical and analytical studies have suggested a different scenario that does not involve any quantum-disordered state. In particular, some of these studies examined the possibility of a transition from an incommensurate spiral state, with highly renormalized **Q**-vector due to quantum fluctuations, to a *collinear antiferromagnetic* (CAF) state at a small J'/J [56, 59, 100, 106, 119]. Schematics of the spiral and CAF states can be seen in Fig. [2.8].

Bocquet *et al.* [120], studied the finite-temperature dynamical response of a this model in the strong anisotropy limit, where it is quasi-one-dimensional. The finite-temperature dynamical response function was obtained by starting with the finite-temperature dynamical susceptibility of decoupled chains and taking into account the effect of interchain couplings within the random phase approximation (RPA). They found a weak instability to an incommensurate long-range ordered state by starting from a high-temperature disordered state.

Dalidovich *et al.* [121] showed that a rather conventional anharmonic spin-wave theory can qualitatively account for the experimental observations as well as that large renormalization in the magnetic moments and the **Q**-vector of the long-range ordered state. A similar result was found by Veillette *et al.* [122].

Starykh *et al.* [56] examined this model at strong anisotropies using the same RG scheme as the one employed here, and suggested a collinear antiferromagnetic state at strong anisotropies. They argued that the dominant interchain coupling is a second-nearest-chain Néel coupling, generated by quantum fluctuations of order $(J'/J)^4$. This interchain term couples second-nearest chains antiferromagnetically, which via the order-by-disorder mechanism stabilizes the CAF state. In contrast, in [59] intense competition between the CAF and incommensurate spiral states, and also ferromagnetic fluctuations of order $(J'/J)^2$ were found, which will be explained in detail in the following sections.

Pardini *et al.* [100], motivated by the proposed CAF state of Starykh and Balents [56] at strong anisotropies, studied magnetic ordered states in this model using linked-cluster series expansions at zero temperature in this model. They compared the energies of the CAF state and the incommensurate spiral state (with a variational **Q**-vector), and found that the CAF state has a slightly higher energy than the spiral state ($J' = 0.1J$ was the smallest non-zero J' value they could access due to the convergence of the series expansions). However, the difference between the energies of the two states was small, and they concluded that both phases can be stabilized.

Weichselbaum *et al.* [106] examined large two-dimensional patches using the DMRG approach for $0.5 \lesssim J'/J \leq 1$. To avoid frustrating the spiral correlations, they used

a cylindrical geometry, where the boundary conditions are periodic in the direction perpendicular to the chains and open in the direction along the chains. To further minimize the finite-size effects, they used a pinning magnetic field on one of the open ends of the cylinder, and exponentially suppressed the couplings near the other end. The pinning field allows for conveniently determining the spin-spin correlations by measuring the induced local moments $\langle \mathbf{S}_i \rangle$. They observed an even-odd effect depending on whether the width of the patch was $4n$ or $4n+2$ chains, which seemed to disappear with increasing n. Specifically, they observed only incommensurate spiral correlations for all systems they studied, with no sign of any collinear state at J'/J values down to 0.5, and found the $\mathbf{Q}$-vector of the form $c_1(\frac{J'}{J})^2\, e^{-c_2\frac{J'}{J}}$ best fits the observed spiral correlations.

Harada [123], using a tensor network approach, supplemented with an entanglement renormalization (ER) step, was able to explore large system sizes: $N = 144$ with one ER level and $N = 2166$ with two ER levels for $0.7 \leq J'/J < 1$. He found a stable incommensurate spiral state in contrast with most studies that suggested a transition to a spin-liquid state at $J'/J \approx 0.8$.

Thesberg *et al.* [119] studied finite-size systems with twisted boundary conditions using ED. The twisted boundary condition allows for accommodating spiral states with wavelengths much larger than the systems sizes that can be handled using ED. Interestingly, their analysis seems to be in good agreement with the DMRG study of Weichselbaum *et al.* [106]. The result of their analysis suggests a phase transition between a long-range spiral phase and a subtle phase with only short-range spiral correlations. Also, they observed close competition between ferromagnetic and antiferromagnetic correlations between second-nearest chains.

In another study, Thesberg and Sorensen [124] examined the phase diagram of the generalized version of this Heisenberg antiferromagnetic triangular model where next-nearest-neighbor couplings along the chains are present (the J_1-J_2-J' model). This study indicated good agreement with the picture expected based on the RG analysis (see Ref. [56]). This case, although different from the model discussed here, is expected to provide an indirect test of the RG predictions. The continuum limit of a J_1-J_2 spin-$\frac{1}{2}$ antiferromagnetic chain for $J_2/J_1 \lesssim 0.24$ is the same as that of a nearest-neighbor spin-$\frac{1}{2}$ antiferromagnetic chain except with $|\gamma_{bs}| < 0.23$ (see the next section). Based on the discussion in the next section and Ref. [56], the J_1-J_2-J' model in the strong anisotropy limit is expected to exhibit a dimer state sufficiently close to $J_2/J_1 = 0.24$. Note that, in comparison with the RG analysis in Ref. [56], the presented RG analysis indicates in this chapter indicates that this model is slightly more resistant to dimer states as $J_2/J_1 \to 0.24$ is approached. This is due to the g_N^2 term in the β-function of γ_{bs} in Eq. (2.8a), which will be discussed in the next section.

The results obtained in careful numerical studies of [100, 106], as well as the RG analyses in [56, 59] are hard to refute. However, if there is no transition to a spin-liquid state, then how can one explain the results of inelastic neutron scattering experiments [53, 54] on Cs_2CuCl_4 that suggest spinons propagating in both spatial

directions? A convincing answer to this question was provided by Kohno *et al.* [125]. They showed that the dynamical structure factor $S(\mathbf{q}, \omega)$, computed within a two-spinon approximation (truncating the Fock space of 1D spin-$\frac{1}{2}$ chains to two-spinon excitations) and taking into account the interchain couplings perturbatively, can account for the experimentally observed continuum being dispersive in both spatial directions. This should be contrasted with some of previous anharmonic spin-wave studies that were able to qualitatively account for the observed continuum. The approximate structure factor, computed within this two-spinon approximation, quantitatively explains the experimental observations without any fitting parameters and only using the experimentally measured exchanges J and J'. Based on this, Kohno *et al.* argued that the observed continuum in the neutron scattering spectrum of Cs_2CuCl_4 is due to the descendants of 1D spinons, and the naive expectation that 1D spinions solely disperse in one direction (only along the chains) was erroneous. Two spinons can hop from one chain to another, which results in dispersion in the direction perpendicular to the chains.

The RG analysis of Starykh and Balents [56], which suggests a CAF state at strong anisotropies, only indicates antiferromagnetic correlations between spins on second-nearest chains on all length scales. This is somewhat puzzling as finite-size systems [59, 106] only exhibit ferromagnetic correlations between second-nearest chains. As shown in Figs. [2.7,2.8], ferromagnetic correlations are compatible with a spiral state, whereas in a CAF spin texture antiferromagnetic correlations are expected. This discrepancy was resolved in [59], which is explained in detail in the remainder of this chapter.

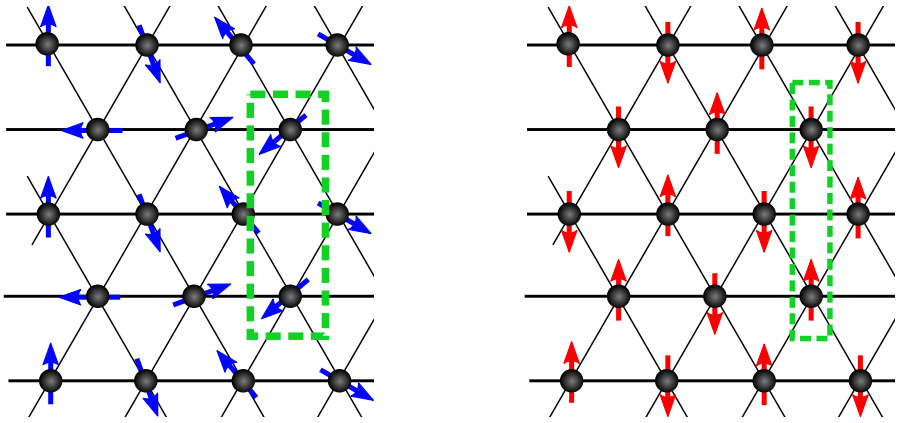

(a) Incommensurate Spiral **(b)** CAF

Figure 2.7: (a) Ferromagnetic correlations between second-neighbor chains in a spiral spin texture. (b) Antiferromagnetic correlations in a CAF configuration.

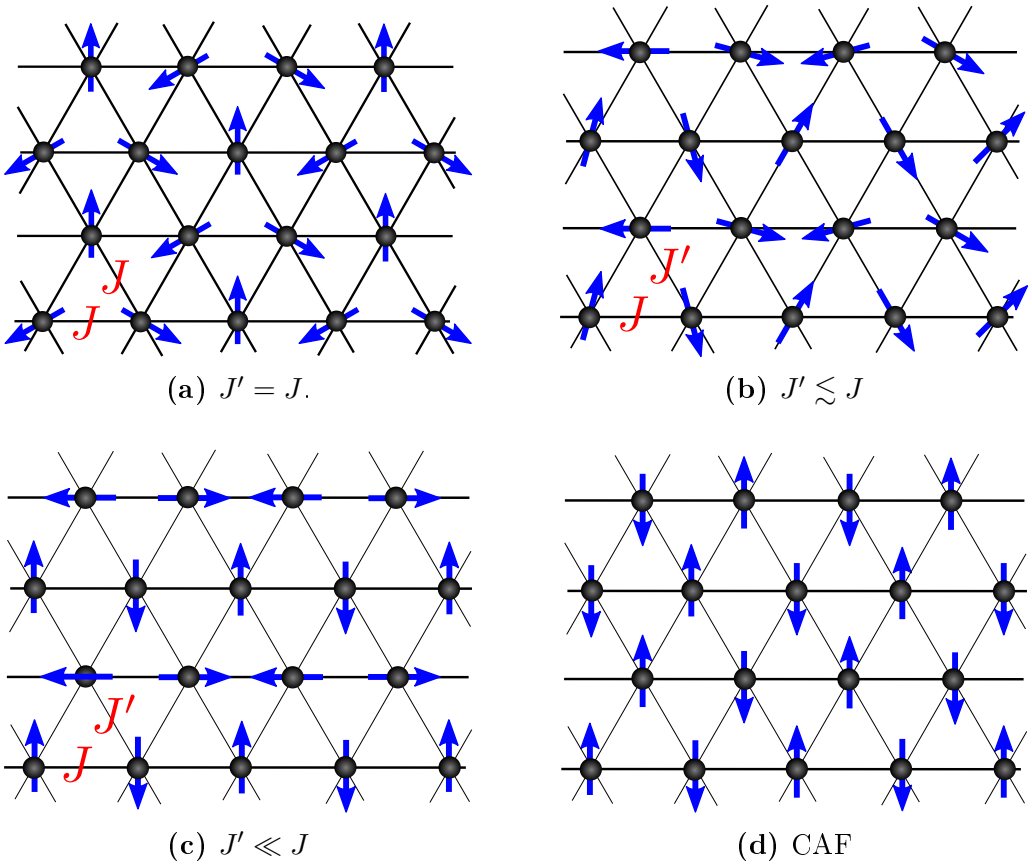

(a) $J' = J$. **(b)** $J' \lesssim J$

(c) $J' \ll J$ **(d)** CAF

Figure 2.8: (a) Commensurate spiral state (120° phase). (b) Incommensurate spiral state for $J' \lesssim J$. (c) Incommensurate spiral state with $\mathbf{Q} \approx \pi$. (d) Collinear antiferromagnetic state (CAF).

2.2 Continuum Model and RG Analysis

In this section we present the details of the RG analysis for spin-$\frac{1}{2}$ HAF model on an anisotropic triangular lattice at strong anisotropies. Employing a one-dimensional RG scheme appropriate for antiferromagnetic spin-$\frac{1}{2}$ chains, we perturbatively determine the running of interchain couplings as the short-distance cutoff of the problem is increased. Since in this RG approach interchain couplings are treated perturbatively, the obtained β-functions can be relied on only up to a length scale L^* where any of the interchain couplings reaches unity (in the units of the intrachain exchange coupling J) and the quasi-one-dimensional picture no longer holds. For the purpose of this one-dimensional RG approach, it is the continuum limit of the chains that is needed and not the full continuum limit in both spatial directions. Thus, the desired continuum Hamiltonian is obtained from the continuum limit of a collection of decoupled spin-$\frac{1}{2}$ chains together with a set of interchain couplings compatible with the symmetries of the lattice Hamiltonian. In this section, we only focus on the Heisenberg part of the Hamiltonian in Eq. (2.1), and postpone the discussion of the effect of a weak DM interaction to Section. [2.4].

The symmetries of the lattice Heisenberg Hamiltonian,

$$\mathcal{H}_{\rm H} = J\sum_{x,y}\mathbf{S}_{x,y}\cdot\mathbf{S}_{x+1,y} + J'\sum_{x,y}\mathbf{S}_{x,y}\cdot\mathbf{S}_{x,y+1} + \mathbf{S}_{i,y}\cdot\mathbf{S}_{x\mp1,y+1}\,, \tag{2.2}$$

determine what interchain couplings are allowed in the continuum limit of this model. The relevant symmetries here are lattice translational symmetry, invariance under a global $SU(2)$ rotation and invariance under reflections with respect to planes perpendicular to the chains as shown in Fig. [2.9]. Note that, a Néel spin configuration or a nearest-neighbor dimer state is odd under a reflection that maps even and odd sites to each other. As shown in Fig. [2.9], under a reflection whose plane intersect a chain at a site, even sites are mapped onto even sites and odd sites to odd sites, whereas when the reflection plane intersects a chain at the centre of a bond, even and odd sites are mapped to each other.

The continuum limit of an antiferromagnetic spin-$\frac{1}{2}$ chain can be described by the $SU(2)_{k=1}$ *Wess-Zumino-Novikov-Witten* (WZNW) model perturbed by a backscattering term (see Appendix [A.1] for more details). Since $J'/J \ll 1$, the leading ($\mathcal{O}(J'/J)$) continuum interchain couplings are the direct descendants of the couplings present in the lattice Hamiltonian in Eq. (2.2). Using the approximation,

$$\mathbf{S}_{x,y} \to \mathbf{M}_y(x) + (-1)^x\mathbf{N}_y(x)\,, \tag{2.3}$$

where $\mathbf{M}_y(x)$ is the uniform magnetization and $\mathbf{N}_y$ the staggered (Néel) magnetiza-

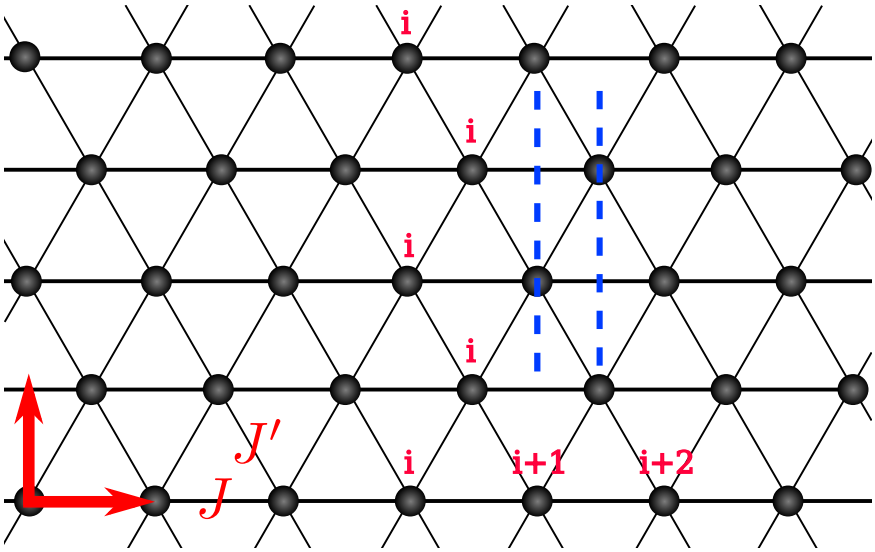

Figure 2.9: Our convention for labelling sites in the y-direction is shown. The dashed blue lines indicate the intersections of two reflection planes with the lattice. Under a reflection with respect to a plane that intersects a chain at a site, even sites are mapped to even sites and odd sites are mapped to odd sites. In contrast, when the reflection plane intersects a chain at the centre of a bond, even sites are mapped to odd sites and vice versa.

tion, we obtain:

$$\begin{aligned}
\mathcal{H}_{\text{Continuum}} &= \mathcal{H}_{\text{Intra}} + \mathcal{H}_{\text{Inter}} \qquad (2.4)\\
\mathcal{H}_{\text{Intra}} &= \sum_y \left\{ \mathcal{H}_y^{\text{WZNW}} + \gamma_{bs} \int \mathrm{d}x\, \mathbf{J}_{L,y}(x) \cdot \mathbf{J}_{R,y}(x) \right\} \\
\mathcal{H}_{\text{Inter}} &= \sum_y \Big\{ \gamma_M \int \mathrm{d}x\, \mathbf{M}_y(x) \cdot \mathbf{M}_{y+1}(x) + \\
&\qquad \gamma_{tw} \frac{(-1)^y}{2} \int \mathrm{d}x \left(\mathbf{N}_y(x) \cdot \partial_x \mathbf{N}_{y+1}(x) - (\partial_x \mathbf{N}_j(x)) \cdot \mathbf{N}_{y+1}(x) \right) + \\
&\qquad \mathcal{O}(J'/J)^2 \Big\},
\end{aligned}$$

Note that $\mathbf{M}$ and $\mathbf{N}$ do not couple with each other due to the rapidly oscillating factor $(-1)^x$ in the above continuum approximation for a single spin operator. This continuum Hamiltonian is valid at length scales larger than a shortest length L_0, which is larger but comparable to the lattice spacing a_0. Here, $\mathbf{J}_L$ ($\mathbf{J}_R$) is the left-(right-) moving current operator (see Appendix [A.1] and Eq. (2.5) below). The coupling constant of the backscattering term, $\gamma_{bs} = -0.23$, which was determined using ED on finite spin-$\frac{1}{2}$ antiferromagnetic chains in [126]. The uniform magnetization operator is given in terms of the chiral current operators as $\mathbf{M} = \mathbf{J}_L + \mathbf{J}_R$. The term in the last line with the coupling γ_{tw} is a twist term, and promotes spiral ordering.

The geometric frustration of the lattice Hamiltonian is dictated on the continuum Hamiltonian by the aforementioned symmetries. These symmetries prevent a direct coupling between Néel magnetization operators (as well as dimerization operators ε) on adjacent chains, and on n^{th}-nearest chains for any odd n. Thus, direct Néel (and ε) coupling between n^{th}-nearest chains for any even n, and, in particular, second-nearest chains are not prohibited and can get generated in the course of RG.

As in any RG analysis, we should include all relevant and marginal terms (as well as any dangerously irrelevant term) compatible with the symmetries of this model. For this purpose, we need to determine the scaling dimension of various operators in the continuum description. Since the fixed-point theory that we perform our perturbative RG analysis with respect to is a conformal field theory (CFT), the scaling dimensions of various operators can be easily obtained. The $SU(2)_{k=1}$ WZNW theory is defined in terms of a $SU(2)$ matrix field g with the conformal scaling dimension $\frac{1}{2}$ [127, 128]. The chiral currents and the Néel magnetization operator are expressed in terms of

this matrix field as follows (see Appendix [A.1]):

$$\mathbf{J}_L = \frac{1}{4\pi}\mathrm{Tr}\{\boldsymbol{\sigma} g^{-1}\partial_{\bar{z}} g\} \tag{2.5a}$$

$$\mathbf{J}_R = \frac{1}{4\pi}\mathrm{Tr}\{\boldsymbol{\sigma} g^{-1}\partial_{z} g\} \tag{2.5b}$$

$$\mathbf{N} = \mathrm{Tr}\{g\boldsymbol{\sigma}\} \tag{2.5c}$$

$$\varepsilon = \mathrm{Tr}\{g\} \tag{2.5d}$$

Here z and $\bar{z}$ and the so-called light-cone coordinates. The operator ε in the last line is the dimerization operator. We see that both $\mathbf{N}$ and ε have the scaling dimension $\frac{1}{2}$. The scaling dimension of the chiral currents is 1. From the scaling dimensions of these operators we can determine the scaling dimensions of interchain couplings.

The interchain coupling terms $\mathbf{N}_y \cdot \mathbf{N}_{y+2n}$ and $\varepsilon_y\, \varepsilon_{y+2n}$ for $n \geq 1$ have the scaling dimension 1, and, therefore, are relevant. In fact these are the only relevant terms in the RG analysis. The presence of spatial derivative in the twist term in Eq. (2.4) (as well as its dimerization analog and their farther-neighbor versions) increases the scaling dimension by 1, and, therefore, the twist term is marginal. Any bilinear of chiral currents has the scaling dimension 2, and, thus, is marginal (here the upper critical dimension $d_{\mathrm{u.c.}} = 2$).

Note that, although there are an infinite number of relevant and marginal interchain couplings in this model (as there are an infinite number of chains), the RG analysis can be restricted to only those that couple nearby chains. The reason for this is that almost all of such terms (except for the interchain terms in Eq. (2.4)) are originally absent in the microscopic Hamiltonian, and will be generated by quantum fluctuations. For this reason, in the strong anisotropy limit ($J'/J \ll 1$), the coupling constants of nearest and second-nearest interchain terms are expected to be much larger than their farther-neighbor counterparts at L_0. The only marginal and relevant interchain couplings included in the RG analysis, in addition to those in Eq. (2.4) are:

$$g_N \int \mathrm{d}x\, \mathbf{N}_y(x) \cdot \mathbf{N}_{y+2}(x) \tag{2.6a}$$

$$g_\varepsilon \int \mathrm{d}x\, \varepsilon_y(x)\varepsilon_{y+2}(x) \tag{2.6b}$$

$$\gamma_\varepsilon \frac{(-1)^y}{2} \int \mathrm{d}x \left(\varepsilon_y(x)\partial_x\varepsilon_{y+1}(x) - \varepsilon_{y+1}(x)\partial_x\varepsilon_y(x)\right) \tag{2.6c}$$

$$g_M \int \mathrm{d}x\, \mathbf{M}_y(x) \cdot \mathbf{M}_{y+2}(x)\,. \tag{2.6d}$$

In addition to the above terms, we also include two irrelevant interchain couplings:

$$\zeta_N \int \mathrm{d}x\, \partial_x \mathbf{N}_y(x) \cdot \partial_x \mathbf{N}_{y+2}(x) \tag{2.6e}$$

$$\zeta_M \int \mathrm{d}x \left[\mathbf{J}_{L,y+1}(x) \cdot \mathbf{J}_{R,y+1}(x)\right] \left[\mathbf{M}_y(x) \cdot \mathbf{M}_{y+2}(x)\right]. \tag{2.6f}$$

The reason for including these two irrelevant terms, as we will see, is that ζ_N, together with g_M, enters in the β-functions of g_N and g_ε, and ζ_M generates g_M.

Before proceding to the RG analysis, let us explain an important point regarding the form of the twist term in the continuum Hamiltonian in Eq. (2.6c) that distinguishes our RG analysis from [56]. The couplings between the Néel operators on nearest chains with the couplings constant γ_{tw} (as well as its farther chain analogs and similar interchain couplings with ε operator instead of $\mathbf{N}$ – all referred to as twist terms) can be reduced to $\gamma_{tw}\,(-1)^y \int \mathrm{d}x\, \mathbf{N}_y(x) \cdot \partial_x \mathbf{N}_{y+1}(x)$ only when the boundary conditions in the x-direction are periodic. As will be discussed in the next section, this can be observed in numerical studies on finite-size systems. The form adopted here for such twist terms is the same as the one in Ref. [129].

We start the RG analysis with the two relevant couplings g_N and g_ε. When the relevant coupling g_N dominates, depending on its sign, second-nearest chains are either ferromagnetically ($g_N < 0$) or antiferromagnetically ($g_N > 0$) coupled. Similarly, a dominant g_ε, depending on its sign, induces either a columnar or staggered dimer state, as depicted in Fig. [2.10].

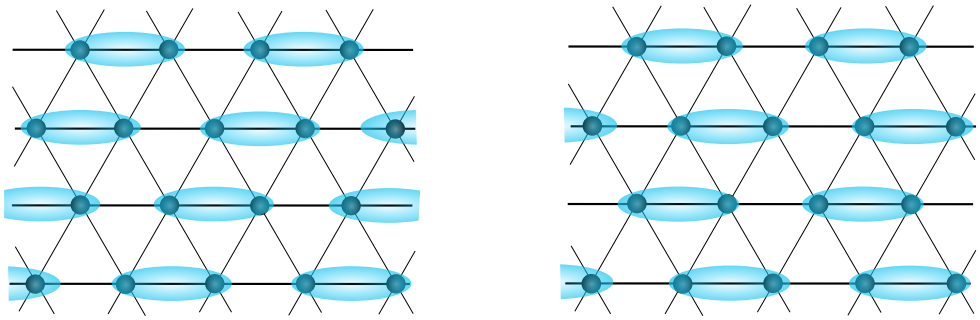

(a) **(b)**

Figure 2.10: (a) Columnar dimer state. (b) Staggered dimer state.

In this real-space RG, the running of couplings is generated by increasing the short-distance cutoff of the theory and integrating out the short-distance modes. Since the fixed-point theory is a CFT, we do not explicitly integrate out short-distance modes and directly use the available n-point functions of the fixed-point theory. For this purpose, we need the *operator product expansions* (OPEs) of various operators in this RG. The derivation of the OPEs are presented in Appendix [A.2]. The OPEs are as

follows:

$$\mathbf{J}_L^a(\bar{z})\,\mathbf{J}_L^b(\bar{w}) \simeq \frac{\delta^{ab}}{8\pi^2(\bar{z}-\bar{w})^2} + \frac{i\epsilon^{abc}}{2\pi(\bar{z}-\bar{w})}J_L^c(\bar{w}) + \mathcal{O}(\bar{z}-\bar{w}) \tag{2.7a}$$

$$\mathbf{J}_R^a(z)\,\mathbf{J}_R^b(w) \simeq \frac{\delta^{ab}}{8\pi^2(z-w)^2} + \frac{i\epsilon^{abc}}{2\pi(z-w)}J_R^c(w) + \mathcal{O}(z-w) \tag{2.7b}$$

$$\mathbf{N}^a(z,\bar{z})\,\mathbf{N}^b(w,\bar{w}) \simeq \frac{\delta^{ab}}{4\pi^2|z-w|^2} + \mathcal{O}(z-z',\bar{z}-\bar{z}') \tag{2.7c}$$

$$\varepsilon(z,\bar{z})\,\varepsilon(z',\bar{z}') \simeq \frac{1}{4\pi^2|z-w|^2} + \mathcal{O}(z-z',\bar{z}-\bar{z}') \tag{2.7d}$$

$$\mathbf{J}_L^a(\bar{z})\,\varepsilon(w,\bar{w}) \simeq \frac{i}{4\pi(\bar{z}-\bar{w})}\mathbf{N}^a(w,\bar{w}) + \mathcal{O}(\bar{z}-\bar{w}) \tag{2.7e}$$

$$\mathbf{J}_R^a(z)\,\varepsilon(w,\bar{w}) \simeq -\frac{i}{4\pi(z-w)}\mathbf{N}^a(w,\bar{w}) + \mathcal{O}(z-w) \tag{2.7f}$$

$$\mathbf{N}^a(z,\bar{z})\,\varepsilon(z',\bar{z}') \simeq 0 + \mathcal{O}(z-z',\bar{z}-\bar{z}') \tag{2.7g}$$

$$\mathbf{J}_L^a(\bar{z})\,\mathbf{N}^b(w,\bar{w}) \simeq \frac{i\delta^{ab}}{4\pi(\bar{z}-\bar{w})}\varepsilon(w,\bar{w}) - \frac{i\epsilon^{abc}}{4\pi(\bar{z}-\bar{w})}\mathbf{N}^c(w,\bar{w}) + \mathcal{O}(\bar{z}-\bar{w}) \tag{2.7h}$$

$$\mathbf{J}_R^a(z)\,\mathbf{N}^b(w,\bar{w}) \simeq -\frac{i\delta^{ab}}{4\pi(z-w)}\varepsilon(w,\bar{w}) - \frac{i\epsilon^{abc}}{4\pi(z-w)}\mathbf{N}^c(w,\bar{w}) + \mathcal{O}(z-w) \tag{2.7i}$$

In this RG, as shown in Appendix. [A.3], using the above OPEs, the one-loop β-functions are derived from the products of the interchain couplings and the backscattering term, which are treated as perturbations to the WZNW term. The one-loop

β-functions are as follows:

$$\partial_l \gamma_{bs} = \gamma_{bs}^2 - 6g_N^2 + 2g_\varepsilon^2 \tag{2.8a}$$

$$\partial_l \gamma_M = \gamma_M^2 \tag{2.8b}$$

$$\partial_l \gamma_{tw} = -\frac{1}{2}\gamma_{bs}\gamma_{tw} + \gamma_M\gamma_{tw} - 3\gamma_{tw}g_N - \frac{1}{2}\gamma_M\gamma_\varepsilon \tag{2.8c}$$

$$\partial_l g_N = g_N - \frac{1}{2}\gamma_{bs}g_N + g_M\zeta_N + \frac{1}{4}\gamma_{tw}^2 + g_M g_N \tag{2.8d}$$

$$\partial_l g_\varepsilon = g_\varepsilon + \frac{3}{2}\gamma_{bs}g_\varepsilon - \frac{3}{2}g_M\zeta_N + \frac{1}{4}\gamma_\varepsilon^2 - \frac{3}{2}g_M g_N \tag{2.8e}$$

$$\partial_l \gamma_\varepsilon = \frac{3}{2}\gamma_{bs}\gamma_\varepsilon - \frac{3}{2}\gamma_{tw}\gamma_M - \frac{3}{2}\gamma_\varepsilon g_\varepsilon \tag{2.8f}$$

$$\partial_l g_M = g_M^2 - \frac{1}{4\pi^2}\gamma_{bs}\zeta_M \tag{2.8g}$$

$$\partial_l \zeta_N = -\zeta_N - \frac{1}{2}\gamma_{bs}\zeta_N - \gamma_{tw}^2 + g_M\zeta_N \tag{2.8h}$$

$$\partial_l \zeta_M = -2\zeta_M - 8\pi^2\gamma_M^2 + \gamma_{bs}\zeta_M \tag{2.8i}$$

Note that we have scaled all couplings by $\pi^2 J$ and $e^\ell = L/L_0$ (ℓ is the RG time and L is the physical length scale). Also irrelevant and relevant couplings are made dimensionless by accompanying them with appropriate powers of the short-distance cutoff (or, alternatively, by setting $L_0 = 1$).

We point out that our β-functions for g_N (Eq. (2.8d)) and g_ε (Eq. (2.8e)) are different from the β-functions of these couplings in the RG analysis of Starykh and Balents [56]. This is the consequence of the form of the twist terms and, in particular, γ_{tw}. Without the γ_{tw}^2 term in the β-function of g_N, this coupling will be of $\mathcal{O}(J'/J)^4$ at the scale L_0 (due to $g_M\,\zeta_N$). As explained below, this extra term in Eq. (2.8d) explains the discrepancy between the RG study of [56] and numerics: $\mathcal{O}(J'/J)^2$ contribution of γ_{tw} does not order the system, rather it is responsible for the ferromagnetic correlations observed in numerical studies on finite-size systems. Another important feature of our β-functions is the g_N^2 term in the β-function of γ_{bs} (Eq. (2.8a)). This term was absent in the RG analysis of [56] as its contribution in their analysis was of $\mathcal{O}(J'/J)^8$. In contrast, here its contribution is of $\mathcal{O}(J'/J)^4$. The g_N^2 term in the β-function of γ_{bs} becomes important when one considers the extension of this problem to the problem of weakly coupled $J_1 - J_2$ chains, near $J_2/J_1 = 0.24$ where γ_{bs} vanishes [126].

Focusing on small J'/J, $\gamma_{tw} = \gamma_M/2 = \frac{J'}{\pi^2 J}$ and $\gamma_{bs} = -0.23$ at L_0, the general analysis of the β-functions is as follows. The couplings g_N and g_ε (Eqs. (2.8d,2.8e)) are the only relevant couplings in the β-functions in [2.8], and, once generated, grow exponential in ℓ (linearly in L/L_0). The marginal couplings γ_{tw}, γ_M, g_M and γ_{bs} grow

linear in ℓ (logarithmic in L/L_0). Note that, due to the negative backscattering term, g_N grows a little faster than g_ε (irrespective of their signs). As discussed in [56], in the case of weakly coupled $J_1 - J_2$ chains at $J_2/J_1 \approx 0.24$, where γ_{bs} vanishes, the system can exhibit a dimer state. Therefore, we conclude that the fate of the this model is determined solely by g_N, which will reach unity at $\ell^* \equiv \ln(L^*/L_0)$ before any other coupling. Thus, the question of the fate of the system described by the Hamiltonian in Eq. (2.2) reduces to the sign of g_N, which in turn determines whether second-nearest chains are coupled ferromagnetically or antiferromagnetically at L^*.

When the initial value of g_N at L_0 is positive, g_N remains positive and flows to $+1$ at ℓ^* while the rest of the couplings remain small. Then, at ℓ^*, the problem becomes similar to the problem of two interpenetrating square lattices coupled to each other by γ_M (γ_{tw} gets suppressed when $g_N > 0$). Via the order-by-disorder mechanism [44, 130, 131], a CAF state is then stabilized. This is the prediction of Starykh and Balents in [56]. They obtained $g_N(0) = -\frac{2}{3} g_\varepsilon(0) = \frac{A_0^x}{\pi^6} (J'/J)^4$ (the normalization factor $A_0^x \approx 0.13$) by integrating out every other chain. Note that, since g_N in this picture remains positive throughout its flow, one expects antiferromagnetic correlations between second-nearest chains, which, as pointed out in the beginning of this chapter, is not what numerical studies find.

When $g_N(0)$ is negative, as the β-function for g_N in Eq. (2.8d) indicates, there are two possibilities: either it stays negative or eventually changes its sign and becomes positive. This depends on the precise initial values of g_N and γ_{tw}, and is shown in the flow diagram of the couplings γ_{tw} and g_N in Fig. [2.11]. The behavior of g_N in this case depends on whether $g_N(0)$ is smaller or larger than a critical initial value $g_N^{\text{crit}}(0) \propto \mathcal{O}(J'/J)^2$ for which g_N is completely fine-tuned, i.e. does not grow at all. Below, we explain these two cases separately.

First, consider the case where $g_N < g_N^{\text{crit}} < 0$ at L_0 such that $g_N(0) - g_N^{\text{crit}}(0) \propto (J'/J)^2$. In this case, g_N does remain negative (ferromagnetic) and grows exponentially. γ_{tw} receives a boost from this negative g_N and grows marginally. At ℓ^*, where $g_N = -1$, second-nearest chains are coupled ferromagnetically. The effective model at ℓ^* is then Néel-ordered block-spins of length L^* that are coupled ferromagnetically. This is because γ_{bs} is marginal and remains negative by the time ℓ^* is reached, which means that intrachain Hamiltonian has not changed much. The renormalization of the $\mathbf{Q}$ vector can be estimated using the value of L^* and treating the effective model classically (partly justified by the fact that this is a model of large block-spins). Thus, we expect a spiral order with $\epsilon_0 \propto (J'/J)^3$. Such a spiral state would be the most robust spiral state possible in this model.

In the case $g_N - g_N^{\text{crit}} \lesssim 0$ at L_0 such that $g_N(0) - g_N^{\text{crit}}(0)$ is cubic or quartic in J'/J, one obtains a fragile spiral state with $\epsilon_0 \propto (J'/J)^n$, where n is 4 or 5 depending on whether $g_N - g_N^{\text{crit}}$ at L_0 is cubic or quartic in J'/J. If $g_N(0)$ is exactly fine-tuned to $g_N^{\text{crit}}(0)$, then a weak spiral order can be stabilized only when γ_{tw} reaches unity first, in which case $\epsilon_0 \sim e^{a(J'/J)^2}$, where, to leading order in J'/J, $a = 2.6$ if the value $\gamma_{bs} = -0.38$ at a_0 is used. For this to happen, none of the relevant

couplings, specifically g_ε, should grow exponentially or even faster than γ_{tw}, which is highly unlikely as such terms are not prohibited from flowing faster than γ_{tw} by the symmetries of this model.

Finally, the case $g_N > g_N^{\rm crit}$ where $g_N(0) - g_N^{\rm crit}(0) \propto (J'/J)^2$ is similar to the case $g_N > 0$ explained above. The only difference is that, as shown in Fig. [2.11], g_N remains briefly negative before changing its sign and becoming positive. The closer $g_N(0)$ to $g_N^{\rm crit}(0)$ in this case, the longer g_N stays negative.

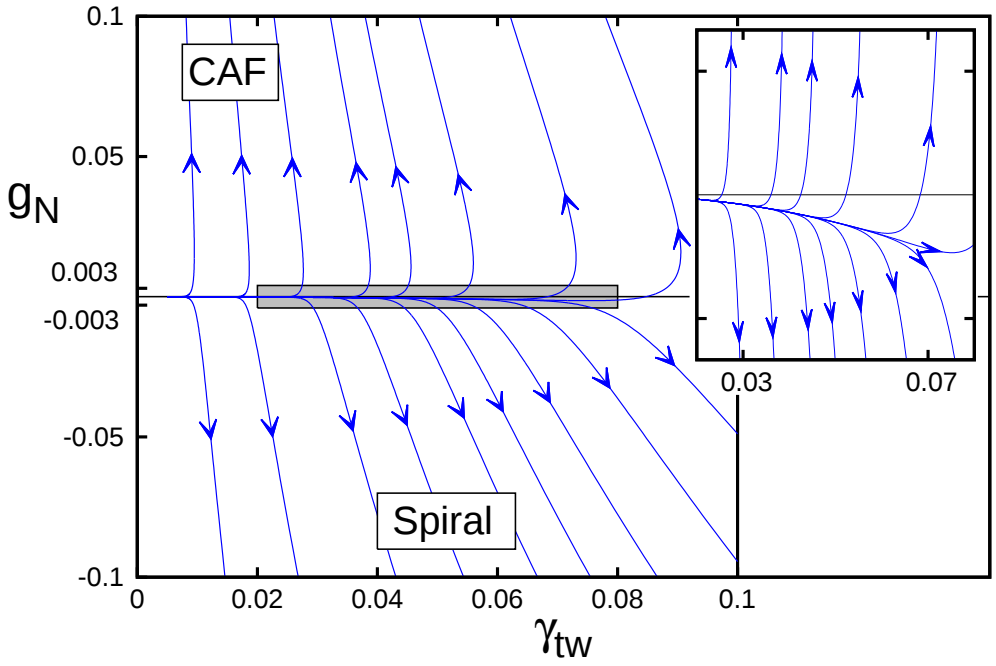

Figure 2.11: The flow diagram of g_N and γ_{tw} for $g_N(0) = \alpha(J'/J)^2 < 0$ (ferromagnetic initial value) for $-0.3 \leq \alpha \leq -0.26$, $g_\varepsilon = \gamma_\varepsilon = 0$ and $J'/J = 0.5$. As in the text, both g_N and γ_{tw} are in scaled units. For $\alpha \simeq -0.26$, the flow lines are close to the vertical axis and reach $+1$ and result in the CAF state. For $\alpha \simeq -0.3$, the flow lines are again close to the vertical axis, but reach -1, which results in a robust spiral state as explained in the text. The inset shows that when $g_N(0)$ is close to $g_N^{\rm crit}(0)$ the flow lines reach $g_N(\ell^*) = \pm 1$ substantially away from $\gamma_{tw} = 0$, as g_N grows considerably slower.

Assuming that the initial value of g_N is such that a CAF state stabilizes in the strong anisotropy limit, one expects either a first-order phase transition or an intermediate state (dimer state would not be a good candidate) separating this CAF state from the spiral phase. As J'/J increases, the initial values of γ_{tw} and γ_M increase. Also, γ_{tw} receives a larger boost from γ_{bs} and γ_M at larger J'/J values, as can be seen in Eq. (2.8c). Thus, even when $g_N(0) - g_N^{\rm crit} < 0$ (i.e., the antiferromagnetic regime), as can be seen in Fig. [2.11], the RG flows reach $g_N(\ell^*) = 1$ at larger $\gamma_{tw}(\ell^*)$. Thus

when J'/J is not too small, γ_{tw} can reach unity before g_N and result in a spiral order. From the β-functions in Eq. (2.8) and using $\gamma_{bs}(0) = -0.23$ we estimate $J'_c \simeq 0.3J$ as the smallest J' for which γ_{tw} reaches unity first.

So far, we have found that the general behavior of the β-functions in this RG analysis indicates that the fate of this system is determined by the precise initial value of g_N at L_0 for $J'/J \ll 1$. At this point one might wonder whether this peculiar behavior of g_N where it changes its sign when $g_N^{\rm crit}(0) < g_N(0) < 0$) is at all physical. The origin of this behavior becomes more clear when one considers the effective action at the length scale L, which can be obtained by integrating out modes between the two length scales L_0 and $L > L_0$ at once using perturbation theory. This results in a quantum correction to $g_N(0)$, given by:

$$-\gamma_{tw}^2 \int \mathrm{d}z\mathrm{d}z'[\partial_x\partial_{x'}\mathcal{G}(z-z')]\mathbf{N}_y(z)\cdot\mathbf{N}_{y+2}(z')\,, \tag{2.9}$$

where, $z = i(vt+x)$ and $\bar{z} = i(vt-x)$ with $v = \pi J/2$, $\mathcal{G}(z-z') = \langle \mathbf{N}_{y+1}(z)\cdot \mathbf{N}_{y+1}(z')\rangle \sim 1/\sqrt{(z-z')^2+L_0^2}$, which is obtained from the OPE of two $\mathbf{N}$ operators (Eq. (2.7c)). We see that the integrand is positive for $0 < |z-z'| < L_0$, which generates a ferromagnetic initial condition for g_N, while negative for $|z-z'| > L_0$.

Note that the above reasoning is independent of the way we chose to regularize the continuum theory. The ferromagnetic (negative) initial value of g_N follows from the fact that $[\partial_x\partial_{x'}\mathcal{G}(z-z')]$ in the integrand of the above expression is a total derivative and integrates to zero. Since the integrand is negative (note that the integral is accompanied by $-\gamma_{tw}^2$) at large distances, the initial value of g_N has to be negative to balance it out. With the same token, in a gradient expansion, the above γ_{tw}^2 contribution to g_N does not contribute to $q = 0$, and, therefore, is not expected to result in ordering. This also explains why ferromagnetic correlations were absent in the RG study of Starykh and Balents [56]. They missed the ferromagnetic correlations due to this γ_{tw}^2 contribution because, as mentioned earlier, they completely integrated out the middle chains. Finally, we point out that the RG results of Starykh and Balents [56] are reproduced by the set of β-functions in Eq. (2.8) if the initial value of g_N is tuned to $g_N^{\rm crit}$ to $\mathcal{O}(J'/J)^4$.

In summary, from the analysis of the β-functions it follows that determining the fate of this model crucially depends on the precise value of g_N at $L_0 \gtrsim a_0$. We argued that initially $g_N(0) \propto (J'/J)^2$ and is negative. Since, the studies of Pardini *et al.* [100] and Bishop *et al.* [132] indicate that the difference between the energies of the CAF and the spiral states is much smaller than $\mathcal{O}(J'/J)^2$, it seems that $g_N(0)$ is enough close to $g_N^{\rm crit}(0)$ so that the order is not stabilized at $\mathcal{O}(J'/J)^2$. Thus, while the quadratic term in the initial value of g_N does not result in the ordering of the system, it, nevertheless, is important as it describes the ferromagnetic fluctuations observed in numerical studies. The projection of the phase diagram of this model onto the $\gamma_{tw} - g_N$ plane is shown in Fig. [2.12].

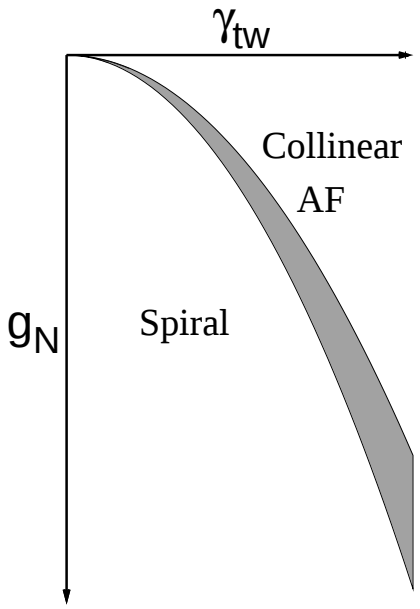

Figure 2.12: The projection of the phase diagram of the spin-$\frac{1}{2}$ HAF model on an anisotropic triangular lattice onto the $\gamma_{tw} - g_N$ plane. The shaded region indicates the case where $g_N(0)$ is too close to $g_N^{\rm crit}(0)$ where a dimer or other ordered states may appear.

2.3 Numerical Analysis on Finite-Size Systems

In the previous section we determined the β-functions of the main interchain terms, and discussed the general flow of the couplings. While we were able to draw some general conclusions about the large-distance behaviour of this model and possible states it can exhibit, we found that the precise initial values of various couplings, and in particular g_N, is needed for determining what kind of order the system exhibits. Often, in RG studies, the knowledge of the precise initial values of the couplings in the continuum description is not necessary for predicting the fate of the system. However, in this model, due to the intense competition between ferromagnetic and antiferromagnetic fluctuations, whether the system exhibits the CAF state or an incommensurate spiral state becomes extremely sensitivity to the initial value of g_N.

Let us first explain why direct determination of couplings in any continuum approximation to a lattice spin model is challenging. Any continuum model is in fact an effective field theory for its underlying lattice model at length scales larger than its short-distance cutoff. Thus, in principle, the couplings in the continuum model should be determined via a matching process: the couplings in the continuum model are chosen so that the continuum model reproduces exactly the same observable (n-point functions) as those obtained from the original lattice model. But, we resorted to continuum description and RG analysis in the first place as we could not compute

the large-distance observables of the lattice model.

Although we cannot solve the lattice Hamiltonian and determine its correlation functions in the thermodynamic limit, we can employ exact diagonalization and high-accuracy DMRG to study relatively small systems with high precision. Such finite-size systems, however, suffer from finite-size effects; nevertheless, one can always extract useful information about correlations at length scales up to the size of the system using the *finite-size scaling theory*. Such correlations can be used in conjunction with the RG analysis to determine the couplings constants at the scale L_0. This is the approach we take to estimate the initial value of g_N.

To connect to the RG analysis, the correlation between 1D block-spins of various sizes on second-nearest chains are needed. In principle, such correlations can be obtained from correlations between spins on second-nearest chains. A more straightforward way of obtaining such correlations between block-spins on second-nearest chains is to use an interchain Néel susceptibility defined as,

$$\chi_s(L) \;=\; -i\sum_{n=1}^{L}(-1)^n \int \mathrm{d}t\,\theta(t)\langle[S^z_{i,y}(t), S^z_{n,y+2}(0)]\rangle\,. \tag{2.10}$$

This is the response of the system to a staggered magnetic field applied to spins on the $y+2$ chain at a site in the middle of the y chain, as depicted in Fig. [2.13].

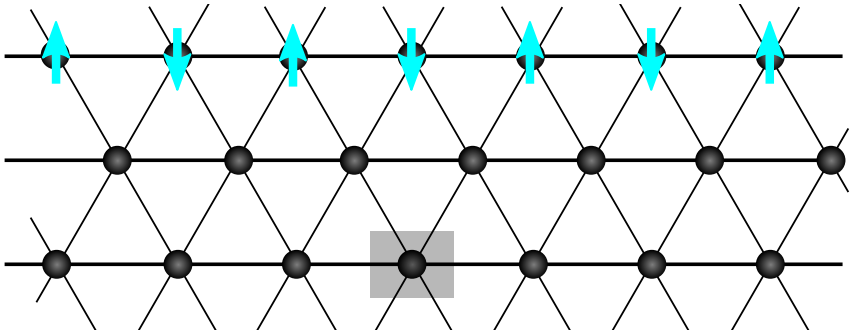

Figure 2.13: The Néel susceptibility is determined numerically by applying a weak staggered magnetic field on one chain (the top chain in the figure), and measuring $\langle S^z\rangle$ on the bottom chain for a site in the middle of the chain. The grey box indicates the site where $\langle S^z\rangle$ is measured, and the staggered magnetic field is indicated with cyan arrows on the top chain.

Since high-precision numerical computations restrict one to small system sizes, we only consider three-chain systems. The reason for this is that, as argued in the previous section, farther neighbor interchain couplings play a less important role than their nearest and second-nearest analogues due to their smaller initial conditions. Thus, restricting the analysis to a three chain system is expected to result in a quantita-

tive error of $\mathcal{O}(J'/J)^3$. Indeed, as argued in [59], the difference between the results of a four-chain system with periodic boundary conditions in the y-direction and a three-chain system is of this order.

Before proceding to the detailed analysis of numerical results obtained from high-accuracy DMRG and ED, let us first confirm that, $\mathcal{O}(J'/J)^2$ ferromagnetic fluctuations associated with the presence of γ_{tw}^2 in the β-function of g_N are present in systems with open boundary conditions along the chains. The response of three-chain systems of lengths 6 to 12 (with open boundary conditions along the direction of the chains) to a weak staggered magnetic field applied to one chain obtained from ED is shown in Fig. [2.14]. We see that this response is ferromagnetic and $\mathcal{O}(J'/J)^2$. In addition, all higher-order terms (cubic and quartic term in J'/J) are also ferromagnetic. As discussed in [59], for periodic boundary conditions along the chains, this response is $\mathcal{O}(J'/J)^4$ in agreement with the discussion of the γ_{tw}^2 in the β-function of g_N in the previous section.

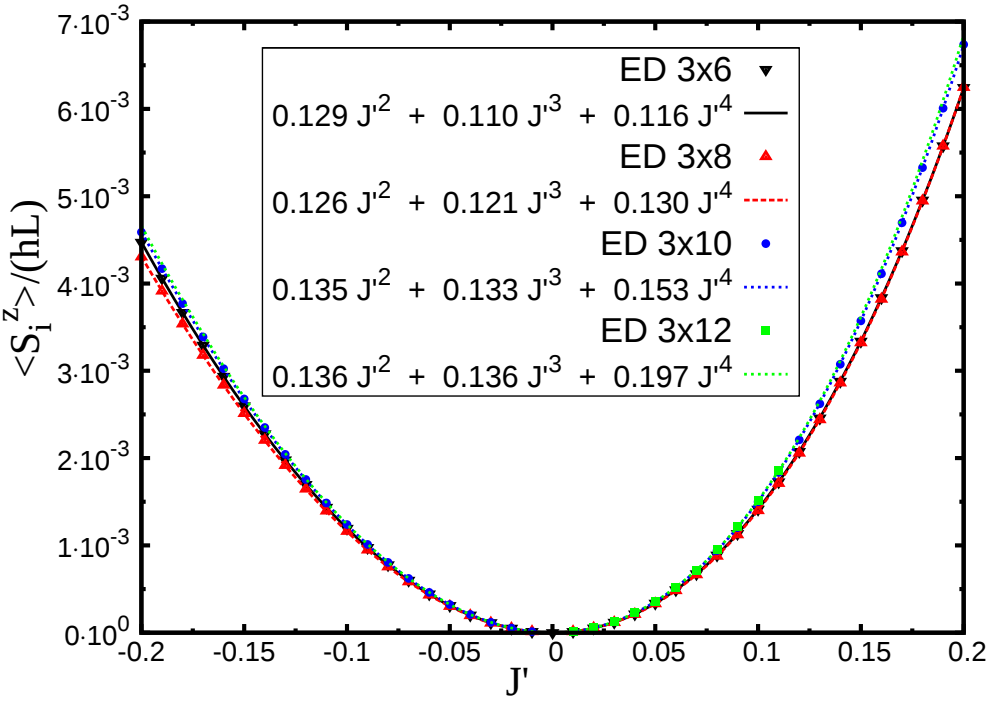

Figure 2.14: Exact diagonalization results for the response of $3 \times L$ systems to a weak staggered magnetic field, h, applied to spins on the first chain for lengths $L = 6$ to $L = 12$ and the interchain exchange J' in the range $-0.2J \leq J' \leq 0.2J$. This response is obtained from $\langle S_i^z \rangle / hL$, where i is a site in the middle of the third chain. The points are the ED results and the dashed curves are the polynomial $A(J'/J)^2 + B(J'/J)^3 + C(J'/J)^4$ fits to the data. The fitting parameters A, B and C are shown in the inset for each system size.

To relate the Néel susceptibility χ_s, obtained from exact diagonalization and DMRG on finite-size systems to the correlations of the system in the thermodynamic limit, we use the finite-size scaling theory. In finite-size scaling theory, the length of the system is treated as a relevant parameter. Thus, the following relation should hold between the susceptibility of a system of the size $L = L_0\, e^{\ell}$ with the set of couplings $\{g_i(\ell = 0)\}$ and that of a system with the size L_0:

$$\chi_s(L, \{g_i(0)\}, L_0) \;=\; C(L)\, \chi_s(L_0, \{g_i(l)\}, L_0)\,, \tag{2.11}$$

where $C(L)$ is a length-dependent function related to the dimension of the operator $\mathbf{N}$, as the staggered susceptibility is proportional to the two-point function $\langle \mathbf{N}(x) \cdot \mathbf{N}(0) \rangle$. To determine $C(L)$, we note that the dimension of the product of two $\mathbf{N}$ operators with respect to the $SU(2)_{k=1}$ WZNW model perturbed with a backscattering term is give by the β-functions of g_N and γ_{bs} as the backscattering term itself runs. Thus, the scaling factor $C(L)$ is in fact the solution of the β-function of g_N (ignoring $\mathcal{O}(J'/J)^2$ terms). We find $C(L) = \frac{L}{L_0}\sqrt{1 - \gamma_{bs}(\ell = 0)\ell}$. The factor $\frac{L}{L_0}$ is due to the dimension of the operator $\mathbf{N}$ with respect to the unperturbed WZNW model and the rest is due to the presence of the backscattering term.

It only remains to relate χ_s to g_N. For small $g_N(\ell)$, $\chi_s(L_0, \{g_i(l)\}, L_0)$ is expected to be approximately proportional to $g_N(\ell)$. Thus, we find:

$$\chi_s(L, \{g_i(0)\}, L_0) \;\propto\; \frac{L}{L_0}\sqrt{1 - \gamma_{bs}(\ell = 0)\ell}, g_N(\ell)\,. \tag{2.12}$$

This relation allows us to directly relate the numerically measured susceptibility χ_s for a finite-size system of the length L to the value of the coupling g_N at $\ell = \log \frac{L}{L_0}$. In what follows, we use the above finite-size scaling relation to determine the coefficients in the expansion of $g_N(\ell = 0)$ in J'/J by fitting g_N to the scaled susceptibility,

$$\tilde{\chi}_s(L) \;=\; \frac{L_0}{L}\frac{\chi_s(L)}{\sqrt{1 - \gamma_{bs}(\ell = 0)\ell}} \;\propto\; g_N(\ell)\,. \tag{2.13}$$

The fitting parameters are the initial values of the couplings in the RG analysis, which we restrict to $\gamma_{tw}(0)$, $\gamma_{bs}(0)$, $\gamma_M(0)$, and $g_N(0)$.

The details of the presented numerical results are as follows. Three-chain systems of lengths $L = 8$ to $L = 28$ sites (24 to 84 site systems) were studied. For systems up to 36 spins ED was used and for larger systems DMRG. In the DMRG analysis up to 2600 states were kept to ensure the accuracy of the results.

The results for system sizes up to 3×28 sites and for $-0.11 \leq J'/J \leq 0.5$ are presented in Fig. [2.15]. We see that the numerical results indicate increasing ferromagnetic correlations without any hint of antiferromagnetism. The β-functions suggest that for $J'/J \simeq 0.5$ one should see the tapering of the ferromagnetic correlations at $L \gtrsim 20$ if the system is destined to CAF ordering; however, J'/J is too

large for this quasi-one-dimensional RG approach to be quantitatively accurate at that point.

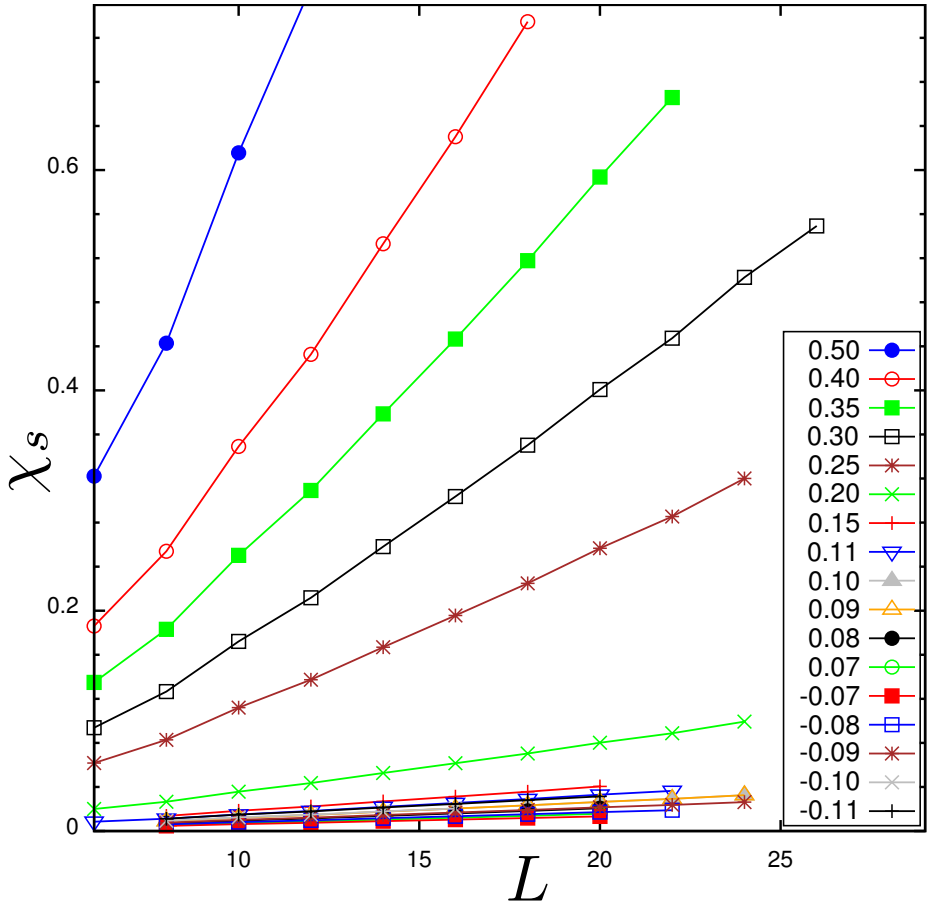

Figure 2.15: DMRG and ED results for χ_s (points) and RG fits for $-0.11 \leq \frac{J'}{J} \leq 0.5$ as a function of chain length L. The sign of χ_s is positive, indicating that chains are coupled ferromagnetically for all analyzed chain lengths L and J'/J values.

Fig. [2.16] shows the scaled Néel susceptibility for $-0.11 \leq J'/J \leq 0.11$, which is more appropriate for determining the initial value of $g_N(0)$ in the strong anisotropy limit. Fitting to the numerical results is done at once, which gives the initial values of the couplings at $L_0 = 10a_0$. We obtain $\gamma_{tw} = 0.416\frac{J'}{J} + 0.121(\frac{J'}{J})^2$, $\gamma_{bs} = -0.072$, $\gamma_M = 0.24\frac{J'}{J}$ and $g_N(0) = -0.0450(\frac{J'}{J})^2 - 0.0425(\frac{J'}{J})^3$. We note that the extracted value for the backscattering term $\gamma_{bs}(L_0 = 10a_0)$ is much smaller than the expected result -0.19 at this length scale base on the ED study of Eggert on J_1-J_2 chains [126].

As pointed out in the previous section, it is $g_N(0) - g_N^{\text{crit}}(0)$ that determines the fate of the system. Using the fit results for γ_{bs}, γ_{tw} and γ_M, we find (see Appendix [A.5]) $g_N^{\text{crit}}(0) = -0.0447(\frac{J'}{J})^2 - 0.0479(\frac{J'}{J})^3 + \mathcal{O}(\frac{J'}{J})^4$. We see that the extracted initial value,

$g_N(0)$, although indicates flowing to large ferromagnetic values, deviates from $g_N^{\text{crit}}(0)$ small enough (1% for the quadratic term and 12% for the cubic term) to be attributed to finite-size effects in the numerical results.

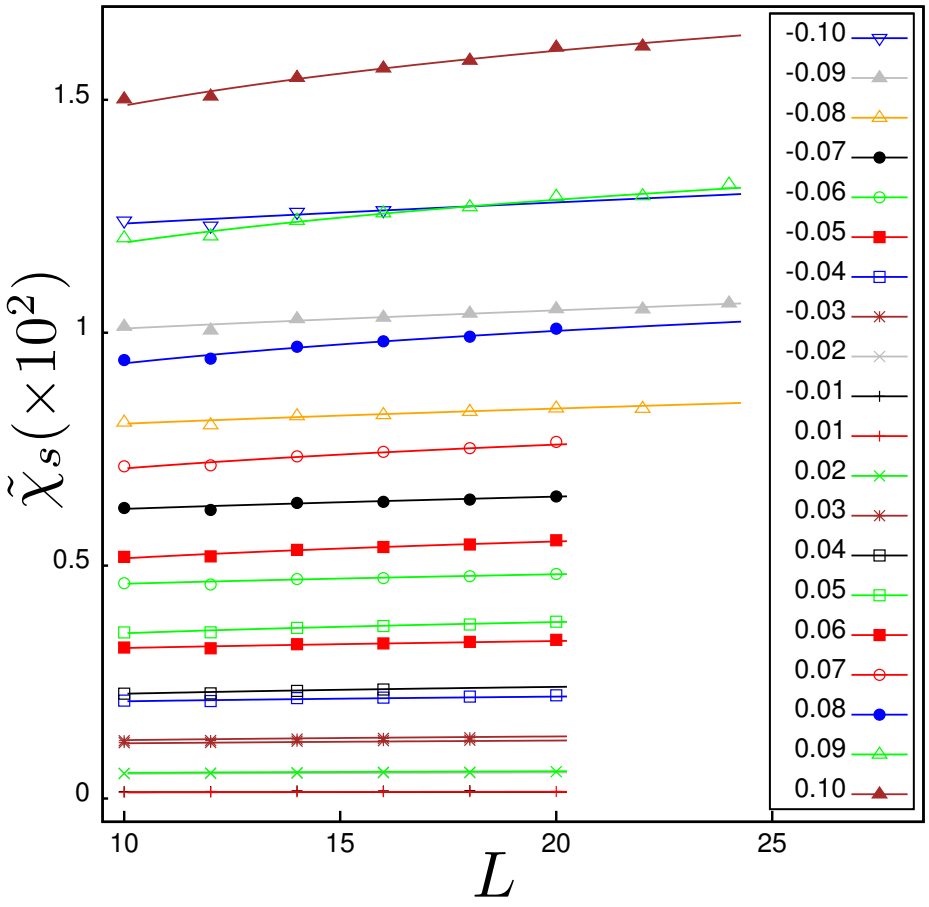

Figure 2.16: DMRG and ED results for the scaled susceptibility $\tilde{\chi}_s$ (points) and RG fits (solid curves) for $-.1 \leq \frac{J'}{J} \leq 0.1$ as a function of chain length L.

Given the limitations of the numerics as well as all the approximations made in the RG analysis (in particular, ignoring the irrelevant terms that are important at small length scales), we conclude that the numerical results are consistent with no order being selected up to $\mathcal{O}(J'/J)^4$.

2.4 Dzyaloshinskii-Moriya Interaction

The RG analysis presented in section [2.2] only took into account the Heisenberg part of the full lattice Hamiltonian in Eq. (2.1). In this section, we extend the RG analysis to the full Hamiltonian and explain how the presence of a weak DM term affects the running of the couplings and in particular g_N. Since our RG scheme is one-dimensional, we need to distinguish between the inter- and intrachain parts of the DM interaction in Eq. (2.1). We start the analysis by absorbing the intrachain DM interaction into the intrachain lattice Hamiltonian, which results in a weakly (as $|\mathbf{D}| \ll J$) anisotropic XXZ intrachain Heisenberg Hamiltonian.

Since the presence of the intrachain DM term introduces easy-plane anisotropy (breaks down the $SU(2)$ symmetry down to a $U(1)$ symmetry), it may seem that there is no advantage in using the WZNW theory for the continuum limit. As explained in Appendix [A.1], one can use a sine-Gordon theory instead of the $SU(2)_{k=1}$ WZNW theory for the continuum limit of the spin-$\frac{1}{2}$ chains, which is more appropriate for spin-$\frac{1}{2}$ XXZ chains. However, since we are assuming that the DM interaction is weak in comparison with the intrachain exchange J, following [133], we regard the resultant XXZ Heisenberg Hamiltonian from absorbing the intrachain DM term into the Heisenberg term as an isotropic Heisenberg Hamiltonian weakly perturbed by a term that breaks the $SU(2)$ symmetry. Such a term will result in an exactly marginal term in the continuum model that breaks the $SU(2)$ symmetry, and, thus, although weak, cannot be ignored. However, since the interchain DM interaction also breaks the $SU(2)$ symmetry in exactly the same way, this perturbation, as argued below, becomes unimportant.

The lattice Hamiltonian in Eq. (2.1) can be written as:

$$\mathcal{H} \;=\; \mathcal{H}_H^{\text{Intra}} + \mathcal{H}_H^{\text{Intra}} + \mathcal{H}_{\text{DM}}^{\text{Intra}} + \mathcal{H}_{\text{DM}}^{\text{Inter}}\,, \tag{2.14a}$$

where,

$$\mathcal{H}_H^{\text{Intra}} = J\sum_{x,y} \mathbf{S}_{x,y}\cdot\mathbf{S}_{x+1,y} \tag{2.14b}$$

$$\mathcal{H}_H^{\text{Inter}} = \sum_{x,y} \mathbf{S}_{x,y}\cdot\mathbf{S}_{x,y+1} + \mathbf{S}_{i,y}\cdot\mathbf{S}_{x\mp1,y+1} \tag{2.14c}$$

$$\mathcal{H}_{\text{DM}}^{\text{Intra}} = D\sum_{x,y}\Big[S^x_{x,y}S^y_{x+1,y} - S^y_{x,y}S^x_{x+1,y}\Big] \tag{2.14d}$$

$$\mathcal{H}_{\text{DM}}^{\text{Inter}} = D\Big[S^x_{x,y}(S^y_{x,y+1}\pm S^y_{x\mp1,y+1}) - S^y_{x,y}(S^x_{x,y+1}\pm S^x_{x\mp1,y+1})\Big]\,. \tag{2.14e}$$

Much the same way that the Heisenberg exchange $\mathbf{S}_n\cdot\mathbf{S}_m$ can be written as $\frac{1}{2}(S^+_mS^-_n + \text{h.c.}) + S^z_mS^z_n$, a DM term with a $\mathbf{D}$-vector in the $\hat{z}$-direction can be written as $\frac{i}{2}(S^+_mS^-_n + \text{h.c.})$. Using this, following [133], we absorb the intrachain part of the DM interaction into the intrachain Heisenberg Hamiltonian by locally rotating the

basis of spin operators as follows:

$$\mathcal{H}_H^{\text{Intra}} + \mathcal{H}_{\text{DM}}^{\text{Intra}} \rightarrow \mathcal{H}_{XXZ}^{\text{Intra}} = \frac{\tilde{J}}{2} \sum_{x,y} \left(\tilde{S}^+_{x,y} \tilde{S}^-_{x+1,y} + \text{h.c.} \right) + J \sum_{x,y} \tilde{S}^z_{x,y} \tilde{S}^z_{x+1,y} \tag{2.15}$$

where, $\tilde{J} = J/\cos\alpha$, and the new spin operators (indicated with twiddles) are defined in the twisted bases: $\tilde{\mathbf{S}} = e^{i\alpha x \tilde{S}^z_{x,y}} \mathbf{S}\, e^{i\alpha x \tilde{S}^z_{x,y}}$. The angle α is given by the equation:

$$J \cos\alpha + D \sin\alpha = \frac{J}{\cos\alpha} \,. \tag{2.16}$$

Next we need to determine the interchain Hamiltonians $\mathcal{H}_{\text{DM}}^{\text{Inter}}$ and $\mathcal{H}_H^{\text{Inter}}$ in terms of the twisted spin operators $\tilde{\mathbf{S}}_{x,y}$. For this, we need the relative twist between the two spins $\tilde{\mathbf{S}}_{x,y}$ and $\tilde{\mathbf{S}}_{x\pm1,y+1}$. Using our convention for labelling sites on the chains (see Fig. [2.9]), we obtain:

$$\begin{aligned} \mathcal{H}_H^{\text{Inter}} \rightarrow \tilde{\mathcal{H}}_H^{\text{Inter}} = & \frac{J'}{2} \sum_{x,y} \left[\tilde{S}^+_{x,y} \left(e^{-i\frac{\alpha}{2}}\, \tilde{S}^-_{x\mp1,y+1} + e^{i\frac{\alpha}{2}}\, \tilde{S}^-_{x,y+1} \right) + \text{h.c.} \right] \\ & + J' \sum_{x,y} \tilde{S}^z_{x,y} \left(\tilde{S}^z_{x\mp1,y+1} + \tilde{S}^z_{x,y+1} \right) , \end{aligned} \tag{2.17}$$

and,

$$\mathcal{H}_{\text{DM}}^{\text{Inter}} \rightarrow \tilde{\mathcal{H}}_{\text{DM}}^{\text{Inter}} = \frac{iD}{2} \sum_{x,y} \left[\tilde{S}^+_{x,y} \left(e^{i\frac{\alpha}{2}}\, \tilde{S}^-_{x,y+1} \mp e^{-i\frac{\alpha}{2}}\, \tilde{S}^-_{x\mp1,y+1} \right) - \text{h.c.} \right] , \tag{2.18}$$

where we have rotated sites on odd chains around the z axis by $-\frac{\alpha}{2}$ for convenience. Thus, the full lattice Hamiltonian can be written in this representation as:

$$\mathcal{H} = \mathcal{H}_{XXZ}^{\text{Intra}} + \tilde{\mathcal{H}}_{XXZ}^{\text{Inter}} + \tilde{\mathcal{H}}_{\text{DM}}^{\text{Inter}} \,. \tag{2.19}$$

Indicating the coupling of the S^zS^z terms with Δ and Δ', and those of the XY term with $\tilde{J}$ and $\tilde{J}'$ in the intra- and interchain XXY Hamiltonians, and $\tilde{D}$ for the interchain DM interaction, we have the following set couplings:

$$\begin{cases} \tilde{\Delta} &= J \\ \tilde{\Delta}' &= J' \\ \tilde{J} &= \frac{1}{\cos\alpha} J \approx J(1 + \frac{D^2}{4J^2}) \\ \tilde{J}' &= \cos\frac{\alpha}{2}\, J' - \sin\frac{\alpha}{2}\, D \\ \tilde{\Delta}' &= \cos\frac{\alpha}{2}\, D + \sin\frac{\alpha}{2}\, J' \end{cases} \tag{2.20}$$

where we have used $\alpha \approx \frac{D}{2J}$, as, by assumption, $J \gg J'$, D. Note that the intrachain

XXZ Hamiltonian is still critical as $\Delta < \tilde{J}$ [134]. Therefore, as an approximation, we ignore $\frac{D^2}{4J^2}$ in $\tilde{J}$ and only consider the interchain DM term. This amounts to regarding the intrachain XXZ Hamiltonian as a weakly perturbed isotropic (XXX) Heisenberg Hamiltonian by an intrachain XY term which we ignore.

The continuum limit of the interchain DM interaction with the coupling $\tilde{D} \approx D$ is:

$$\mathcal{H}_{\rm DM} \;=\; D \int \mathrm{d}x\, \epsilon^{ab\mathbf{z}} \Big[N_y^a(x)\, N_{y+1}^b(x) + \cdots \Big] \,. \tag{2.21}$$

Since the presence of the DM interaction results in easy-plane anisotropy, all coupling constants for the product of vector operators (except those involving ε, which is a pseudoscalar operator) in the previous RG analysis should be split into the XY and Z couplings. In what follows, we only focus on the XY couplings where the DM interaction enters. As we will see, the DM interaction promotes spiral ordering in the x-y plane.

The β-functions for $g_{\rm DM}$ and XY part of g_N are (see Appendix [A.4]):

$$\partial_l g_{\rm DM} \;=\; g_{\rm DM} - \frac{1}{2}\gamma_{bs}\, g_{\rm DM} + \frac{1}{2}\gamma_M g_{\rm DM} - 4 g_N\, g_{\rm DM} \tag{2.22a}$$

$$\partial_l g_N \;=\; g_N - \frac{1}{2}\gamma_{bs} g_N + g_M \zeta_N + \frac{1}{4}\gamma_{tw}^2 + g_M g_N - 2 g_{\rm DM}^2 \,, \tag{2.22b}$$

Where $g_{\rm DM}(0) \approx \dfrac{2|\mathbf{D}|}{\pi^2 J}$ is the scaled coupling constant. The β-functions of other couplings and, in particular, that of γ_{tw} remain the same. Note that, this new term, $g_{\rm DM}$, promotes and gets enhanced by a ferromagnetic g_N. Also, the $\beta-$function in Eq. (2.22a) indicates that, in the presence of a weak DM interaction, the initial value of g_N at L_0 receives a contribution from $g_{\rm DM}$, which is approximately $-2g_{\rm DM}^2(0)$. We see that the presence of the DM interaction is detrimental to the CAF state.

Both g_N and $g_{\rm DM}$ are relevant couplings, and are boosted the same by a negative γ_{bs}. Therefore, in the limit $J'/J \ll 1$, where the rest of the terms in the β-functions of g_N and $g_{\rm DM}$ are negligible, both of these couplings grow at the same rate. If $g_{\rm DM}(0)$ is larger than $g_N(0) - g_N^{\rm crit}(0)$, which was argued to be $\mathcal{O}(J'/J)^4$, the DM interaction will suppress the CAF state. Note that classically the DM interaction favours a spin configuration where spins on adjacent chains are oriented perpendicular to each other; however, the presence of γ_{tw} results in a spiral state.

A suggested phase diagram in the $J' - D$ plane based on the above analysis is shown in Fig. [2.17]. The transition between CAF and spiral states at small J'/J occurs at the critical DM strength $D^{\rm crit} \propto J'^4/J^3$. The maximum $D^{\rm crit}$ where the CAF state survives is expected to be small (smaller than $\left(\frac{J'_c}{J}\right)^4$).

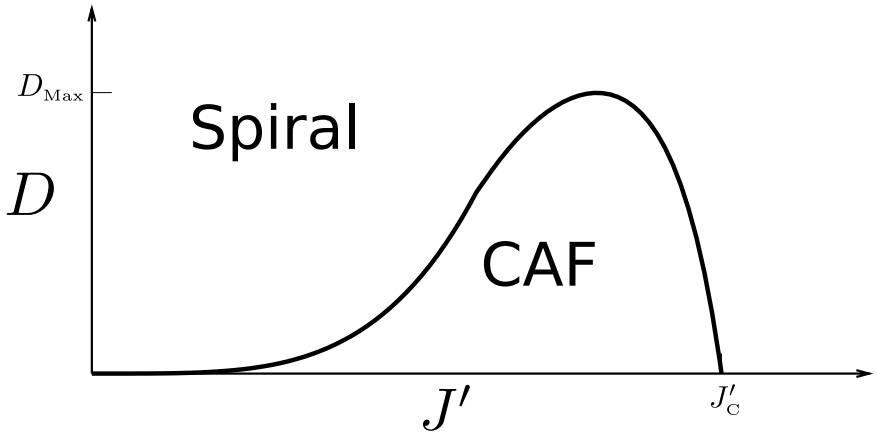

Figure 2.17: Cartoon phase diagram in the $J' - D$ plane. As explained in the text, the DM interaction promotes ferromagnetic coupling between second-nearest chains, and, thus, suppresses the CAF state. In the limit $J'/J \ll 1$, the critical DM strength $D^{\rm crit}$, which defines the boundary between CAF and spiral states in the figure, vanishes as J'^4/J^3.

2.5 Summary and Conclusions

In summary, in this chapter we presented careful RG analysis for the spin-$\frac{1}{2}$ Heisenberg antiferromagnetic model on a spatially anisotropic triangular lattice. Also we discussed the effect of a weak DM interaction with a **D** vector in the z-direction, which is relevant to Cs_2CuCl_4, within this RG approach. To determine the initial values of the coupling constant of the second-nearest interchain Néel coupling, which was argued to be crucial for determining the fate of this system, we studied finite-size systems using exact diagonalization and high-accuracy density-matrix renormalization group.

The presented RG analysis revealed intense competition between ferromagnetic and antiferromagnetic second-nearest chain fluctuations. It was argued that the dominance of antiferromagnetic correlations results in a collinear antiferromagnetic (CAF) state via the order-by-disorder mechanism, while ferromagnetically coupled chains, together with the interchain twist term, result in an incommensurate spiral (non-collinear) state. In agreement with a similar study by Starykh and Balents [56], we found that the CAF state can be stabilized at strong anisotropies. However, a small ($\mathcal{O}(J'/J)^4$) ferromagnetic second-nearest chain coupling or a weak DM interaction suffices to replace this tenuous CAF state with a spiral state.

As shown in Fig. [2.12], the RG analysis does not indicate any sign of an extended quantum-disordered state, and suggests that the phase diagram of this model is dominated by spiral and CAF states. This is in contrast with many numerical and theoretical studies that suggest that the appearance of a spin-liquid state at small

or even moderate anisotropies in this model. Careful numerical studies of Pardini *et al.* [100] and Weichselbaum *et al.* [106], which suggest the prevalence of the spiral order in the phase diagram of this model, lend support the picture presented in this chapter. The CAF and spiral states are likely separated by a direct first-order transition, which was estimated to be at $J'_c \lesssim 0.3J$.

The striking outcome of our RG analysis that was absent in the similar RG study of Starykh and Balents [56] is the fine-tuning of the coupling constant of the second-nearest interchain Néel coupling. Due to this fine-tuning there will be $\mathcal{O}(J'/J)^2$ ferromagnetic correlations that do not result in ordering. We argued that these correlations are sensitive to the boundary conditions along the chains. Specifically, such second-nearest-chain ferromagnetic correlations persist over large length scales ($L_{\text{FM}} \propto (J/J')^2$) even in the CAF state, where the system eventually manifests antiferromagnetic correlations. This reconciles the observation of only ferromagnetic correlations in numerical studies on finite-size systems with the existence of the CAF state at sufficiently strong anisotropies. Our analysis of the scaling of an interchain Néel susceptibility in small three-chain systems obtained from ED and high-accuracy DMRG in section [2.3] clearly indicates these ferromagnetic correlations, and, as discussed, is in agreement with no order being selected up to $\mathcal{O}(J'/J)^4$. Therefore, our results, while consistent with the presence of the CAF state at strong anisotropies, do not provide direct evidence for the presence of such a state.

We showed that the presence of a weak DM interaction term enhances ferromagnetic second-nearest chain couplings, and, thereby, helps to stabilize the spiral order. This is shown in the illustrative phase diagram in Fig. [2.17]. Based on this and the fact the the estimated crossover between CAF and spiral states $J'_c \lesssim 0.3J$, we conclude that Cs_2CuCl_4 with $J'/J \simeq 0.3$ and $D/J = 0.053$ is well within the stability range of the spiral order.

In the future, it would be interesting to further explore the nature of the transition between the CAF and spiral states more rigorously. Specifically, to examine the possibility of the appearance of an intermediate dimer state brought about by g_ε at a point or over a small sliver in the phase diagram of this model. Also, as pointed out above, the results of our numerical analysis and the study of Pardini *et al.* [100], although compatible with the presence of the CAF state at sufficiently strong anisotropies, do not directly support the presence of such a state. Thus, the presence of the CAF state at strong anisotropies, while certainly very likely and strongly suggested by the RG analysis, has not yet been fully established.

The fine-tuning of the relevant coupling g_N in the presented RG analysis has important implications on how the results of numerical studies should be interpreted. As discussed earlier in this chapter, g_N is responsible for magnetic ordering in this model. Given that, due to its fine-tuning, this coupling does not run as fast as a relevant coupling is expected it is not surprising that many numerical studies on finite-size systems concluded that at strong anisotropies a quantum-disordered state appears. Likely, those studies mistook this rather peculiar behavior of g_N for a spin-

liquid state, which, to appear, requires g_N to remain small on all length scales.

With the understanding gained from the RG analysis in the strong anisotropy limit available, confirming and further elucidating the structure of the phase diagram of this model demands careful numerical analysis. Several numerical studies have already pursued this line of thought, and this is still an ongoing effort [100, 106, 119, 124]. Due to convergence issues, accessing the strong anisotropy regime in this mode using series expansions and large-system DMRG approaches, which are more suited for studying relatively large system sizes, has so far been somewhat problematic. It might be possible to circumvent such issues by resorting to other numerical approaches that are tailored for this model such as the study in Ref. [119]. This study seems to show good agreement with the picture proposed here. Thesberg *et al.* found a phase transition from a long-range spiral state to another state with short-range spiral correlations at $J'/J \simeq 0.5$. However, they were unable to identify the latter phase. Thus, despite many hints, it still remains to find direct evidence for the putative CAF state at high anisotropies, which demands further numerical investigations.

Chapter 3

Renormalization Group Analysis for a Neck-Narrowing Lifshitz Transition in Two Dimensions

This chapter discusses the effect of weak interactions on a neck-narrowing Lifshitz transition in two dimensions using an RG approach. The model studied here is described by the dispersion relation $\varepsilon(\mathbf{k}) = k_x^2 - k_y^2$ together with a momentum cutoff that plays the role of the size of the Fermi surface. The neck-narrowing transition in this model is controlled by the chemical potential with the critical point of the transition at $\mu_c = 0$. It is shown that, at the critical point of this transition, the Wilsonian effective action is intrinsically non-local. The appearance of non-locality in the effective action at the critical point is attributed to integrating out an emergent soft degree of freedom.

Slightly away from the critical point of the neck-narrowing transition, where the Fermi surface has a narrow neck, locality can be restored only in the presence of the momentum cutoff, which keeps the size of the Fermi surface finite. It is found that the coupling of a weak attractive contact density-density interaction grows as $\log^2 L$ in this RG. Nevertheless, quantum corrections are analytic only within a finite momentum range that shrinks as the critical point is approached. The analysis presented in this chapter is largely based on [135].

3.1 Introduction

Determining the fate of Fermi surfaces in the presence of interactions in two and three dimensions is a problem of great significance in condensed matter physics. The importance of this problem arises from the fact that a wide range of condensed matter systems are described by fermions that form a Fermi surface and interact with each other via short- or long-range interactions. Such systems not only include common

examples such as metals and liquid ^{3}He [136] but also rather more abstract models such as the *Halperin-Lee-Read* state (a compressible phase of $\nu = \frac{1}{2}$ fractional quantum Hall liquid) and spin-liquid states that are described by fermionic spinons, which, at the mean-field level, form a Fermi surface [1, 137, 47].

Depending on the nature of low-energy interactions, i.e., whether the low-energy interactions are short-range or long-range, entirely different physics is expected. Our understanding of the low-energy effective field theories of Fermi surfaces in the presence of long-range interactions, mediated by a soft boson or a gauge field, where a non-Fermi liquid state can appear, despite great progresses in recent years [137, 138, 139, 140, 141, 142] still remains incomplete. In contrast, for Fermi surfaces in the presence of weak short-range interactions we seem to have a fairly complete understanding: Landau's celebrated *Fermi liquid* theory together with its well-known pairing and density wave instabilities.

Landau's *Fermi liquid theory* [143, 144, 145, 136, 146] is, in fact, one of the pillars of modern condensed matter physics. This theory not only describes the low-energy (energies much smaller than the Fermi energy) properties of normal metals, but also is the cornerstone of our understanding of conventional superconductivity. What lies at the heart of the Fermi liquid theory is the notion of well-defined fermionic quasi-particles that are adiabatically connected to non-interacting fermions [136, 146]. More technically, this is the assumption that the single-particle propagator, $\mathcal{G}(\mathbf{k}, \omega) = -i \langle \psi_{\mathbf{k},\omega}\, \psi^\dagger_{\mathbf{k},\omega} \rangle$, in a Fermi liquid state has a well-defined single-particle pole. This, in fact, is a statement about many-particle states in Fermi liquids: the presence of this well-defined single-particle pole can be equivalently expressed as the finiteness of the so-called *wave-function renormalization* parameter Z [146].

Fermi liquid behavior is fairly resilient and very common in real systems. This raises the question of what the origin of Fermi liquid behavior is. The original proof given for the Fermi liquid theory [136, 146] was a self-consistency argument: assuming a finite wave-function renormalization Z and showing that to any order in the perturbation theory this assumption holds. However, this approach obscures the crucial role of the Fermi surface. In the early 90s, an alternative approach for explaining the Fermi liquid behavior based on the notions of low-energy effective field theories and the RG theory was developed by J. Polchinski [21], R. Shankar [147, 148] and others [149]. This approach provides a much simpler conceptual picture of Fermi liquid behavior in terms of a fixed-point theory. Also the role of the Fermi surface is much more transparent. However, as discussed later in this section, this RG approach is not particularly suited for determining the fate of a given Fermi surface starting from a microscopic scale: this RG program – henceforth referred to as *Shankar's RG* – solely describes the Fermi liquid fixed point.[1]

Before describing Shankar's RG approach, it is worth pointing out a subtle point

[1]Note that, Shankar's RG approach provides a qualitative explanation for why Fermi liquid behavior arises at low energies: it shows that non-forward and non-BCS scattering processes are kinematically suppressed.

in RG approaches to Fermi surfaces. A marked characteristic of many-body fermion systems is that they can form Fermi surfaces, which are extended zero-energy manifolds as opposed to isolated points. Note that systems with zero-dimensional (point) zero-energy manifolds not only include ordinary many-body boson systems but also certain many-body fermion systems whose zero-energy manifolds are consisted of a few isolated points. Instances of such fermion systems include Graphene at half-filling, where Dirac points appear, *quantum electrodynamics* in 3+1 dimensions (QED4) [39], superconductors that have nodal superconducting gap structures such as a d-wave superconductor [150], and 1D fermion systems where the Fermi surface consists of Fermi points [69]. The significance of this point becomes clear once one notices that low-energy modes become synonymous with long-distance observables only when the zero-energy manifold that one renormalizes towards is a point in the momentum space. In fact, this poses a serious problem when there is a coupling to a boson degree of freedom whose zero-energy manifold is a point. Developing appropriate scaling relations in such cases that apply to 3D Fermi surfaces or to the whole Fermi surface in two-dimensions (i.e., beyond the so-called patch approximation) still remains an unsolved problem [38, 151, 152].

3.1.1 Shankar's RG

Shankar's RG is based on normalizing towards the Fermi surface, along the normal to the Fermi surface, while keeping the Fermi surface fixed at tree level [148].[2] Therefore, this RG scheme only applies to regular Fermi surfaces, i.e., Fermi surfaces that do not contain *van Hove* singularities [153]. This is because, at a van Hove singularity, the normal to the Fermi surface does not exist, and, therefore, renormalizing towards the Fermi surface becomes meaningless.

To put our RG approach in context, here we briefly review the main points of Shankar's RG for a circular Fermi surface described by the dispersion $\varepsilon_{\mathbf{k}} = |\mathbf{k}|^2$ and the chemical potential $\mu = k_F^2$. At the end, following Shankar, we explain how this RG approach can, in principle, be extended to non-rotationally-invariant regular Fermi surfaces, which will clarify why not only van Hove singular Fermi surfaces but also Fermi surfaces that are sufficiently close to such singular points may deviate from the Fermi-liquid paradigm.

The starting point of Shankar's RG is the following (imaginary-time) fermion path-integral for a rotationally-invariant two-dimensional Fermi surface in the presence of weak short-range interactions:

$$\mathcal{Z} = \int_{|\xi_{\mathbf{k}}|<\Lambda} \mathcal{D}\psi\, \mathcal{D}\bar{\psi}\, \exp\left\{ \int \frac{\mathrm{d}\mathbf{k}\mathrm{d}\omega}{(2\pi)^3} \bar{\psi}_{\mathbf{k},\omega}(i\omega - \xi_{\mathbf{k}})\psi_{\mathbf{k},\omega} - \mathcal{S}_{\text{int}} \right\}, \tag{3.1}$$

[2] Note that the Fermi surface in general may run in the course of RG due to quantum corrections to the quadratic part of the action (chemical potential and self-energy corrections).

where the energy cutoff $\Lambda \ll E_F = k_F^2$ and $\bar{\psi}$ and ψ are Grassmann field variables. Here $\mathcal{G}^0(\mathbf{k},\omega) = -\frac{1}{i\omega - \xi_{\mathbf{k}}}$ and $\xi_{\mathbf{k}} = \varepsilon(\mathbf{k}) - k_F^2$. Since the interactions are short range, the vertex function, $\Gamma(\mathbf{k}_1,\mathbf{k}_2,\mathbf{k}_3,\mathbf{k}_4)$, in the interaction term,

$$\mathcal{S}_{\text{int}} = g\left[\prod_{i=1}^{4}\int \frac{\mathrm{d}\mathbf{k}_i}{(2\pi)^2}\int\frac{\mathrm{d}\omega_i}{2\pi}\right]\Gamma(\mathbf{k}_1,\mathbf{k}_2,\mathbf{k}_3,\mathbf{k}_4)\,\delta(\omega_1+\omega_2-\omega_3-\omega_4) \tag{3.2}$$
$$\delta(\mathbf{k}_1+\mathbf{k}_2-\mathbf{k}_3-\mathbf{k}_4)\,\bar{\psi}(\mathbf{k}_1,\omega_1)\bar{\psi}(\mathbf{k}_2,\omega_2)\psi(\mathbf{k}_3,\omega_3)\psi(\mathbf{k}_4,\omega_4)\,,$$

is an analytic function of the momenta.[3]

In Shankar's RG it is the momentum measured from the Fermi surface $(\mathbf{k}-\mathbf{k}_F)$ that is rescaled. The interaction vertex $\Gamma(\mathbf{k}_1,\mathbf{k}_2,\mathbf{k}_3,\mathbf{k}_4)$ can be Taylor expanded in $\mathbf{k}_i - \mathbf{k}_F$. The leading term of this expansion, $\Gamma(\mathbf{K}_1,\mathbf{K}_2,\mathbf{K}_3,\mathbf{K}_4)$ ($|\mathbf{K_i}| = k_F$), defines the dimensionless interaction vertex. However, this does not mean that the four-fermion interaction term with the vertex $\Gamma(\mathbf{K}_1,\mathbf{K}_2,\mathbf{K}_3,\mathbf{K}_4)$ is marginal at tree level. This is because of the δ-function, which, under the non-linear scaling[4] $(\mathbf{k}_i - \mathbf{K}_i) \to s^{-1}(\mathbf{k}_i - \mathbf{K}_i)$, transforms in a non-trivial way for an arbitrary set of momenta $\{\mathbf{K}_i\}$. Therefore, not all four-fermion scattering processes with the interaction vertex $\Gamma(\mathbf{K}_1,\mathbf{K}_2,\mathbf{K}_3,\mathbf{K}_4)$ are marginal at tree level. This is a kinematic constraint brought about by the presence of the Fermi surface, and, as we will see shortly, results in the suppression of all scattering processes except for *forward* ($\mathbf{K}_1 = \mathbf{K}_4$ and $\mathbf{K}_2 = \mathbf{K}_3$, or $\mathbf{K}_1 = \mathbf{K}_3$ and $\mathbf{K}_2 = \mathbf{K}_4$) and *pairing (BCS)* ($\mathbf{K}_1 = -\mathbf{K}_2$ and $\mathbf{K}_3 = -\mathbf{K}_4$) scatterings at low energies [148] (see Fig. [3.1]). This kinematic constraint is the origin of the infinite life-time of quasi-particles in Fermi liquids at the Fermi surface [21]. Let us see how this kinematic constraint that arises from the presence of the Fermi surface in Shankar's RG in regular Fermi surfaces (excluding nested Fermi surfaces) and at low energies only leaves forward and pairing scatterings marginal at tree level. Because of the momentum-conserving δ-function not all the momenta in an arbitrary four-fermion interaction with the by-power-counting marginal vertex $\Gamma(\mathbf{K}_1,\mathbf{K}_2,\mathbf{K}_3,\mathbf{K}_4)$ can be laid on the Fermi surface. Therefore, as the result of scaling momenta measured from the Fermi surface, the "legs" that are left out will grow as the energy cutoff is lowered towards the Fermi surface. Using a geometrical argument, it can be easily shown that for a two-dimensional regular Fermi surface that is not nested only forward and pairing scatterings satisfy this constraint, and, thus, are marginal at tree level [148, 21].[5]

At one-loop order, it is found that the forward scattering channel does not re-

[3] Although the interaction vertex is an analytic function, it may have a finite convergence radius. For example, suppose $\Gamma(\mathbf{k}_1,\mathbf{k}_2,\mathbf{k}_3,\mathbf{k}_4) = \Gamma(\mathbf{p} = \mathbf{k}_1 - \mathbf{k}_4) = \frac{1}{|\mathbf{p}|^2+m^2}$ (density-density interaction mediated by a massive boson), which is analytic only within $|\mathbf{p}| < m$.

[4] This scaling is non-linear because $\mathbf{K}$, the Fermi momentum, changes its orientation. See, for example, [49, 154, 155].

[5] For nested regular 2D Fermi surfaces there will be an extra scattering process, characterized by the nesting vector, that satisfies this constraint, which, at one-loop order, suggests a density-wave instability [148].

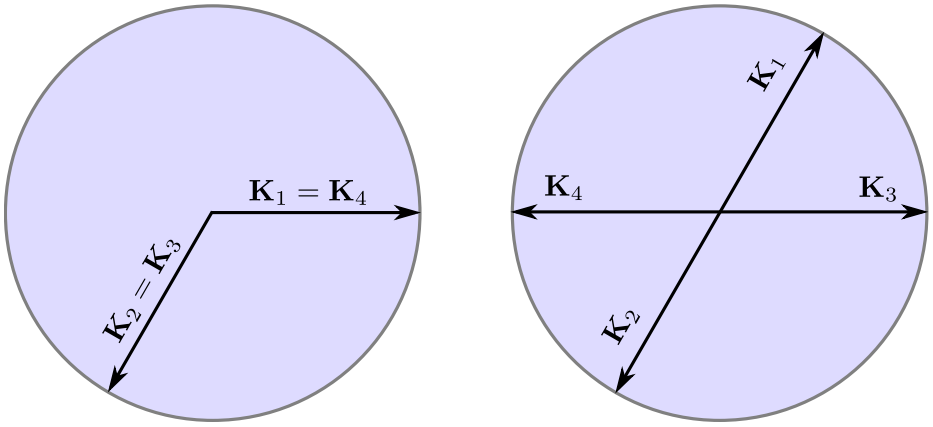

Figure 3.1: Instances of forward and BCS scatterings in a 2D rotationally invariant Fermi surface. (a) A forward scattering with momenta on the Fermi surface. (b) A BCS scattering.

ceive any quantum corrections, while the BCS scattering, depending on whether the interactions are attractive or repulsive is either marginally relevant (for attractive interactions) or marginally irrelevant (for repulsive interactions). Shankar, invoking a large-N-like argument, showed [148] that based on $\Lambda \ll k_F^2$ the one-loop scenario persists to all loop orders, and, therefore, the forward scattering is exactly marginal. Note that owing to the rotational symmetry of this problem, there is only one coupling constant for the pairing scatterings and one for the forward scatterings. This is the advantage of rotational symmetry; otherwise, even at one-loop order, one encounters functional β-functions (not to be confused with functional β-functions in functional RG approaches that do not rely on the analyticity of quantum corrections) as each scattering process will have its own coupling constant (each BCS or forward scattering process can be labeled by two angles, associated with the orientations of the vectors $\mathbf{K}_i$ – see Fig. [3.1]) [148, 156].

Finally, let us outline how this RG approach can be extended to regular Fermi surfaces that are not rotationally-invariant. This will show why not only van Hove singular Fermi surfaces but also Fermi surfaces close to a singular point are pathological. For a generic Fermi surface with an energy cutoff much smaller than the Fermi energy, one can use a different set of coordinates to describe modes in the vicinity of the Fermi surface: $(k_x, k_y) \to (\xi, \theta)$. Here $\xi = \xi_{\mathbf{k}}$ is the energy measured from the Fermi surface, and θ is a coordinate that parameterizes the constant energy contours labelled by ξ. For regular Fermi surfaces, the Jacobian associated with this change of coordinates, $J(\xi, \theta)$, can be Taylor expanded in ξ. If this Taylor expansion holds for

$|\xi| < \Lambda$, then one can write the quadratic part of the action at low-energies as:

$$\mathcal{S}_0 = \int \mathrm{d}\omega \int \mathrm{d}\theta \int \mathrm{d}\xi \left[J(0,\theta) + \xi\, J'(0,\theta) + \cdots \right] \bar{\psi}_\sigma(\xi,\theta) \left(i\omega - \xi \right) \psi_\sigma(\xi,\theta)\,. \quad (3.3)$$

In the above expansion, the first-order and all higher-order terms (indicated by ellipses) are accompanied by powers of ξ, and, therefore, are irrelevant in Shankar's RG and will eventually renormalize to zero. Ignoring these terms and absorbing the $J(0,\theta)$ factor in the field variables, one arrives at a description (for the quadratic part of the action) very similar to that of a rotationally-invariant Fermi surface. Note that the anisotropy of the Fermi surface is encoded in $J(0,\theta)$, which in general is not a constant.[6]

Regardless of whether the Fermi surface is rotationally invariant or not, due to the non-trivial transformation of the δ-function in Eq. (3.2), it is not feasible to incorporate the effect of non-forward and non-pairing scattering processes to determine how various parameters, such as the effective mass [158], are renormalized as one lowers the energy cutoff in the course of this RG. This is why Shankar's RG is only suited for describing the fixed-point theory, i.e., the Fermi liquid theory. To determine the fate of a Fermi surface in the presence of weak short-range interactions, starting from a microscopic scale, it is important to know how exactly the low-energy effective interactions are renormalized by non-forward and non-BCS scatterings [156, 159]. For example, it is well known that even starting with repulsive weak interactions an attractive interaction can be generated through the *Kohn-Luttinger* mechanism in 3D [160], or its 2D version [161].

3.1.2 Neck-Narrowing Lifshitz Transitions

We saw that 2D Fermi surfaces that contain van Hove singularities cannot be addressed using Shankar's RG. The fate of such Fermi surfaces in the presence of weak short-range interactions is a question of great theoretical interest and very relevant to real materials (see Fig. [3.2]). From a simple scaling analysis based on renormalizing towards the singular point one can readily see that there is no analog of the kinematic constraint in Shankar's RG in a van-Hove singular Fermi surface [21, 162]. This argument already suggests departure from the Fermi-liquid theory. This raises the question of the fate of Fermi surfaces that contain van Hove singularities in the presence of interactions. Specifically, what happens to such Fermi surfaces in the presence of weak interactions near the singular points, and how the singular points

[6] This procedure tacitly assumes that the Fermi surface does not change its shape in the course of RG. However, the shape of the Fermi surface is expected to change while maintaining a fixed density (volume enclosed by the Fermi surface) to respect Luttinger's theorem [157]. Shankar showed that this ultimate (renormalized) Fermi surface can be determined self-consistently by including an initially unknown deviation from the ultimate Fermi surface, $\delta\xi(\theta)$, and requiring that this to be the fixed point [148].

affect the rest of the Fermi surface.

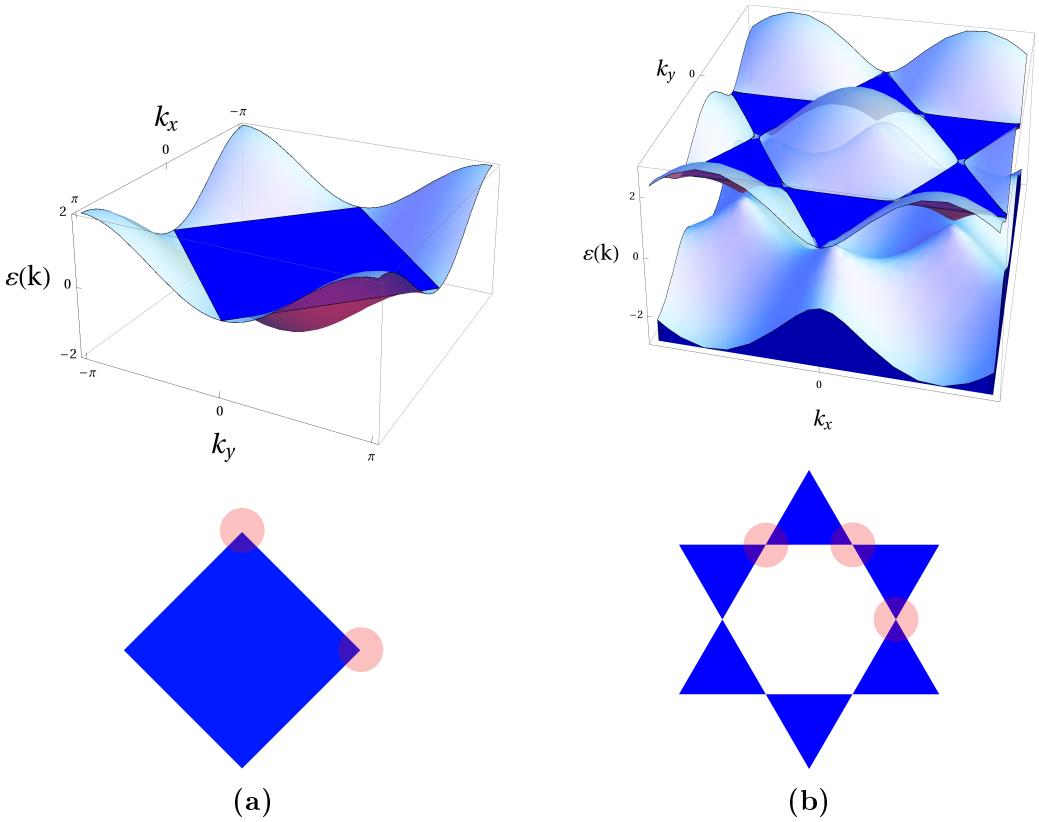

Figure 3.2: Instances of Fermi surfaces in real systems that contains van Hove singular points. (a) Hubbard model on a square lattice at half filling. (b) Graphene at $\frac{5}{8}$ filling.

Here we discuss the effect of weak short-range interaction on Fermi surfaces that contain or are in close proximity to a van Hove singularity in a simple model using an RG approach. We saw that a Fermi surface that is close to a van Hove singularity although formally regular cannot be treated using Shankar's RG due to close proximity to the singular point, which potentially can have a dramatic effect on the low-energy interactions. This is because Shankar's prescription is inapplicable as long as the singular point is at an energy scale smaller than the energy cutoff (see Fig. [3.3]). Such Fermi surfaces that are in close proximity to a van Hove singular point are actually more common than Fermi surfaces that contain a van Hove singularity as realizing a van Hove singular Fermi surface requires fine-tuning the chemical potential or some other parameters such as hopping amplitudes in the underlying tight binding model. In fact, in the absence of interactions, the appearance of a van Hove singularity upon tuning the chemical potential in a Fermi surface is an instance of *neck-narrowing Lifshitz transitions*.

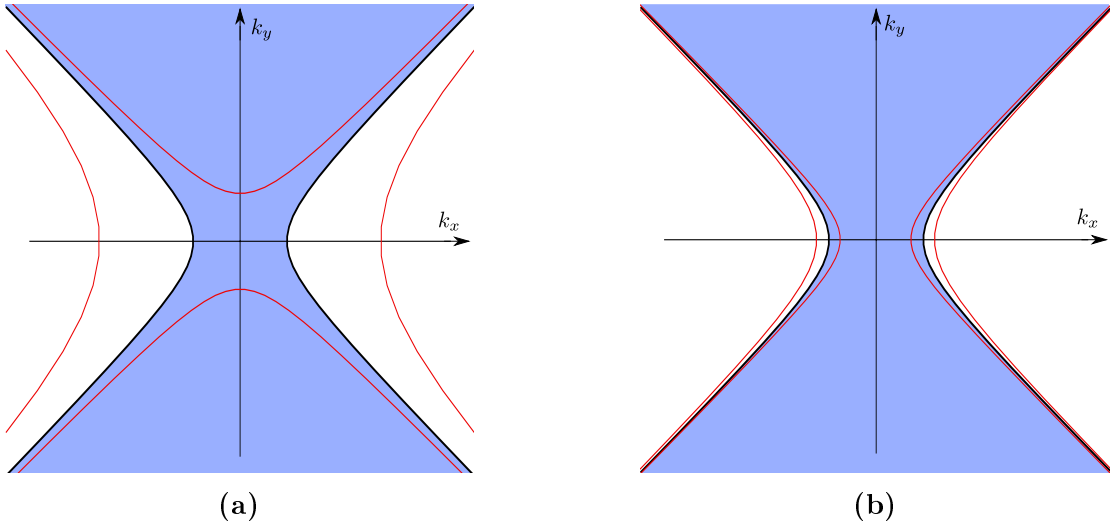

Figure 3.3: The neck region of a Fermi surface near a singular point that has a narrow neck. (a) When the energy cutoff is larger than the energy scale of the singular point (the momentum scale corresponding to the energy cutoff is larger than the width of the neck). Thus the Fermi surface seems van Hove singular and Shankar's RG in inapplicable. (b) The energy cutoff is much smaller than the energy scale of the singular point. In this regime one may apply Shankar's RG.

Lifshitz transitions are quantum phase transitions where the topology of the Fermi surface changes [163, 164]. Lifshitz classified such phase transitions into *pocket-disappearing* and *neck-narrowing* transitions [165]. An instance of the former transitions is Graphene at half-filling, where Dirac points appear. Lifshitz transitions are, in fact, *topological quantum phase transitions* where only the topology of the Fermi surface changes while all symmetries remain unchanged throughout the transition [1]. Here we are interested in neck-narrowing Lifshitz transitions. How the change in topology in a neck-narrowing Lifshitz transition manifests itself in the *entanglement entropy* of the system [166] is an interesting question at its own right, which we do not discuss here.

The neck-narrowing Lifshitz transition that we examine in this chapter is described by the quadratic dispersion $\varepsilon(\mathbf{k}) = k_x^2 - k_y^2$ with a momentum cutoff K that keeps the size of the Fermi surface finite. In fact, this model can be regarded as a crude approximation to realistic Fermi surfaces that undergo neck-narrowing Lifshitz transitions and are described by this quadratic dispersion near the neck, such as those shown in Fig. [3.2]. Then, the momentum cutoff roughly plays the role of the size of the Fermi surface. At the critical point of this class of neck-narrowing transitions a van Hove singularity, with its characteristic logarithmically divergent density of states (DOS) appears. In fact, these are the most common neck-narrowing transitions in two-dimensions as neck-narrowing transitions that are described by other dispersion

relations near the neck (e.g., $\varepsilon(\mathbf{k}) = k_x^4 - k_y^4$ with a more singular DOS) require fine-tuning the hopping matrix elements in the underlying lattice model.[7]

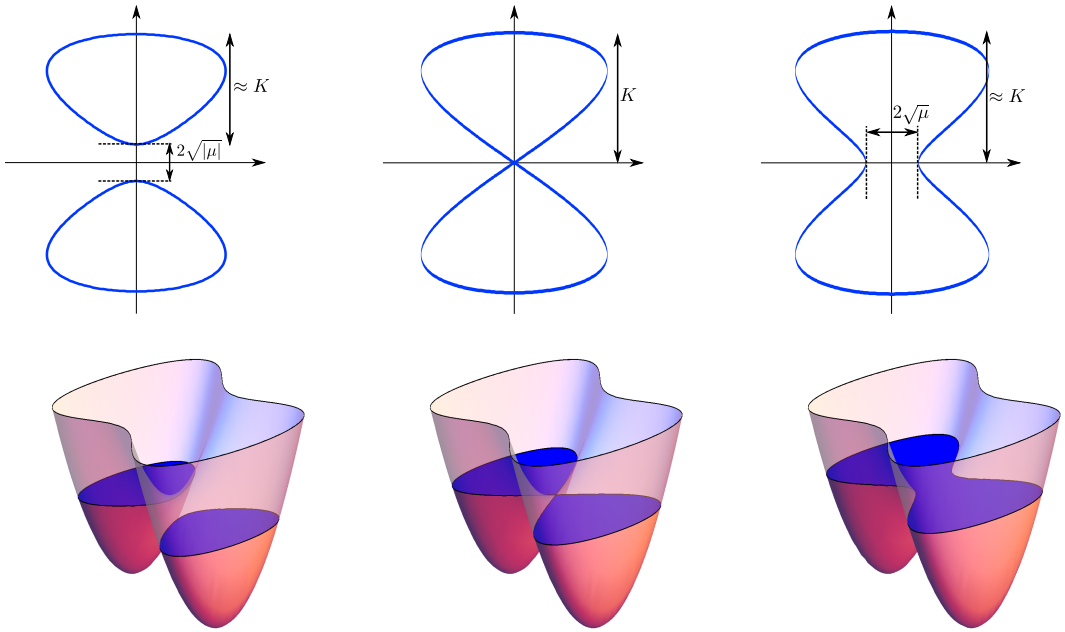

(a) $\mu < 0$ **(b)** $\mu = 0$ **(c)** $\mu > 0$

Figure 3.4: A neck-narrowing Lifshitz phase transition in 2D for a non-interacting Fermion model with the dispersion $\varepsilon(\mathbf{k}) = k_x^2 - k_y^2 + \frac{1}{K^2}k_y^4$ at (a) $\mu < 0$, where the Fermi surface is made up of two separate lobes, (b) the critical point, $\mu = 0$, where the two lobes first touch and a van Hove singularity is developed, and (c) $\mu > 0$ at which point a smooth monolithic Fermi surface is formed.

As we will see in this Chapter, the Wilsonian effective action of this model at the critical point of the neck-narrowing transition is intrinsically non-local. This intrinsic non-locality can be regarded as the result of integrating out an emergent soft degree of freedom. Therefore, a question of great theoretical interest regarding Fermi surfaces that undergo such neck-narrowing Lifshitz transitions in the presence of interactions is whether the effect of the change in topology on the low-energy effective interactions can somehow be captured by an independent degree of freedom at low-energies of perhaps a topological nature. To clarify this idea, it is instructive to draw a parallel between neck-narrowing Lifshitz transitions and *Ising-nematic* phase transitions in metals [167].

Ising-nematic phase transitions in metals are phase transitions driven by interactions where the point-group symmetry is spontaneously broken. The phase transition

[7] Note that dispersion relations of the form $\varepsilon(\mathbf{k}) = |k_x|^3 - |k_y|^3$ are non-local and cannot be obtained from any microscopic tight-binding model with short-range hoppings.

can be described by an *Ising order parameter* that undergoes a symmetry breaking Ising phase transition and is coupled with the Fermi surface. At the critical point of such Ising-nematic transitions the Ising order parameter is gapless and mediates long-range interactions between fermions, where a non-Fermi liquid state may appear [137, 141, 139, 140, 168, 151]. In fact, this Ising order parameter is a convenient way to represent collective excitations of fermions and have a local description. With this analogy in mind, we will look for hints of description in terms of an emergent independent degree of freedom in our RG analysis.

3.1.3 Previous Studies

The fate of 2D van Hove singular Fermi surfaces in the presence of weak, short-range interactions has already been addressed by numerous studies [169, 170, 171, 172, 173, 174, 175, 176, 177, 178, 179, 180, 181] using various approaches and, in particular, RG [162, 182, 183, 184, 185, 186, 187, 188, 189, 190]. However, none of these studies based on RG has been successful in achieving a consistent RG description. This is because these studies encountered non-locality in the effective low-energy action. Since non-local terms typically proliferate under RG (unless a symmetry constraints the form of non-local terms that can get generated), these studies are not, strictly speaking, consistent.

The problem with the appearance of non-local terms in the low-energy action is that it is not clear how to restrict the RG analysis to a closed set of operators. This is in contrast with local perturbative RG approaches where analyticity makes it possible to classify all allowed terms into local tree-level relevant, marginal and irrelevant terms. Then, all or most of irrelevant terms are ignored, which restricts the RG analysis to a much smaller set of marginal and relevant couplings. Therefore, it is not clear whether one can trust any conclusion drawn from restricting the RG analysis to marginal local terms when quantum corrections are non-local (non-analytic in momentum space), as done in the aforementioned studies.

Gonzalez *et al.* [162], studied an isolated van Hove singularity described by the dispersion relation $\varepsilon_{\mathbf{k}} = k_x^2 - k_y^2$ at zero chemical potential, using a field-theoretic RG approach. In their analysis, they encountered a non-analytic two-loop self-energy of the form $\frac{1}{8\pi^4}\frac{U^2}{t^2}\xi_{\mathbf{q}}(\log\frac{\Lambda}{|\xi_{\mathbf{q}}|})^2$ (where $\xi_{\mathbf{q}} = q_x^2 - q_y^2$, and t and U are the usual hopping and on-site repulsion parameters in the Hubbard model), which required a non-analytic counterterm. In spite of the appearance of this non-local self-energy term, they argued that due to the topological character of the dispersion relation, one can ignore the effect of this two-loop self-energy and focus on the renormalization of interactions. They concluded that, in the weak-coupling limit, the interaction strength of repulsive interactions renormalizes to zero, and also suggested the existence of a strong-coupling phase arising from the flattening of the dispersion near the van Hove singularity.

Furukawa *et al.* [183], examined the diamond Fermi surface of the Hubbard model on a square lattice at half filling, where the Fermi surface contains two distinct van

Hove singularities. Relying on a patch approximation, they only focused on the two van Hove singularities and restricting the interactions to intra- and inter-singularity interactions (the so-called *g-ology* approach). The non-locality can be seen in the one-loop intra-particle-particle and inter-particle-hole diagrams, which they found to be $\propto \log^2 \omega/E_0$ (ω is the transfer frequency and E_0 is their energy cutoff). Due to this log-square form of intra-particle-particle and inter-particle-hole susceptibilities, they defined their β-functions by taking the derivative of the running couplings with respect to $(\log E_0)^2$, which implies undermining non-analyticity of quantum corrections.

Nandkishore *et al.* [187], extended the analysis of Furukawa *et al.* [183] to the case of Graphene at $\frac{5}{8}$ filling where the Fermi surface contains three distinct singular points. As far as the physics near an isolated van Hove singularity is concerned, this study follows the same approach as that of Furukawa *et al.* [183].

Kapustin *et al.* [188], studied and isolated van Hove singularity described by the dispersion $\varepsilon_{\mathbf{k}} = k_x^2 - k_y^2$ in the presence of weak short-range interactions using dimensional regularization as to regularize the theory and extract counter terms. At one-loop order, they encountered a non-local interaction counter term of the particle-particle nature.

The main message of this chapter is that non-locality of the Wilsonian effective action at the critical point of the neck-narrowing Lifshitz transition is intrinsic and unavoidable, which was not paid enough attention to in the previous studies. By intrinsic non-locality of the effective action we mean that it is not an artifact of the specific regularization scheme that one chooses. Imposing a sharp cutoff results in the appearance of extrinsic non-local terms in the Wilsonian effective action, which can be removed by resorting to a soft energy cutoff. This is not the case here, and we encounter non-local terms even when all cutoffs are smooth. In addition, we show how one can recover the $\log^2 L$ growth of interactions within a consistent local perturbative RG approach, away from the critical point and in the presence of a finite momentum cutoff.

3.2 RG Analysis

In this section we present the details of our RG analysis. We start with the model that we study. Then we explain our RG scheme. Finally, the structure of one-loop quantum corrections and their implications are discussed.

3.2.1 Model

We study Fermi surfaces described by the quadratic dispersion relation $\varepsilon(\mathbf{k}) = k_x^2 - k_y^2$ together with a momentum cutoff K. The need for the momentum cutoff arises from the fact that this quadratic dispersion entails a non-compact Fermi surface. This momentum cutoff, in fact, plays the role of the size of the Fermi surface. Ideally, in studying neck-narrowing Lifshitz transitions, one should study dispersion relations that describe compact Fermi surfaces, such as the dispersion relation $\varepsilon(\mathbf{k}) = k_x^2 - k_y^2 + \frac{1}{K^2}k_y^4$ as shown in Fig. [3.4c]. However, such cases are more difficult to treat analytically. In this model the chemical potential controls the neck-narrowing transition with the critical point at $\mu_c = 0$ (see Fig. [3.5a]). At finite but small chemical potentials ($0 < \mu \ll K^2$) the Fermi surface has a narrow neck of the width $2\sqrt{\mu}$ as shown in Fig. [3.5b].

Note that, despite the fact that the momentum cutoff alone suppresses both high-energy and large-momentum modes, one should not treat the momentum cutoff as an energy cutoff and lower it in the course of RG. Lowering the momentum cutoff amounts to integrating out zero-energy modes (portions of the Fermi surface), which results in the appearance of non-analytic (hence non-local) terms. In this RG scheme the running of the couplings is generated by integrating out high-energy modes away from the Fermi surface.

The starting point of our RG analysis is the following regulated action:

$$
\begin{aligned}
\mathcal{S} &= \mathcal{S}_0 + \mathcal{S}_{\text{int}} \qquad (3.4)\\
\mathcal{S}_0 &= \int \frac{\mathrm{d}\mathbf{k}}{(2\pi)^2} \int \frac{\mathrm{d}\omega}{2\pi} \bar{\psi}_\sigma(\mathbf{k},\omega)\, \mathcal{G}_0^{-1}(\mathbf{k},\omega)\, \psi_\sigma(\mathbf{k},\omega)\\
\mathcal{S}_{int} &= g\Big[\prod_{i=1}^{3} \int \frac{\mathrm{d}\mathbf{k}_i}{(2\pi)^2} \int \frac{\mathrm{d}\omega_i}{2\pi}\Big]\\
&\qquad \bar{\psi}_\sigma(\mathbf{k}_1,\omega_1)\bar{\psi}_{\sigma'}(\mathbf{k}_2,\omega_2)\psi_{\sigma'}(\mathbf{k}_3,\omega_3)\psi_\sigma(\mathbf{k}_4,\omega_4)\\
&\qquad \delta(\mathbf{k}_1+\mathbf{k}_2-\mathbf{k}_3-\mathbf{k}_4)\,\delta(\omega_1+\omega_2-\omega_3-\omega_4)\,,
\end{aligned}
$$

where the partition function is given by,

$$
\mathcal{Z} = \int \mathcal{D}\psi\mathcal{D}\bar{\psi}\, e^{-\mathcal{S}}\,, \qquad (3.5)
$$

and,

$$\mathcal{G}_0(\mathbf{k},\omega) \;=\; -\frac{e^{-\frac{\xi(\mathbf{k})^2}{\Lambda^2}}\, e^{-\frac{|\mathbf{k}|^2}{K^2}}}{i\omega - \xi(\mathbf{k})} \tag{3.6}$$

is the regularized free propagator, and $\xi(\mathbf{k}) = k_x^2 - k_y^2 - \mu$. Here $|g| \ll 1$ is the coupling of the four-fermion contact density-density interaction. Note that the choice of smooth cutoffs is to maintain locality in the regulated theory. Since the energy and momentum cutoffs are included in the free propagator, the contribution of high-energy ($|\xi_{\mathbf{k}}| > \Lambda$) and large-momentum ($|\mathbf{k}| > K$) modes in computing diagrams are automatically suppressed.

The vertex of a quartic short-range interaction term is an analytic function of the form $\Gamma_{\sigma,\sigma'}(\mathbf{k}_1,\mathbf{k}_2,\mathbf{k}_3,\mathbf{k}_4)$, where $\sigma,\sigma' = \uparrow,\downarrow$. A marked difference between the RG scheme that we employ here and Shankar's RG is in the way that the momenta are rescaled. As explained in the previous section, in Shankar's RG it is $\Gamma_{\sigma,\sigma'}(\mathbf{K}_1,\mathbf{K}_2,\mathbf{K}_3,\mathbf{K}_4)$ ($\mathbf{K}_i = \mathbf{k}_F$) that is taken as the dimensionless marginal interaction vertex. In contrast, in our RG scheme, the momentum $\mathbf{k}$ is rescaled. Therefore, it is the leading term in the Taylor expansion of $\Gamma_{\sigma,\sigma'}(\mathbf{k}_1,\mathbf{k}_2,\mathbf{k}_3,\mathbf{k}_4)$ that gives the marginal quartic interaction vertex in our RG scheme, i.e., $g \equiv \Gamma_{\sigma,\sigma'}(0,0,0,0)$. Note that, because of the anticommutativity of fermions, the spin indices should be dissimilar ($\sigma \neq \sigma'$), as $\Gamma_{\sigma,\sigma'}(0,0,0,0)$ for $\sigma = \sigma'$ reduces to a chemical potential term.

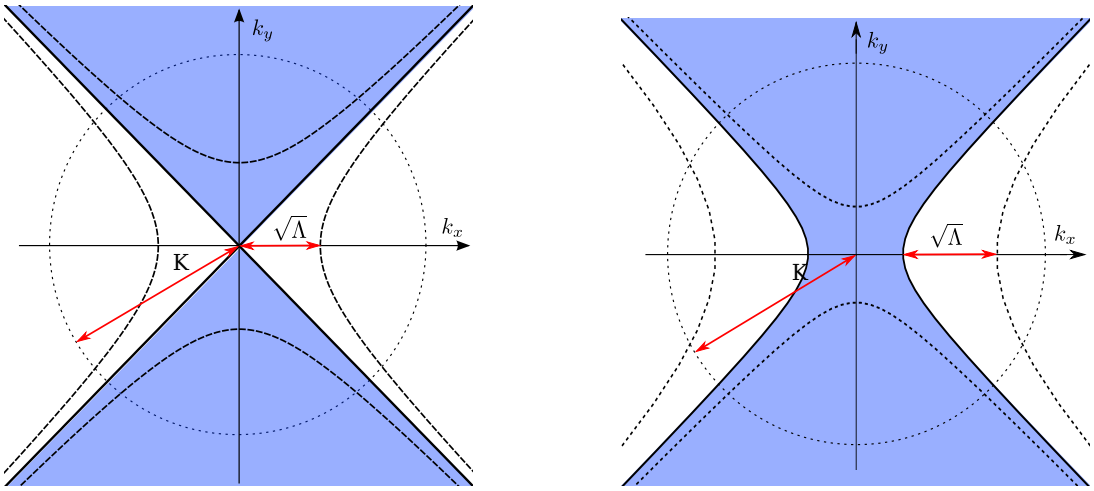

(a) $\mu = 0$ **(b)** $\mu > 0$

Figure 3.5: Fermi surfaces together with energy and momentum cutoffs at (a) the critical point of the neck-narrowing Lifshitz transition ($\mu = 0$), and (b) away from the transition point ($0 < \mu < \Lambda$). In (b) the width of the neck is $2\sqrt{\mu}$.

This model, at zero chemical potential, possesses a "pseudo-particle-hole" symmetry: invariance under the particle-hole transformation together with a $\frac{\pi}{2}$ rotation

in momentum space, which reverses the sign of $k_x^2 - k_y^2$. In the limit $K \to \infty$, this model manifests $O(1,1)$ symmetry in momentum space. However, the presence of the momentum cutoff spoils this symmetry.

3.2.2 RG Scheme

Since renormalizing towards the Fermi surface, when the Fermi surface contains a van Hove singularity, at the singular point is nonsensical, an RG approach different from Shankar's RG is required for Fermi surfaces that contain a van Hove singularity. In the model that we study here, at $\mu = 0$, lowering the energy cutoff Λ results in getting closer to the van Hove singularity. Rescaling momenta restores the lowered energy cutoff. As a result, in this RG scheme, the momentum cutoff K runs. Thus, in contrast with Shankar's RG, there is no kinematic constraint, and therefore all dimensionless vertices are equally important at tree level (i.e., all momentum-independent quartic interactions are marginal at tree level).

Slightly away from the critical point ($0 < \mu \ll \Lambda$), despite the fact that the van Hove singularity is no longer on the Fermi surface, we continue using the same RG scheme outlined above: renormalizing towards the singular point, which is now away from the Fermi surface. This results in the running of the chemical potential μ, in addition to the momentum cutoff K, and, thereby, the whole Fermi surface (at tree level, μ/K^2 remains constant) as shown in Fig. [3.6]. Our intention of employing this scheme is that we are interested in the evolution of the effective action as the energy cutoff is lowered: running of μ and K while Λ is held fixed, serves as a proxy for systematically lowering the energy cutoff.

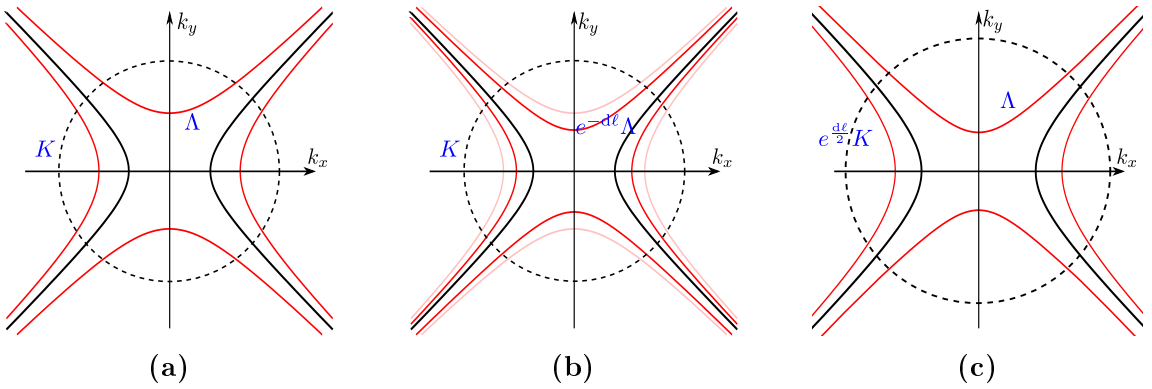

Figure 3.6: Running of K and μ in our RG scheme. (a) The Fermi surface with the momentum cutoff K, the energy cutoff Λ and the chemical potential $\mu > 0$. (b) The energy cutoff is lowered to $e^{-\mathrm{d}\ell}\Lambda$. (c) The energy cutoff is restored to Λ by rescaling momenta: $\mathbf{k} \to e^{\frac{\mathrm{d}\ell}{2}}\mathbf{k}$. This results in $\mu \to e^{\mathrm{d}\ell}\mu$ and $K \to e^{\frac{\mathrm{d}\ell}{2}}K$.

At tree level, the lowered energy cutoff $e^{-\mathrm{d}\ell}\Lambda$ (ℓ is the RG "time") can be restored

to Λ by:

$$\begin{cases} \mathbf{k} & \to & e^{\frac{1}{2}\mathrm{d}\ell}\ \mathbf{k} \\ \mu & \to & e^{\mathrm{d}\ell}\ \mu \\ \omega & \to & e^{\mathrm{d}\ell}\ \omega \\ K & \to & e^{\frac{1}{2}\mathrm{d}\ell}\ K \\ \{\psi,\psi^\dagger\} & \to & e^{-\frac{3}{2}\mathrm{d}\ell}\,\{\psi,\psi^\dagger\} \end{cases} \quad \to \quad \begin{cases} [\mathbf{k}] & = & \frac{1}{2} \\ [\mu] & = & 1 \\ [\omega] & = & 1 \\ [K] & = & \frac{1}{2} \\ [\psi] = [\psi^\dagger] & = & -\frac{3}{2} \end{cases} \tag{3.7}$$

From the above tree-level scaling dimensions we obtain $[g] = 0$, which implies that g is marginal.

At one-loop order, we have diagrams shown in Figs. [3.7,3.8]. Among the diagrams in Fig. [3.7] that renormalize the interaction vertex, the diagram in Fig. [3.7b] (the so-called penguin diagram) is not allowed as it requires same spin indices on all four legs of one of the vertices. Diagrams in Fig. [3.7a] and Fig. [3.7c] do not vanish and involve the exchange of a particle and a hole, while the diagram in Fig. [3.7d] involves a pair of particles. Note that the contributions of the diagrams in Fig. [3.7a] and Fig. [3.7c] to the interaction vertex are distinct due to the spin indices of the external legs, nevertheless they have the same loop integral:

$$\begin{aligned} \Gamma^{\text{Ladder}}_{\text{PH}}(\mathbf{q},\Omega) \ &= \ -\,\Pi_{\text{PH}}(\mathbf{q},\Omega) \ = \ \int \frac{\mathrm{d}\mathbf{k}}{(2\pi)^2} \int_{-\infty}^{\infty} \frac{\mathrm{d}\omega}{2\pi}\, \mathcal{G}^0(\omega,\mathbf{k})\, \mathcal{G}^0(\omega+\Omega,\mathbf{k}+\mathbf{q}) \\ &= \int \frac{\mathrm{d}\mathbf{k}}{(2\pi)^2} \frac{\theta(\xi_{\mathbf{k}}) - \theta(\xi_{\mathbf{k}+\mathbf{q}})}{i\Omega - \xi(\mathbf{k}+\mathbf{q}) + \xi(\mathbf{k})} e^{-\frac{\xi^2_{\mathbf{k}}+\xi^2_{\mathbf{k}+\mathbf{q}}}{\Lambda^2}} e^{-\frac{|\mathbf{k}|^2+|\mathbf{k}+\mathbf{q}|^2}{K^2}} . \end{aligned} \tag{3.8}$$

The diagram in Fig. [3.7d] is given by:

$$\begin{aligned} \Gamma_{\text{PP}}(\mathbf{q},\Omega) \ &= \int \frac{\mathrm{d}\mathbf{k}}{(2\pi)^2} \int_{-\infty}^{\infty} \frac{\mathrm{d}\omega}{2\pi}\, \mathcal{G}^0(-\omega,-\mathbf{k})\, \mathcal{G}^0(\omega+\Omega,\mathbf{k}+\mathbf{q}) \\ &= -\int \frac{\mathrm{d}\mathbf{k}}{(2\pi)^2} \frac{\theta(\xi_{\mathbf{k}}) - \theta(-\xi_{\mathbf{k}+\mathbf{q}})}{i\Omega - \xi(\mathbf{k}+\mathbf{q}) - \xi(\mathbf{k})} e^{-\frac{\xi^2_{\mathbf{k}}+\xi^2_{\mathbf{k}+\mathbf{q}}}{\Lambda^2}} e^{-\frac{|\mathbf{k}|^2+|\mathbf{k}+\mathbf{q}|^2}{K^2}} . \end{aligned} \tag{3.9}$$

The renormalized interaction term at one-loop order is given by:

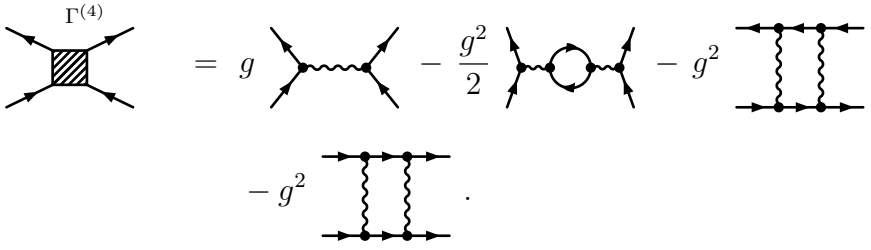

(3.10)

We postpone the discussion of the structure of $\partial_{\log\Lambda}\Gamma^{\text{Ladder}}_{\text{PH}}(\mathbf{q},0)$ and $\partial_{\log\Lambda}\Gamma_{\text{PP}}(\mathbf{q},0)$ to the next subsection.

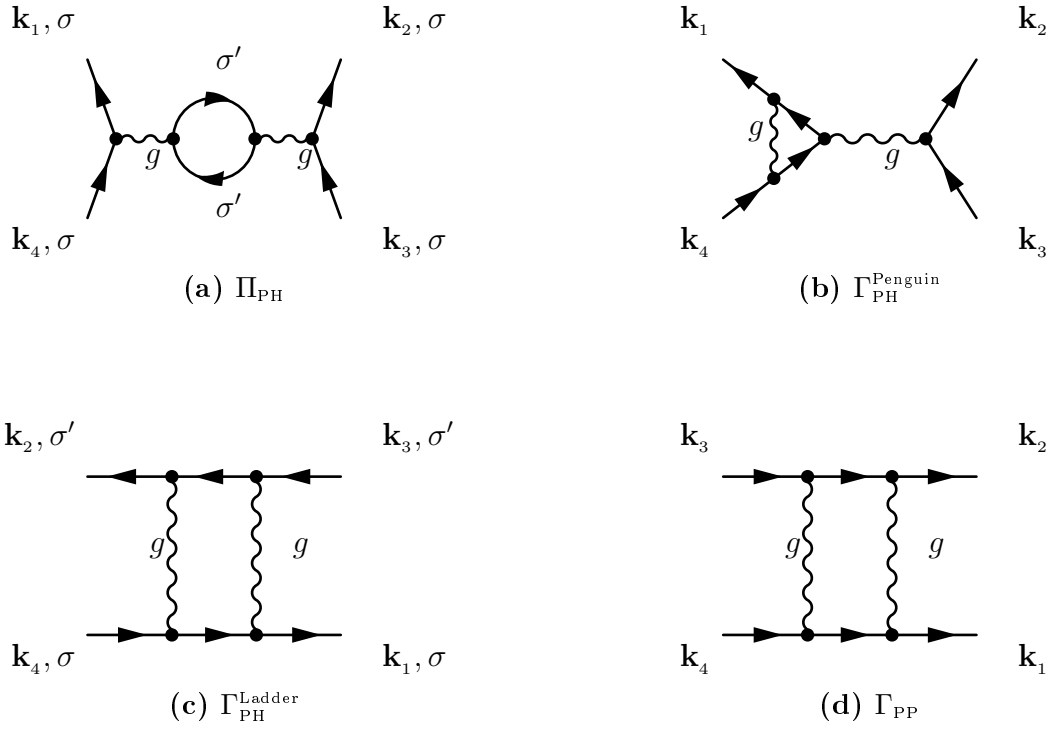

Figure 3.7: Diagrams that renormalize four-fermion interactions at one-loop order. In order to keep track of the spin indices, a wiggly line is used for the marginal density-density interaction even though the vertex of this interaction is momentum-independent. Diagrams (a), (b) and (c) involve the exchange of a particle and a hole, whereas diagram (d) is a particle-particle diagram. Diagram (a) is the usual particle-hole bubble Π_{PH}, diagram (b) is the penguin diagram, diagram (c) is a one-loop ladder diagram $\Gamma_{\mathrm{PH}}^{\mathrm{Ladder}}$.

Diagrams shown in Fig. [3.8] contribute to the renormalization of the chemical potential at one-loop order. The pseudo-particle-hole symmetry at $\mu = 0$ ensures that the contribution of these diagrams (as well as all higher-order corrections to the chemical potential) vanishes. For $\mu > 0$, $\partial_{\log\Lambda}\Sigma^{(1)} \propto g\mu$ (with no singular dependence on K as $K \to \infty$), and is negligible. Since we assume that the bare interaction vertex is momentum independent, momentum-dependent self-energy contribution first appears at a two-loop self-energy diagram. Note that, the momentum dependent self-energy obtained from the diagram in Fig. [3.8b] with weak, short-range interactions instead of the contact density-density interactions that we consider here, will only result in trivial ($\propto \mu$ and $\mathcal{O}(g)$) field renormalizations.

(a) $\Sigma^{(1)}$ **(b)** $\Sigma^{(1)}$

Figure 3.8: Self-energy diagrams at one-loop order. Since we are considering a momentum-independent bare interaction vertex with different spin indices the Fock diagram, (b), is not allowed.

Assuming analyticity of quantum corrections, one-loop $\beta-$functions for local operators are obtained from the Taylor expansion of the one-loop quantum corrections:

$$\begin{aligned}
\dot{g} &= -g^2\,\partial_{\log\Lambda}\Gamma^{\text{Ladder}}_{\text{PH}}(0,0) - g^2\,\partial_{\log\Lambda}\Gamma_{\text{PP}}(0,0)\\
\dot{g}^{\{n,m\}}_{\text{PH}} &= -(n+m)\,g^{\{n,m\}}_{\text{PH}} - g^2\,\frac{\partial^{2n}}{\partial q_x^{2n}}\frac{\partial^{2m}}{\partial q_y^{2m}}\partial_{\log\Lambda}\Gamma^{\text{Ladder}}_{\text{PH}}(\mathbf{q},0)\big|_{q=0}\\
\dot{h}^{\{n,m\}}_{\text{PH}} &= -(n+m)\,h^{\{n,m\}}_{\text{PH}} - \frac{g^2}{2}\,\frac{\partial^{2n}}{\partial q_x^{2n}}\frac{\partial^{2m}}{\partial q_y^{2m}}\partial_{\log\Lambda}\Pi_{\text{PH}}(\mathbf{q},0)\big|_{q=0}\\
\dot{g}^{\{n,m\}}_{\text{PP}} &= -(n+m)\,g^{\{n,m\}}_{\text{PP}} - g^2\,\frac{\partial^{2n}}{\partial q_x^{2n}}\frac{\partial^{2m}}{\partial q_y^{2m}}\partial_{\log\Lambda}\Gamma_{\text{PP}}(\mathbf{q},0)\big|_{q=0}\\
\dot{K} &= \frac{1}{2}K\\
\dot{\mu} &= \mu + \mathcal{O}(g)\,.
\end{aligned} \tag{3.11}$$

Here, g is the coupling of the momentum-independent interaction term, $g^{\{n,m\}}_{\text{PH}}$ (differ-

ent spin) and $h_{\rm PH}^{\{n,m\}}$ (same spin) are the couplings of the following (by-power-counting) irrelevant interaction term:

$$\mathcal{S}_{\rm PH}^{\{n,m\}} = \Big[g_{\rm PH}^{\{n,m\}}(1-\delta_{\sigma,\sigma'}) + h_{\rm PH}^{\{n,m\}}\delta_{\sigma,\sigma'}\Big] \int \frac{\mathrm{d}\mathbf{k}}{(2\pi)^2}\frac{\mathrm{d}\omega}{2\pi}\int \frac{\mathrm{d}\mathbf{k}'}{(2\pi)^2}\frac{\mathrm{d}\omega'}{2\pi}\int \frac{\mathrm{d}\mathbf{q}}{(2\pi)^2}\frac{\mathrm{d}\Omega}{2\pi}$$
$$\bar\psi_\sigma(\mathbf{k},\omega)\,\psi_\sigma(\mathbf{k}+\mathbf{q},\omega+\Omega)\,\frac{q_x^{2n}}{\Lambda^n}\frac{q_y^{2m}}{\Lambda^m}\,\bar\psi_{\sigma'}(\mathbf{k}'+\mathbf{q},\omega'+\Omega)\,\psi_{\sigma'}(\mathbf{k}',\omega')\,, \quad (3.12)$$

and $g_{\rm PP}^{\{n,m\}}$ is the coupling constant of:

$$\mathcal{S}_{\rm PP}^{\{n,m\}} = g_{\rm PP}^{\{n,m\}} \int \frac{\mathrm{d}\mathbf{k}}{(2\pi)^2}\frac{\mathrm{d}\omega}{2\pi}\int \frac{\mathrm{d}\mathbf{k}'}{(2\pi)^2}\frac{\mathrm{d}\omega'}{2\pi}\int \frac{\mathrm{d}\mathbf{q}}{(2\pi)^2}\frac{\mathrm{d}\Omega}{2\pi} \quad (3.13)$$
$$\bar\psi_{\sigma'}(\mathbf{k}+\mathbf{q},\omega+\Omega)\,\bar\psi_\sigma(-\mathbf{k},-\omega)\,\frac{q_x^{2n}}{\Lambda^n}\frac{q_y^{2m}}{\Lambda^m}\,\psi_\sigma(\mathbf{k}'+\mathbf{q},\omega'+\Omega)\,\psi_{\sigma'},(-\mathbf{k}',-\omega')\,.$$

Diagramatic representation of these irrelevant interactions are shown in Fig. [3.9].

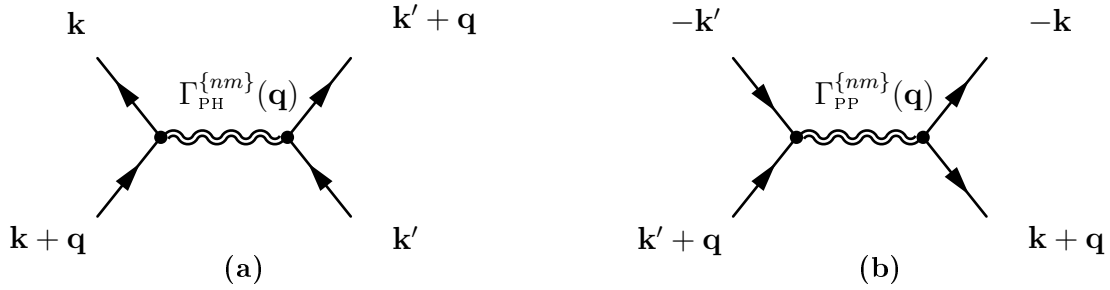

Figure 3.9: Diagramatic representation of irrelevant particle-particle and particle-hole interactions $\mathcal{S}_{\rm PP}^{\{n,m\}}$ and $\mathcal{S}_{\rm PH}^{\{n,m\}}$.

3.2.3 One-Loop Quantum Corrections

Here we show that the Wilsonian effective action at the critical point of the neck-narrowing transition is intrinsically non-local. Also, we demonstrate that slightly away from the critical point, locality can be retained only in the presence of the momentum cutoff in our model that keeps the size of the Fermi surface finite. Even then, the quantum corrections are analytic within a finite momentum range, related to the width of the neck. Within this analytic range, we determine the β-functions and find that, due to the running of K in this RG scheme, a negative g (attractive four-fermion contact interactions) grows as $\ell^2 = \log^2 L$.

To lay out our arguments, we primarily focus on one-loop particle-hole quantum corrections $\partial_{\log\Lambda}\Gamma_{\rm PH}(\mathbf{q},\omega=0)$ (form here on, we use $\Gamma_{\rm PH} \equiv \Gamma_{\rm PH}^{\rm Ladder} = -\Pi_{\rm PH}$) for $\mathbf{q} = q\hat{x}$. In the absence of any momentum regulator ($K\to\infty$), where the $O(1,1)$

symmetry of the model is intact, any dependence on $\mathbf{q}$ is through $q_x^2 - q_y^2$. Thus, it suffices to determine the dependence of any diagram with the transfer momentum $\mathbf{q}$ on $q_x^2 - q_y^2$ for only three representative directions: $\mathbf{q} = q\hat{x}$ for x-like momenta ($q_x^2 - q_y^2 > 0$), $\mathbf{q} = q\hat{y}$ for y-like momenta ($q_x^2 - q_y^2 < 0$) and $\mathbf{q} = \frac{q}{\sqrt{2}}(\hat{x} + \hat{y})$ for null momenta ($q_x^2 - q_y^2 = 0$). The presence of the momentum regulator ($K < \infty$), however, spoils this symmetry. Despite this, we restrict the computation of $\partial_{\log\Lambda}\Gamma_{\text{PH}}$ to $\mathbf{q} = q\hat{x}$. Thus, assuming the analyticity of quantum corrections, of the interaction vertices in Eq. (3.12) we only have access to those with $m = 0$.

Slightly away from the critical point of the neck-narrowing transition ($0 < \mu \ll K^2, \Lambda$), for any x-like transfer momentum $\mathbf{q}$ ($q_x^2 - q_y^2 > 0$), $\partial_{\log\Lambda}\Gamma_{\text{PH}}(\mathbf{q}, 0)$ is analytic as long as $q_x^2 - q_y^2 < 4\mu$. Non-analyticity at $q_x^2 - q_y^2 = 4\mu$ stems from the well-known $2k_F$ singularity, which arises when the transfer momentum $\mathbf{q}$ connects antipodal points on the Fermi surface, as shown in Fig. [3.10]. For $\mathbf{q} = q\hat{x}$, this implies that $\partial_{\log\Lambda}\Gamma_{\text{PH}}(q\hat{x}, 0)$ is non-analytic at $q = 2\sqrt{\mu}$.

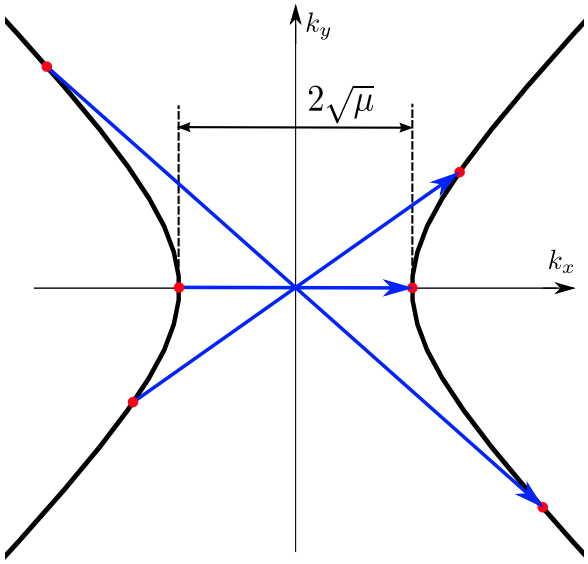

Figure 3.10: All three indicated vectors satisfying $\xi_{\mathbf{q}} = 4\mu$ and connecting antipodal points correspond to "$2k_F$" momentum transfers $\mathbf{q}$ on the Fermi surface.

For $\partial_{\log\Lambda}\Gamma_{\text{PH}}(q\hat{x},0)$ we obtain the following series expansion in q (see Appendix [B.3]):

$$\begin{aligned}\partial_{\log\Lambda}\Gamma_{\text{PH}}(q\hat{x},0) \approx \frac{1}{2(2\pi)^2}\Bigg[&8\frac{K^2}{\Lambda}\frac{q^2}{\Lambda}+\Big(19.7\log\frac{\mu}{K^2}+101-5.6\frac{K^4}{\Lambda^2}\Big)\frac{q^4}{\Lambda^2}\\
&+\Big(-1.87\frac{\Lambda}{\mu}+\Big[22.8\frac{K^2}{\Lambda}+86\frac{\Lambda}{K^2}\Big]\log\frac{\mu}{K^2}+4.11\frac{K^6}{\Lambda^3}+162\frac{K^2}{\Lambda}\Big)\frac{q^6}{\Lambda^3}\\
&+\Big(-0.13\frac{\Lambda^2}{\mu^2}-2.06\frac{K^2}{\mu}+\Big[237\frac{\Lambda^2}{K^4}+255+8.7\frac{K^4}{\Lambda^2}\Big]\log\frac{\mu}{K^2}+1462\\
&-71.5\frac{K^4}{\Lambda^2}-3.16\frac{K^8}{\Lambda^4}\Big)\frac{q^8}{\Lambda^4}+\Big(-0.014\frac{\Lambda^3}{\mu^3}-0.138\frac{K^2}{\Lambda\mu^2}-0.326\frac{\Lambda^3}{K^2\mu^2}\\
&-0.716\frac{K^4}{\Lambda\mu}-17.13\frac{\Lambda}{\mu}-12.98\frac{\Lambda^3}{K^4\mu}+\Big[-1.262\frac{K^6}{\Lambda^3}+305\frac{K^2}{\Lambda}+1082\frac{\Lambda}{K^2}\\
&+483\frac{\Lambda^3}{K^6}\Big]\log\frac{\mu}{K^2}+2.52\frac{K^{10}}{\Lambda^5}+9.235\frac{K^6}{\Lambda^3}+1987\frac{K^2}{\Lambda}\Big)\frac{q^{10}}{\Lambda^5}+\mathcal{O}(q)^{12}\Bigg],\end{aligned}\tag{3.14}$$

where we have ignored all $\mathcal{O}(\mu)$ and $\mathcal{O}(1/K)$ terms.

Let us explain the origin of different K- and μ-dependent terms in this series expansion. First consider terms singular in μ. Since the above series expansion is valid only for $q < 2\sqrt{\mu}$ and singular terms in μ are accompanied by sufficiently high powers of q, there is no divergence in Eq. (3.14) as $\mu \to 0$. Singular dependence on μ first appears at $\mathcal{O}(q^4)$. This feature depends on the choice of the energy cutoff. If instead of $\exp(-\xi_{\mathbf{k}}^2/\Lambda^2)$ we imposed, for example, $\exp(-\xi_{\mathbf{k}}^4/\Lambda^4)$, singular dependence on μ would first appear at $\mathcal{O}(q^6)$. More generally, for an energy cutoff of the form $\exp(-\xi_{\mathbf{k}}^{2n}/\Lambda^{2n})$, singular terms in μ appear at $\mathcal{O}(q^{2n+2})$. Note that, in the limit $n \to \infty$, where the energy cutoff becomes the sharp energy cutoff $\theta(1-\frac{|\xi_{\mathbf{k}}|}{\Lambda})$, the singular terms completely disappear. This can be understood as follows. With a soft-energy cutoff, although quantum corrections are most sensitive to modes at the energy scale Λ, they nevertheless weakly sense all other modes. This is because the derivative of a soft energy regulator with respect to $\log\Lambda$ is not a δ-function. Thus, the appearance of an IR singularity upon setting μ to zero is "sensed" by quantum corrections (in this case, $\partial_{\log\Lambda}\Gamma_{\text{PH}}$).

Another important feature of the series expansion in Eq. (3.14) is the presence of terms with positive powers of K. These terms indicate that the series expansion breaks down not only when $q = 2\sqrt{\mu}$, as discussed above, but also when $q < \frac{\Lambda}{K}$. Note that, unlike terms singular in μ, the appearance of these terms is not sensitive to the details of the energy cutoff. The origin of non-analyticity at $q \simeq \Lambda/K$ becomes evident when both cutoffs are imposed sharply. As depicted in Fig [3.11], when both cutoffs are sharp the smaller $|\mathbf{q}|$, the farther from the origin the modes that are decimated

lie. This will result in non-analyticity of $\partial_{\log\Lambda}\Gamma_{\text{PH}}(\mathbf{q},0)$ as it will be proportional to $\theta(1-\frac{\Lambda^2}{q^2K^2})$. Note that this applies to both $\mu=0$ and $\mu\ll\Lambda,K^2$. Imposing a soft momentum cutoff, while maintaining a sharp energy cutoff, will not cure this non-analyticity and only results in a softer non-analytic dependence on q. For our momentum regulator $\exp(-|\mathbf{k}|^2/K^2)$, one finds non-analytic dependence on $|\mathbf{q}|$ in $\partial_{\log\Lambda}\Gamma_{\text{PH}}(\mathbf{q},\Omega)$ of the form $\exp(-\frac{\Lambda^2}{|\mathbf{q}|^2K^2})$. When both cutoffs are imposed softly, this aspect of the problem manifests itself as a finite convergence radius $q<\Lambda/K$.

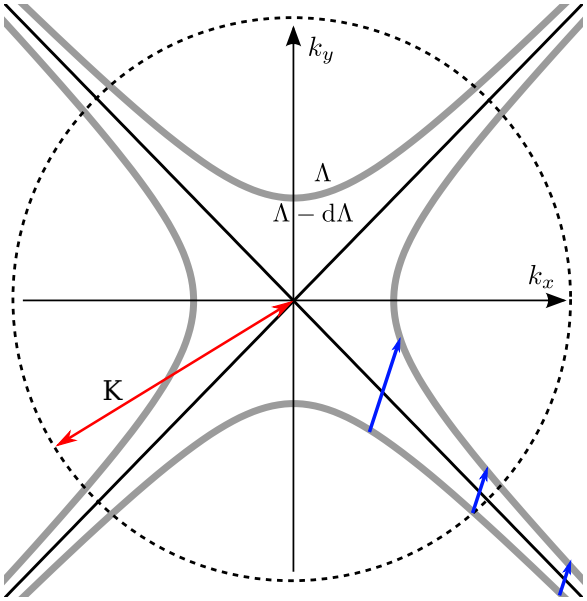

Figure 3.11: When both cutoffs are imposed sharply, as depicted in this figure, for smaller $|\mathbf{q}|$, the eliminated modes will be farther from the origin. Thus, if $|\mathbf{q}|$ is sufficiently small ($<\frac{\Lambda}{K}$) $\partial_{\log\Lambda}\Gamma_{\text{PH}}(\mathbf{q},\Omega)$ suddenly vanishes (as a result of using sharp cutoffs). When both cutoffs are imposed softly, as discussed in the text, this feature results in the convergence radius $q<\Lambda/K$ in $\partial_{\log\Lambda}\Gamma_{\text{PH}}$.

As shown in the previous subsection, the β-function of g (the coupling of the contact density-density interaction) receives a contribution from $\partial_{\log\Lambda}\Gamma_{\text{PP}}(0,0)$ (see Eq. (3.11)). For $\Gamma_{\text{PP}}(\mathbf{q}=0,\Omega\ll\Lambda)$ we obtain:

$$\Gamma_{\text{PP}}(\mathbf{q}=0,\Omega\ll\Lambda)\approx\frac{1}{(2\pi)^2}\left[\log\frac{K^2}{\Lambda}\log\left(1+\frac{4\Lambda^2}{\Omega^2}\right)+\frac{1}{4}\log^2\left(\frac{\Omega^2}{4\Lambda^2}\right)\right], \tag{3.15}$$

where, we have only kept singular terms in Ω. From Eq. (3.15) we find:

$$\partial_{\log\Lambda}\Gamma_{\text{PP}}^{\mu=0}(0,\Omega)\approx\frac{1}{(2\pi)^2}\left[\frac{8\Lambda^2}{4\Lambda^2+\Omega^2}\log\frac{K^2}{\Lambda}-\log\left(1+\frac{\Omega^2}{4\Lambda^2}\right)+\mathcal{O}(\frac{\Omega^2}{\Lambda^2})\right], \tag{3.16}$$

which, in the limit $\Omega \to 0$, reduces to $\frac{1}{2\pi^2}\log\frac{K^2}{\Lambda}$.

The series expansion in Eq. (3.14) indicates that as $\mu \to 0$ the quantum corrections become non-analytic. Indeed, we find that at the critical point of the neck-narrowing transition ($\mu = 0$), $\partial_{\log\Lambda}\Gamma_{\text{PH}}(q\hat{x}, 0)$ is non-analytic in q. Isolating the non-analytic terms, for small q we obtain the following series expansion in q (see Appendix [B.2] for the computational details):

$$\partial_{\log\Lambda}\Gamma^{\text{non-analytic}}_{\text{PH}}(q\hat{x},0) = \frac{1}{(2\pi)^2}\Bigg[-0.028\frac{q^4}{\Lambda^2} - 0.368\frac{K^2}{\Lambda}\frac{q^6}{\Lambda^3} + \Big(0.473\frac{K^4}{\Lambda^2} + 0.448\Big)\frac{q^8}{\Lambda^4} - \Big(0.55\frac{K^6}{\Lambda^3} + 0.6\frac{K^2}{\Lambda}\Big)\frac{q^{10}}{\Lambda^5} + \mathcal{O}(\frac{q^{12}}{\Lambda^6})\Bigg]\log\frac{q^2}{K^2}\,. \tag{3.17}$$

The β-functions of g, and the couplings of the first five tree-level irrelevant vertices $g^{\{n\}}_{\text{PH}} \equiv g^{\{n,0\}}_{\text{PH}}$ are obtained from Eq. (3.14). These β-functions describe the evolution of the effective action when $\mu > 0$ and for transfer momenta within the convergence radius of quantum corrections. From here on we set Λ to 1 for brevity (Λ can be restored by $K^2 \to K^2/\Lambda$ and $\mu \to \mu/\Lambda$). The one-loop β-functions are:

$$\dot{g} = -\frac{g^2}{2\pi^2}\log K^2 \tag{3.18a}$$

$$\dot{g}^{\{1\}}_{\text{PH}} = -g^{\{1\}}_{\text{PH}} - \frac{g^2}{2(2\pi)^2}8K^2 \tag{3.18b}$$

$$\dot{g}^{\{2\}}_{\text{PH}} = -2g^{\{2\}}_{\text{PH}} - \frac{g^2}{2(2\pi)^2}\Big(19.7\log\frac{\mu}{K^2} + 101 - 5.6K^4\Big) \tag{3.18c}$$

$$\dot{g}^{\{3\}}_{\text{PH}} = -3g^{\{3\}}_{\text{PH}} - \frac{g^2}{2(2\pi)^2}\Big(-\frac{1.87}{\mu} + \Big[22.8K^2 + \frac{86}{K^2}\Big]\log\frac{\mu}{K^2} + 4.11K^6 + 162K^2\Big) \tag{3.18d}$$

$$\dot{g}^{\{4\}}_{\text{PH}} = -4g^{\{4\}}_{\text{PH}} - \frac{g^2}{2(2\pi)^2}\Big(-\frac{0.13}{\mu^2} - 2.06\frac{K^2}{\mu} + \Big[\frac{237}{K^4} + 255 + 8.7K^4\Big]\log\frac{\mu}{K^2} + 1462 - 71.5K^4 - 3.16K^8\Big) \tag{3.18e}$$

$$\dot{g}^{\{5\}}_{\text{PH}} = -5g^{\{5\}}_{\text{PH}} - \frac{g^2}{2(2\pi)^2}\Big(-\frac{0.014}{\mu^3} - \frac{0.138K^2}{\mu^2} - \frac{0.326}{K^2\mu^2} - 0.716\frac{K^4}{\mu} - \frac{17.13}{\mu} - \frac{12.98}{K^4\mu} + \Big[-1.262K^6 + 305K^2 + \frac{1082}{K^2} + \frac{483}{K^6}\Big]\log\frac{\mu}{K^2} + 2.52K^{10} + 9.235K^6 + 1987K^2\Big)\,. \tag{3.18f}$$

where, $K = K_0 e^{\ell/2}$ and $\mu = \mu_0 e^{\ell}$ (ℓ is the RG "time", $\mu_0 = \mu_{\ell=0}$ and $K_0 = K_{\ell=0}$ are

the initial values). The β-function of g can be solved analytically:

$$g(\ell) = \frac{2\pi^2}{\ell \log K_0^2 + \frac{1}{2}\ell^2 + \frac{1}{g_0}}, \tag{3.19}$$

where $g_0 = g_{\ell=0}$. Thus, g is marginally relevant if $g_0 < 0$ (attractive) and is marginally irrelevant if $g_0 > 0$ (repulsive). The quadratic term in ℓ in the denominator of Eq. (3.19) is due to the running of K from the $\log K$ contribution of $\partial_{\log\Lambda}\Gamma_{\rm PP}(\mathbf{q} = 0, \Omega = 0)$ to the marginal four-fermion interaction term. For an attractive bare interaction ($g_0 < 0$), $|g(\ell)|$ reaches unity at $\ell^* = -\log K_0^2 + \sqrt{\log^2 K_0^2 + \frac{2}{|g_0|} + 4\pi^2}$. Thus, for $|g_0| \ll 1$ and $K_0^2 \simeq 1$ (recall that we set $\Lambda = 1$), $\ell^* \propto 1/\sqrt{|g_0|}$. The rest of the β-functions can be solved numerically.

Observe that, the β-functions of more irrelevant couplings contain higher powers of K. For example, there is a K^{10} term in the in the β-function of $g_{\rm PH}^{\{5\}}$ (Eq. (3.18f)). This is the reflection of the finiteness of the convergence radius. Note that, although the coupling constants of irrelevant interactions grow large, the overall strength of such irrelevant interaction vertices remains small, due to the restriction of the transfer momentum to the convergence radius of the Taylor expansion of $\partial_{\log\Lambda}\Gamma_{\rm PH}$.

The analytic window, within which one can describe the evolution of effective interactions by the above β-functions, changes in the course of RG as shown in Fig. [3.12]. Regardless of the details of the cutoffs (even for a sharp cutoff), by the time that the energy cutoff has been sufficiently lowered ($\Lambda \lesssim \mu$) this analytic window has shrunk to $\mathcal{O}(\frac{\mu}{K})$. This indicates the strong dependence of quantum corrections on $\mathbf{q}$ that cannot be captured entirely in terms of local operators.

Finally, we point out that the this feature of this model that there is a non-analyticity at $|\mathbf{q}| \simeq \frac{\Lambda}{K}$, independent of the details of the energy and momentum regulator, is already manifest in the imaginary part of the particle-hole susceptibility $\chi''_{\rm PH}(q\hat{x}, \Omega)$, as shown in Fig. [3.13].

3.3 Summary and Conclusions

In summary, in this chapter we examined a two-dimensional neck-narrowing Lifshitz transition in the presence of weak interactions using an RG approach in a model described by the dispersion $\varepsilon(\mathbf{k}) = k_x^2 - k_y^2$ together with a momentum cutoff K. We argued that this simple model serves as an approximation to more realistic Fermi surfaces, and is expected to capture the essential features of common neck-narrowing Lifshitz transitions in two-dimensions in the presence of interactions. Thus, the momentum cutoff K in our simple model, which keeps the size of the Fermi surface finite, should be regarded as the full size of the Fermi surface. This model undergoes a neck-narrowing Lifshitz transition as the chemical potential is varied, with the critical point at $\mu_c = 0$. Slightly away from the critical point, the Fermi surface has a narrow neck of the width $2\sqrt{\mu}$. Our main goals were to determine the effect of interactions on the

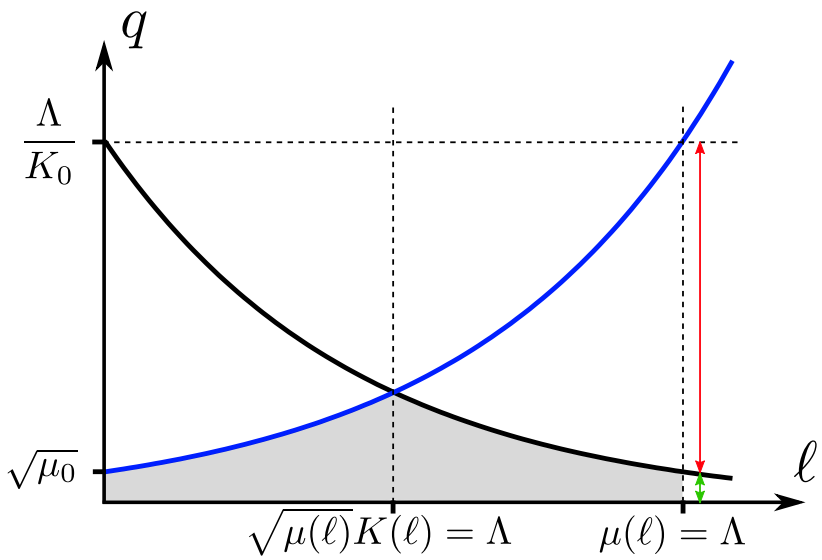

Figure 3.12: The analytic range of $\partial_{\log\Lambda}\Gamma_{\text{PH}}(q)$ in the course of RG is indicated by the shaded region. Initially, the width of the neck (due to the $2k_F$ physics) determines this analytic window (blue curve). Beyond the point $\sqrt{\mu(\ell)}K(\ell) = \Lambda$, it is Λ/K that dictates analytic range of quantum corrections (the black curve). Starting from a microscopic scale ($\Lambda \simeq K^2$), by the time that the energy cutoff has been sufficiently lowered, the analytic window has shrunk to $\mathcal{O}(\frac{\mu}{K})$.

Fermi surface at and close to the critical point of the transition.

We rigorously showed that, at the critical point of the neck-narrowing Lifshitz transition, the Wilsonian effective action is intrinsically non-local. This non-locality is due to the presence of the van Hove singularity, which results in non-analytic quantum corrections, and is not the artifact of the regularization scheme we chose. The non-locality of the effective action at the critical point is attributed to integrating out an emergent soft collective degree of freedom related to the critical fluctuations of the Fermi surface topology.

Precise identification of this emergent degree of freedom and devising a completely local description similar to those in symmetry breaking phase transitions in metals are left to future works. In principle, the nature of the suggested emergent soft degree of freedom at the critical point of the neck-narrowing Lifshitz transition can be inferred from the generated non-local terms. However, in contrast with the Ising-nematic phase transitions, this emergent degree of freedom may not be as simple. More precisely, if this emergent soft mode, aside from the coupling to the low-energy fermions, is an interacting mode, then identifying it based on the non-locality it entails upon being integrated out becomes extremely challenging and most likely practically impossible. An equally important and related question is how exactly this emergent soft mode is coupled to low-energy fermions, which again in principle can be addressed based on the structure of the non-local terms. Further insight into the nature of this emergent

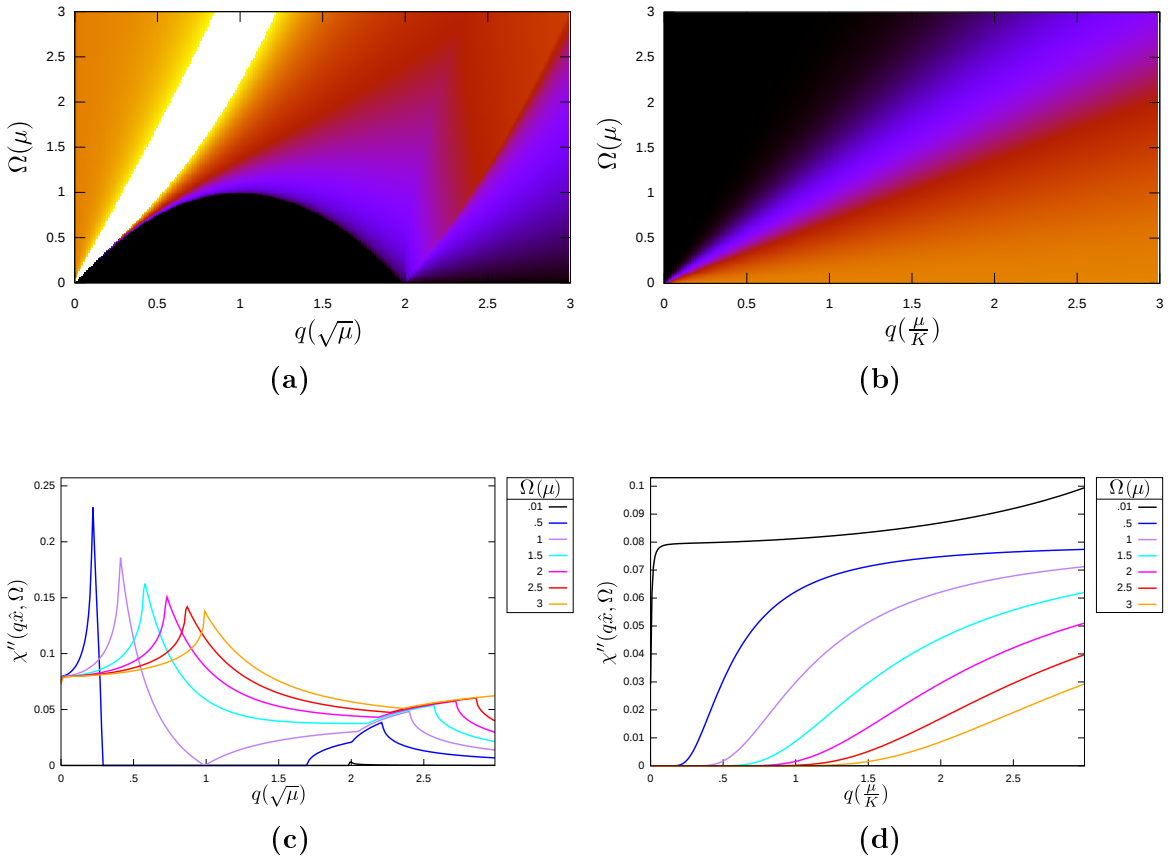

Figure 3.13: (a) Density plot of the imaginary part of the particle-hole susceptibility, $\chi''_{\rm PH}(q\hat{x},\Omega)$ computed for $K = 1000\sqrt{\mu}$. (b) Density plot of $\chi''_{\rm PH}(q\hat{x},\Omega)$ to small q values. (c) Constant Ω slices. (D) Constant Ω slices in the small q region. Non-analytic behavior for $q < \frac{\Omega}{K}$ is reflected by the sudden drop close to the vertical axis in (a) and almost flat curves at small q in (b).

degree of freedom may be gained based on the topological role that it plays in this transition.

As discussed here, due to the non-localities that appear at the critical point in the low-energy effective action, the application of local RG approaches are inconclusive. Aside from the above proposal to retain locality by isolating the emergent gapless mode responsible for the appearance of the non-local terms, it might be illuminating to try to recover locality by introducing a control parameter. One viable route is to extend the co-dimension of the Fermi surface, which suppresses the divergent density of states. Starting from the co-dimension $1+\epsilon$, this approach may allows for determining how precisely non-locality is developed as one approaches the physical co-dimension 1.

We demonstrated that the locality of the effective action can be restored only away from the critical point ($\mu \neq 0$) and in the presence of the momentum cutoff. Even then, the quantum corrections are analytic within a finite momentum range, which shrinks as the critical point is approached. Within this analytic window, we derived the β-functions for the couplings of marginal and irrelevant interactions, and captured the $\log^2 L$ growth of weak attractive contact density-density interactions in a consistent RG picture. This growth is faster than $\log L$ expected for ordinary marginal couplings due to the running of the momentum cutoff in this RG, which is treated as a dimensionful coupling constant. The finiteness of the analytic window, which is proportional to the width of the neck is indicative of the strong momentum dependence of quantum corrections that cannot be entirely captured by local operators. In analogy with Ising-nematic phase transitions in metals, this development of non-locality as the critical point of the neck-narrowing transition is approached lends further support to the idea of an independent degree of freedom at low energies (the analog of the Ising order parameter) that couples to the Fermi surface and becomes gapless at the critical point.

Chapter 4

Conclusions and Outlook

In this final chapter, we draw some general conclusions about the use of RG approaches in studying strongly correlated condensed matter systems based on what we saw in the RG analyses of the preceding chapters. We conclude this short chapter by a few comments on the prospect of RG-based approaches that reach beyond the scope of local perturbative RG schemes.

4.1 Summary

We started with the premise that condensed matter systems fall into universality classes that are uniquely labelled by the common phase of systems within each class. We argued that, while any system in a universality class serves as a representative for that universality class, universality classes are best typified by fixed-point theories, which are theories that possess no non-universal properties and are scale invariant. We illustrated how these ideas materialize as effective field theory and RG statements about the low-energy effective field theories of condensed matter systems. We learned that fixed-point theories are indeed privileged as they are invariant under the action of RG, and all systems within the same universality class ultimately flow to the fixed-point theory that characterizes that universality class. Thus, the question of the fate of a given system becomes synonymous to the question of to what fixed point the low-energy effective field theory of the system flows under RG.

While the notion of RG is very elegant and powerful, implementing it in practice may not be easy. Nonetheless, as we saw, under the assumptions of locality and perturbativity it becomes possible to systematically carry out the RG transformation approximately in the vicinity of a fixed point. Such RG approaches are referred to as local perturbative RG schemes, which we utilized in the presented RG analyses in this thesis. As briefly explained in Chapter 1, perturbativity allows us to systematically integrate out high-energy modes within a loop-expansion approximation, and locality, together with perturbativity, enables us to consistently restrict the RG analysis to a

manageable set of coupling constants.

Before further discussing practical challenges of implementing RG, let us point out a more basic problem in studying some lattice models that we encountered an instance of in Chapter 2: sensitivity to the precise values of the coupling constants in the continuum field theory of a lattice model. Sometimes the RG analysis of the quantum field theory of a lattice model can be carried out without much difficulty and what prevents us from accurately determining the fate of the system is the lack of the precise values of the couplings in the continuum field theory, i.e., the initial values of the running couplings. A simple and well-known example of this is the so-called spin-$\frac{1}{2}$ $J_1 - J_2$ model in one dimension, which is an isotropic Heisenberg antiferromagnetic spin-$\frac{1}{2}$ chain with nearest and next-nearest-neighbor exchanges J_1 and J_2. This model undergoes a phase transition to a gapped phase at $J_2^{\text{crit}} = 0.241167\, J_1$, and, in the continuum limit, just like a nearest-neighbor isotropic Heisenberg antiferromagnetic chain, is described by the $SU(2)_{k=1}$ WZNW theory perturbed by a backscattering term. The sign of the coupling constant of the backscattering term changes at the critical point J_2^{crit}, which brings about the transition. Precise determination of this critical next nearest exchange, J_2^{crit}, has only been possible by numerical calculations [126, 191]. Nevertheless, as we saw in Chapter 2, being able to identify main instabilities based on the general flow of the coupling constants in an RG analysis is extremely valuable.

The analysis of the flow of coupling constants in local perturbative RG schemes is typically restricted to the vicinity of the fixed point with respect to which the calculations are carried out (the UV fixed point). As a result of this, often we are unable to track the flow of the low-energy effective field theory of the system all the way to its fixed point (the IR fixed point) in these RG schemes. One possible solution to circumvent this shortcoming of local perturbative RG schemes is to introduce another control parameter (e.g. increasing a flavour number, or extending the dimensions of the system) that allows for making a systematic approximation. A well-known example of this is the flow from the Gaussian fixed point to the Wilson-Fisher fixed point in a ϕ^4 scalar field theory in $(4-\epsilon)$-dimensions. There, extending the physical dimensions from $\epsilon = 1$ (or even $\epsilon = 2$) to $\epsilon \ll 1$, allows for systematically accessing the Wilson-Fisher fixed point [5, 29, 192, 193]. Other recent examples of such approaches are the RG studies in Refs. [138, 141, 194].

In general it may not be possible to harness the RG flow, away from the UV fixed point, by increasing the flavour index, or it may not be easy to define the theory in non-integer dimensions. An instance of the former is the insufficiency of the large-N approximation in the case of a $U(1)$ gauge field coupled to a single patch of a Fermi surface in two dimensions that was pointed out in Ref. [151]. In cases where the UV fixed point is a $(1+1)$D CFT, such as the RG analysis in Chapter 2, extending to non-integer dimensions is not yet fully understood [195].

The above discussion of the flow of the low-energy effective field theory of a system from the vicinity of its UV fixed point to its IR fixed point allows us to bet-

ter understand the rationale behind the RG analysis of Chapter 2. Specifically, the meaning of the length scale L^* where an interchain coupling reaches $\mathcal{O}(1)$ and quasi-one-dimensionality is lost. This will also explain why in both the RG analysis and the numerical calculations three chains were enough while the system is two-dimensional. The length scale L^* marks a dimensional crossover. At length scales smaller than L^* the model is controlled by the one-dimensional fixed point of decoupled spin-$\frac{1}{2}$ chains. On the other hand, at length scales larger than L^* the system is controlled by its true two-dimensional fixed point.

In Chapter 3, we encountered two other obstacles in implementing RG for fermion systems that possess Fermi surfaces. The first problem was related to applying RG to fermion systems with Fermi surfaces in general. The second problem was the breakdown of locality, which was more specific to that model and Fermi surfaces that undergo symmetry-breaking phase transitions.

We argued that in applying RG to Fermi surfaces, one has two options: either renormalizing towards a point on the Fermi surface or renormalizing towards the entire Fermi surface. The former is the underlying idea in the so-called patch approximation, and the latter is the central idea in Shankar's RG. Patch approximations have their own limitations [151, 38]. On the other hand, RG schemes based on renormalizing towards the Fermi surface entail non-linear scaling relations [148, 154, 155]. Thus, despite great progresses, the application of RG approaches to Fermi surfaces even after twenty years since Shankar's and Polchinski's works still remains incomplete.

The loss of locality in the RG analysis of Chapter 3 at the critical point was attributed to the emergence of a gapless mode at the critical point. It was argued that, similar to more conventional symmetry-breaking phase transitions, locality can be retained if one isolates the putative emergent gapless mode. Nonetheless, this indicated that loss of locality poses a serious problem to systematic implementation of RG in practice.

4.2 Future Directions

Being able to treat strongly interacting systems is of great importance. Here we briefly mention three possible approaches that are based on or are related to RG and may allows us to address a wider range of problems.

As briefly mentioned in Chapter 1, exact, or more precisely, functional RG approaches can serve as better alternatives in cases where local perturbative RG approaches are problematic. In particular, in cases where the low-energy effective theory is non-local but still perturbative functional RG schemes can be useful.

While tracing RG flows from UV fixed points to IR fixed points in general may seem too far-fetched, one can attempt addressing a more modest question: whether there are general restrictions (no-go theorems) on the RG flows between various fixed points. A perfect instance of such "no-go" theorems for the RG flows between fixed points already exists in one dimension: Zamolodchikov's celebrated c-theorem. In one

dimension, a fixed point with dynamical critical exponent $z = 1$ is scale invariant and must be a CFT [196]. A Conformal field theory is characterized by its central charge, c, which is a measure of the total number of degrees of freedom in the system [197, 127]. Zamolodchikov [198] showed that it is not possible to flow from a CFT with a smaller central charge to another one with a larger central charge. There has been attempts to extend this theorem to higher dimensions, most notable Cardy's a-theorem in four-dimensions [199, 200]. Also, there has been proposals to use *entanglement entropy* to impose constraints on RG flows between various fixed points [201, 202, 203].

Another recent promising direction in dealing with strongly interacting quantum field theories is the use of *holography* [204, 205, 206].

Appendices

Appendix A

Appendix to Chapter 2

In this appendix we present the detailed derivation of the OPEs and the β-functions that were used in the RG analysis of Chapter 2. We begin with a brief review of the continuum limit of spin-$\frac{1}{2}$ Heisenberg antiferromagnetic chains. Then the derivation of the OPEs, β-functions and the modified β-functions in the presence of the DM interaction are presented. Finally, an approximate analytic computation of g_N^{crit} is given.

A.1 Continuum Limit of Spin-$\frac{1}{2}$ Heisenberg Antiferromagnetic Chains

The continuum limit of a spin-$\frac{1}{2}$ Heisenberg antiferromagnetic chain is given by a conformal field theory together with a tree-level marginal term that, depending on the precise details of the Hamiltonian, may or may not be relevant [207, 208, 209]. For critical chains, which are described by solely the CFT at low-energies, the tree-level marginal term is irrelevant. The continuum limit of spin-$\frac{1}{2}$ isotropic Heisenberg antiferromagnetic chains can be represented in two equivalent ways: either by a so-called *sine-Gordon* theory, or the $SU(2)_{k=1}$ *Wess-Zumino-Novikov-Witten* (WZNW) model perturbed by a marginally backscattering term. The backscattering term is marginally irrelevant for critical Heisenberg chains and, in particular, chains with only nearest-neighbor Heisenberg exchanges. Here, $k = 1$ is the *level* of this WZNW theory which, together with the symmetry group $SU(2)$, determines the central charge of this CFT, and is related to the fact that this theory describes spin-$\frac{1}{2}$ ($\frac{k}{2}$ is the highest conformal spin of the primary operators in this CFT) [128, 127, 197]. Note that, the precise microscopic continuum limit theory involves an infinite number of irrelevant terms, which are typically ignored. Nevertheless, such terms are potentially important if one is interest in short-distance correlations [210].

Let us start with the continuum description based on a sine-Gordon model, which is more appropriate for anisotropic Heisenberg (XXZ) chains. A spin-$\frac{1}{2}$ isotropic

antiferromagnetic nearest-neighbor Heisenberg chain can be regarded as the isotropic ($\Delta = J$) point of an XXZ chain with the Hamiltonian,

$$\mathcal{H}_{XXZ} = \frac{J}{2}\sum_i \Big[S_i^+ S_{i+1}^- + \text{h.c.}\Big] + \Delta \sum_i S_i^z S_{i+1}^z \,. \tag{A.1}$$

To obtain the continuum limit of the above Hamiltonian, it is more convenient to first *fermionize* the model using the *Jordan-Wigner* transformation, which results in a Hubbard model for spin-less fermions in 1D, and then bosnize the continuum limit of the Hubbard model [41, 129]. Using the Jordan-Wigner transformation,

$$S_i^+ = c_i\, e^{i\pi \sum_{j=1}^{i-1} c_j^\dagger c_j} \qquad , \qquad S_i^z = \hat{n}_i \,, \tag{A.2}$$

where $\hat{n}_i = c_i^\dagger\, c_i$. One obtains the following *fermionized* XXZ Hamiltonian [208]:

$$\mathcal{H}_{XXZ} = \frac{J}{2}\sum_i \Big[c_i^\dagger\, c_{i+1} + \text{h.c.}\Big] + \Delta \sum_i \hat{n}_i\, \hat{n}_{i+1} \,. \tag{A.3}$$

The continuum limit of the above one-dimensional Hubbard chain can be *bosonized* (Abelian bosonization) [207, 129], which results in a sine-Gordon Hamiltonian [207, 211]:

$$\mathcal{H}_{\text{SG}} = \frac{\nu}{2}\int \mathrm{d}x \left[\hat{\Pi}^2 + (1+\frac{4\Delta}{\pi})(\partial_x \hat{\Phi})^2\right] + \frac{\nu\Delta}{(\pi a_0)^2} : \cos(4\sqrt{\pi}\hat{\Phi}) : \,, \tag{A.4}$$

where $\hat{\Pi}$ is the momentum conjugate to the boson field operator $\hat{\Phi}$, a_0 is the lattice spacing and $: \mathcal{O} :$ indicates the normal-ordered operator $\mathcal{O}$. The velocity ν can be extracted from the *Bethe ansatz* solution of the XXZ Hamiltonian, which is integrable [212, 213]. The cosine term in the above Hamiltonian is irrelevant for $|\Delta| \leq J$, and is relevant and results in a finite gap when $\Delta > J$. Thus, as stated in Chapter 2, the XXZ spin-$\frac{1}{2}$ antiferromagnetic chains for $|\Delta| \leq J$ are critical [134]. In a critical sine-Gorodon theory the cosine term is irrelevant and the fixed-point theory, which is a CFT, is the free boson theory.

Let us now turn to the continuum description based on the $SU(2)_{k=1}$ WZNW model. The main disadvantage of the above continuum description based on the sine-Gordon theory is that it conceals the $SU(2)$ symmetry of the isotropic Heisenberg chains. As Witten showed [214], it is possible to construct a CFT that is explicitly invariant under a Lie group [127, 197]. In this case, this is the $SU(2)_{k=1}$ WZNW theory, which is a CFT explicitly invariant under the $SU(2)$ group with the same central charge as the free-boson CFT ($c = 1$).

A convenient way to obtain the continuum description for an isotropic spin-$\frac{1}{2}$ Heisenberg antiferromagnetic chain based on the $SU(2)_{k=1}$ WZNW theory is to start with the parent Hubbard model of the Heisenberg chain. This approach offers a particularly convenient way for deriving (most of) the OPEs, which we will use the next

section. The main idea is to take advantage of the *spin-charge* separation phenomenon in one dimension that occurs at any U/t (as opposed to in the limit $U/t \to \infty$ in higher dimension) [215, 208].[1] Then using *non-Abelian bosonization* [214], the spin sector of the Hubbard model is represented by the $SU(2)_{k=1}$ WZNW model perturbed by a backscattering term.

The continuum limit of the 1D Hubbard model for spin-$\frac{1}{2}$ fermions at low energies can be written in terms of the left- and right-moving fermion fields (field operators near the two Fermi points – left and right Fermi points), $\psi_{L,\alpha}$ and $\psi_{R,\alpha}$ as [208]:

$$\begin{aligned}\mathcal{H}_{\text{Hubbard}} \;=\; \int \mathrm{d}x\, \mathcal{H}_0 \;+\; \int \mathrm{d}x \Big\{ \lambda_1 J_L(x) J_R(x) \;+\; \lambda_3\, \mathbf{J}_L(x)\cdot \mathbf{J}_R(x) \\ +\; \lambda_2 \Big[\big(\varepsilon^{\alpha\beta} \psi^\dagger_{L,\alpha} \psi^\dagger_{R,\beta}\big) \big(\varepsilon^{\gamma\eta} \psi_{L,\gamma} \psi_{R,\eta}\big) + \text{h.c.} \Big] \Big\}\,,\end{aligned} \tag{A.5}$$

where λ_i are the couplings constants. The free continuum Hamiltonian can be written in terms of the chiral spin and charge currents as follows:

$$\begin{aligned}\mathcal{H}_0 \;=& \frac{\pi}{2}\, \nu_c \int \mathrm{d}x \Big[:J_L(x) J_L(x): + :J_R(x) J_R(x): \Big] + \\ & \frac{\pi}{2}\, \nu_s \int \mathrm{d}x \Big[:\mathbf{J}_L(x)\cdot \mathbf{J}_L(x): + :\mathbf{J}_R(x)\cdot \mathbf{J}_R(x): \Big]\,,\end{aligned} \tag{A.6}$$

where, ν_c and ν_s are charge and spin velocities, respectively, which are the same in general [129]. The left- and right-moving spin currents are given by:

$$\mathbf{J}_L \;=\; \psi^\dagger_{L,\alpha} \boldsymbol{\sigma}^{\alpha,\beta} \psi_{L,\beta} \qquad , \qquad \mathbf{J}_R \;=\; \psi^\dagger_{R,\alpha} \boldsymbol{\sigma}^{\alpha,\beta} \psi_{R,\beta}\,. \tag{A.7}$$

Similarly, the chiral charge currents are given by:

$$J_L \;=\; \psi^\dagger_{L,\alpha}\, \psi_{L,\alpha} \qquad , \qquad J_R \;=\; \psi^\dagger_{R,\alpha}\, \psi_{R,\alpha}\,. \tag{A.8}$$

Note that, normal ordering of bilinear products of fermion operators using point splitting [41], one can easily show that the normal-ordered currents in $\mathcal{H}_0$ are the same as the usual $\psi^\dagger \partial_x \psi$ term in the continuum Hubbard Hamiltonian.

Using non-Abelian bosonization [208, 134], the continuum Hubbard model in Eq. (A.5) can be bosonized. Then, an ordinary boson field Φ describes the charge sector and a matrix field g describes the dynamics in the spin sector,[2] which makes the aforementioned spin-charge separation manifest, as there will be no coupling between the spin and charge sectors. This way, $\mathcal{H}_0$ is mapped onto a free boson for the charge

[1] Strictly speaking, spin-charge separation occurs at low energies where one can use a linear approximation near the two Fermi points. The spin-charge separation would have been exact if one was dealing with a perfectly linear dispersion, i.e., the *Tomonaga-Luttinger* model [215].

[2] In Abelian bosonization, a separate ordinary boson field is used for the spin sector, which results in the sine-Gordon theory in Eq. (A.4).

sector and the $SU(2)_{k=1}$ WZNW model for the spin sector. The charge sector of $\mathcal{H}_0$ we have the following action,

$$\mathcal{S}_{\text{charge}} = -\frac{1}{2}\int \mathrm{d}\tau \mathrm{d}x \Big[\frac{1}{\nu_c}(\partial_\tau \Phi)^2 + \nu_c(\partial_x \Phi)^2\Big], \tag{A.9}$$

and the $SU(2)_{k=1}$ WZNW model is given by the action,

$$\mathcal{S}_{\text{WZNW}} = \frac{1}{8\pi}\int \mathrm{d}^2x \mathrm{Tr}\{\partial_\mu g^\dagger \partial^\mu g\} + \frac{1}{12\pi}\int \mathrm{d}^3x \varepsilon^{\mu\nu\lambda}\mathrm{Tr}\{g^\dagger\partial_\mu g\, g^\dagger \partial_\mu g\, g^\dagger \partial_\lambda g\}. \tag{A.10}$$

The bosonized form of the interaction terms in Eq. (A.5) are obtained from the following non-Abelian bosonization dictionary [134]:

Boson Operators	Fermion Bilinears
$\frac{1}{2\pi}e^{i\frac{1}{\sqrt{2\pi}}\Phi}g_{\alpha,\beta}$	$\psi^\dagger_{R,\alpha}\psi_{L,\beta}$
$i\frac{1}{\sqrt{2\pi}}\partial_{\bar{z}}\Phi$	$\frac{1}{2}:\psi^\dagger_{L,\alpha}\psi_{L,\alpha}:$
$i\frac{1}{\sqrt{2\pi}}\partial_z\Phi$	$\frac{1}{2}:\psi^\dagger_{R,\alpha}\psi_{R,\alpha}:$
$\frac{1}{2\pi}\mathrm{Tr}\{\boldsymbol{\sigma} g^{-1}\partial_z g\}$	$:\psi^\dagger_{R,\alpha}\boldsymbol{\sigma}_{\alpha,\beta}\psi_{R,\beta}:$
$\frac{1}{2\pi}\mathrm{Tr}\{\boldsymbol{\sigma} g^{-1}\partial_{\bar{z}} g\}$	$:\psi^\dagger_{L,\alpha}\boldsymbol{\sigma}_{\alpha,\beta}\psi_{L,\beta}:$

Table A.1: Non-Abelian Bosonization "dictionary".

Finally, let us turn to how magnetization operators $\mathbf{M}$ and $\mathbf{N}$, as well as, the dimerization operator ε are represented in terms of the $SU(2)$ matrix field of the $SU(2)_{k=1}$ WZNW model, g. These are given by [216]:

$$\mathbf{J}_L = \frac{k}{4\pi}\mathrm{Tr}\{\boldsymbol{\sigma} g^{-1}\partial_{\bar{z}} g\} \tag{A.11a}$$

$$\mathbf{J}_R = \frac{k}{4\pi}\mathrm{Tr}\{\boldsymbol{\sigma} g^{-1}\partial_z g\} \tag{A.11b}$$

$$\mathbf{N} = \mathrm{Tr}\{g\boldsymbol{\sigma}\} \tag{A.11c}$$

$$\varepsilon = \mathrm{Tr}\{g\}. \tag{A.11d}$$

where $k = 1$ is the level of the $SU(2)_{k=1}$ WZNW model. We see that the chiral currents are expressed in terms of fermion bilinears. However, the dimerization operator, ε, and the staggered magnetization, $\mathbf{N}$, cannot be expressed in terms of the chiral fermion operators due to the presence of the boson field Φ for the charge sector (see

Table [A.1]). Thus, the following naive fermionic representations are incorrect:

$$\varepsilon \neq \frac{1}{2}\sum_{\alpha}\psi^{\dagger}_{R,\alpha}\psi_{L,\alpha} + \text{h.c.} = \frac{1}{2\pi}\cos\big(\frac{1}{\sqrt{2\pi}}\Phi\big)\,\text{Tr}\{g\}\,. \tag{A.12a}$$

$$\mathbf{N} \neq \frac{1}{2}\sum_{\alpha,\beta}\psi^{\dagger}_{R,\alpha}\boldsymbol{\sigma}_{\alpha,\beta}\psi_{L,\beta} + \text{h.c.} = \frac{1}{2\pi}\cos\big(\frac{1}{\sqrt{2\pi}}\Phi\big)\,\text{Tr}\{g\boldsymbol{\sigma}\}\,. \tag{A.12b}$$

This point becomes important in the next section where we compute OPEs.

A.2 Derivation of the OPEs

In this section, the derivation of the OPEs for the set of operators in Chapter 2 are presented. These OPEs are needed for the derivation of the β-functions in the next section. In determining the OPEs of the chiral currents with each other and other operators, we use the fermion representation of the spin-$\frac{1}{2}$ operators $\mathbf{S} = \psi^\dagger_\alpha \frac{\boldsymbol{\sigma}_{\alpha\beta}}{2} \psi_\beta$. The justification for this is that, as shown in the previous section, the fermion representations of the chiral currents,

$$\mathbf{J}_L = \psi^\dagger_{L,\alpha} \frac{\boldsymbol{\sigma}_{\alpha\beta}}{2} \psi_{L,\beta} \,, \tag{A.13a}$$

$$\mathbf{J}_R = \psi^\dagger_{R,\alpha} \frac{\boldsymbol{\sigma}_{\alpha\beta}}{2} \psi_{R,\beta} \,, \tag{A.13b}$$

once bosonized, solely depend on the matrix field of the $SU(2)_{k=1}$ WZNW model,i.e., are operators in the spin sector of the Hubbard model. Thus the OPEs obtained in this fermionic representation are the same as those obtained using the representation of the operators in terms of the matrix field of the WZNW model. In contrast, the naive representation of $\mathbf{N}$ and ε in terms of the chiral fermion fields do not completely belong to the spin sector and their bosonized form contain both g and Φ fields. Thus, their correct OPEs cannot be computed directly from their fermion representation [209].

OPEs of the Chiral Currents

The OPE of the right-moving current with itself is obtained as follows:

$$\begin{aligned} J^a_R(z')J^b_R(z) &= :\psi^\dagger_{R,\alpha}(z') \frac{\sigma^a_{\alpha\beta}}{2} \psi_{R,\beta}(z') :: \psi^\dagger_{R,\gamma}(z) \frac{\sigma^b_{\gamma\nu}}{2} \psi_{R,\gamma}(z) : \\ &= :\psi^\dagger_{R,\alpha}(z') \frac{\sigma^a_{\alpha\beta}}{2} \psi_{R,\beta}(z') \psi^\dagger_{R,\gamma}(z) \frac{\sigma^b_{\gamma\nu}}{2} \psi_{R,\gamma}(z) : + \{\text{cross contractions}\} \,. \end{aligned} \tag{A.14}$$

Cross contractions that contain singular terms in the space-time separation between the two operators are (see, for example, Chapter 2 in [217]):

$$: \overbrace{\psi^\dagger_{R,\alpha}(z') \psi_{R,\beta}(z') \psi^\dagger_{R,\gamma}(z) \psi_{R,\nu}}(z) : \frac{1}{4} \sigma^a_{\alpha\beta} \sigma^b_{\gamma\nu} \tag{A.15a}$$

$$: \psi^\dagger_{R,\alpha}(z') \overbrace{\psi_{R,\beta}(z') \psi^\dagger_{R,\gamma}}(z) \psi_{R,\nu}(z) : \frac{1}{4} \sigma^a_{\alpha\beta} \sigma^b_{\gamma\nu} \tag{A.15b}$$

$$: \overbrace{\psi^\dagger_{R,\alpha}(z') \overbrace{\psi_{R,\beta}(z') \psi^\dagger_{R,\gamma}}(z) \psi_{R,\nu}}(z) : \frac{1}{4} \sigma^a_{\alpha\beta} \sigma^b_{\gamma\nu} \,. \tag{A.15c}$$

Using the OPE of the right-moving fermion field,

$$\psi_{R,\alpha}(w)\psi^\dagger_{R,\beta}(z) = \frac{\delta_{\alpha\beta}}{2\pi(w-z)}\,, \tag{A.16}$$

we obtain:

$$\begin{aligned} J^a_R(z')J^b_R(z) \;=& \frac{\delta_{\alpha\nu}}{2\pi(z'-z)} : \psi_{R,\beta}(z')\psi^\dagger_{R,\gamma}(z) : \frac{1}{4}\sigma^a_{\alpha\beta}\sigma^b_{\gamma\nu} \\ &+ \frac{\delta_{\beta\gamma}}{2\pi(z'-z)} : \psi^\dagger_{R,\alpha}(z')\psi_{R,\nu}(z) : \frac{1}{4}\sigma^a_{\alpha\beta}\sigma^b_{\gamma\nu} + \frac{\delta_{\beta\gamma}\delta_{\alpha\nu}}{4\pi^2(z'-z)^2}\frac{1}{4}\sigma^a_{\alpha\beta}\sigma^b_{\gamma\nu}\,, \end{aligned} \tag{A.17}$$

which, using the identity,

$$\sigma^a\sigma^b = \delta^{ab}I + i\epsilon^{abc}\sigma^c\,, \tag{A.18}$$

is written as:

$$\boxed{J^a_R(\bar z')J^b_R(\bar z) \;=\; \frac{\delta^{ab}}{8\pi^2(\bar z'-\bar z)^2} + \frac{i\epsilon^{abc}J^c_R(\bar z)}{2\pi(\bar z'-\bar z)}} \tag{A.19}$$

Similarly, for the OPE of the left-moving current we find:

$$\boxed{J^a_L(\bar z')J^b_L(\bar z) \;=\; \frac{\delta^{ab}}{8\pi^2(\bar z'-\bar z)^2} + \frac{i\epsilon^{abc}J^c_L(\bar z)}{2\pi(z'-\bar z)}} \tag{A.20}$$

OPEs of the Chiral Currents with N

Next, let us determine the OPE of $\mathbf{J}_R$ with $\mathbf{N}(z,\bar z)$:

$$\begin{aligned} J^a_R(z')N^b(z,\bar z) \;=& : \psi^\dagger_{R,\alpha}(z')\frac{\sigma^a_{\alpha\beta}}{2}\psi_{R,\beta}(z') :: \psi^\dagger_{R,\gamma}(z)\frac{\sigma^b_{\gamma\nu}}{2}\psi_{L,\nu}(\bar z) : \\ &+ : \psi^\dagger_{R,\alpha}(z')\frac{\sigma^a_{\alpha\beta}}{2}\psi_{R,\beta}(z') :: \psi^\dagger_{L,\gamma}(\bar z)\frac{\sigma^b_{\gamma\nu}}{2}\psi_{R,\nu}(z) : \\ =& : \psi^\dagger_{R,\alpha}(z')\frac{\sigma^a_{\alpha\beta}}{2}\psi_{R,\beta}(z')\psi^\dagger_{R,\gamma}(z)\frac{\sigma^b_{\gamma\nu}}{2}\psi_{L,\nu}(\bar z) : \\ &+ : \psi^\dagger_{R,\alpha}(z')\frac{\sigma^a_{\alpha\beta}}{2}\psi_{R,\beta}(z')\psi^\dagger_{L,\gamma}(\bar z)\frac{\sigma^b_{\gamma\nu}}{2}\psi_{R,\nu}(z) : + \{\text{cross contractions}\}\,. \end{aligned} \tag{A.21}$$

Again, the cross contractions are:

$$: \psi^\dagger_{R,\alpha}(z')\overbrace{\psi_{R,\beta}(z')\psi^\dagger_{R,\gamma}}(z)\psi_{L,\nu}(\bar z) : \frac{1}{4}\sigma^a_{\alpha\beta}\sigma^b_{\gamma\nu} \tag{A.22a}$$

$$: \overbrace{\psi^\dagger_{R,\alpha}(z')\psi_{R,\beta}(z')\psi^\dagger_{L,\gamma}(\bar z)}\psi_{R,\nu}(z) : \frac{1}{4}\sigma^a_{\alpha\beta}\sigma^b_{\gamma\nu}\,. \tag{A.22b}$$

Note that there are no double contractions in this OPE. We obtain:

$$J_R^b(z')N^a(z,\bar{z}) = \frac{1}{2\pi(z'-z)}\Big[\delta_{\beta\gamma} : \psi_{R,\alpha}^\dagger(z')\psi_{L,\gamma}(\bar{z}) : + \delta_{\alpha\nu} : \psi_{R,\beta}(z')\psi_{L,\gamma}^\dagger(\bar{z}) : \Big]\frac{1}{4}\sigma_{\alpha\beta}^a\sigma_{\gamma\nu}^b\,. \tag{A.23}$$

Again, using the identity [A.18], we get:

$$\boxed{J_R^b(z')N^a(z,\bar{z}) = \frac{-i\delta^{ab}\varepsilon(z,\bar{z})}{4\pi(z'-z)} + \frac{i\epsilon^{abc}N^c(z,\bar{z})}{4\pi(z'-z)}} \tag{A.24}$$

And, similarly, for the OPE of the left-moving current $\mathbf{J}_L$ and $\mathbf{N}$ we get:

$$\boxed{J_L^b(\bar{z}')N^a(z,\bar{z}) = \frac{i\delta^{ab}\varepsilon(z,\bar{z})}{4\pi(\bar{z}'-\bar{z})} + \frac{i\epsilon^{abc}N^c(z,\bar{z})}{4\pi(\bar{z}'-\bar{z})}} \tag{A.25}$$

OPEs of the Chiral Currents with ε

The OPE of the right-moving current $\mathbf{J}_R$ with the dimerization operator ε is obtained as follows:

$$J_R^a(z')\varepsilon(z,\bar{z}) = \frac{i}{2}\Big[: \psi_{R,\alpha}^\dagger(z')\frac{\sigma_{\alpha\beta}^a}{2}\psi_{R,\beta}(z') :: \psi_{R,\gamma}^\dagger(z)\psi_{L,\gamma}(\bar{z}) : - : \psi_{R,\alpha}^\dagger(z')\frac{\sigma_{\alpha\beta}^a}{2}\psi_{R,\beta}(z') :: \psi_{L,\gamma}^\dagger(\bar{z})\psi_{R,\gamma}(z) : \Big]\,. \tag{A.26}$$

There are only two cross contractions possible:

$$: \psi_{R,\alpha}^\dagger(z')\overbrace{\psi_{R,\beta}(z')\psi_{R,\gamma}^\dagger}(z)\psi_{L,\gamma}(\bar{z}) : \frac{\sigma_{\alpha\beta}^a}{2}\,, \tag{A.27a}$$

$$: \overbrace{\psi_{R,\alpha}^\dagger(z')\psi_{R,\beta}(z')\psi_{L,\gamma}^\dagger(\bar{z})}\psi_{R,\gamma}(z) : \frac{\sigma_{\alpha\beta}^a}{2}\,. \tag{A.27b}$$

We get:

$$\boxed{J_R^a(z')\varepsilon(z,\bar{z}) = \frac{iN^a(z,\bar{z})}{4\pi(z'-z)}} \tag{A.28}$$

Similarly, for the OPE of the left-moving current operator with ε we get:

$$\boxed{J_L^a(\bar{z}')\varepsilon(z,\bar{z}) = \frac{-iN^a(z,\bar{z})}{4\pi(\bar{z}'-\bar{z})}} \tag{A.29}$$

OPE of N with ε

The OPE of $\mathbf{N}$ with ε:

$$\begin{aligned} N^a(z',\bar{z}')\varepsilon(z,\bar{z}) \;=\; \frac{i}{2}\Bigg[& - :\psi^\dagger_{R,\alpha}(z')\frac{\sigma^a_{\alpha,\beta}}{2}\psi_{L,\beta}(\bar{z}') :: \psi^\dagger_{L,\gamma}(\bar{z})\psi_{R,\gamma}(z) : \\ & + :\psi^\dagger_{L,\alpha}(\bar{z}')\frac{\sigma^a_{\alpha,\beta}}{2}\psi_{R,\beta}(z') :: \psi^\dagger_{R,\gamma}(z)\psi_{L,\nu}(\bar{z}) : \\ & - :\psi^\dagger_{L,\alpha}(\bar{z}')\frac{\sigma^a_{\alpha,\beta}}{2}\psi_{R,\beta}(z') :: \psi^\dagger_{L,\gamma}(\bar{z})\psi_{R,\gamma}(z) : \\ & + :\psi^\dagger_{R,\alpha}(z')\frac{\sigma^a_{\alpha,\beta}}{2}\psi_{L,\beta}(\bar{z}') :: \psi^\dagger_{R,\gamma}(z)\psi_{L,\gamma}(\bar{z}) :\Bigg] . \end{aligned} \tag{A.30}$$

The only possible contraction is:

$$\begin{aligned} & :\overbrace{\psi^\dagger_{R,\alpha}(z')\overbrace{\psi_{L,\beta}(\bar{z}')\psi^\dagger_{L,\gamma}(\bar{z})}\psi_{R,\gamma}(z)}: \frac{\sigma^a_{\alpha,\beta}}{2} \\ =& \frac{\delta_{\alpha\gamma}}{2\pi(z'-z)}\frac{\delta_{\beta\gamma}}{2\pi(\bar{z}'-\bar{z})}\frac{\sigma^a_{\alpha,\beta}}{2} \;=\; \frac{\mathrm{Tr}\{\sigma^a\}}{4\pi^2|z'-z|^2} \;=\; 0\,. \end{aligned} \tag{A.31}$$

Therefore,

$$\boxed{N^a(z',\bar{z}')\varepsilon(z,\bar{z}) \;=\; 0\,.} \tag{A.32}$$

One may wonder whether the above result for the OPE of $\mathbf{N}$ with ε, which was obtained from their naive fermion representation, can be trusted. The fact that there are no singular terms in this OPE can be understood based on the $SU(2)$ symmetry. Nevertheless, at the the end of this section, we reexamine this OPE in the Abelian bosonization formulation and confirm that the result is indeed zero.

OPE of ε with itself

The derivation of the OPE of ε requires more attentions, and, as pointed out in the beginning of this section, cannot be obtained from its naive fermion representation. The (Abelian) bosonized form of $\varepsilon(z,\bar{z})$ is:

$$\varepsilon(z,\bar{z}) \;=\; \frac{\lambda}{\pi a_0} :\cos(\sqrt{2\pi}\Phi(z,\bar{z})) : \tag{A.33}$$

where $\lambda \simeq 1$ is a constant, and Φ is the boson field of the spin sector in the Abelian bosonization. Then the OPE of ε with itself can be readily computed:

$$\varepsilon(z',\bar{z}')\,\varepsilon(z,\bar{z}) \;=\; \frac{\lambda^2}{(\pi a_0)^2} : \cos(\sqrt{2\pi}\Phi(z',\bar{z}')) :: \cos(\sqrt{2\pi}\Phi(z,\bar{z})) : \,. \tag{A.34}$$

Writing the cosine term of exponential terms, we get:

$$\begin{aligned}\varepsilon(z',\bar{z}')\,\varepsilon(z,\bar{z}) \;=& \frac{\lambda^2}{(2\pi a_0)^2}\Big[: \exp(i\sqrt{2\pi}\Phi(z',\bar{z}')) :: \exp(i\sqrt{2\pi}\Phi(z,\bar{z})) : \; + \\ & : \exp(i\sqrt{2\pi}\Phi(z',\bar{z}')) :: \exp(-i\sqrt{2\pi}\Phi(z,\bar{z})) : \; + \\ & : \exp(-i\sqrt{2\pi}\Phi(z',\bar{z}')) :: \exp(i\sqrt{2\pi}\Phi(z,\bar{z})) : \; + \\ & : \exp(-i\sqrt{2\pi}\Phi(z',\bar{z}')) :: \exp(-i\sqrt{2\pi}\Phi(z,\bar{z})) : \Big] \,. \end{aligned} \tag{A.35}$$

Using the normal ordering prescription for these so-called *vertex operators* (see [215] or Ch.2 in [217]),

$$: e^A :: e^B :=: e^{A+B} : e^{\langle AB\rangle} \,, \tag{A.36}$$

the OPE can be readily computed as follows:

$$\begin{aligned}\varepsilon(z',\bar{z}')\,\varepsilon(z,\bar{z}) \;=& \Big[: \exp\Big(i\sqrt{2\pi}[\Phi(z',\bar{z}')+\Phi(z,\bar{z})]\Big) : \; \exp\Big(-2\pi\frac{-1}{4\pi}\ln(|z'-z|^2)\Big) + \\ & : \exp\Big(i\sqrt{2\pi}[\Phi(z',\bar{z}')-\Phi(z,\bar{z})]\Big) : \; \exp\Big(2\pi\frac{-1}{4\pi}\ln(|z'-z|^2)\Big) + \\ & : \exp\Big(-i\sqrt{2\pi}[\Phi(z',\bar{z}')-\Phi(z,\bar{z})]\Big) : \; \exp\Big(2\pi\frac{-1}{4\pi}\ln(|z'-z|^2)\Big) + \\ & : \exp\Big(-i\sqrt{2\pi}[\Phi(z',\bar{z}')+\Phi(z,\bar{z})]\Big) : \; \exp\Big(-2\pi\frac{-1}{4\pi}\ln(|z'-z|^2)\Big)\Big] \,. \end{aligned} \tag{A.37}$$

Since we are only interested in the singular terms of the OPEs, we ignore the first and the last terms. Finally, Taylor expanding the argument of the normal ordered vertex operators, we get:

$$\boxed{\varepsilon(z',\bar{z}')\varepsilon(z,\bar{z}) \;=\; \frac{2\lambda^2}{(2\pi a_0)^2}\frac{1}{|z'-z|} \,.} \tag{A.38}$$

OPE of N with itself

The OPE of $\mathbf{N}$ with itself is obtained similar to that of ε. However, since $\mathbf{N}$ is a vector operator, we need to treat its z-component different from its other components for the purpose of the Abelian bosonization. This is the disadvantage of Abelian

bosonization where the $SU(2)$ symmetry is not manifest. The bosonized version of $\mathbf{N}$ in the Abelian bosonization is:

$$N^z(z,\bar{z}) \;=\; \frac{-\lambda}{\pi a_0} : \sin(\sqrt{2\pi}\Phi(z,\bar{z})) :, \tag{A.39a}$$

$$N^{\pm}(z,\bar{z}) \;=\; \frac{\lambda}{\pi a_0} : \exp(\pm i\sqrt{2\pi}\Theta(z,\bar{z})) :, \tag{A.39b}$$

where, again, λ is some parameter, and Θ is the so-called *dual boson* field [209, 215]:

$$\begin{cases} \Phi(z,\bar{z}) \;=\; \varphi_L(\bar{z}) + \varphi_R(z) \\ \Theta(z,\bar{z}) \;=\; \varphi_L(\bar{z}) - \varphi_R(z) \end{cases} \tag{A.40}$$

The two-point functions of the left- and right-moving boson fields, φ_L and φ_R, are:

$$\begin{cases} \langle \varphi_L(\bar{z}')\varphi_L(\bar{z})\rangle \;=\; \frac{-1}{4\pi}\ln(\bar{z}'-\bar{z}) \\ \langle \varphi_R(z')\varphi_R(z)\rangle \;=\; \frac{-1}{4\pi}\ln(z'-z) \end{cases} \tag{A.41}$$

Now, we can easily compute the OPE of $\mathbf{N}$ with itself. Let us start with N^z:

$$\begin{aligned} N^z(z',\bar{z}')N^z(z,\bar{z}) \;&=\frac{\lambda^2}{(\pi a_0)^2} : \sin(\sqrt{2\pi}\Phi(z',\bar{z}')) :: \sin(\sqrt{2\pi}\Phi(z,\bar{z})) : \\ &=\frac{\lambda^2}{(2i\pi a_0)^2}\Big[: \exp(i\sqrt{2\pi}\Phi(z',\bar{z}')) :: \exp(i\sqrt{2\pi}\Phi(z,\bar{z})) : \; - \\ &\quad : \exp(i\sqrt{2\pi}\Phi(z',\bar{z}')) :: \exp(-i\sqrt{2\pi}\Phi(z,\bar{z})) : \; - \\ &\quad : \exp(-i\sqrt{2\pi}\Phi(z',\bar{z}')) :: \exp(i\sqrt{2\pi}\Phi(z,\bar{z})) : \; + \\ &\quad : \exp(-i\sqrt{2\pi}\Phi(z',\bar{z}')) :: \exp(-i\sqrt{2\pi}\Phi(z,\bar{z})) : \Big] \end{aligned} \tag{A.42}$$

$$\begin{aligned} =\; \frac{\lambda^2}{(2i\pi a_0)^2}\Big[&: \exp\Big(i\sqrt{2\pi}[\Phi(z',\bar{z}')+\Phi(z,\bar{z})]\Big) : \; \exp\Big(-2\pi\frac{-1}{4\pi}\ln(|z'-z|^2)\Big) - \\ &: \exp\Big(i\sqrt{2\pi}[\Phi(z',\bar{z}')-\Phi(z,\bar{z})]\Big) : \; \exp\Big(2\pi\frac{-1}{4\pi}\ln(|z'-z|^2)\Big) - \\ &: \exp\Big(-i\sqrt{2\pi}[\Phi(z',\bar{z}')-\Phi(z,\bar{z})]\Big) : \; \exp\Big(2\pi\frac{-1}{4\pi}\ln(|z'-z|^2)\Big) + \\ &: \exp\Big(-i\sqrt{2\pi}[\Phi(z',\bar{z}')+\Phi(z,\bar{z})]\Big) : \; \exp\Big(-2\pi\frac{-1}{4\pi}\ln(|z'-z|^2)\Big)\Big]. \end{aligned}$$

Again, the first and the last terms produce no singular term and thus can be ignored. We arrive at:

$$\boxed{N^z(z',\bar{z}')N^z(z,\bar{z}) \;=\; \frac{\lambda^2}{2(\pi a_0)^2}\frac{1}{|z'-z|}\,.} \tag{A.43}$$

Next, consider the OPE of $N^{\pm}$ with $N^{\pm}$:

$$\begin{aligned} N^+N^+ \;&=\frac{\lambda^2}{(\pi a_0)^2} : \exp\Big(i\sqrt{2\pi}\Theta(z',\bar{z}')\Big) :: \exp\Big(i\sqrt{2\pi}\Theta(z,\bar{z})\Big) : \\ &=\frac{\lambda^2}{(\pi a_0)^2} : \exp\Big(i\sqrt{2\pi}(\varphi_L(\bar{z}')-\varphi_R(z'))\Big) :: \exp\Big(i\sqrt{2\pi}(\varphi_L(\bar{z})-\varphi_R(z))\Big) : \,. \end{aligned} \tag{A.44}$$

$$\begin{aligned} N^+N^+ \;&=\frac{\lambda^2}{(\pi a_0)^2} : \exp\Big(i\sqrt{2\pi}(\Theta(z',\bar{z}')+\Theta(z,\bar{z}))\Big) : \\ &\qquad \exp\Big[-2\pi[\langle\varphi_L(\bar{z}')\varphi_L(\bar{z})\rangle+\langle\varphi_R(z')\varphi_R(z')\rangle]\Big] \\ &=\frac{\lambda^2}{(\pi a_0)^2} : \exp\Big(i\sqrt{2\pi}(\Theta(z',\bar{z}')+\Theta(z,\bar{z}))\Big) : \\ &\qquad \exp\Big[-2\pi[\frac{-1}{4\pi}\ln(z'-z)+\frac{-1}{4\pi}\ln(\bar{z}'-\bar{z})]\Big]\,. \end{aligned} \tag{A.45}$$

Similarly, for other OPEs we get:

$$\begin{aligned} N^-N^- \;&=\; : \exp\Big(-i\sqrt{2\pi}(\Theta(z',\bar{z}')+\Theta(z,\bar{z}))\Big) : \\ &= \exp\big[\frac{1}{2}[\ln(z'-z)+\ln(\bar{z}'-\bar{z})]\big]\,. \end{aligned} \tag{A.46}$$

Also, for the cross products, we get:

$$\begin{aligned} N^-N^+ \;&=\; : \exp\Big(-i\sqrt{2\pi}(\Theta(z,\bar{z})-\Theta(0,0))\Big) : \\ &\qquad \exp\Big[\frac{-1}{2}[\ln(z'-z)+\ln(\bar{z}'-\bar{z})]\Big]\,, \end{aligned} \tag{A.47}$$

and,

$$\begin{aligned} N^+N^- \;&=\; : \exp\Big(i\sqrt{2\pi}(\Theta(z,\bar{z})-\Theta(0,0))\Big) : \\ &\qquad \exp\Big[\frac{-1}{2}[\ln(z'-z)+\ln(\bar{z}'-\bar{z})]\Big]\,. \end{aligned} \tag{A.48}$$

Therefore, as expected from the $SU(2)$ symmetry, the product $N^x N^y$ has no singular terms in its OPE. Thus,

$$\boxed{\mathbf{N}(z',\bar{z}')\cdot\mathbf{N}(z,\bar{z}) \;\propto\; \frac{1}{|z'-z|}\,.} \tag{A.49}$$

OPE of N with ε

Finally, for the sake of completeness, let us confirm that the OPE of $\mathbf{N}$ with ε is zero.

$$N^z(z,\bar{z})\varepsilon(z,\bar{z}) \;=\; \frac{-\lambda^2}{(\pi a_0)^2} : \sin\left(\sqrt{2\pi}\Phi(z',\bar{z}')\right) :: \cos\left(\sqrt{2\pi}\Phi(z,\bar{z})\right) : \tag{A.50}$$

$$\begin{aligned} &= \frac{-\lambda^2}{i(2\pi a_0)^2}\Big[: \exp(i\sqrt{2\pi}\Phi(z',\bar{z}')) :: \exp(i\sqrt{2\pi}\Phi(z,\bar{z})) : \; + \\ &: \exp(i\sqrt{2\pi}\Phi(z',\bar{z}')) :: \exp(-i\sqrt{2\pi}\Phi(z,\bar{z})) : \; - \\ &: \exp(-i\sqrt{2\pi}\Phi(z',\bar{z}')) :: \exp(i\sqrt{2\pi}\Phi(z,\bar{z})) : \; - \\ &: \exp(-i\sqrt{2\pi}\Phi(z',\bar{z}')) :: \exp(-i\sqrt{2\pi}\Phi(z,\bar{z})) : \Big]\,. \end{aligned} \tag{A.51}$$

Following the same steps as in above, it is clear this OPE does not contain any singular terms. Therefore,

$$N^z(z',\bar{z}')\varepsilon(z,\bar{z}) \;=\; 0\,. \tag{A.52}$$

A.3 Derivation of the β-Functions

Here we present the derivation of the β-functions. Let us first explain how in this real-space perturbative local RG approach the β-functions are obtained directly from the OPEs of the interaction terms. For simplicity, suppose we only have one interaction term $\mathcal{S}_{\rm int} = \lambda \int \mathrm{d}z\mathrm{d}\bar{z}\mathcal{O}(z,\bar{z})$. As mentioned in Chapter 2, this RG approach is based on gradually increasing a short-distance cutoff, which we indicate by Λ^{-1} (starting RG at the length scale $\Lambda^{-1} = L_0$). The quantum corrections can be conveniently obtained from the OPEs of the operators as follows.

As usual, one starts by the expansion of the full action in the weak perturbation parameter(s):

$$\int \mathcal{D}g\; e^{-\mathcal{S}_{\rm WZNW}}\Big(1 - \lambda\mathcal{S}_{\rm int} + \frac{\lambda^2}{2}\mathcal{S}_{\rm int}\mathcal{S}_{\rm int} + \cdots\Big) \tag{A.53}$$

The scaling dimension of the operators is given by their scaling dimension with respect to the conformal WZNW model. One-loop quantum corrections are given by,

$$\partial_\ell \int \mathcal{D}g e^{-\mathcal{S}_{\rm WZNW}}\mathcal{S}_{\rm int}^2 = \int \mathrm{d}z'\mathrm{d}\bar{z}' \int \mathrm{d}z\mathrm{d}\bar{z}\langle\mathcal{O}(z',\bar{z}')\mathcal{O}(z,\bar{z})\rangle\,\big|_{e^{-\mathrm{d}\ell}\Lambda^{-1}<x'-x<\Lambda^{-1}}\,, \tag{A.54}$$

which can be conveniently obtained from the OPE of $\mathcal{O}$,

$$\mathcal{O}(z',\bar{z}')\mathcal{O}(z,\bar{z}) = \sum_{n=-2h_{\mathcal{O}}}^{-1} c_n\,|z'-z|^n\,\mathcal{O}^{(n)}(z,\bar{z}) + :\mathcal{O}(z',\bar{z}')\mathcal{O}(z,\bar{z}):\,. \tag{A.55}$$

The scaling dimensions on both sides should be the same, which implies that the scaling dimension of $\mathcal{O}^{(n)}$ and $\mathcal{O}$ should satisfy: $2h_{\mathcal{O}} = n + h_{\mathcal{O}^{(n)}}$.

We see that the quantum corrections are dominated by the singular terms in the OPEs as non-singular terms (those that originate from $:\mathcal{O}(z',\bar{z}')\mathcal{O}(z,\bar{z}):$ upon expanding in $(z'-z)$ and $(\bar{z}'-\bar{z})$) are accompanied by Λ^{-1}, which is small. Also, following the same dimensional analysis for the singular terms above, operators that appear in the non-singular part of the OPEs will have the scaling dimension $2h_{\mathcal{O}}$ and are often irrelevant. Therefore, the one-loop quantum corrections are given by the OPEs of the product of interaction terms in $\mathcal{S}_{\rm int}$.

Now let us turn to the derivation of the β-functions in Chapter 2 (Eqs. (2.8a-2.8i)), which are obtained from integrating out short-distance fluctuations. In the

determining the β-functions, we will encounter the following integrals:

$$\partial_\ell \int_{-\infty}^{\infty} \mathrm{d}\tau \int_{e^{-\mathrm{d}\ell}\Lambda^{-1}}^{\Lambda^{-1}} \mathrm{d}x \, \frac{1}{z^n} = 0 \tag{A.56a}$$

$$\partial_\ell \int_{-\infty}^{\infty} \mathrm{d}\tau \int_{e^{-\mathrm{d}\ell}\Lambda^{-1}}^{\Lambda^{-1}} \mathrm{d}x \, \frac{1}{\bar{z}^n} = 0 \tag{A.56b}$$

$$\partial_\ell \int_{-\infty}^{\infty} \mathrm{d}\tau \int_{e^{-\mathrm{d}\ell}\Lambda^{-1}}^{\Lambda^{-1}} \mathrm{d}x \, \frac{1}{|z|^n} = \frac{8\sqrt{\pi}}{n} \left(\Lambda^{-1}\right)^{n-2} \tag{A.56c}$$

where, in the last equation $n \geq 2$. Note that the fact that the first two integrals vanish is independent of the our RG scheme (imposing the cutoff on spatial separations – Fig. [A.1] (a)). One obtains the same result if the regularization scheme in Fig. [A.1](b) is used, which suppresses short separations in both space and time.

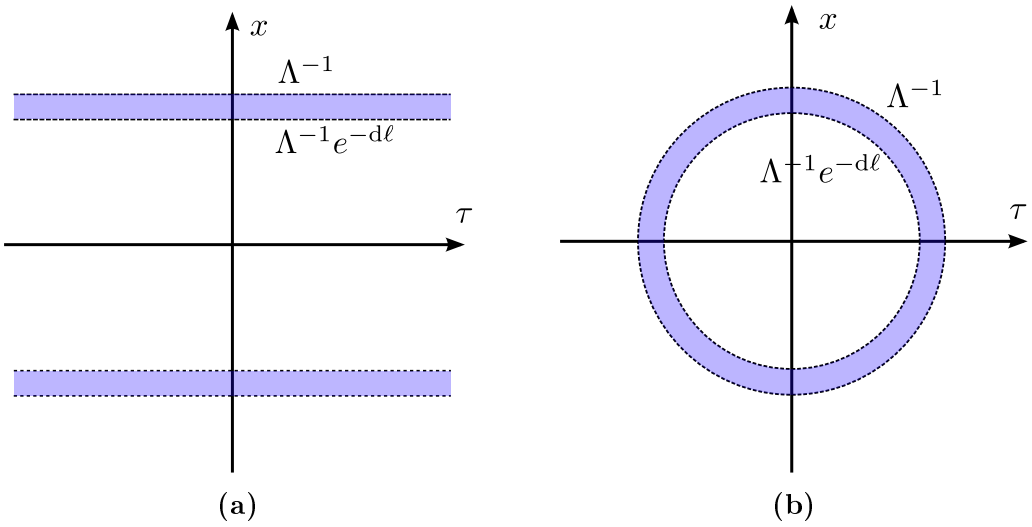

Figure A.1: Different regularization schemes: (a) The short-distance cutoff is imposed only on the spatial separations. (b) The cutoff is imposed on both spatial and temporal separations: $|z|$. The purple region is the region integrated over at each iteration of RG.

- γ_{bs} - γ_{bs}

For the product of two backscattering terms we have:

$$
\begin{aligned}
& J^b_{R,y'}(z')J^b_{L,y'}(\bar{z}')\, J^a_{R,y}(z)J^a_{L,y}(\bar{z}) \qquad (A.57)\\
&= \delta_{y,y'}\Big[\frac{\delta^{ab}}{8\pi^2(\bar{z}-\bar{z}_0)^2}+\frac{i\epsilon^{abc}J^c_{R,y}(\bar{z}_0)}{2\pi(\bar{z}-\bar{z}_0)}\Big]\Big[\frac{\delta^{ab}}{8\pi^2(z-z_0)^2}+\frac{i\epsilon^{abd}J^d_{L,y'}(z_0)}{2\pi(z-z_0)}\Big]\\
&= \frac{\delta^{ab}}{(8\pi^2)^2|z-z_0|^4}+\frac{-|\epsilon^{abc}|J^c_{R,y}(\bar{z}_0)J^c_{L,y}(z_0)}{4\pi^2|z-z_0|^2}\,.
\end{aligned}
$$

- γ_{tw} - γ_{tw}

The product of two twist terms gives:

$$
\begin{aligned}
& (-1)^{y+y'}N^a_y(z',\bar{z}')\partial_x N^a_{y+1}(z',\bar{z}')N^b_{y'}(z,\bar{z})\partial_x N^b_{y'+1}(z,\bar{z}) \qquad (A.58)\\
& (-1)^{y+y'}\partial_x N^a_y(z',\bar{z}')N^a_{y+1}(z',\bar{z}')\partial_x N^b_{y'}(z,\bar{z})N^b_{y'+1}(z,\bar{z})\\
& -(-1)^{y+y'}\partial_x N^a_y(z',\bar{z}')N^a_{y+1}(z',\bar{z}')N^b_{y'}(z,\bar{z})\partial_x N^b_{y'+1}(z,\bar{z})\\
& -(-1)^{y+y'}N^a_y(z',\bar{z}')\partial_x N^a_{y+1}(z',\bar{z}')\partial_x N^b_{y'}(z,\bar{z})N^b_{y'+1}(z,\bar{z})
\end{aligned}
$$

There are three choices for the chain indices, $y = y'$, $y = y' + 1$ and $y = y' - 1$. Since the singular part of the OPE of $\mathbf{N}$ with itself contains no operators, we ignore the first choice ($y = y'$) as it results only in a numerical factor. On the other hand, for the

other two case $y = y' \pm 1$ we get (the following expressions are for the case $y = y' + 1$):

$$(-1)^{y+y-1} N_y^a(z', \bar{z}') \partial_x N_{y+1}^a(z', \bar{z}') N_{y+1}^b(z, \bar{z}) \partial_x N_{y+2}^b(z, \bar{z}) \tag{A.59}$$

$$= -\frac{-\delta^{ab}(x - x_0)}{2\pi^2 |z' - z|^3} N_y^a(z) \partial_x N_{y+2}^b(z, \bar{z})$$

$$= -\frac{-\delta^{ab}(x - x_0)}{2\pi^2 |z' - z|^3} N_y^a(z, \bar{z}) \partial_x N_{y+2}^b(z, \bar{z}) \; - \; \frac{-\delta^{ab}(x - x_0)^2}{2\pi^2 |z' - z|^3} \partial_x N_y^a(z) \partial_x N_{y+2}^b(z, \bar{z})$$

$$(-1)^{y+y-1} \partial_x N_y^a(z', \bar{z}') N_{y+1}^a(z', \bar{z}') \partial_x N_{y+1}^b(z, \bar{z}) N_{y+2}^b(z, \bar{z}) \tag{A.60}$$

$$= -\frac{\delta^{ab}(x - x_0)}{2\pi^2 |z' - z|^3} \partial_x N_y^a(z) N_{y+2}^b(z, \bar{z})$$

$$= -\frac{\delta^{ab}(x - x_0)}{2\pi^2 |z' - z|^3} \partial_x N_y^a(z) N_{y+2}^b(z) \; + \; \frac{\delta^{ab}(x - x_0)^2}{2\pi^2 |z' - z|^3} \partial_x N_y^a(z) \partial_x N_{y+2}^b(z)$$

$$- (-1)^{y+y-1} \partial_x N_y^a(z', \bar{z}') N_{y+1}^a(z', \bar{z}') N_{y+1}^b(z, \bar{z}) \partial_x N_{y+2}^b(z, \bar{z}) \tag{A.61}$$

$$= \frac{\delta^{ab}}{2\pi^2 |z' - z|} \partial_x N_y^a(z) \partial_x N_{y+2}^b(z, \bar{z})$$

$$- (-1)^{y+y-1} N_y^a(z', \bar{z}') \partial_x N_{y+1}^a(z', \bar{z}') \partial_x N_{y+1}^b(z, \bar{z}) N_{y+2}^b(z, \bar{z}) \tag{A.62}$$

$$= \partial_x \partial_{x_0} \left[\frac{\delta^{ab}}{2\pi^2 |z' - z|} \right] N_y^a(z) N_{y+2}^b(z, \bar{z})$$

$$= \left[\frac{\delta^{ab}}{2\pi^2 |z' - z|^3} + \frac{-3\delta^{ab}(x - x_0)^2}{2\pi^2 |z' - z|^5} \right] N_y^a(z) N_{y+2}^b(z, \bar{z})$$

- γ_M - γ_M

The product of the nearest interchain uniform magnetization coupling terms is:

$$M_y^a(z', \bar{z}') M_{y+1}^a(z', \bar{z}') \; M_{y'}^b(z, \bar{z}) M_{y'+1}^b(z, \bar{z}) \tag{A.63}$$

where,

$$\mathbf{M}_y(z, \bar{z}) = \mathbf{J}_{R,y}(z) + \mathbf{J}_{L,y}(\bar{z})$$

Thus in terms of the products of the chiral currents we have the following 16 terms:

$$
\begin{aligned}
& M^a_y(z',\bar{z}')M^a_{y+1}(z',\bar{z}')\ M^b_{y'}(z,\bar{z})M^b_{y'+1}(z,\bar{z}) \qquad \text{(A.64)}\\
&= J^a_{R,y}(z')J^a_{R,y+1}(z')J^b_{R,y'}(z)J^b_{R,y'+1}(z) + \\
& J^a_{L,y}(\bar{z}')J^a_{L,y+1}(\bar{z}')J^b_{L,y'}(\bar{z})J^b_{L,y'+1}(\bar{z}) + \\
& J^a_{R,y}(z')J^a_{L,y+1}(\bar{z}')J^b_{R,y'}(z)J^b_{L,y'+1}(\bar{z}) + \\
& J^a_{L,y}(\bar{z}')J^a_{R,y+1}(z')J^b_{L,y'}(\bar{z})J^b_{R,y'+1}(z) + \\
& J^a_{R,y}(z')J^a_{R,y+1}(z')J^b_{R,y'}(z)J^b_{L,y'+1}(\bar{z}) + \\
& J^a_{R,y}(z')J^a_{R,y+1}(z')J^b_{L,y'}(\bar{z})J^b_{R,y'+1}(z) + \\
& J^a_{R,y}(z')J^a_{L,y+1}(z')J^b_{R,y'}(z)J^b_{R,y'+1}(z) + \\
& J^a_{L,y}(\bar{z}')J^a_{R,y+1}(z')J^b_{R,y'}(z)J^b_{R,y'+1}(z) + \\
& J^a_{L,y}(\bar{z}')J^a_{L,y+1}(\bar{z}')J^b_{L,y'}(\bar{z})J^b_{R,y'+1}(z) + \\
& J^a_{L,y}(\bar{z}')J^a_{L,y+1}(\bar{z}')J^b_{R,y'}(z)J^b_{L,y'+1}(\bar{z}) + \\
& J^a_{L,y}(\bar{z}')J^a_{R,y+1}(z')J^b_{L,y'}(\bar{z})J^b_{L,y'+1}(\bar{z}) + \\
& J^a_{R,y}(z')J^a_{L,y+1}(\bar{z}')J^b_{L,y'}(\bar{z})J^b_{L,y'+1}(\bar{z}) + \\
& J^a_{R,y}(z')J^a_{R,y+1}(z')J^b_{L,y'}(\bar{z})J^b_{L,y'+1}(\bar{z}) + \\
& J^a_{L,y}(\bar{z}')J^a_{L,y+1}(\bar{z}')J^b_{R,y'}(z)J^b_{R,y'+1}(z) + \\
& J^a_{R,y}(z')J^a_{L,y+1}(\bar{z}')J^b_{L,y'}(\bar{z})J^b_{R,y'+1}(z) + \\
& J^a_{L,y}(\bar{z}')J^a_{R,y+1}(z')J^b_{R,y'}(z)J^b_{L,y'+1}(\bar{z})\,.
\end{aligned}
$$

Now there are two possibilities for y and y': either $y = y'$ or $y = y' - 1$. Ignoring numerical factors and four-current terms (as well as other irrelevant terms), in the

case $y = y'$ we find:

$$
\begin{aligned}
\propto \Big[& \frac{\delta^{ab}}{8\pi^2(z'-z)^2} J^a_{R,y}(z) J^b_{R,y}(z) + \frac{\delta^{ab}}{8\pi^2(z'-z)^2} J^a_{R,y+1}(z) J^b_{R,y+1}(z) \\
& + \frac{-\varepsilon^{abc}\varepsilon^{abc'}}{4\pi^2(z'-z)^2} J^c_{R,y}(z) J^{c'}_{R,y+1}(z) \Big] + \\
\Big[& \frac{\delta^{ab}}{8\pi^2(\bar{z}'-\bar{z})^2} J^a_{L,y}(\bar{z}) J^b_{L,y}(\bar{z}) + \frac{\delta^{ab}}{8\pi^2(\bar{z}'-\bar{z})^2} J^a_{L,y+1}(\bar{z}) J^b_{L,y+1}(\bar{z}) \\
& + \frac{-\varepsilon^{abc}\varepsilon^{abc'}}{4\pi^2(\bar{z}'-\bar{z})^2} J^c_{L,y}(\bar{z}) J^{c'}_{L,y+1}(\bar{z}) \Big] + \\
\Big[& \frac{\delta^{ab}}{8\pi^2(z'-z)^2} J^a_{R,y}(z) J^b_{R,y}(z) + \frac{\delta^{ab}}{8\pi^2(\bar{z}'-\bar{z})^2} J^a_{L,y+1}(\bar{z}) J^b_{L,y+1}(\bar{z}) \\
& + \frac{-\varepsilon^{abc}\varepsilon^{abc'}}{4\pi^2|z'-z|^2} J^c_{R,y}(z) J^{c'}_{L,y+1}(\bar{z}) \Big] + \\
\Big[& \frac{\delta^{ab}}{8\pi^2(\bar{z}'-\bar{z})^2} J^a_{L,y}(\bar{z}) J^b_{L,y}(\bar{z}) + \frac{\delta^{ab}}{8\pi^2(z'-z)^2} J^a_{R,y+1}(z) J^b_{R,y+1}(z) \\
& + \frac{-\varepsilon^{abc}\varepsilon^{abc'}}{4\pi^2|z'-z|^2} J^c_{L,y+1}(\bar{z}) J^{c'}_{R,y}(z) \Big] + \\
\Big[& \frac{\delta^{ab}}{8\pi^2(z'-z)^2} J^a_{R,y+1}(z) J^b_{L,y+1}(\bar{z}) \Big] \; + \; \Big[\frac{\delta^{ab}}{8\pi^2(z'-z)^2} J^a_{R,y}(z) J^b_{L,y}(\bar{z}) \Big] + \\
\Big[& \frac{\delta^{ab}}{8\pi^2(z'-z)^2} J^a_{L,y+1}(\bar{z}) J^b_{R,y+1}(z) \Big] \; + \; \Big[\frac{\delta^{ab}}{8\pi^2(z'-z)^2} J^a_{L,y}(\bar{z}) J^b_{R,y}(z) \Big] + \\
\Big[& \frac{\delta^{ab}}{8\pi^2(\bar{z}'-\bar{z})^2} J^a_{L,y+1}(\bar{z}) J^b_{R,y+1}(z) \Big] \; + \; \Big[\frac{\delta^{ab}}{8\pi^2(\bar{z}'-\bar{z})^2} J^a_{L,y}(\bar{z}) J^b_{R,y}(z) \Big] + \\
\Big[& \frac{\delta^{ab}}{8\pi^2(\bar{z}'-\bar{z})^2} J^a_{R,y+1}(z) J^b_{L,y+1}(\bar{z}) \Big] \; + \; \Big[\frac{\delta^{ab}}{8\pi^2(\bar{z}'-\bar{z})^2} J^a_{R,y}(z) J^b_{L,y}(\bar{z}) \Big]
\end{aligned}
\tag{A.65}
$$

Next, consider the case $y = y' - 1$. This time we get:

$$\begin{aligned}
\propto & \left[\frac{\delta^{ab}}{8\pi^2(z'-z)^2} J^a_{R,y}(z) J^b_{R,y+2}(z)\right] + \left[\frac{\delta^{ab}}{8\pi^2(\bar{z}'-\bar{z})^2} J^a_{L,y}(\bar{z}) J^b_{L,y+2}(\bar{z})\right] + \\
& \left[\frac{\delta^{ab}}{8\pi^2(z'-z)^2} J^a_{R,y}(z) J^b_{L,y+2}(\bar{z})\right] + \left[\frac{\delta^{ab}}{8\pi^2(z'-z)^2} J^a_{L,y}(\bar{z}) J^b_{R,y+2}(z)\right] + \\
& \left[\frac{\delta^{ab}}{8\pi^2(\bar{z}'-\bar{z})^2} J^a_{L,y}(\bar{z}) J^b_{R,y+2}(z)\right] + \left[\frac{\delta^{ab}}{8\pi^2(\bar{z}'-\bar{z})^2} J^a_{R,y}(z) J^b_{L,y+2}(\bar{z})\right] + \\
& \left[\frac{\delta^{ab}}{8\pi^2(\bar{z}'-\bar{z})^2} J^a_{R,y}(z) J^b_{R,y+2}(z)\right] + \left[\frac{\delta^{ab}}{8\pi^2(z'-z)^2} J^a_{L,y}(\bar{z}) J^b_{L,y+2}(\bar{z})\right]. \qquad \text{(A.66)}
\end{aligned}$$

Note that since integrals of the form $\int \frac{1}{z^n}$ and $\int \frac{1}{\bar{z}^m}$ vanish, the above OPEs do not result in a $\mathbf{M}_y \cdot \mathbf{M}_{y+2}$. Such a term is generated from the irrelevant interaction the product of $\left(\mathbf{J}_{L,y+2} \cdot \mathbf{J}_{R,y+1}\right)\left(\mathbf{M}_y \cdot \mathbf{M}_{y+2}\right)$ with the backscattering term on the $y+1$ chain.

- γ_{bs} - γ_{tw}

The backscattering term in this product can either be on the first chain or the second chain, which in both cases gives the same result. In the case where the backscattering term is on the first chain, we have:

$$\begin{aligned}
& \frac{(-1)^y}{2} J^a_{R,y}(z') J^a_{L,y}(\bar{z}') N^b_y(z,\bar{z}) \partial_x N^b_{y+1}(z,\bar{z}) - \qquad \text{(A.67)} \\
& \frac{(-1)^y}{2} J^a_{R,y}(z') J^a_{L,y}(\bar{z}') N^b_{y+1}(z,\bar{z}) \partial_x N^b_y(z,\bar{z}) \,,
\end{aligned}$$

which gives:

$$\begin{aligned}
&\propto \frac{(-1)^y}{2} J^a_{R,y}(z')\Big[\frac{i\delta^{ab}\varepsilon_y(z,\bar z)}{4\pi\bar z' - \bar z} + \frac{i\epsilon^{abc}N^c_y(z,\bar z)}{4\pi(\bar z' - \bar z)}\Big]\partial_x N^b_{y+1}(z,\bar z) - \qquad \text{(A.68)}\\
&\quad \frac{(-1)^y}{2} J^a_{R,y}(z') N^b_{y+1}(z,\bar z)\partial_x\Big[\frac{i\delta^{ab}\varepsilon_y(z,\bar z)}{4\pi(\bar z' - \bar z)} + \frac{i\epsilon^{abc}N^c_y(z,\bar z)}{4\pi(\bar z' - \bar z)}\Big]\,,\\
&= \frac{(-1)^y}{2}\Big[\frac{i^2\delta^{ab}N^a_y(z,\bar z)}{(4\pi)^2(\bar z' - \bar z)(z' - z)} + \frac{(i)^2\epsilon^{acd}\epsilon^{abc}N^d_y(z,\bar z)}{(4\pi)^2(\bar z' - \bar z)(z' - z)}\Big]\partial_x N^b_{y+1}(z,\bar z) -\\
&\quad \frac{(-1)^y}{2} N^b_{y+1}(z,\bar z)\partial_x\Big[\frac{i^2\delta^{ab}N^a_y(z,\bar z)}{(4\pi)^2(\bar z' - \bar z)(z' - z)} + \frac{(i)^2\epsilon^{acd}\epsilon^{abc}N^d_y(z,\bar z)}{(4\pi)^2(\bar z' - \bar z)(z' - z)}\Big]\,,\\
&= \frac{(-1)^y}{2}[\underbrace{-\delta^{ab} - \epsilon^{acb}\epsilon^{abc}}_{\delta^{ab}}]\frac{N^b_y(z,\bar z)}{16\pi^2|z' - z|^2}\partial_x N^b_{y+1}(z,\bar z) -\\
&\quad \frac{(-1)^y}{2} N^b_{y+1}(z,\bar z)[\underbrace{-\delta^{ab} - \epsilon^{acb}\epsilon^{abc}}_{\delta^{ab}}]\partial_x\frac{N^b_y(z,\bar z)}{16\pi^2|z' - z|^2}\,,
\end{aligned}$$

- γ_{bs} - γ_M

$$\begin{aligned}
&J^a_{R,y}(z')J^a_{L,y}(\bar z')\, M^b_{y'}(\bar z, z)M^b_{y'+1}(\bar z, z) \;=\; J^a_{R,y}(z')J^a_{L,y}(\bar z')\;J^b_{R,y'}(z)J^b_{R,y'+1}(z) +\\
&J^a_{R,y}(z')J^a_{L,y}(\bar z')\;J^b_{L,y'}(\bar z)J^b_{L,y'+1}(\bar z) \;+\; J^a_{R,y}(z')J^a_{L,y}(\bar z')\;J^b_{L,y'}(\bar z)J^b_{R,y'+1}(z) +\\
&J^a_{R,y}(z')J^a_{L,y}(\bar z')\;J^b_{R,y'}(z)J^b_{L,y'+1}(\bar z)\,. \qquad \text{(A.69)}
\end{aligned}$$

Again, the backscattering term can either be on the first chain or the second term. Here we focus on the latter case and include a factor of 2 at the end. Ignoring $\mathbb{C}$-numbers and irrelevant interactions, we find:

$$\begin{aligned}
&= \Big[\frac{\delta^{ab}}{8\pi^2(z' - z)^2} + \frac{i\epsilon^{abc}J^c_{R,y}(z)}{2\pi(z' - z)}\Big]J^a_{L,y}(\bar z')\;J^b_{R,y+1}(z) +\\
&\quad \Big[\frac{\delta^{ab}}{8\pi^2(\bar z' - \bar z)^2} + \frac{i\epsilon^{abc}J^c_{L,y}(\bar z)}{2\pi(\bar z' - \bar z)}\Big]J^a_{R,y}(z')\;J^b_{L,y+1}(\bar z) +\\
&\quad \Big[\frac{\delta^{ab}}{8\pi^2(\bar z' - \bar z)^2} + \frac{i\epsilon^{abc}J^c_{L,y}(\bar z)}{2\pi(\bar z' - \bar z)}\Big]J^a_{R,y}(z')\;J^b_{R,y+1}(z) +\\
&\quad \Big[\frac{\delta^{ab}}{8\pi^2(z' - z)^2} + \frac{i\epsilon^{abc}J^c_{R,y}(z)}{2\pi(z' - z)}\Big]J^a_{L,y}(\bar z')\;J^b_{L,y+1}(\bar z)\,, \qquad \text{(A.70)}
\end{aligned}$$

which all vanish due to the vanishing integrals $\int \frac{1}{z^n}$ and $\int \frac{1}{\bar{z}^n}$.

- γ_M - γ_{tw}

$$\frac{(-1)^{y'}}{2} M^a_y(\bar{z}', z') M^a_{y+1}(\bar{z}', z') \left[N^b_{y'}(\bar{z}, z) \partial_x N^b_{y'+1}(\bar{z}, z) \; - \; N^b_{y'+1}(\bar{z}, z) \partial_x N^b_{y'}(\bar{z}, z) \right]. \tag{A.71}$$

The case $y = y' - 1$ does not result in anything of interest. In the case $y' = y$, only have:

$$\begin{aligned}
= & \frac{(-1)^y}{2} J^a_{R,y}(z') J^a_{R,y+1}(z') \left[N^b_y(\bar{z}, z) \partial_x N^b_{y+1}(\bar{z}, z) \; - \; N^b_{y+1}(\bar{z}, z) \partial_x N^b_y(\bar{z}, z) \right] + \\
& \frac{(-1)^y}{2} J^a_{L,y}(\bar{z}') J^a_{L,y+1}(\bar{z}') \left[N^b_y(\bar{z}, z) \partial_x N^b_{y+1}(\bar{z}, z) \; - \; N^b_{y+1}(\bar{z}, z) \partial_x N^b_y(\bar{z}, z) \right] + \\
& \frac{(-1)^y}{2} J^a_{L,y}(\bar{z}') J^a_{R,y+1}(\bar{z}') \left[N^b_y(\bar{z}, z) \partial_x N^b_{y+1}(\bar{z}, z) \; - \; N^b_{y+1}(\bar{z}, z) \partial_x N^b_y(\bar{z}, z) \right] + \\
& \frac{(-1)^y}{2} J^a_{R,y}(z') J^a_{L,y+1}(\bar{z}') \left[N^b_y(\bar{z}, z) \partial_x N^b_{y+1}(\bar{z}, z) \; - \; N^b_{y+1}(\bar{z}, z) \partial_x N^b_y(\bar{z}, z) \right].
\end{aligned} \tag{A.72}$$

Of the above products, the first two will result in $\frac{1}{(\bar{z}' - \bar{z})}$ and $\frac{1}{(z' - z)}$, which will vanish and thus we ignore. The remaining two terms give:

$$\begin{aligned}
= \; \frac{(-1)^y}{2} \Big[& J^a_{L,y}(\bar{z}') J^a_{R,y+1}(\bar{z}') \, N^b_y(\bar{z}, z) \partial_x N^b_{y+1}(\bar{z}, z) - \\
& J^a_{L,y}(\bar{z}') J^a_{R,y+1}(\bar{z}') \, N^b_{y+1}(\bar{z}, z) \partial_x N^b_y(\bar{z}, z) + \\
& J^a_{R,y}(z') J^a_{L,y+1}(\bar{z}') \, N^b_y(\bar{z}, z) \partial_x N^b_{y+1}(\bar{z}, z) - \\
& J^a_{R,y}(z') J^a_{L,y+1}(\bar{z}') \, N^b_{y+1}(\bar{z}, z) \partial_x N^b_y(\bar{z}, z) \Big].
\end{aligned} \tag{A.73}$$

We get:

$$
\begin{aligned}
= \frac{(-1)^y}{2}\Bigg[& \Big[\frac{i\delta^{ab}\varepsilon_y(\bar{z},z)}{4\pi(\bar{z}'-\bar{z})}+\frac{i\epsilon^{abc}N^c_y(\bar{z},z)}{4\pi(\bar{z}'-\bar{z})}\Big]\partial_x\Big[\frac{-i\delta^{ab}\varepsilon_{y+1}(\bar{z},z)}{4\pi(z'-z)}+\frac{i\epsilon^{abc}N^c_{y+1}(\bar{z},z)}{4\pi(z'-z)}\Big]- \\
& \Big[\frac{-i\delta^{ab}\varepsilon_{y+1}(\bar{z},z)}{4\pi(z'-z)}+\frac{i\epsilon^{abc}N^c_{y+1}(\bar{z},z)}{4\pi(z'-z)}\Big]\partial_x\Big[\frac{i\delta^{ab}\varepsilon_y(\bar{z},z)}{4\pi(\bar{z}'-\bar{z})}+\frac{i\epsilon^{abc}N^c_y(\bar{z},z)}{4\pi(\bar{z}'-\bar{z})}\Big]+ \\
& \Big[\frac{i\delta^{ab}\varepsilon_y(\bar{z},z)}{4\pi(z'-z)}+\frac{i\epsilon^{abc}N^c_y(\bar{z},z)}{4\pi(z'-z)}\Big]\partial_x\Big[\frac{-i\delta^{ab}\varepsilon_{y+1}(\bar{z},z)}{4\pi(\bar{z}'-\bar{z})}+\frac{i\epsilon^{abc}N^c_{y+1}(\bar{z},z)}{4\pi(\bar{z}'-\bar{z})}\Big]- \\
& \Big[\frac{i\delta^{ab}\varepsilon_{y+1}(\bar{z},z)}{4\pi(\bar{z}'-\bar{z})}+\frac{i\epsilon^{abc}N^c_{y+1}(\bar{z},z)}{4\pi(\bar{z}'-\bar{z})}\Big]\partial_x\Big[\frac{-i\delta^{ab}\varepsilon_y(\bar{z},z)}{4\pi(z'-z)}+\frac{i\epsilon^{abc}N^c_y(\bar{z},z)}{4\pi(z'-z)}\Big]\Bigg].
\end{aligned}
\tag{A.74}
$$

Finally we obtain:

$$
\begin{aligned}
= \frac{(-1)^y}{2}\Bigg[& \Big[-\delta^{ab}\varepsilon_y(\bar{z},z)\partial_x\varepsilon_{y+1}(\bar{z},z)+\epsilon^{abc}\epsilon^{abd}N^c_y(\bar{z},z)\partial_x N^d_{y+1}(\bar{z},z)\Big]\frac{-1}{16\pi^2|z'-z|^2}- \\
& \Big[-\delta^{ab}\varepsilon_{y+1}(\bar{z},z)\partial_x\varepsilon_y(\bar{z},z)+\epsilon^{abc}\epsilon^{abd}N^c_{y+1}(\bar{z},z)\partial_x N^d_y(\bar{z},z)\Big]\frac{-1}{16\pi^2|z'-z|^2}+ \\
& \Big[-\delta^{ab}\varepsilon_y(\bar{z},z)\partial_x\varepsilon_{y+1}(\bar{z},z)+\epsilon^{abc}\epsilon^{abd}N^c_y(\bar{z},z)\partial_x N^d_{y+1}(\bar{z},z)\Big]\frac{-1}{16\pi^2|z'-z|^2}- \\
& \Big[-\delta^{ab}\varepsilon_{y+1}(\bar{z},z)\partial_x\varepsilon_y(\bar{z},z)+\epsilon^{abc}\epsilon^{abd}N^c_{y+1}(\bar{z},z)\partial_x N^d_y(\bar{z},z)\Big]\frac{-1}{16\pi^2|z'-z|^2}\Bigg].
\end{aligned}
\tag{A.75}
$$

Note that the terms that result from applying the spatial derivative on $\frac{1}{|z'-z|^2}$ factors vanish and thus have not been shown. Therefore, this product generates γ_{tw} and γ_ε.

γ_{bs} - g_N

$$
J^a_{R,y}(z')J^a_{L,y}(\bar{z}')\,N^b_{y'}(\bar{z},z)N^b_{y'+2}(\bar{z},z) \tag{A.76}
$$

There are two possibilities for the chain indices: $y = y'$ and $y = y' - 2$. We only consider the case $y = y'$ and at the end include a factor of 2.

$$J^a_{R,y}(z')J^a_{L,y}(\bar{z}')\, N^b_y(\bar{z},z)N^b_{y+2}(\bar{z},z) \tag{A.77}$$

$$= J^a_{R,y}(z')\Big[\frac{i\delta^{ab}\varepsilon_y(\bar{z},z)}{4\pi(\bar{z}'-\bar{z})} + \frac{i\epsilon^{abc}N^c_y(\bar{z},z)}{4\pi(\bar{z}'-\bar{z})}\Big]N^b_{y+2}(\bar{z},z)$$

$$= \Big[\frac{i\delta^{ab}}{4\pi(\bar{z}'-\bar{z})}\frac{iN^a_y(\bar{z},z)}{4\pi(z'-z)} + \frac{i\epsilon^{abc}}{4\pi(\bar{z}'-\bar{z})}\frac{i\epsilon^{acd}N^d_y(\bar{z},z)}{4\pi(z'-z)}\Big]N^b_{y+2}(\bar{z},z)$$

$$= \big[\underbrace{\delta^{ab} + \epsilon^{abc}\epsilon^{acd}}_{\delta^{ab}}\big]\frac{-1}{16\pi^2|z'-z|^2}N^b_y(\bar{z},z)N^b_{y+2}(\bar{z},z)\,.$$

- γ_{bs} - g_ε

$$J^a_{R,y}(z')J^a_{L,y}(\bar{z}')\,\varepsilon_{y'}(z,\bar{z})\varepsilon_{y'+2}(z,\bar{z}) \tag{A.78}$$

Just like in the previous case, here we have two choices for y'. Following the same steps as in the previous case, we find:

$$J^a_{R,y}(z')J^a_{L,y}(\bar{z}')\,\varepsilon_{y'}(z,\bar{z})\varepsilon_{y'+2}(z,\bar{z}) \tag{A.79}$$

$$= J^a_{R,y}(z')\,\frac{-iN^a_y(z,\bar{z})}{4\pi(\bar{z}'-\bar{z})}\varepsilon_{y+2}(z,\bar{z})$$

$$= \frac{-i}{4\pi(\bar{z}'-\bar{z})}\Big[\frac{-i\delta^{aa}\varepsilon_y(z,\bar{z})}{4\pi(z'-z)} + \frac{i\epsilon^{aac}N^c_y(z,\bar{z})}{4\pi(z'-z)}\Big]\varepsilon_{y+2}(z,\bar{z})$$

$$= \frac{-\delta^{aa}}{16\pi^2|z'-z|^2}\varepsilon_y(z,\bar{z})\varepsilon_{y+2}(z,\bar{z})\,.$$

- **γ_M-g_N, γ_M-g_ε, γ_{tw}-g_ε, and g_N-g_ε**

None of these products results in the renormalizaion of any of the couplings we are considering here.

$$M^a_y(z',\bar{z}')M^a_{y+1}(z',\bar{z}')\,\varepsilon_{y'}(z,\bar{z})\varepsilon_{y'+2}(z,\bar{z}) \tag{A.80}$$

$$M^a_y(z',\bar{z}')M^a_{y+1}(z',\bar{z}')\,N^b_{y'}(z,\bar{z})N^b_{y'+2}(z,\bar{z}) \tag{A.81}$$

$$\frac{(-1)^y}{2}\Big[N^a_y(z',\bar{z}')\partial_x N^a_{y+1}(z',\bar{z}') - N^a_{y+1}(z',\bar{z}')\partial_x N^a_y(z',\bar{z}')\Big]\,\varepsilon_{y'}(z,\bar{z})\varepsilon_{y'+2}(z,\bar{z}) \tag{A.82}$$

and,

$$N^a_y(z',\bar{z}')N^a_{y+2}(z',\bar{z}')\,\varepsilon_{y'}(z,\bar{z})\varepsilon_{y'+2}(z,\bar{z}) \tag{A.83}$$

- γ_{tw} - g_N

The product of a twist term with a second chain Néel coupling is:

$$\frac{(-1)^y}{2}\Big[N^a_y(z',\bar{z}')\partial_x N^a_{y+1}(z',\bar{z}') - N^a_{y+1}(z',\bar{z}')\partial_x N^a_y(z',\bar{z}')\Big]N^b_{y'}(z,\bar{z})N^b_{y'+2}(z,\bar{z}) \tag{A.84}$$

Several choice are possible for the indecies. In particular, we ignore $y+1=y'$ and $y=y'+2$ that result in farther chain analogs of the twist term. Here we only focus on $y=y'$ and $y=y'+1$. First consider the case $y=y'$:

$$\begin{aligned}&\frac{(-1)^y}{2}\Big[N^a_y(z',\bar{z}')\partial_x N^a_{y+1}(z',\bar{z}') - N^a_{y+1}(z',\bar{z}')\partial_x N^a_y(z',\bar{z}')\Big]N^b_y(z,\bar{z})N^b_{y+2}(z,\bar{z})\\ =&-\frac{(-1)^{y+1}}{2}\Big[\frac{\delta^{ab}}{2\pi^2|z'-z|}\partial_x N^a_{y+1}(z',\bar{z}') - N^a_{y+1}(z',\bar{z}')\partial_x\frac{\delta^{ab}}{2\pi^2|z'-z|}\Big]N^b_{y+2}(z,\bar{z})\end{aligned} \tag{A.85}$$

Similarly, the case $y=y'+1$ gives:

$$\begin{aligned}&\frac{(-1)^y}{2}\Big[N^a_y(z',\bar{z}')\partial_x N^a_{y+1}(z',\bar{z}') - N^a_{y+1}(z',\bar{z}')\partial_x N^a_y(z',\bar{z}')\Big]N^b_{y-1}(z,\bar{z})N^b_{y+1}(z,\bar{z})\\ =&-\frac{(-1)^{y-1}}{2}\Big[N^a_y(z',\bar{z}')\partial_x\frac{\delta^{ab}}{2\pi^2|z'-z|} - \frac{\delta^{ab}}{2\pi^2|z'-z|}\partial_x N^a_y(z',\bar{z}')\Big]N^b_{y-1}(z,\bar{z})\end{aligned} \tag{A.86}$$

The results of Eqs. (A.85,A.86) together contribute to the renormalization of the twist term.

- g_N - g_N

$$N^a_y(z',\bar{z}')N^a_{y+2}(z',\bar{z}')\,N^b_{y'}(z,\bar{z})N^b_{y'+2}(z,\bar{z}) \tag{A.87}$$

The case $y=y'$ results in a $\mathbb{C}$-number and the intrachain : $\vec{N}\cdot\vec{N}$: term, which we ignore as it will be $\mathcal{O}(J'/J)^4 \ll 1$. Consider the case $y+2=y'$. We have:

$$\begin{aligned}&N^a_y(z',\bar{z}')N^a_{y+2}(z',\bar{z}')\,N^b_{y+2}(z,\bar{z})N^b_{y+4}(z,\bar{z})\\ =&\,N^a_y(z',\bar{z}')\frac{\delta^{ab}}{2\pi^2|z'-z|}N^b_{y+4}(z,\bar{z})\,.\end{aligned} \tag{A.88}$$

This is a farther neighbor analog of g_N.

- g_ε - g_ε

$$\varepsilon_y(z',\bar{z}')\varepsilon_{y+2}(z',\bar{z}')\,\varepsilon_{y'}(z,\bar{z})\varepsilon_{y'+2}(z,\bar{z}) \tag{A.89}$$

Similar to the previous product, the case $y = y'$ only results in a $\mathbb{C}$-number and a weak intrachain term, which we ignore. The case $y + 2 = y'$ gives a farther neighbor analog of g_ε:

$$\begin{aligned}&\varepsilon_y(z',\bar{z}')\varepsilon_{y+2}(z',\bar{z}')\,\varepsilon_{y'}(z,\bar{z})\varepsilon_{y'+2}(z,\bar{z}) \\ =&\,\varepsilon_y(z',\bar{z}')\frac{1}{2\pi^2|z'-z|}\varepsilon_{y'+2}(z,\bar{z})\,.\end{aligned} \tag{A.90}$$

- γ_{bs} - g_M

$$J^a_{R,y}(z')J^a_{L,y}(\bar{z}')\,M^b_{y'}(z,\bar{z})M^b_{y'+2}(z,\bar{z}) \tag{A.91}$$

Similar to other products of the backscattering term with an interchain term, the backscattering term can either be on the first chain or the third chain. Here we consider the latter case and will include a factor of 2 at the end. We have:

$$\begin{aligned}&J^a_{R,y}(z')J^a_{L,y}(\bar{z}')\,M^b_{y}(z,\bar{z})M^b_{y+2}(z,\bar{z}) \\ =&\,J^a_{R,y}(z')J^a_{L,y}(\bar{z}')\big[J^b_{L,y}(\bar{z})+J^b_{R,y}(z)\big]M^b_{y+2}(z,\bar{z}) \\ =&\,\Bigg[\Big[\frac{i\delta^{ab}}{8\pi^2(\bar{z}'-\bar{z})^2}+\frac{i\epsilon^{abs}J^c_{L,y}(\bar{z})}{2\pi(\bar{z}'-\bar{z})}\Big]J^a_{R,y}(z') \\ &+\Big[\frac{i\delta^{ab}}{8\pi^2(z'-z)^2}+\frac{i\epsilon^{abs}J^c_{R,y}(z)}{2\pi(z'-z)}\Big]J^a_{L,y}(\bar{z}')\Bigg]M^b_{y+2}(z,\bar{z})\,.\end{aligned} \tag{A.92}$$

None of the above terms results in the renormalization of g_M.

- γ_M - g_M

For the same reason that $\vec{M}_y\cdot\vec{M}_{y+2}$ cannot be generated from the products of two $\vec{M}_y\cdot\vec{M}_{y+1}$, this product does not renormalize any of the interchain interaction terms considered in the RG analysis (can only generate unimportant irrelevant terms). Nevertheless, this product generates the irrelevant interaction term:

$$\vec{M}_y\cdot\vec{M}_{y+3}\vec{J}_{L,y+1}\cdot\vec{J}_{R,y+1}\,, \tag{A.93}$$

which, in the subsequent RG iterations an upon contraction with the backscattering term on the $y+1$ chain, generates $\vec{M}_y\cdot\vec{M}_{y+3}$.

- γ_{tw} - g_M

$$\frac{(-1)^y}{2}\Big[N^a_y(z',\bar{z}')\partial_x N^a_{y+1}(z',\bar{z}') \;-\; N^a_{y+1}(z',\bar{z}')\partial_x N^a_y(z',\bar{z}')\Big]\, M^b_{y'}(z,\bar{z})M^b_{y'+2}(z,\bar{z}) \tag{A.94}$$

Regardless of the choice of indices, as can be inferred from the OPEs, this will not result in the renormalization of any of the interchain couplings considered here.

- g_N - g_M

$$N^a_y(z',\bar{z}')N^a_{y+2}(z',\bar{z}')\, M^b_{y'}(z,\bar{z})M^b_{y'+2}(z,\bar{z}) \tag{A.95}$$

The only choice of chain indices that result in the renormalization of the couplings is $y' = y$. In this case we have:

$$\begin{aligned} &N^a_y(z',\bar{z}')N^a_{y+2}(z',\bar{z}')\big[J^b_{L,y}(\bar{z}) + J^b_{R,y}(z)\big]\big[J^b_{L,y+2}(\bar{z}) + J^b_{R,y+2}(z)\big] \qquad (A.96)\\ &\propto \Big[\frac{i\delta^{ab}\varepsilon_y(z,\bar{z})}{4\pi(\bar{z}'-\bar{z})} + \frac{i\epsilon^{abc}N^c_y(z,\bar{z})}{4\pi(\bar{z}'-\bar{z})} \;+\; \frac{-i\delta^{ab}\varepsilon_y(z,\bar{z})}{4\pi(z'-z)} + \frac{i\epsilon^{abc}N^c_y(z,\bar{z})}{4\pi(z'-z)}\Big]\\ &\quad\Big[\frac{i\delta^{ab}\varepsilon_{y+2}(z,\bar{z})}{4\pi(\bar{z}'-\bar{z})} + \frac{i\epsilon^{abd}N^d_{y+2}(z,\bar{z})}{4\pi(\bar{z}'-\bar{z})} \;+\; \frac{-i\delta^{ab}\varepsilon_{y+2}(z,\bar{z})}{4\pi(z'-z)} + \frac{i\epsilon^{abd}N^d_{y+2}(z,\bar{z})}{4\pi(z'-z)}\Big]\\ &\rightsquigarrow \frac{2\delta^{ab}}{16\pi^2(\bar{z}'-\bar{z})}\varepsilon_y(z,\bar{z})\varepsilon_{y+2}(z,\bar{z}) \;+\; \frac{-2\epsilon^{abc}\epsilon^{abd}}{16\pi^2(\bar{z}'-\bar{z})}N^c_y(z,\bar{z})N^d_{y+2}(z,\bar{z})\,, \end{aligned}$$

where, in the last line, we have ignored terms that vanish upon loop integration.

- g_ε - g_M

$$\varepsilon_y(z',\bar{z}')\varepsilon_{y+2}(z',\bar{z}')\, M^b_{y'}(z,\bar{z})M^b_{y'+2}(z,\bar{z}) \tag{A.97}$$

This is similar to the previous case. Consider the case $y = y'$:

$$\begin{aligned} &\varepsilon_y(z',\bar{z}')\varepsilon_{y+2}(z',\bar{z}')\big[J^b_{L,y}(\bar{z}) + J^b_{R,y}(z)\big]\big[J^b_{L,y+2}(\bar{z}) + J^b_{R,y+2}(z)\big] \qquad (A.98)\\ &\propto \Big[\frac{-iN^c_y(z,\bar{z})}{4\pi(\bar{z}'-\bar{z})} \;+\; \frac{iN^c_y(z,\bar{z})}{4\pi(z'-z)}\Big]\Big[\frac{-iN^c_y(z,\bar{z})}{4\pi(\bar{z}'-\bar{z})} \;+\; \frac{iN^c_y(z,\bar{z})}{4\pi(z'-z)}\Big]\\ &\rightsquigarrow \frac{-2}{16\pi^2(\bar{z}'-\bar{z})}N^a_y(z,\bar{z})N^a_{y+2}(z,\bar{z})\,. \end{aligned}$$

- γ_{bs} - ζ_N

$$J^a_{R,y}(z')J^a_{L,y}(\bar{z}')\,\partial_x N^b_{y'}(z,\bar{z})\partial_x N^b_{y'+2}(z,\bar{z}) \tag{A.99}$$

As in the previous cases involving a backscattering term, the backscattering term can either be on the first chain or the third chain. Again, we consider the latter and will include a factor of 2 at the end. We have:

$$
\begin{aligned}
& J^a_{R,y}(z')J^a_{L,y}(\bar{z}')\partial_x N^b_y(z,\bar{z})\partial_x N^b_{y+2}(z,\bar{z}) \qquad (A.100)\\
&\propto J^a_{R,y}(z')\partial_x\Big[\frac{i\delta^{ab}\varepsilon_y(z,\bar{z})}{4\pi(\bar{z}'-\bar{z})}+\frac{i\epsilon^{abc}N^c_y(z,\bar{z})}{4\pi(\bar{z}'-\bar{z})}\Big]\partial_x N^b_{y+2}(z,\bar{z})\\
&\propto \partial_x\Big[\frac{-\delta^{ab}N^a_y(z,\bar{z})}{16\pi^2|z'-z|^2}+\frac{1}{16\pi^2|z'-z|^2}\Big(\epsilon^{abc}\delta^{ab}\varepsilon_y(z,\bar{z})\,\epsilon^{abc}\epsilon^{acd}N^d_y(z,\bar{z})\Big)\Big]\partial_x N^b_{y+2}(z,\bar{z})\\
&= \partial_x\frac{1}{16\pi^2|z'-z|^2}\big[\underbrace{-\delta^{ab}+|\epsilon^{abc}|}_{1}\big]N^b_y(z,\bar{z})\partial_x N^b_{y+2}(z,\bar{z})\,.
\end{aligned}
$$

- γ_M - ζ_N

$$M^a_y(z',\bar{z}')M^a_{y+1}(z',\bar{z}')\partial_x N^b_{y'}(z,\bar{z})\partial_x N^b_{y'+2}(z,\bar{z}) \qquad (A.101)$$

This product results in no renormalized interaction due to the vanishing integrals $\int\frac{1}{z'-z}$ and $\int\frac{1}{\bar{z}'-\bar{z}}$.

- γ_{tw} - ζ_N

$$\frac{(-1)^y}{2}\Big[N^a_y(z',\bar{z}')\partial_x N^a_{y+1}(z',\bar{z}') \;-\; N^a_{y+1}(z',\bar{z}')\partial_x N^a_y(z',\bar{z}')\Big]\partial_x N^b_{y'}(z,\bar{z})\partial_x N^b_{y'+2}(z,\bar{z}) \qquad (A.102)$$

This will result in the renormalization of the twist term. There are two choices of indices. First consider the case $y = y'$. We have:

$$
\begin{aligned}
& \frac{(-1)^y}{2}\Big[N^a_y(z',\bar{z}')\partial_x N^a_{y+1}(z',\bar{z}') \;-\; N^a_{y+1}(z',\bar{z}')\partial_x N^a_y(z',\bar{z}')\Big]\partial_x N^b_y(z,\bar{z})\partial_x N^b_{y+2}(z,\bar{z})\\
&\propto \frac{(-1)^y}{2}\Big[\partial_x\frac{\delta^{ab}}{2\pi^2|z'-z|}\partial_x N^a_{y+1}(z',\bar{z}') \;-\; N^a_{y+1}(z',\bar{z}')\partial_x^2\frac{\delta^{ab}}{2\pi^2|z'-z|}\Big]\partial_x N^b_{y+2}(z,\bar{z}) \qquad (A.103)
\end{aligned}
$$

Similarly, for the case $y = y'+1$ we have:

$$
\begin{aligned}
& \frac{(-1)^y}{2}\Big[N^a_y(z',\bar{z}')\partial_x N^a_{y+1}(z',\bar{z}') \;-\; N^a_{y+1}(z',\bar{z}')\partial_x N^a_y(z',\bar{z}')\Big]\partial_x N^b_{y-1}(z,\bar{z})\partial_x N^b_{y+1}(z,\bar{z})\\
&\propto \frac{(-1)^y}{2}\Big[N^a_y(z',\bar{z}')\partial_x^2\frac{\delta^{ab}}{2\pi^2|z'-z|} \;-\; \partial_x N^a_y(z',\bar{z}')\partial_x\frac{\delta^{ab}}{2\pi^2|z'-z|}\Big]\partial_x N^b_{y-1}(z,\bar{z})\,. \qquad (A.104)
\end{aligned}
$$

These two result in the renormalization of the twist term as the contractions with a single spatial derivative are odd in x and will vanish.

- g_N - ζ_N

$$N^a_y(z',\bar{z}')N^a_{y+2}(z',\bar{z}')\,\partial_x N^b_{y'}(z,\bar{z})\partial_x N^b_{y'+2}(z,\bar{z}) \tag{A.105}$$

This product will not result in the renormalization of any of the interaction terms in the set of terms kept in the RG analysis.

- g_ε - ζ_N

$$\varepsilon_y(z',\bar{z}')\varepsilon_{y+2}(z',\bar{z}')\partial_x N^b_{y'}(z,\bar{z})\partial_x N^b_{y'+2}(z,\bar{z}) \tag{A.106}$$

Since the OPE of $\mathbf{N}$ with ε does not contain any singular terms, this product is ignored.

- g_M - ζ_N

$$M^a_{y'}(z',\bar{z}')M^a_{y'+2}(z',\bar{z}')\partial_x N^b_{y'}(z,\bar{z})\partial_x N^b_{y'+2}(z,\bar{z}) \tag{A.107}$$

The only choice of indices that result in anything of interest is $y = y'$. We have:

$$\begin{aligned}
&\big[J^b_{L,y}(\bar{z}) + J^b_{R,y}(z)\big]\big[J^b_{L,y+2}(\bar{z}) + J^b_{R,y+2}(z)\big]\partial_x N^b_y(z,\bar{z})\partial_x N^b_{y+2}(z,\bar{z}) \qquad (A.108)\\
&\propto \partial_x\Big[\frac{i\delta^{ab}\varepsilon_y(z,\bar{z})}{4\pi(\bar{z}'-\bar{z})} + \frac{i\epsilon^{abc}N^c_y(z,\bar{z})}{4\pi(\bar{z}'-\bar{z})} + \frac{-i\delta^{ab}\varepsilon_y(z,\bar{z})}{4\pi(z'-z)} + \frac{i\epsilon^{abc}N^c_y(z,\bar{z})}{4\pi(z'-z)}\Big]\times\\
&\quad \partial_x\Big[\frac{i\delta^{ab}\varepsilon_{y+2}(z,\bar{z})}{4\pi(\bar{z}'-\bar{z})} + \frac{i\epsilon^{abd}N^d_{y+2}(z,\bar{z})}{4\pi(\bar{z}'-\bar{z})} + \frac{-i\delta^{ab}\varepsilon_{y+2}(z,\bar{z})}{4\pi(z'-z)} + \frac{i\epsilon^{abd}N^d_{y+2}(z,\bar{z})}{4\pi(z'-z)}\Big]\\
&\rightsquigarrow \Big[\frac{2\delta^{ab}}{16\pi^2|z'-z|^2}\partial_x\varepsilon_y(z,\bar{z})\partial_x\varepsilon_{y+2}(z,\bar{z}) + \frac{2\delta^{ab}}{16\pi^2|z'-z|^4}\varepsilon_y(z,\bar{z})\varepsilon_{y+2}(z,\bar{z})\Big] +\\
&\quad \Big[\frac{-2|\epsilon^{abc}|}{16\pi^2|z'-z|^2}\partial_x N^d_{y+2}(z,\bar{z})\partial_x N^d_{y+2}(z,\bar{z}) + \frac{-2|\epsilon^{abc}|}{16\pi^2|z'-z|^4}N^c_{y+2}(z,\bar{z})N^c_{y+2}(z,\bar{z})\Big].
\end{aligned}$$

- γ_{bs} - γ_ε

$$\frac{(-1)^y}{2}J^a_{R,y}(z')J^a_{L,y}(\bar{z}')\Big[\varepsilon_{y'}(z,\bar{z})\partial_x\varepsilon_{y'+1}(z,\bar{z}) - \varepsilon_{y'+1}(z,\bar{z})\partial_x\varepsilon_{y'}(z,\bar{z})\Big] \tag{A.109}$$

This product is similar to the product of a twist term and a backscattering term. For the case $y = y'$, we have:

$$\frac{(-1)^y}{2} J^a_{R,y}(z') J^a_{L,y}(\bar{z}') \Big[\varepsilon_{y'}(z,\bar{z}) \partial_x \varepsilon_{y+1}(z,\bar{z}) - \varepsilon_{y'+1}(z,\bar{z}) \partial_x \varepsilon_y(z,\bar{z}) \Big] \tag{A.110}$$

$$\propto \frac{(-1)^y}{2} J^a_{R,y}(z') \Big[\frac{-iN^a}{4\pi(\bar{z}'-\bar{z})} \partial_x \varepsilon_{y+1}(z,\bar{z}) \; - \; \varepsilon_{y'+1}(z,\bar{z}) \partial_x \frac{-iN^a}{4\pi(z'-z)} \Big]$$

$$\propto \frac{(-1)^y}{2} J^a_{R,y}(z') \Big[\frac{-\varepsilon_y(z,\bar{z})}{16\pi^2 |z'-z|^2} \partial_x \varepsilon_{y+1}(z,\bar{z}) \; - \; \varepsilon_{y'+1}(z,\bar{z}) \partial_x \frac{-\varepsilon_y(z,\bar{z})}{16\pi^2 |z'-z|^2} \Big] .$$

- γ_M - γ_ε

$$\frac{(-1)^{y'}}{2} M^a_{y'}(z',\bar{z}') M^a_{y'+1}(z',\bar{z}') \Big[\varepsilon_{y'}(z,\bar{z}) \partial_x \varepsilon_{y'+1}(z,\bar{z}) \; - \; \varepsilon_{y'+1}(z,\bar{z}) \partial_x \varepsilon_{y'}(z,\bar{z}) \Big] \tag{A.111}$$

This is similar to the product of γ_M and γ_ε. First consider the case $y = y'$:

$$\frac{(-1)^y}{2} M^a_{y'}(z',\bar{z}') M^a_{y'+1}(z',\bar{z}') \Big[\varepsilon_y(z,\bar{z}) \partial_x \varepsilon_{y+1}(z,\bar{z}) - \varepsilon_{y+1}(z,\bar{z}) \partial_x \varepsilon_y(z,\bar{z}) \Big]$$

$$\propto \frac{(-1)^y}{2} M^a_{y'+1}(z',\bar{z}') \Bigg[\Big[\frac{-iN^a_y(z,\bar{z})}{4\pi(\bar{z}'-\bar{z})} + \frac{iN^a_y(z,\bar{z})}{4\pi(z'-z)} \Big] \partial_x \varepsilon_{y+1}(z,\bar{z})$$

$$- \; \varepsilon_{y+1}(z,\bar{z}) \partial_x \Big[\frac{-iN^a_y(z,\bar{z})}{4\pi(\bar{z}'-\bar{z})} + \frac{iN^a_y(z,\bar{z})}{4\pi(z'-z)} \Big] \Bigg]$$

$$\rightsquigarrow \frac{(-1)^y}{2} \Bigg[\Big[\frac{-iN^a_y(z,\bar{z})}{4\pi(\bar{z}'-\bar{z})} + \frac{iN^a_y(z,\bar{z})}{4\pi(z'-z)} \Big] \partial_x \Big[\frac{-iN^a_{y+1}(z,\bar{z})}{4\pi(\bar{z}'-\bar{z})} + \frac{iN^a_{y+1}(z,\bar{z})}{4\pi(z'-z)} \Big]$$

$$- \; \Big[\frac{-iN^a_{y+1}(z,\bar{z})}{4\pi(\bar{z}'-\bar{z})} + \frac{iN^a_{y+1}(z,\bar{z})}{4\pi(z'-z)} \Big] \partial_x \Big[\frac{-iN^a_y(z,\bar{z})}{4\pi(\bar{z}'-\bar{z})} + \frac{iN^a_y(z,\bar{z})}{4\pi(z'-z)} \Big] \Bigg]$$

$$\rightsquigarrow \frac{(-1)^y}{2} \frac{2}{16\pi^2 |z'-z|^2} \Big[N^a_y(z,\bar{z}) \partial_x N^a_{y+1}(z,\bar{z}) - N^a_{y+1}(z,\bar{z}) \partial_x N^a_y(z,\bar{z}) \Big] , \tag{A.112}$$

- γ_{tw} - γ_ε, $g_N - \gamma_\varepsilon$, $\zeta_N - \gamma_\varepsilon$ **and** g_N - ζ_ε

None of these products results in anything of interest as the OPE of $\mathbf{N}$ with ε does not contain any singular terms.

- g_ε - γ_ε

$$\frac{(-1)^{y'}}{2} \varepsilon_y(z',\bar{z}') \varepsilon_{y+2}(z',\bar{z}') \Big[\varepsilon_{y'}(z,\bar{z}) \partial_x \varepsilon_{y'+1}(z,\bar{z}) \; - \; \varepsilon_{y'+1}(z,\bar{z}) \partial_x \varepsilon_{y'}(z,\bar{z}) \Big] \tag{A.113}$$

This is similar to the product of g_N and γ_{tw}. First consider the case $y = y'$:

$$\begin{aligned}
&\frac{(-1)^y}{2}\varepsilon_y(z',\bar{z}')\varepsilon_{y+2}(z',\bar{z}')\Big[\varepsilon_{y'}(z,\bar{z})\partial_x\varepsilon_{y'+1}(z,\bar{z}) \;-\; \varepsilon_{y+1}(z,\bar{z})\partial_x\varepsilon_y(z,\bar{z})\Big] \\
&\propto \frac{(-1)^y}{2}\varepsilon_{y+2}(z',\bar{z}')\Big[\frac{1}{2\pi^2|z'-z|}\partial_x\varepsilon_{y'+1}(z,\bar{z}) \;-\; \varepsilon_{y+1}(z,\bar{z})\partial_x\frac{1}{2\pi^2|z'-z|}\Big]. \qquad \text{(A.114)}
\end{aligned}$$

Similarly, in the case $y = y' + 1$, we get:

$$\begin{aligned}
&\frac{(-1)^{y+1}}{2}\varepsilon_y(z',\bar{z}')\varepsilon_{y+2}(z',\bar{z}')\Big[\varepsilon_{y+1}(z,\bar{z})\partial_x\varepsilon_{y+2}(z,\bar{z}) \;-\; \varepsilon_{y+2}(z,\bar{z})\partial_x\varepsilon_{y+1}(z,\bar{z})\Big] \\
&\propto \frac{(-1)^{y+1}}{2}\varepsilon_y(z',\bar{z}')\Big[\varepsilon_{y+1}(z,\bar{z})\partial_x\frac{1}{2\pi^2|z'-z|} \;-\; \frac{1}{2\pi^2|z'-z|}\partial_x\varepsilon_{y+1}(z,\bar{z})\Big]. \qquad \text{(A.115)}
\end{aligned}$$

These two together result in the renormalization of γ_ε.

- γ_ε - γ_ε

$$\begin{aligned}
&\frac{(-1)^{y'+y}}{4}\Big[\varepsilon_{y'}(z',\bar{z}')\partial_x\varepsilon_{y'+1}(z',\bar{z}') \;-\; \varepsilon_{y+1}(z',\bar{z}')\partial_x\varepsilon_y(z',\bar{z}')\Big]\times \qquad \text{(A.116)} \\
&\qquad\Big[\varepsilon_{y'}(z,\bar{z})\partial_x\varepsilon_{y'+1}(z,\bar{z}) \;-\; \varepsilon_{y'+1}(z,\bar{z})\partial_x\varepsilon_{y'}(z,\bar{z})\Big].
\end{aligned}$$

There are three choices for the chain indices : $y = y'$, $y = y' + 1$, and $y + 1 = y'$. The first one only results in an intrachain term, which we ignore. The second and third choices are similar. We only consider the second one and will include a factor of 2 at the end:

$$\begin{aligned}
&\frac{(-1)^{y+y+1}}{4}\Big[\varepsilon_y(z',\bar{z}')\partial_x\varepsilon_{y+1}(z',\bar{z}') \;-\; \varepsilon_{y+1}(z',\bar{z}')\partial_x\varepsilon_y(z',\bar{z}')\Big] \qquad \text{(A.117)} \\
&\qquad\Big[\varepsilon_{y+1}(z,\bar{z})\partial_x\varepsilon_{y+2}(z,\bar{z}) \;-\; \varepsilon_{y+2}(z,\bar{z})\partial_x\varepsilon_{y+1}(z,\bar{z})\Big] \\
&\propto \frac{-1}{4}\Big[\varepsilon_y(z',\bar{z}')\partial_x\frac{1}{2\pi^2|z'-z|}\partial_x\varepsilon_{y+2}(z,\bar{z}) \;+\; \partial_x\varepsilon_y(z',\bar{z}')\partial_x\frac{1}{2\pi^2|z'-z|}\varepsilon_{y+2}(z,\bar{z}) \\
&\quad - \;\varepsilon_{y'}(z',\bar{z}')\partial_x^2\frac{1}{2\pi^2|z'-z|}\varepsilon_{y+2}(z,\bar{z}) \;-\; \partial_x\varepsilon_y(z',\bar{z}')\frac{1}{2\pi^2|z'-z|}\partial_x\varepsilon_{y+2}(z,\bar{z})\Big].
\end{aligned}$$

The only terms that survive the loop integration are:

$$\frac{1}{4}\left[\frac{1}{2}\frac{1}{2\pi^2|z'-z|^3}\,\varepsilon_{y'}(z',\bar{z}')\varepsilon_{y+2}(z,\bar{z}) \;+\; \frac{1}{2\pi^2|z'-z|}\,\partial_x\varepsilon_y(z',\bar{z}')\partial_x\varepsilon_{y+2}(z,\bar{z})\right]. \qquad \text{(A.118)}$$

- γ_{bs} - ζ_ε

This product results in the renormalization of ζ_ε:

$$J^a_{R,y}(z')J^a_{L,y}(\bar{z}')\partial_x\varepsilon_{y'}(z,\bar{z})\partial_x\varepsilon_{y'+2}(z,\bar{z}) \tag{A.119}$$

Again, the backscattering term can either reside on the first chain or the third chain. We consider the first case and will include a factor of 2 at the end:

$$\begin{aligned} & J^a_{R,y}(z')J^a_{L,y}(\bar{z}')\partial_x\varepsilon_y(z,\bar{z})\partial_x\varepsilon_{y+2}(z,\bar{z}) \qquad (A.120)\\ & \propto J^a_{R,y}(z')\partial_x \frac{-iN^a_y(z,\bar{z})}{4\pi(\bar{z}'-\bar{z})}\partial_x\varepsilon_{y+2}(z,\bar{z}) \\ & \propto \partial_x \frac{-i}{4\pi(\bar{z}'-\bar{z})}\Big[\frac{-i\delta^{aa}\varepsilon_y(z,\bar{z})}{4\pi(z'-z)} + \frac{i\epsilon^{aac}N^c_y(z,\bar{z})}{4\pi(z'-z)}\Big]\partial_x\varepsilon_{y+2}(z,\bar{z}) \\ & \rightsquigarrow \frac{-1}{16\pi^2|z'-z|^2}\partial_x\varepsilon_y(z,\bar{z})\partial_x\varepsilon_{y+2}(z,\bar{z})\,. \end{aligned}$$

- γ_M - ζ_ε **and** γ_{tw} - ζ_ε

We ignore these two products as they do not result in the renormalization of any of the relevant terms.

- g_M - ζ_ε

$$M^a_y(z',\bar{z}')M^a_{y+2}(z',\bar{z}')\ \partial_x\varepsilon_{y'}(z,\bar{z})\partial_x\varepsilon_{y'+2}(z,\bar{z}) \tag{A.121}$$

The only choice of indices that results in anything of interest is $y = y'$:

$$\big[J^b_{L,y}(\bar{z}')+J^b_{R,y}(z')\big]\big[J^b_{L,y+2}(\bar{z}')+J^b_{R,y+2}(z')\big]\partial_x\varepsilon_y(z,\bar{z})\partial_x\varepsilon_{y+2}(z,\bar{z}) \tag{A.122}$$

$$\propto \partial_x\Big[\frac{-iN^a_y(z,\bar{z})}{4\pi(\bar{z}'-\bar{z})} + \frac{iN^a_y(z,\bar{z})}{4\pi(z'-z)}\Big]\partial_x\Big[\frac{-iN^a_{y+2}(z,\bar{z})}{4\pi(\bar{z}'-\bar{z})} + \frac{iN^a_{y+2}(z,\bar{z})}{4\pi(z'-z)}\Big] \tag{A.123}$$

$$\propto \Big[\frac{1}{16\pi^2|z'-z|^2}\partial_x N^a_y(z,\bar{z})\partial_x N^a_{y+2}(z,\bar{z}) + \frac{1}{16\pi^2|z'-z|^4}N^a_y(z,\bar{z})N^a_{y+2}(z,\bar{z})\Big]\,.$$

- γ_ε - ζ_ε

$$\frac{(-1)^y}{2}\Big[\varepsilon_y(z',\bar{z}')\partial_x\varepsilon_{y+1}(z',\bar{z}') - \varepsilon_{y+1}(z',\bar{z}')\partial_x\varepsilon_y(z',\bar{z}')\Big]\partial_x\varepsilon_{y'}(z,\bar{z})\partial_x\varepsilon_{y'+2}(z,\bar{z}) \tag{A.124}$$

There are four possible choices for the chain indices: $y = y'$, $y+1 = y'$, $y = y'+2$, and $y = y'+1$. The only ones that result in the renormalization of ζ_ε are $y = y'$ and $y = y'+1$, while the rest result in the generation of farther chain analogs of ζ_ε. For $y = y'$ we have:

$$\begin{aligned}&\frac{(-1)^y}{2}\Big[\varepsilon_y(z',\bar{z}')\partial_x\varepsilon_{y+1}(z',\bar{z}') \;-\; \varepsilon_{y+1}(z',\bar{z}')\partial_x\varepsilon_y(z',\bar{z}')\Big]\partial_x\varepsilon_y(z,\bar{z})\partial_x\varepsilon_{y+2}(z,\bar{z})\\ &\propto \frac{(-1)^y}{2}\left[\frac{1}{2\pi^2|z'-z|}\partial_x\varepsilon_{y+1}(z',\bar{z}') \;-\; \varepsilon_{y+1}(z',\bar{z}')\partial_x\frac{1}{2\pi^2|z'-z|}\right]\partial_x\varepsilon_{y+2}(z,\bar{z})\,.\end{aligned} \tag{A.125}$$

Similarly, for the case $y = y'+1$ we get:

$$\begin{aligned}&\frac{(-1)^y}{2}\Big[\varepsilon_y(z',\bar{z}')\partial_x\varepsilon_{y+1}(z',\bar{z}') \;-\; \varepsilon_{y+1}(z',\bar{z}')\partial_x\varepsilon_y(z',\bar{z}')\Big]\partial_x\varepsilon_{y-1}(z,\bar{z})\partial_x\varepsilon_{y+1}(z,\bar{z})\\ &\propto \frac{(-1)^y}{2}\Big[\varepsilon_y(z',\bar{z}')\partial_x\frac{1}{2\pi^2|z'-z|} \;-\; \frac{1}{2\pi^2|z'-z|}\partial_x\varepsilon_y(z',\bar{z}')\Big]\partial_x\varepsilon_{y-1}(z,\bar{z})\,.\end{aligned} \tag{A.126}$$

- **g_ε - ζ_ε and ζ_ε - ζ_ε**

$$\varepsilon_y(z',\bar{z}')\varepsilon_{y+2}(z',\bar{z}')\;\partial_x\varepsilon_{y'}(z,\bar{z})\partial_x\varepsilon_{y'+2}(z,\bar{z}) \tag{A.127}$$

$$\partial_x\varepsilon_{y'}(z',\bar{z}')\partial_x\varepsilon_{y'+2}(z',\bar{z}')\;\partial_x\varepsilon_{y'}(z,\bar{z})\partial_x\varepsilon_{y'+2}(z,\bar{z}) \tag{A.128}$$

The case $y = y'$ will result in a $\mathbb{C}$-number and an intrachain term, which we ignore.

- **γ_{bs} - ζ_M**

Finally, let us demonstrate how g_M is generated from the product of γ_{bs} with ζ_M:

$$J^a_{R,y}(z')J^a_{L,y}(\bar{z}')\;J^b_{R,y'+1}(z)J^b_{L,y'+1}(\bar{z})M^c_{y'}(z,\bar{z})M^c_{y'+2}(z,\bar{z}) \tag{A.129}$$

The only choice of indices that result in the generation of g_M is $y = y'+1$:

$$\begin{aligned}&J^a_{R,y}(z')J^a_{L,y}(\bar{z}')\;J^b_{R,y+1}(z)J^b_{L,y+1}(\bar{z})M^c_y(z,\bar{z})M^c_{y+2}(z,\bar{z}) \qquad (A.130)\\ &\propto \Big[\frac{\delta^{ab}}{8\pi^2(\bar{z}'-\bar{z})^2} + \frac{i\epsilon^{abc}J^c_{L,y+1}(\bar{z})}{2\pi(\bar{z}'-\bar{z})}\Big]\Big[\frac{\delta^{ab}}{8\pi^2(z'-z)^2} + \frac{i\epsilon^{abc}J^c_{R,y+1}(z)}{2\pi(z'-z)}\Big]\\ &\quad M^c_y(z,\bar{z})M^c_{y+2}(z,\bar{z})\\ &\propto \Big[\frac{\delta^{ab}}{64\pi^4|z'-z|^4} + \frac{-\epsilon^{abc}\epsilon^{abd}}{4\pi^2|z'-z|^2}J^c_{L,y+1}(\bar{z})J^d_{R,y+1}(z)\Big]M^c_y(z,\bar{z})M^c_{y+2}(z,\bar{z})\,.\end{aligned}$$

• β-functions

Using the above results, we obtain the following β-functions for the dimensionless couplings constants (after scaling couplings by $2\pi\nu = \pi^2 J$ and setting $J = 1$):

$$\partial_l \gamma_{bs} = \gamma_{bs}^2 - 6g_N^2 + 2g_\varepsilon^2 \tag{A.131}$$

$$\partial_l \gamma_M = \gamma_M^2 \tag{A.132}$$

$$\partial_l \gamma_{tw} = -\frac{1}{2}\gamma_{bs}\gamma_{tw} + \gamma_M\gamma_{tw} - 3\gamma_{tw}g_N + 2\gamma_{tw}\zeta_N - \frac{1}{2}\gamma_M\gamma_\varepsilon \tag{A.133}$$

$$\partial_l g_N = g_N + \frac{1}{4}\gamma_{tw}^2 - \frac{1}{2}\gamma_{bs}g_N + g_M g_N - \frac{1}{2}g_M g_\varepsilon + g_M\zeta_N - \frac{1}{2}g_M\zeta_\varepsilon \tag{A.134}$$

$$\partial_l g_\varepsilon = g_\varepsilon + \frac{1}{2}\gamma_\varepsilon^2 + \frac{3}{2}\gamma_{bs}g_\varepsilon - \frac{3}{2}g_M g_N - \frac{3}{2}g_M\zeta_N \tag{A.135}$$

$$\partial_l \zeta_N = -\zeta_N - \frac{1}{2}\gamma_{bs}\zeta_N - \gamma_{tw}^2 + g_M\zeta_N - \frac{1}{2}g_M\zeta_\varepsilon \tag{A.136}$$

$$\partial_l g_M = g_M^2 - \frac{1}{4\pi^2}\gamma_{bs}\zeta_M \tag{A.137}$$

$$\partial_l \gamma_\varepsilon = \frac{3}{2}\gamma_{bs}\gamma_\varepsilon - \frac{3}{2}\gamma_{tw}\gamma_M - \frac{3}{2}g_\varepsilon\gamma_\varepsilon + 2\gamma_\varepsilon\zeta_\varepsilon \tag{A.138}$$

$$\partial_l \zeta_\varepsilon = -\zeta_\varepsilon - \frac{1}{2}\gamma_{bs}\zeta_\varepsilon - \gamma_\varepsilon^2 - \frac{3}{2}g_M\zeta_N \tag{A.139}$$

$$\partial_l \zeta_M = -2\zeta_M + \gamma_{bs}\zeta_M - 8\pi^2\gamma_M^2 \tag{A.140}$$

A.4 β-Functions with g_{DM}

In this section we present how the inclusion of a relevant interchain term that originates from the interchain DM interaction in the continuum limit modifies the β-functions. For this purpose we only focus on a subset of the couplings, and in particular g_N and γ_{tw}.

- γ_{bs} - g_{DM}

$$\epsilon^{bc\mathbf{z}}\, J^a_{R,y}(z')J^a_{L,y}(\bar{z}')\, N^b_{y'}(z,\bar{z})N^c_{y'+1}(z,\bar{z}) \tag{A.141}$$

The backscattering term can either reside on the first chain or the second chain, $y = y'$ and $y = y' + 1$. We consider the latter and will include a factor of 2 at the end:

$$\epsilon^{bc\mathbf{z}}\, J^a_{R,y}(z')J^a_{L,y}(\bar{z}')\, N^b_{y'}(z,\bar{z})N^c_{y'+1}(z,\bar{z}) \;\propto\; \frac{\epsilon^{bc\mathbf{z}}(-\delta^{ab}-\epsilon^{abd}\epsilon^{adb})}{16\pi^2|z-z_0|^2} N^b_y(z_0)N^c_{y+1}(z_0) \tag{A.142}$$

- γ_{tw} - g_{DM}

$$\epsilon^{bc\mathbf{z}}\frac{(-1)^y}{2}\Big[N^a_y(z',\bar{z}')\partial_x N^a_{y+1}(z',\bar{z}') \;-\; N^a_{y+1}(z',\bar{z}')\partial_x N^a_y(z',\bar{z}')\Big] N^b_{y'}(z,\bar{z})N^c_{y'+1}(z,\bar{z}) \tag{A.143}$$

Now we have two distinct choices for the chain indices: $y = y'$ or $y - 1 = y'$. The latter, aside from irrelevant terms, only results in an intrachain marginal term and a $\mathbb{C}$-number. For the case $y = y' + 1$, we have:

$$\begin{aligned}
&\epsilon^{bc\mathbf{z}}\frac{(-1)^y}{2}\Big[N^a_y(z',\bar{z}')\partial_x N^a_{y+1}(z',\bar{z}') \;-\; N^a_{y+1}(z',\bar{z}')\partial_x N^a_y(z',\bar{z}')\Big] N^b_{y-1}(z,\bar{z})N^c_y(z,\bar{z}) \\
&\quad\propto\; \epsilon^{bc\mathbf{z}}\frac{(-1)^y}{2}\left[\frac{\delta^a}{2\pi^2|z'-z|}\partial_x N^a_{y+1}(z',\bar{z}') \;-\; N^a_{y+1}(z',\bar{z}')\partial_x\frac{\delta^{ab}}{2\pi^2|z'-z|}\right] N^b_{y-1}(z,\bar{z})\,,
\end{aligned} \tag{A.144}$$

which is a farther chain coupling.

- γ_M - g_{DM}

$$\epsilon^{bc\mathbf{z}}\, M^a_y(z',\bar{z}')M^a_{y+1}(z',\bar{z}')\, N^b_{y'}(z,\bar{z})N^c_{y'+1}(z,\bar{z}) \tag{A.145}$$

The only choice of chain indices that results in anything of interest is $y = y'$. We have:

$$\epsilon^{bc\mathbf{z}}\, \overbrace{M^a_y(z',\bar{z}')\overbrace{M^a_{y+1}(z',\bar{z}')\, N^b_y(z,\bar{z})}N^c_{y+1}(z,\bar{z})} \tag{A.146}$$

$$\propto \epsilon^{bc\mathbf{z}} \left[\frac{-i\delta^{ab}\varepsilon_y(z,\bar{z})}{4\pi(z'-z)} + \frac{i\epsilon^{abd}N^d_y(z,\bar{z})}{4\pi(z'-z)} + \frac{i\delta^{ab}\varepsilon_y(z,\bar{z})}{4\pi(\bar{z}'-\bar{z})} + \frac{i\epsilon^{abd}N^d_y(z,\bar{z})}{4\pi(\bar{z}'-\bar{z})}\right]$$

$$\left[\frac{-i\delta^{ac}\varepsilon_{y+1}(z,\bar{z})}{4\pi(z'-z)} + \frac{i\epsilon^{ace}N^e_{y+1}(z,\bar{z})}{4\pi(z'-z)} + \frac{i\delta^{ac}\varepsilon_{y+1}(z,\bar{z})}{4\pi(\bar{z}'-\bar{z})} + \frac{i\epsilon^{ace}N^e_{y+1}(z,\bar{z})}{4\pi(\bar{z}'-\bar{z})}\right]$$

$$\rightsquigarrow \epsilon^{bc\mathbf{z}}\, \frac{-2\,\epsilon^{abd}\epsilon^{ace}}{16\pi^2|z'-z|^2} N^d_y(z,\bar{z})N^e_{y+1}(z,\bar{z})\,,$$

where, in the last line we have ignored all terms that vanish upon performing the loop integrals.

- g_N - g_{DM}

$$\epsilon^{bc\mathbf{z}}\, N^a_y(z',\bar{z}')N^a_{y+2}(z',\bar{z}')\, N^b_{y'}(z,\bar{z})N^c_{y'+1}(z,\bar{z}) \tag{A.147}$$

There are four choices for the chain indices: $y = y'$, $y+2 = y'$, $y = y'+1$, and $y+1 = y'$. The two choices $y = y'$ and $y+1 = y'$ may result in the renormalization of g_{DM}, whereas the other two choices only result in the generation of farther-chain analogs of g_{DM}. For the case $y = y'$ we have:

$$\epsilon^{bc\mathbf{z}}\, N^a_y(z',\bar{z}')N^a_{y+2}(z',\bar{z}')\, N^b_y(z,\bar{z})N^c_{y+1}(z,\bar{z}) \tag{A.148}$$

$$\propto \epsilon^{bc\mathbf{z}}\, \frac{\delta^{ab}}{2\pi^2|z'-z|} N^a_{y+2}(z,\bar{z})\, N^c_{y+1}(z,\bar{z})\,.$$

And for the case $y+1 = y'$, we have:

$$\epsilon^{bc\mathbf{z}}\, N^a_y(z',\bar{z}')N^a_{y+2}(z',\bar{z}')\, N^b_{y+1}(z,\bar{z})N^c_{y+2}(z,\bar{z}) \tag{A.149}$$

$$\propto \epsilon^{bc\mathbf{z}}\, \frac{\delta^{ac}}{2\pi^2|z'-z|} N^a_y(z,\bar{z})N^b_{y+1}(z,\bar{z})\,.$$

Note that these two results are the same and do not cancel each other. Therefore the product of g_N and g_{DM} does renormalize g_{DM}.

- g_ε - g_{DM}

Since the OPE of $\vec{N}$ with ε does not contain any singular terms, this product result in no renormalized interaction.

g_{DM} - g_{DM}

$$\epsilon^{ab\mathbf{z}}\epsilon^{cd\mathbf{z}}\, N^a_y(z',\bar{z}')N^b_{y+1}(z',\bar{z}')\, N^c_{y'}(z,\bar{z})N^d_{y'+1}(z,\bar{z}) \tag{A.150}$$

The choice $y = y'$ results in a c-number and an intrachain term, which we ignore. However, the choice $y = y' + 1$ will result in the renormalization of g_N as follows.

$$\begin{aligned}
&\epsilon^{ab\mathbf{z}}\epsilon^{cd\mathbf{z}}\, N^a_y(z',\bar{z}')N^b_{y+1}(z',\bar{z}')\, N^c_{y+1}(z,\bar{z})N^d_{y+2}(z,\bar{z}) \qquad \text{(A.151)}\\
&\propto \epsilon^{ab\mathbf{z}}\epsilon^{cd\mathbf{z}}\, N^a_y(z,\bar{z})\frac{\delta^{bc}}{2\pi^2|z'-z|}N^d_{y+2}(z,\bar{z})\\
&= \frac{-\overbrace{\delta^{bc}\epsilon^{ab\mathbf{z}}\epsilon^{dc\mathbf{z}}}^{\delta^{ad}}}{2\pi^2|z'-z|}N^a_y(z,\bar{z})N^d_{y+2}(z,\bar{z})\,.
\end{aligned}$$

Putting these together, we obtain the following β-functions for the couplings of the XY part of the interactions when the DM interaction is present:

$$\partial_l g_{\text{DM}} \;=\; g_{\text{DM}} - 4g_N g_{\text{DM}} - \frac{1}{2}\gamma_{bs}g_{\text{DM}} + \frac{1}{2}\gamma_M g_{\text{DM}} \tag{A.152}$$

$$\partial_l g_N \;=\; g_N - 2g^2_{\text{DM}} + \frac{1}{4}\gamma^2_{tw} - \frac{1}{2}\gamma_{bs}g_N + \cdots \tag{A.153}$$

while the rest of the β-functions remain the same.

A.5 Computation of g_N^{crit}

The critical initial value of the interchain Néel coupling, $g_N^{\text{crit}}(0)$, can be computed by numerically solving the β-functions given in Eqs. (2.8a-2.8i). For this purpose, the β-functions are solves repeatedly and the initial value of g_N is refined while keeping the initial value of other couplings fixed until tuning, i.e., to no exponential growth in g_N, is achieved. Nevertheless, to better understand the flow of g_N and γ_{tw} under RG, one may attempt solving a reduced subset of the β-functions analytically. If one drops terms in the β-functions that contribute at quartic and higher orders (in J'/J) to g_N, partial analytic solutions can be obtained that yield insight into the initial conditions corresponding to tuning. This leaves us with the following reduced β-functions:

$$\partial_\ell \gamma_{bs} = \gamma_{bs}^2 \tag{A.154a}$$

$$\partial_\ell \gamma_M = \gamma_M^2 \tag{A.154b}$$

$$\partial_\ell \gamma_{tw} = -\tfrac{1}{2}\gamma_{bs}\gamma_{tw} + \gamma_M \gamma_{tw} \tag{A.154c}$$

$$\partial_\ell g_N = g_N - \tfrac{1}{2}\gamma_{bs} g_N + \tfrac{1}{4}\gamma_{tw}^2 \,. \tag{A.154d}$$

From these, we obtain the following analytic expressions for the couplings:

$$\gamma_{bs}(\ell) = \frac{\gamma_{bs}(0)}{1-\gamma_{bs}(0)\ell} \tag{A.155a}$$

$$\gamma_M(\ell) = \frac{\gamma_M(0)}{1-\gamma_M(0)\ell} \tag{A.155b}$$

$$\gamma_{tw}(\ell) = \gamma_{tw}(0)\frac{\sqrt{1-\gamma_{bs}(0)\ell}}{1-\gamma_M(0)\ell} \tag{A.155c}$$

$$g_N(\ell) = \left[\frac{\gamma_{tw}^2(0)}{4}\int_0^\ell \frac{e^{-t}\sqrt{1-\gamma_{bs}(0)t}}{(1-\gamma_M(0)t)^2}\mathrm{d}t + g_N(0)\right] e^\ell \sqrt{1-\gamma_{bs}(0)\ell}\,. \tag{A.155d}$$

For a non-zero $\gamma_M(0)$, the integral in Eq. (A.155d) cannot be expressed in terms of elementary functions. However, assuming $\gamma_M(0)\ell \ll 1$, it is possible to expand $\frac{1}{(1-\gamma_M t)^2}$ and find an expression for $g_N(\ell)$ as series in terms of the lower incomplete Γ-function,$\gamma_{\text{Lower}}(m,z)$, as follows:

$$g_N(l) = \left[\frac{\gamma_{tw}^2(0)}{4}\, e^{-\frac{1}{\gamma_{bs}(0)}}\, \sqrt{-\gamma_{bs}(0)} \sum_n (n+1)\,\gamma_M^n\, F_n(\ell) + g_N(0)\right] e^\ell\, \sqrt{1-\gamma_{bs}(0)\ell}\,, \tag{A.156}$$

where $F_n(\ell)$ is given recursively by:

$$F_n(\ell) = \Big[\gamma_{\text{Lower}}(n+\tfrac{3}{2}, \ell + \tfrac{1}{-\gamma_{bs}(0)}) - \gamma_{\text{Lower}}(n+\tfrac{3}{2}, \tfrac{1}{-\gamma_{bs}(0)}) - \sum_{m=1}^{n} \frac{(-1)^m n!}{\gamma_{bs}^m(0)(n-m)!} F_{n-m}(\ell)\Big]. \tag{A.157}$$

Each term in Eq. (A.156) is accompanied by a power of $\gamma_M(0)$, and also we have a $\gamma_{tw}^2(0)$ factor that multiplies the sum. Since the above analytic expressions for the couplings were derived by neglecting quartic and higher-order contributions, we dismiss all terms in the expansion except the first two terms. Finally, using the above analytic expressions, the tuned initial condition for the interchain Néel coupling, $g_N^{\text{crit}}(0)$, is found (assuming $\gamma_{bs}(0) = -0.23$):

$$g_N^{\text{crit}}(0) = -\Big[0.27620(J'/J)^2 + 1.20152(J'/J)^3 + \mathcal{O}(J'/J)^4\Big]. \tag{A.158}$$

It is possible to determine the coefficient of the quartic term in the above expansion numerically, which gives 8.0. Note that we have taken $g_N^{\text{crit}}(0)$ as the initial value of g_N such that $g_N(\tilde{\ell}) = 0$ and $\gamma_{tw}(\tilde{\ell}) = 1$, which for any $J'/J \lesssim 0.2$ is not any different from other ways of defining tuning (e.g. $g_N(\tilde{\ell}) = -1$), as the difference for these small J'/J values would be due to quartic and higher-order terms. However, the estimated value, J_c'/J, for the transition from CAF to spiral, would be smaller if $g_N(\tilde{\ell}) < 0$ was used.

Finally, note that in the above calculation $\gamma_{bs}(0) = -0.23$ was used, which is the coupling of the backscattering term at the length scale $4a_0$ rather than the lattice spacing a_0, where γ_M and γ_{tw} have their bare values. Of course, with the knowledge of the value of these couplings at the scale $4a_0$ one can repeat the whole calculations and determine g_N^{crit} at $4a_0$. Thus what has been neglected is the small growth in γ_M and particularly γ_{tw} from a_0 to $4a_0$. Taking into account the growth of these couplings, for the quadratic and cubic parts of g_N^{crit} at $4a_0$ we obtain 0.291374 and 1.31288, respectively.

Appendix B

Appendix to Chapter 3

In this appendix the computational details of $\Gamma_{\text{PH}}(q\hat{x}, \Omega = 0)$ and $\Gamma_{\text{PP}}(\mathbf{q} = 0, \Omega \ll \Lambda)$ for the model in Chapter 3 are presented. From these, the one-loop quantum corrections $\partial_{\log\Lambda}\Gamma_{\text{PH}}(q\hat{x}, 0)$ and $\partial_{\log\Lambda}\Gamma_{\text{PP}}(\mathbf{q} = 0, \Omega\Lambda)$, at $(\mu = 0)$ and slightly away $(\mu > 0)$ from the critical point of the neck-narrowing Lifshitz transition are obtained. For $\partial_{\log\Lambda}\Gamma_{\text{PH}}(q\hat{x}, 0)$, a series expansion in q is determined from which we obtain the β-functions presented in Chapter 3. At the end, the computational details of the imaginary part of the one-loop particle-hole susceptibility, $\chi''_{\text{PH}}(q\hat{x}, \Omega)$, are given.

B.1 Computation of $\Gamma_{\text{PH}}(q\hat{x}, 0)$ for $\mu > 0$ and the β-Functions

The one-loop particle-hole diagram $\Gamma_{\text{PH}}(q\hat{x}, \Omega = 0)$ for $\mu > 0$ is given by:

$$\Gamma_{\text{PH}}(q\hat{x}, \Omega = 0) \;=\; \frac{1}{(2\pi)^2}\int \mathrm{d}\mathbf{k}\, \frac{\theta(\xi_{\mathbf{k}}) - \theta(\xi_{\mathbf{k}+\mathbf{q}})}{\xi_{\mathbf{k}} - \xi_{\mathbf{k}+\mathbf{q}}}\; e^{-\frac{|\mathbf{k}|^2+|\mathbf{k}+\mathbf{q}|^2}{K^2}}\; e^{-\frac{\xi_{\mathbf{k}}^2+\xi_{\mathbf{k}+\mathbf{q}}^2}{\Lambda^2}}\,. \tag{B.1}$$

For the purpose of computing the above integral, it is more convenient to change the integration variables: $(k_x, k_y > 0) \to (\xi, \xi')$, where $\xi = \xi_{\mathbf{k}}$ and $\xi' = \xi_{\mathbf{k}+\mathbf{q}}$.

$$\begin{cases} \xi \;=\; k_x^2 - k_y^2 - \mu \\ \xi' \;=\; k_x^2 + q^2 + 2qk_x - k_y^2 - \mu \end{cases} \to \begin{cases} k_x \;=\; \frac{1}{2q}(\xi' - \xi - q^2) \\ k_y \;=\; \pm\sqrt{-\xi - \mu + \frac{1}{4q^2}(\xi' - \xi - q^2)^2} \end{cases} \tag{B.2}$$

The Jacobian of this change of integration variables is:

$$\mathcal{J} \;=\; \Big|\frac{-1}{2\sqrt{(\xi' - \xi - q^2)^2 - 4q^2(\xi + \mu)}}\Big| \tag{B.3}$$

with the constraint $(\xi' - \xi - q^2)^2 \geq 4q^2(\xi + \mu)$. The integral in Eq. (B.1) becomes:

$$\Gamma_{\text{PH}}(q\hat{x}, 0) = \frac{1}{(2\pi)^2} \int_{-\infty}^{\infty} \mathrm{d}\xi \int_{-\infty}^{\infty} \mathrm{d}\xi' \, \frac{\theta(\xi) - \theta(\xi')}{\xi - \xi'} \frac{e^{-\frac{\xi^2 + \xi'^2}{\Lambda^2}} \, e^{-\frac{|\mathbf{k}|^2 + |\mathbf{k}+\mathbf{q}|^2}{K^2}}}{\sqrt{(\xi' - \xi - q^2)^2 - 4q^2(\xi + \mu)}}, \tag{B.4}$$

The above integral is further simplified using the new variables $X = \xi - \xi'$ and $t|X| = \xi + \xi'$:

$$\begin{aligned}\Gamma_{\text{PH}}(q\hat{x}, 0) =& \frac{1}{2(2\pi)^2} \int_{-\infty}^{\infty} \mathrm{d}X \int_{-1}^{1} \mathrm{d}t \, \frac{|X|}{X} \frac{\theta\big(X(t+1)\big) - \theta\big(X(t-1)\big)}{\sqrt{(-X - q^2)^2 - 4q^2(\frac{t+1}{2}X + \mu)}} \\ & e^{-\frac{1}{K^2}(tX + \frac{X^2}{q^2} - 2\mu - q^2)} \, e^{-\frac{X^2(1+t^2)}{2\Lambda^2}},\end{aligned} \tag{B.5}$$

where the integration domain is restricted to the region where $(X + q^2)^2 \geq 2q^2(t + 1)X + 4q^2\mu$. For $q \leq 2\sqrt{\mu}$, applying the Heaviside functions and imposing the constraint $(X + q^2)^2 \geq 2q^2(t + 1)X + 4q^2\mu$, we obtain:

$$\Gamma_{\text{PH}}(q\hat{x}, 0) = \frac{1}{(2\pi)^2} \int_{X_{\min}}^{\infty} \mathrm{d}X \int_{-1}^{1} \mathrm{d}t \, \frac{e^{-\frac{1}{K^2}(tX + \frac{X^2}{q^2} - 2\mu - q^2)} \, e^{-\frac{X^2(1+t^2)}{2\Lambda^2}}}{\sqrt{X^2 + q^4 - 4q^2\mu^2 + 2q^2tX}}, \tag{B.6}$$

where $X_{\min} = tq^2 + q^2\sqrt{4\frac{\mu}{q^2} - (1 - t^2)}$. To further simplify the above integral we first need to rewrite the exponential terms as:

$$\begin{aligned}& \exp\left\{ -\frac{1}{K^2}(tX + \frac{X^2}{q^2} \cancel{-2\mu - q^2}) - \frac{X^2(1+t^2)}{2\Lambda^2} \right\} \\ =& \exp\left\{ -\frac{2\Lambda^2 + q^2K^2(1+t^2)}{2\Lambda^2q^2K^2} \Big(X + \frac{tq^2\Lambda^2}{q^2K^2(1+t^2) + 2\Lambda^2} \Big)^2 \right. \\ & \left. - \frac{q^2t^2\Lambda^2}{2q^2K^4(1+t^2) + 4K^2\Lambda^2} \right\},\end{aligned} \tag{B.7}$$

where in the last line we dropped the two unimportant terms $\frac{2\mu}{K^2}$ and $\frac{q^2}{K^2}$. Using $X \to qK\mathcal{Y} + X_{\min}$, the integral in Eq. (B.6) becomes:

$$\begin{aligned}\Gamma_{\text{PH}}(q\hat{x}, 0) =& \frac{1}{(2\pi)^2} \int_{-1}^{1} \mathrm{d}t \; e^{-\frac{q^2t^2\Lambda^2}{2q^2K^4(1+t^2) + 4K^2\Lambda^2}} \int_{0}^{\infty} \mathrm{d}\mathcal{Y} \, \frac{1}{\sqrt{\mathcal{Y}(\mathcal{Y} + 2a(t))}} \\ & e^{-\frac{2\Lambda^2 + q^2K^2(1+t^2)}{2\Lambda^2} \left(\mathcal{Y} + \frac{tq}{K} + a(t) + \frac{tq\Lambda^2}{q^2K^3(1+t^2) + 2K\Lambda^2}\right)^2},\end{aligned} \tag{B.8}$$

where, $a(t) = \sqrt{4\frac{\mu}{K^2} - (1-t^2)\frac{q^2}{K^2}}$. Using, $\mathcal{Y} \to \mathcal{Y} + a(t)$, we get:

$$\Gamma_{\text{PH}}(q\hat{x}, 0) = \frac{1}{(2\pi)^2}\int_{-1}^{1} \mathrm{d}t\, e^{-\frac{q^2t^2\Lambda^2}{2q^2K^4(1+t^2)+4K^2\Lambda^2}} \int_{a(t)}^{\infty} \mathrm{d}\mathcal{Y}\, \frac{1}{\sqrt{\mathcal{Y}^2 - a(t)^2}} \\ e^{-\frac{2\Lambda^2+q^2K^2(1+t^2)}{2\Lambda^2}\left(\mathcal{Y}+\frac{tq}{K}+\frac{tq\Lambda^2}{q^2K^3(1+t^2)+2K\Lambda^2}\right)^2}. \tag{B.9}$$

The above integral can be written as:

$$\Gamma_{\text{PH}}(q\hat{x}, 0) = \frac{1}{(2\pi)^2}\int_{-1}^{1} \mathrm{d}t\, e^{-\frac{q^2t^2}{K^2}\beta(t)} \int_{\frac{a(t)}{\beta(t)}}^{\infty} \frac{\mathrm{d}\mathcal{Y}}{\sqrt{\mathcal{Y}^2 - \frac{a(t)^2}{\beta(t)^2}}}\, e^{-\frac{1}{\beta(t)}\left(\mathcal{Y}+\frac{tq}{K\beta(t)}+\frac{tq}{K}\right)^2}, \tag{B.10}$$

where $\beta(t) = \frac{\Lambda^2}{q^2K^2(1+t^2)+2\Lambda^2}$. Note that non-analyticity at $\mathcal{O}(\frac{\Lambda}{K})$ mentioned in Chapter 3 stems from $\beta(t)$. Finally, $\Gamma_{\text{PH}}(q\hat{x}, i\Omega = 0)$ can be approximately computed by expanding the inverse square root term in the integrand in large $\mathcal{Y}$:

$$\Gamma_{\text{PH}}(q\hat{x}, 0) = \frac{1}{(2\pi)^2}\int_{-1}^{1} \mathrm{d}t\, e^{-\frac{q^2t^2}{K^2}\beta(t)} \int_{\frac{a(t)}{\beta(t)}}^{\infty} \frac{\mathrm{d}\mathcal{Y}}{\sqrt{\mathcal{Y}^2 - \frac{a(t)^2}{\beta(t)^2}}}\, e^{-\frac{1}{\beta(t)}\mathcal{Y}^2} \tag{B.11}$$

$$= \frac{-1}{(2\pi)^2}\int_{-1}^{1} \mathrm{d}t\, e^{-\frac{q^2t^2}{K^2}\beta(t)} \int_{\frac{a(t)}{\beta(t)}}^{\infty} \mathrm{d}\mathcal{Y}\, e^{-\frac{1}{\beta(t)}\mathcal{Y}^2}\left[\frac{1}{\mathcal{Y}} + \frac{a(t)^2}{\beta(t)^2}\frac{1}{\mathcal{Y}^3} + \frac{a(t)^4}{\beta(t)^4}\frac{3}{8\mathcal{Y}^5} + \right. \\ \left. \frac{a(t)^6}{\beta(t)^6}\frac{5}{16\mathcal{Y}^7} + \frac{a(t)^8}{\beta(t)^8}\frac{35}{128\mathcal{Y}^9} + \frac{a(t)^{10}}{\beta(t)^{10}}\frac{63}{256\mathcal{Y}^{11}} + \frac{a(t)^{12}}{\beta(t)^{12}}\frac{231}{1024\mathcal{Y}^{13}} + \cdots\right]$$

$$= \frac{1}{(2\pi)^2}\int_{-1}^{1} \mathrm{d}t\, e^{-\frac{q^2t^2}{K^2}\beta(t)}\frac{1}{2}\int_{\frac{a(t)^2}{\beta(t)^2}}^{\infty} \mathrm{d}y\, e^{-\frac{y}{\beta(t)}}\left[\frac{1}{y} - \frac{a(t)^2}{\beta(t)^2}\frac{1}{y^2} + \frac{a(t)^4}{\beta(t)^4}\frac{3}{8y^3}\right. \\ \left. - \frac{a(t)^6}{\beta(t)^6}\frac{5}{16y^4} + \frac{a(t)^8}{\beta(t)^8}\frac{35}{128y^5} + \frac{a(t)^{10}}{\beta(t)^{10}}\frac{63}{256y^6} + \frac{a(t)^{12}}{\beta(t)^{12}}\frac{231}{1024y^7} + \cdots\right]$$

$$= \frac{1}{(2\pi)^2}\int_{-1}^{1} \mathrm{d}t\, e^{-\frac{q^2t^2}{K^2}\beta(t)}\frac{1}{2}\int_{\frac{a(t)^2}{\beta(t)^3}}^{\infty} \mathrm{d}y\, e^{-y}\left[\frac{1}{y} - \frac{a(t)^2}{\beta(t)^3}\frac{1}{y^2} + \frac{a(t)^4}{\beta(t)^6}\frac{3}{8y^3}\right. \\ \left. - \frac{a(t)^6}{\beta(t)^9}\frac{5}{16y^4} + \frac{a(t)^8}{\beta(t)^{12}}\frac{35}{128y^5} + \frac{a(t)^{10}}{\beta(t)^{15}}\frac{63}{256y^6} + \frac{a(t)^{12}}{\beta(t)^{18}}\frac{231}{1024y^7} + \cdots\right].$$

Performing the y-integral in the last line, we obtain:

$$\Gamma_{\text{PH}}(q\hat{x},0) \;=\; \frac{1}{2(2\pi)^2}\int_{-1}^{1}\mathrm{d}t\, e^{-\frac{q^2t^2}{K^2}\beta(t)}\;\Bigg[\Gamma(0,\frac{a(t)^2}{\beta(t)^3}) \;+\; \frac{1}{2}\frac{a(t)^2}{\beta(t)^3}\Gamma(-1,\frac{a(t)^2}{\beta(t)^3})$$
$$+\;\frac{3}{8}\frac{a(t)^4}{\beta(t)^6}\Gamma(-2,\frac{a(t)^2}{\beta(t)^3}) \;+\; \frac{5}{16}\frac{a(t)^6}{\beta(t)^{10}}\Gamma(-3,\frac{a(t)^2}{\beta(t)^3}) \;+\; \frac{35}{128}\frac{a(t)^8}{\beta(t)^{12}}\Gamma(-4,\frac{a(t)^2}{\beta(t)^3})$$
$$+\;\frac{63}{256}\frac{a(t)^{10}}{\beta(t)^{15}}\Gamma(-5,\frac{a(t)^2}{\beta(t)^3}) \;+\; \frac{231}{1024}\frac{a(t)^{12}}{\beta(t)^{18}}\frac{231}{1024y^7}\Gamma(-6,\frac{a(t)^2}{\beta(t)^3}) \;+\;\cdots\Bigg], \qquad \text{(B.12)}$$

where $\Gamma(-n,a)$ is the upper incomplete Γ-function. Using the identity,

$$\Gamma(-n,a) \;=\; \frac{(-1)^n}{n!}\Gamma(0,a) \;+\; e^{-a}\sum_{i=n}^{1}\frac{(-1)^{n-i}}{a^i}\frac{(i-1)!}{n!} \qquad \text{(B.13)}$$

$\Gamma_{\text{PH}}(q\hat{x},0)$ can be written as:

$$\Gamma_{\text{PH}}(q\hat{x},0) \;=\frac{1}{2(2\pi)^2}\int_{-1}^{1}\mathrm{d}t\, e^{-\frac{q^2t^2}{K^2}\beta(t)}\;\sum_{n=0}^{\infty}C_n\Big(\frac{a(t)^2}{\beta(t)^3}\Big)^n\Gamma\big(-n,\frac{a(t)^2}{\beta(t)^3}\big) \qquad \text{(B.14)}$$
$$=\frac{-1}{2(2\pi)^2}\int_{-1}^{1}\mathrm{d}t\, e^{-\frac{q^2t^2}{K^2}\beta(t)}\;\sum_{n=0}^{\infty}C_n\Bigg[e^{-\frac{a(t)^2}{\beta(t)^3}}\sum_{m=n}^{1}\frac{(m-1)!}{n!}(-1)^{n-m}$$
$$\Big(\frac{a(t)^2}{\beta(t)^3}\Big)^{n-m} \;+\; \frac{(-1)^n}{n!}\Big(\frac{a(t)^2}{\beta(t)^3}\Big)^n\Gamma\big(0,\frac{a(t)^2}{\beta(t)^3}\big)\Bigg],$$

where C_n are the coefficients in the series expansion of $\frac{1}{\sqrt{y^2-1}}$ in $\frac{1}{y}$, and

$$\frac{\alpha(t)^2}{\beta(t)^3} = 32\frac{\mu}{K^2} + \Big(\frac{8(t^2-1)}{K^2} + \frac{48\mu(1+t^2)}{\Lambda^2}\Big)q^2 + \Big(\frac{12(t^4-1)}{\Lambda^2} + \frac{24K^2\mu(1+t^2)^2}{\Lambda^4}\Big)q^4$$
$$+\Big(\frac{6K^2(t^2-1)(t^2+1)^2}{\Lambda^4} + \frac{4\mu K^4(1+t^2)^3}{\Lambda^6}\Big)q^6 + \frac{K^4}{\Lambda^6}(t^2-1)(t^2+1)^3q^8\,. \qquad \text{(B.15)}$$

From Eqs. (B.14,B.15), one can systematically determine the coefficients of the series expansion of $\Gamma_{\text{PH}}(q\hat{x},0)$ in q by ignoring all $\mathcal{O}(\mu)$ and $\mathcal{O}(1/K)$ terms as accurately as desired. Using *Mathematica 8*, we expand the integral in Eq. (B.12) (keeping up to

$\Gamma(-14, \frac{a(t)^2}{\beta(t)^3}))$ in q and then perform the t-integral. We find:

$$\begin{aligned}\Gamma_{\text{PH}}(q\hat{x},0) \approx \frac{1}{2(2\pi)^2}\Bigg[&\Big(-5.9-2\log\frac{\mu}{K^2}\Big)+\Big(-4\frac{K^2}{\Lambda}+0.33\frac{\Lambda}{\mu}-5\frac{\Lambda}{K^2}\log\frac{\mu}{K^2}\\&\Big)\frac{q^2}{\Lambda}+\Big(1.4\frac{K^4}{\Lambda^2}-50.4+\frac{\Lambda^2}{\mu^2}+0.5\frac{\Lambda^2}{\mu K^2}-12.3\frac{\Lambda^2}{K^4}\log\frac{\mu}{K^2}-9.86\log\frac{\mu}{K^2}\Big)\frac{q^4}{\Lambda^2}\\&+\Big(-0.68\frac{K^6}{\Lambda^3}-40.5\frac{K^2}{\Lambda}+0.0047\frac{\Lambda^3}{\mu^3}+0.035\frac{\Lambda^3}{\mu^2K^2}+0.879\frac{\Lambda^3}{\mu K^4}+0.938\frac{\Lambda}{\mu}\\&-23.5\frac{\Lambda^3}{K^6}\log\frac{\mu}{K^2}-43.0\frac{\Lambda}{K^2}\log\frac{\mu}{K^2}-5.7\frac{K^2}{\Lambda}\log\frac{\mu}{K^2}\Big)\frac{q^6}{\Lambda^3}+\cdots\Bigg].\end{aligned}\tag{B.16}$$

From this, we finally obtain the derivative of $\Gamma_{\text{PH}}(q\hat{x},0)$ with respect to $\log\Lambda$:

$$\begin{aligned}\partial_{\log\Lambda}\Gamma_{\text{PH}}(q\hat{x},0) \approx \frac{1}{2(2\pi)^2}\Bigg[&8\frac{K^2}{\Lambda}\frac{q^2}{\Lambda}+\Big(19.7\log\frac{\mu}{K^2}+101-5.6\frac{K^4}{\Lambda^2}\Big)\frac{q^4}{\Lambda^2}\\&+\Big(-1.87\frac{\Lambda}{\mu}+\Big[22.8\frac{K^2}{\Lambda}+86\frac{\Lambda}{K^2}\Big]\log\frac{\mu}{K^2}+4.11\frac{K^6}{\Lambda^3}+\\&162\frac{K^2}{\Lambda}\Big)\frac{q^6}{\Lambda^3}+\Big(-0.13\frac{\Lambda^2}{\mu^2}-2.06\frac{K^2}{\mu}+\Big[237\frac{\Lambda^2}{K^4}+255+\\&8.7\frac{K^4}{\Lambda^2}\Big]\log\frac{\mu}{K^2}+1462-71.5\frac{K^4}{\Lambda^2}-3.16\frac{K^8}{\Lambda^4}\Big)\frac{q^8}{\Lambda^4}+\Big(-0.014\frac{\Lambda^3}{\mu^3}\\&-0.138\frac{K^2}{\Lambda\mu^2}-0.326\frac{\Lambda^3}{K^2\mu^2}-0.716\frac{K^4}{\Lambda\mu}-17.13\frac{\Lambda}{\mu}-12.98\frac{\Lambda^3}{K^4\mu}+\\&\Big[-1.262\frac{K^6}{\Lambda^3}+305\frac{K^2}{\Lambda}+1082\frac{\Lambda}{K^2}+483\frac{\Lambda^3}{K^6}\Big]\log\frac{\mu}{K^2}+2.52\frac{K^{10}}{\Lambda^5}\\&+9.235\frac{K^6}{\Lambda^3}+1987\frac{K^2}{\Lambda}\Big)\frac{q^{10}}{\Lambda^5}+\mathcal{O}(q)^{12}\Bigg],\end{aligned}\tag{B.17}$$

B.2 Computation of $\Gamma_{\text{PH}}(q\hat{x}, 0)$ for $\mu = 0$

Starting from Eq. (B.5), for the case $\mu = 0$ we have:

$$\Gamma_{\text{PH}}(q\hat{x}, \Omega = 0) = \frac{1}{2(2\pi)^2} \int_{-\infty}^{\infty} \mathrm{d}X \int_{-1}^{1} \mathrm{d}t \, \frac{|X|}{X} \frac{\theta\big(X(t+1)\big) - \theta\big(X(t-1)\big)}{\sqrt{(-X-q^2)^2 - 2q^2(t+1)X}} \\ e^{-\frac{1}{K^2}(tX + \frac{X^2}{q^2} - q^2)} \, e^{-\frac{X^2(1+t^2)}{2\Lambda^2}} \,, \tag{B.18}$$

with no constraint. This can be written as:

$$\Gamma_{\text{PH}}(q\hat{x}, 0) = \frac{1}{(2\pi)^2} \int_{0}^{\infty} \mathrm{d}X \int_{-1}^{1} \mathrm{d}t \, \frac{1}{\sqrt{(X+q^2)^2 - 2q^2(t+1)X}} \\ \exp\left\{ - \frac{2\Lambda^2 + q^2K^2(1+t^2)}{2\Lambda^2 q^2 K^2} \Big(X + \frac{tq^2\Lambda^2}{q^2K^2(1+t^2) + 2\Lambda^2} \Big)^2 \right. \\ \left. - \frac{q^2t^2\Lambda^2}{2q^2K^4(1+t^2) + 4K^2\Lambda^2} \right\}. \tag{B.19}$$

Using, $\beta(t) = \frac{\Lambda^2}{q^2K^2(1+t^2)+2\Lambda^2}$, the above integral becomes:

$$\Gamma_{\text{PH}}(q\hat{x}, 0) = \frac{1}{(2\pi)^2} \int_{-1}^{1} \mathrm{d}t \, e^{-\frac{q^2t^2}{2K^2}\beta(t)} \int_{0}^{\infty} \frac{\mathrm{d}X \, e^{-\frac{1}{2q^2K^2\beta(t)}(X + tq^2\beta(t))^2}}{\sqrt{(X+q^2)^2 - 2q^2(t+1)X}} \,. \tag{B.20}$$

Using, $X \to \tilde{X} = \frac{1}{q^2\beta(t)} X$, we get:

$$\Gamma_{\text{PH}}(q\hat{x}, 0) = \frac{1}{(2\pi)^2} \int_{-1}^{1} \mathrm{d}t \, e^{-\frac{q^2t^2}{2K^2}\beta(t)} \int_{0}^{\infty} \frac{\mathrm{d}\tilde{X} \, \cancel{q^2\beta(t)} \, e^{-\frac{t^2q^2\beta(t)}{2K^2}(\tilde{X}+t)^2}}{\cancel{q^2\beta(t)} \sqrt{(\tilde{X} + \frac{1}{\beta(t)})^2 - 2\tilde{X}\frac{(t+1)}{\beta(t)}}} \,. \tag{B.21}$$

The inverse square root in the integrand can be simplified as follows:

$$(\tilde{X} + \frac{1}{\beta(t)})^2 - 2\tilde{X}\frac{(t+1)}{\beta(t)} = \tilde{X}^2 - 2t\tilde{X}\frac{1}{\beta(t)} + \frac{1}{\beta(t)^2} = \big(\tilde{X} - \frac{t}{\beta(t)}\big)^2 + \frac{1-t^2}{\beta(t)^2} \,. \tag{B.22}$$

Now, let us break up the $\tilde{X}$ integral. This is because we want to Taylor expand the inverse square root term in the integrand.

$$\Gamma_{\text{PH}}(q\hat{x},0) = \frac{1}{(2\pi)^2}\int_{-1}^{1} \mathrm{d}t\, e^{-\frac{q^2t^2}{2K^2}\beta(t)} \Bigg[\underbrace{\int_0^{\frac{1}{\beta(t)}} \mathrm{d}\tilde{X}}_{I_1} + \underbrace{\int_{\frac{1}{\beta(t)}}^{\infty} \mathrm{d}\tilde{X}}_{I_2}\Bigg] \frac{e^{-\frac{t^2q^2\beta(t)}{2K^2}(\tilde{X}+t)^2}}{\sqrt{(\tilde{X}-\frac{t}{\beta(t)})^2+\frac{1-t^2}{\beta(t)^2}}}\,. \tag{B.23}$$

Using *Mathematica*, the first integral is approximately computed as following:

$$\begin{aligned} I_1 &\approx \frac{1}{(2\pi)^2}\int_{-1}^{1} \mathrm{d}t\, e^{-\frac{q^2t^2}{2K^2}\beta(t)} \int_0^{\frac{1}{\beta(t)}} \mathrm{d}\tilde{X} \frac{1}{\sqrt{(\tilde{X}-\frac{t}{\beta(t)})^2+\frac{1-t^2}{\beta(t)^2}}} \Big[1 - \frac{t^2q^2\beta(t)}{2K^2}(\tilde{X}+t)^2 + \cdots\Big] \\ &\approx \frac{1}{(2\pi)^2}\int_{-1}^{1} \mathrm{d}t\, e^{-\frac{q^2t^2}{2K^2}\beta(t)} \Big[\log\frac{1+\sqrt{2(1-t)}-t}{1-t} - \frac{t^2q^2\beta(t)}{2K^2}\frac{1}{2\Lambda^4}\Big(\cdots\Big) + \cdots\Big]\,. \end{aligned} \tag{B.24}$$

we find no singular dependence on q in I_1. Next, let us consider I_2. Expanding the inverse square root in the integrand of I_2 in large $\tilde{X}$, we find:

$$\begin{aligned} I_2 &= \frac{1}{(2\pi)^2}\int_{-1}^{1} \mathrm{d}t\, e^{-\frac{q^2t^2}{2K^2}\beta(t)} \int_{\frac{1}{\beta(t)}}^{\infty} \mathrm{d}\tilde{X} \frac{e^{-\frac{t^2q^2\beta(t)}{2K^2}(\tilde{X}+t)^2}}{\sqrt{(\tilde{X}-\frac{t}{\beta(t)})^2+\frac{1-t^2}{\beta(t)^2}}} \\ &\approx \frac{-1}{(2\pi)^2}\int_{-1}^{1} \mathrm{d}t\, e^{-\frac{q^2t^2}{2K^2}\beta(t)} \int_{\frac{1}{\beta(t)}}^{\infty} \mathrm{d}\tilde{X} \Bigg[\frac{1}{\tilde{X}} + \frac{t}{\beta(t)}\frac{1}{\tilde{X}^2} + \frac{3t^2-1}{2\beta(t)^2}\frac{1}{\tilde{X}^3} + \frac{t(5t^2-3)}{2\beta(t)^3}\frac{1}{\tilde{X}^4} \\ &\quad + \frac{3-30t^2+35t^4}{8\beta(t)^4}\frac{1}{\tilde{X}^5} + \frac{t(15-70t^2+63t^4)}{8\beta(t)^5}\frac{1}{\tilde{X}^6} + \frac{-5+21t^2(5-15t^2+11t^4)}{16\beta(t)^6} \\ &\quad \times \frac{1}{\tilde{X}^7} + \cdots\Bigg] e^{-\frac{t^2q^2\beta(t)}{2K^2}\tilde{X}^2}\Big[1 - 2\frac{t^2q^2\beta(t)}{2K^2}(\tilde{X}+t) + \cdots\Big]\,. \end{aligned} \tag{B.25}$$

The leading term in the above expansion in $\frac{1}{\tilde{X}}$ results in a singular dependence on q of the form $\log q^2$. Similarly, the remaining terms result in logarithmic dependence on q but accompanied by polynomials in q^2. If desired, using *Mathematica*, one can obtain a series expansion in q as accurately as desired.

Using *Mathematica 8*, we determine non-analytic terms in $\partial_{\log\Lambda}\Gamma_{\text{PH}}(q\hat{x},0)$. These

terms are all of the form $q^{2n+2}\log\frac{q^2}{K^2}$ $(n \geq 1)$:

$$\partial_{\log\Lambda}\Gamma^{\text{n.-a.}}_{\text{PH}}(q\hat{x},0) = \frac{1}{(2\pi)^2}\Bigg[-0.028\frac{q^4}{\Lambda^2} - 0.368\frac{K^2}{\Lambda}\frac{q^6}{\Lambda^3} + \Big(0.473\frac{K^4}{\Lambda^2} + 0.448\Big)\frac{q^8}{\Lambda^4} - \Big(0.55\frac{K^6}{\Lambda^3} + 0.6\frac{K^2}{\Lambda}\Big)\frac{q^{10}}{\Lambda^5} + \mathcal{O}(\frac{q^{12}}{\Lambda^6})\Bigg]\log\frac{q^2}{K^2}\,, \tag{B.26}$$

where we have ignored $\mathcal{O}(\frac{1}{K})$ terms.

B.3 Computation of $\Gamma_{\text{PP}}(\mathbf{q}=0,\Omega\ll\Lambda)$

The particle-particle diagram, $\Gamma_{\text{PP}}(\mathbf{q},\Omega)$ is given by:

$$\begin{aligned}\Gamma_{\text{PP}}(\mathbf{q},\Omega) &= \int' \frac{\mathrm{d}\mathbf{k}}{(2\pi)^2}\int\frac{\mathrm{d}\omega}{2\pi}\,\mathcal{G}_0(\mathbf{k}+\mathbf{q},\omega+\Omega)\,\mathcal{G}_0(-\mathbf{k},-\omega)\\ &= \int' \frac{\mathrm{d}\mathbf{k}}{(2\pi)^2}\int\frac{\mathrm{d}\omega}{2\pi}\,\frac{1}{i(\omega+\Omega)-(\xi_{\mathbf{k}+\mathbf{q}}-\mu)}\,\frac{1}{-i\omega-(\xi_{-\mathbf{k}}-\mu)}\\ &= \frac{-1}{(2\pi)^2}\int' \mathrm{d}\mathbf{k}\frac{\theta(\xi_{\mathbf{k}}-\mu)-\theta(-\xi_{\mathbf{k}+\mathbf{q}}+\mu)}{i\Omega-\xi_{\mathbf{k}}-\xi_{\mathbf{k}+\mathbf{q}}+2\mu}\,,\end{aligned} \tag{B.27}$$

where the primes on the integrals indicate that the $\mathbf{k}$-integration is restricted to $|\xi_{\mathbf{k}}|,|\xi_{\mathbf{k}+\mathbf{q}}|<\Lambda$ and $|k_+|,|k_-|<K$ (where $k_\pm=k_x\pm k_y$ are the light-cone coordinates) – see Fig. [B.1]. The reason that we use sharp cutoffs instead of soft cutoffs is for convenience. Note that since we are computing $\Gamma_{\text{PP}}(\mathbf{q},\Omega\ll\Omega)$ at $\mathbf{q}=0$ the question of whether the cutoffs are soft or sharp becomes irrelevant. Setting the

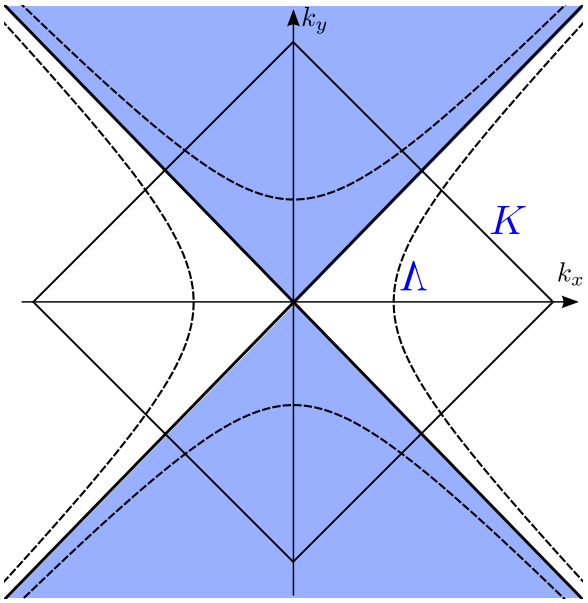

Figure B.1: The Fermi surface and the sharp energy and momentum cutoffs. The sharp momentum cutoff is indicated by the "diamond". This specific choice of the momentum cutoff is for convenience.

transfer momentum $\mathbf{q}$ to zero, for the case $\mu = 0$ I have:

$$\Gamma_{\text{PP}}^{\mu=0}(\mathbf{q}=0,\Omega) = \frac{-1}{(2\pi)^2}\int' \mathrm{d}\mathbf{k}\frac{\theta(\xi_{\mathbf{k}})-\theta(-\xi_{\mathbf{k}})}{i\Omega-\xi_{\mathbf{k}}-\xi_{\mathbf{k}}} = \frac{-1}{(2\pi)^2}\frac{1}{2}\int_{\substack{|k_+K_-|<\Lambda\\|k_\pm|<K}} \mathrm{d}k_+\mathrm{d}k_-\frac{2\,\mathrm{sgn}(\xi_{\mathbf{k}})}{i\Omega-2\xi_{\mathbf{k}}}$$

$$= -\frac{1}{(2\pi)^2}\int_{-K}^{K}\frac{\mathrm{d}k_+}{|k_+|}\underbrace{\int_{-\min\{\Lambda,|k_+|K\}}^{\min\{\Lambda,|k_+|K\}}\mathrm{d}\xi\,\frac{\mathrm{sgn}(\xi)}{i\Omega-2\xi}}_{I(k_+)}, \tag{B.28}$$

where, in the second line, we used $(k_+,k_-)\to(k_+,\xi=k_+k_-)$ with the Jacobian $\frac{1}{|k_+|}$. The $I(k_+)$ integral gives:

$$\begin{aligned} I(k_+) &= \int_{-\min\{\Lambda,|k_+|K\}}^{\min\{\Lambda,|k_+|K\}}\mathrm{d}\xi\,\frac{\mathrm{sgn}(\xi)}{i\Omega-2\xi}\\ &= \int_0^{\min\{\Lambda,|k_+|K\}}\mathrm{d}\xi\left[\frac{1}{i\Omega-2\xi}-\frac{1}{i\Omega+2\xi}\right]\\ &= \int_0^{\min\{\Lambda,|k_+|K\}}\frac{4\xi\,\mathrm{d}\xi}{-\Omega^2-4\xi^2}\\ &= \frac{-1}{2}\ln\left[\frac{\Omega^2+4\big(\min\{\Lambda,|k_+|K\}\big)^2}{\Omega^2}\right] \end{aligned} \tag{B.29}$$

Plugging this result for $I(k_+)$ into Eq. (B.28) and performing the k_+-integral, we obtain:

$$\Gamma_{\text{PP}}^{\mu=0}(\mathbf{q}=0,\Omega) = \frac{1}{(2\pi)^2}\int_0^K\frac{\mathrm{d}k_+}{k_+}\ln\left[\frac{\Omega^2+4\big(\min\{\Lambda,k_+K\}\big)^2}{\Omega^2}\right] \tag{B.30}$$

$$= \frac{1}{(2\pi)^2}\left[\int_0^{\frac{\Lambda}{K}}\frac{\mathrm{d}k_+}{k_+}\ln\left(1+\frac{4k_+^2K^2}{\Omega^2}\right)+\int_{\frac{\Lambda}{K}}^K\frac{\mathrm{d}k_+}{k_+}\ln\left(1+\frac{4\Lambda^2}{\Omega^2}\right)\right]$$

$$= \frac{1}{(2\pi)^2}\left[\frac{1}{2}\int_0^{\frac{4\Lambda^2}{\Omega^2}}\frac{\mathrm{d}\kappa}{\kappa}\ln(1+\kappa)+\ln\frac{K^2}{\Lambda}\ln\left(1+\frac{4\Lambda^2}{\Omega^2}\right)\right]$$

$$= \frac{1}{(2\pi)^2}\left[-\frac{1}{2}\,\mathrm{Li}_2(-\frac{4\Lambda^2}{\Omega^2})+\ln\frac{K^2}{\Lambda}\ln\left(1+\frac{4\Lambda^2}{\Omega^2}\right)\right],$$

where, for the first term in the second last line, $\kappa = \frac{\Omega^2}{4K^2}k_+^2$. Using the expansion of the *dilogarithm* function in the large $\frac{4\Lambda^2}{\Omega^2}$ limit,

$$-\operatorname{Li}_2(-x) \approx \frac{\pi^2}{6} + \frac{1}{2}\Big(\ln\frac{1}{x}\Big)^2 + \mathcal{O}(\frac{1}{a})\,, \tag{B.31}$$

we get:

$$\Gamma_{\text{PP}}^{\mu=0}(\mathbf{q}=0,\Omega\ll\Lambda) \approx \frac{1}{(2\pi)^2}\Bigg[\ln\frac{K^2}{\Lambda}\ln\Big(1+\frac{4\Lambda^2}{\Omega^2}\Big) + \frac{\pi^2}{12} + \frac{1}{4}\Big(\ln\frac{\Omega^2}{4\Lambda^2}\Big)^2 + \mathcal{O}(\frac{\Omega^2}{4\Lambda^2})\Bigg]\,. \tag{B.32}$$

For $\partial_{\ln\Lambda}\Gamma_{\text{PP}}^{\mu=0}(\mathbf{q}=0,\Omega\ll\Lambda)$ I obtain:

$$\partial_{\ln\Lambda}\Gamma_{\text{PP}}^{\mu=0}(0,\Omega) \approx \frac{1}{(2\pi)^2}\Bigg[\frac{8\Lambda^2}{4\Lambda^2+\Omega^2}\ln\frac{K^2}{\Lambda} - \ln\Big(1+\frac{\Omega^2}{4\Lambda^2}\Big) + \mathcal{O}(\frac{\Omega^2}{4\Lambda^2})\Bigg]\,. \tag{B.33}$$

Repeating the same calculations for $\mu \neq 0$, we find:

$$\begin{aligned}\Gamma_{\text{PP}}^{\mu>0}(0,\Omega) \approx \frac{-1}{2\pi^2}\Bigg[&\frac{1}{2}\Bigg(-\frac{\pi^2}{6}+\operatorname{Li}_2(\frac{1}{2})+\frac{\pi^2}{6}+\frac{1}{2}\Big(\ln(2)\Big)^2-\operatorname{Li}_2(1)\Bigg)+\frac{1}{2}\Bigg(\\ &\ln\Big(\frac{\Lambda-2\mu}{\Lambda}\Big)\ln\Big(\frac{\Lambda-\mu}{\mu}\Big)-\frac{1}{2}\Big(\ln 2\Big)^2+\operatorname{Li}_2(\frac{1}{2})+\operatorname{Li}_2(\frac{\mu}{\Lambda})+\frac{1}{2}\Big(\ln(\frac{\Lambda}{\mu})\Big)^2\\ &+\operatorname{Li}_2(\frac{\Lambda-2\mu}{-\mu})\Bigg)-\frac{1}{2}\Bigg(\ln(\Omega^2)\ln\Big(\frac{\mu}{\Lambda-\mu}\Big)-2\ln(2\mu)\ln(2\Lambda-4\mu)\\ &+\ln(2\Lambda-2\mu)\ln(4(\Lambda-2\mu)^2)+2\operatorname{Li}_2(\frac{\Lambda-2\mu}{-\mu})\Bigg)-\frac{1}{2}\Bigg(\\ &\ln\Big(\frac{\Lambda+\mu}{\Lambda-\mu}\Big)\ln(1+\frac{4\Lambda^2}{\Omega^2})+\ln\Big(\frac{\Lambda-\mu}{\mu}\Big)\ln\Big(\frac{\Lambda}{\Lambda-2\mu}\Big)-\operatorname{Li}_2(\frac{\Lambda-2\mu}{-\mu})\\ &+\operatorname{Li}_2(-\frac{\Lambda}{\mu})\Big)-\frac{1}{2}\Bigg(\ln\big(\frac{K^2}{\Lambda+\mu}\big)\ln\big(1+4\frac{\Lambda^2}{\Omega^2}\big)\Bigg)\Bigg]\,.\end{aligned} \tag{B.34}$$

where, in the last line, we have only kept singular terms in Ω in the limit $\Omega \to 0$. Note that taking the two limits $\Omega \to 0$ and $\mu \to 0$ do not commute. The latter should reduce to Eq. (B.32). Taking the derivative of the above expression w.r.t. $\ln\Lambda$, for the leading term in the Taylor expansion in Ω I find:

$$\Gamma_{\mathrm{PP}}^{\mu>0}(0,\Omega\to 0) \;\approx\; \frac{-1}{(2\pi)^2}\ln\Big(\frac{\Lambda^2-\mu^2}{K^4}\Big)\,. \tag{B.35}$$

B.4 Computation of $\chi''_{\mathrm{PH}}(q\hat{x},\Omega)$

Here we present the computation of the imaginary part of the one-loop particle-hole susceptibility, $\chi''_{\mathrm{PH}}(q\hat{x},\Omega)$, for the dispersion $\varepsilon_{\mathbf{k}} = k_x^2 - k_y^2$ at a finite chemical potential and with a smooth momentum cutoff K. This susceptibility is obtained from the imaginary-time (Matsubara) susceptibility $\chi_{\mathrm{PH}}(q\hat{x},\Omega)$ by analytically continuing $\chi_{\mathrm{PH}}(q\hat{x}, i\Omega \to \Omega + i0^+)$ [40]. The imaginary-time particle-hole susceptibility is given by:

$$\chi_{\mathrm{PH}}(q\hat{x}, i\Omega) \;=\; \frac{-1}{(2\pi)^2}\int \mathrm{d}\mathbf{k}\, \frac{\theta(\xi_{\mathbf{k}}-\mu)-\theta(\xi_{\mathbf{k}+\mathbf{q}}-\mu)}{i\Omega+\xi_{\mathbf{k}}-\xi_{\mathbf{k}+\mathbf{q}}}\; e^{-\frac{|\mathbf{k}|^2+|\mathbf{k}+\mathbf{q}|}{K^2}}\,. \tag{B.36}$$

Following the same steps as in Section [B.1] (see Eq. (B.5)), the above integral is written as:

$$\begin{aligned}\chi_{\mathrm{PH}}(\mathbf{q}, i\Omega) \;=& \frac{-2}{2(2\pi)^2}\mathrm{Re}\left\{\int_0^\infty \mathrm{d}X \int_{-1}^{1}\mathrm{d}t\; \frac{X}{i\Omega+X}\frac{e^{-\frac{1}{K^2}(tX+\frac{X^2}{q^2}-2\mu-q^2)}}{\sqrt{(X+q^2)^2-4q^2(\frac{t+1}{2}X+\mu)}}\right\}\\ &\frac{-1}{(2\pi)^2}\int_0^\infty \mathrm{d}X \int_{-1}^{1}\mathrm{d}t\; \frac{X^2}{\Omega^2+X^2}\frac{e^{-\frac{1}{K^2}(tX+\frac{X^2}{q^2}-2\mu-q^2)}}{\sqrt{(X+q^2)^2-4q^2(\frac{t+1}{2}X+\mu)}}\,,\end{aligned} \tag{B.37}$$

with the constraint $X^2+2tq^2X+q^4-4q^2\mu \geq 0$. The constraint $X^2+2tq^2X+q^4-4q^2\mu \geq 0$, for a generic q, implies $X \notin (X_-, X_+)$ where $X_\pm = -tq^2 \pm \sqrt{4q^2\mu - q^4(1-t^2)}$. As in Section [B.1], for $q \leq 2\sqrt{\mu}$ this constraint restricts the integration over X to $[X_{\mathrm{min}}, \infty)$ where $X_{\mathrm{min}} = -tq^2 + \sqrt{4q^2\mu - q^4(1-t^2)}$.

Since we are interested in $\chi''_{\mathrm{PH}}(\mathbf{q},\Omega)$ not only at small q ($q \leq 2\sqrt{\mu}$) but also as $q \simeq \mathbf{O}(\mu)$ we need to consider the two cases $q \leq 2\sqrt{\mu}$ and $q > 2\sqrt{\mu}$ separately.

$q < 2\sqrt{\mu}$

For $q < 2\sqrt{\mu}$, using $X \to \mathcal{Y} = X - X_{\mathrm{min}}$, the above integral becomes:

$$\begin{aligned}\chi_{\mathrm{PH}}(\mathbf{q}, i\Omega) \;=& \frac{-1}{(2\pi)^2}e^{\frac{2\mu+q^2}{K^2}}\int_0^\infty \mathrm{d}\mathcal{Y}\int_{-1}^{1}\mathrm{d}t\; \frac{(\mathcal{Y}-tq^2+\sqrt{4q^2\mu-q^4(1-t^2)})^2}{-(i\Omega)^2+(\mathcal{Y}-tq^2+\sqrt{4q^2\mu-q^4(1-t^2)})^2}\\ &\frac{e^{-\frac{t}{K^2}(\mathcal{Y}-tq^2+\sqrt{4q^2\mu-q^4(1-t^2)})-\frac{1}{q^2K^2}(\mathcal{Y}-tq^2+\sqrt{4q^2\mu-q^4(1-t^2)})^2}}{\sqrt{\mathcal{Y}(\mathcal{Y}+2\sqrt{4q^2\mu-q^4(1-t^2)})}}\,.\end{aligned} \tag{B.38}$$

Analytically continuing $i\Omega \to \Omega + i0^+$, we find the retarded particle hole susceptibility:

$$\chi^R_{\rm PH}(\mathbf{q},\Omega) = \frac{-e^{\frac{2\mu+q^2}{K^2}}}{(2\pi)^2}\int_0^\infty \mathrm{d}\mathcal{Y}\int_{-1}^1 \mathrm{d}t \frac{(\mathcal{Y}-tq^2+\sqrt{4q^2\mu-q^4(1-t^2)})^2}{-(\Omega+i0^+)^2+(\mathcal{Y}-tq^2+\sqrt{4q^2\mu-q^4(1-t^2)})^2} \frac{e^{-\frac{t}{K^2}(\mathcal{Y}-tq^2+\sqrt{4q^2\mu-q^4(1-t^2)})-\frac{1}{q^2K^2}(\mathcal{Y}-tq^2+\sqrt{4q^2\mu-q^4(1-t^2)})^2}}{\sqrt{\mathcal{Y}(\mathcal{Y}+2\sqrt{4q^2\mu-q^4(1-t^2)})}}\,. \tag{B.39}$$

In the part of the integrand that contains Ω, using the Dirac identity, we get:

$$\frac{1}{\underbrace{(\mathcal{Y}-tq^2+\sqrt{4q^2\mu-q^4(1-t^2)})^2}_{\mathcal{X}>0}-(\Omega+i0^+)^2} = \frac{1}{(\mathcal{X}-\Omega-i0^+)(\mathcal{X}+\Omega+i0^+)}\,. \tag{B.40}$$

Without loss of generality, let us assume $\Omega > 0$. We can write:

$$\frac{1}{\mathcal{X}-(\Omega+i0^+)^2} = \frac{1}{(\mathcal{X}-\Omega-i0^+)(\mathcal{X}+\Omega)}\,. \tag{B.41}$$

Therefore, for $\Omega > 0$, the imaginary part of the retarded real-time particle-hole susceptibility is given by:

$$\chi''_{\rm PH}(\mathbf{q},\Omega) = \frac{-(-\pi)}{(2\pi)^2}e^{\frac{2\mu+q^2}{K^2}}\int_0^\infty \mathrm{d}\mathcal{Y}\int_{-1}^1 \mathrm{d}t\, \frac{(\mathcal{Y}-tq^2+\sqrt{4q^2\mu-q^4(1-t^2)})^2}{\Omega+\mathcal{Y}-tq^2+\sqrt{4q^2\mu-q^4(1-t^2)}} \frac{e^{-\frac{t}{K^2}(\mathcal{Y}-tq^2+\sqrt{4q^2\mu-q^4(1-t^2)})-\frac{1}{q^2K^2}(\mathcal{Y}-tq^2+\sqrt{4q^2\mu-q^4(1-t^2)})^2}}{\sqrt{\mathcal{Y}(\mathcal{Y}+2\sqrt{4q^2\mu-q^4(1-t^2)})}} \delta\Big(\mathcal{Y}-tq^2+\sqrt{4q^2\mu-q^4(1-t^2)}-\Omega\Big)\,. \tag{B.42}$$

Imposing the δ-function, we finally obtain:

$$\chi''_{\rm PH}(\mathbf{q},\Omega) = -\frac{\Omega}{8\pi}\,e^{\frac{2\mu+q^2}{K^2}-\frac{\Omega^2}{q^2K^2}}\int_{-1}^1 \mathrm{d}t\, \frac{e^{-\frac{t\Omega}{K^2}}}{\sqrt{\Omega^2+2t\Omega q^2-4q^2\mu+q^4}}\,.. \tag{B.43}$$

with the constraint $\Omega + tq^2 - \sqrt{4q^2\mu - q^4(1-t^2)} \geq 0$. This constraint restricts the integration over t:

$$t \geq \frac{q^2}{2\Omega}\Big(\frac{4\mu}{q^2}-1-\frac{\Omega^2}{q^4}\Big) \tag{B.44}$$

Finally we find:

$$\chi''_{\rm PH}(\mathbf{q},\Omega) \;=\; -\frac{\Omega}{8\pi}\, e^{\frac{2\mu+q^2}{K^2}-\frac{\Omega^2}{q^2K^2}} \int_{\rm Max\{-1,\frac{4\mu-q^2}{2\Omega^2}-\frac{\Omega}{2q^2}\}}^{1} {\rm d}t\; \frac{e^{-\frac{t\Omega}{K^2}}}{\sqrt{\Omega^2+2t\Omega q^2-4q^2\mu+q^4}}\,. \tag{B.45}$$

$$q \geq 2\sqrt{\mu}$$

Next, we consider the $q \geq 2\sqrt{\mu}$. Starting from Eq. (B.37) after analytically continuing $i\Omega \to \Omega + i0^+$ and assuming that $\Omega > 0$, we get:

$$\begin{aligned}\chi^R_{\rm PH}(\mathbf{q},\Omega>0) \;=& \frac{-1}{(2\pi)^2}\int_0^\infty {\rm d}X \int_{-1}^{1} {\rm d}t\; \frac{X^2}{(X+\Omega)(X-\Omega-i0^+)} \\ & \frac{e^{-\frac{1}{K^2}(tX+\frac{X^2}{q^2}-2\mu-q^2)}}{\sqrt{(X+q^2)^2-4q^2(\frac{t+1}{2}X+\mu)}}\,,\end{aligned} \tag{B.46}$$

with the constraint $X^2+q^4+2tq^2X-4q^2\mu \geq 0$. Imposing this constraint restricts the X and t integrals as following:

$$\begin{aligned}\chi^R_{\rm PH}(q\geq 2\sqrt{\mu},\Omega>0) \;=\; \frac{-1}{(2\pi)^2}\Bigg[& \underbrace{\int_0^\infty {\rm d}X \int_{-\sqrt{1-\frac{4\mu}{q^2}}}^{1} {\rm d}t}_{I_1} + \underbrace{\int_{X_+}^\infty {\rm d}X \int_{-1}^{-\sqrt{1-\frac{4\mu}{q^2}}} {\rm d}t}_{I_2} \\ & + \underbrace{\int_0^{X_-} {\rm d}X \int_{-1}^{-\sqrt{1-\frac{4\mu}{q^2}}} {\rm d}t}_{I_3}\Bigg](\cdots)\,,\end{aligned} \tag{B.47}$$

where, $(\cdots)$ stands for the integrand, which is the integrand in Eq. (B.46). We compute the above three integrals I_1, I_2 and I_3 separately.

For I_1 we find:

$$I_1 \;=\frac{-1}{(2\pi)^2}\int_0^\infty {\rm d}X \int_{-\sqrt{1-\frac{4\mu}{q^2}}}^{1} {\rm d}t\; \frac{X^2}{(X+\Omega)(X-\Omega-i0^+)} \frac{e^{-\frac{1}{K^2}(tX+\frac{X^2}{q^2}-2\mu-q^2)}}{\sqrt{X^2+q^4+2tq^2X-4q^2\mu}}\,. \tag{B.48}$$

Thus the imaginary part of I_I is given by:

$$\begin{aligned}\mathrm{Im}\{I_1\} &= \frac{-\pi}{(2\pi)^2}\int_0^\infty \mathrm{d}X \int_{-\sqrt{1-\frac{4\mu}{q^2}}}^1 \mathrm{d}t\ \frac{X^2\delta(X-\Omega)}{(X+\Omega)}\frac{e^{-\frac{1}{K^2}(tX+\frac{X^2}{q^2}-2\mu-q^2)}}{\sqrt{X^2+q^4+2tq^2X-4q^2\mu}} \\ &= \frac{-\pi}{(2\pi)^2}\int_{-\sqrt{1-\frac{4\mu}{q^2}}}^1 \mathrm{d}t\ \frac{\Omega}{2}\frac{e^{-\frac{1}{K^2}(t\Omega+\frac{\Omega^2}{q^2}-2\mu-q^2)}}{\sqrt{\Omega^2+q^4+2tq^2\Omega-4q^2\mu}}\,. \end{aligned} \tag{B.49}$$

I_2 is given by a similar integral to the one for the case $q < 2\sqrt{\mu}$,

$$I_2 = \frac{-1}{(2\pi)^2}\int_{X_+}^\infty \mathrm{d}X \int_{-1}^{-\sqrt{1-\frac{4\mu}{q^2}}} \mathrm{d}t\ \frac{X^2}{(X+\Omega)(X-\Omega-i0^+)}\frac{e^{-\frac{1}{K^2}(tX+\frac{X^2}{q^2}-2\mu-q^2)}}{\sqrt{X^2+q^4+2tq^2X-4q^2\mu}}\,, \tag{B.50}$$

except that the upper limit of the t integral is different. Thus for the imaginary part of I_2 we obtain:

$$\mathrm{Im}\{I_2\} = \frac{-\Omega}{8\pi}\,e^{\frac{2\mu+q^2}{K^2}-\frac{\Omega^2}{q^2K^2}} \int_{\mathrm{Max}\{-1,\frac{4\mu-q^2}{2\Omega}-\frac{\Omega}{2q^2}\}}^{-\sqrt{1-\frac{4\mu}{q^2}}} \mathrm{d}t\ \frac{e^{-\frac{t\Omega}{K^2}}}{\sqrt{\Omega^2+2t\Omega q^2-4q^2\mu+q^4}}\,, \tag{B.51}$$

For I_3 we have:

$$I_3 = \frac{-1}{(2\pi)^2}\int_0^{X_-} \mathrm{d}X \int_{-1}^{-\sqrt{1-\frac{4\mu}{q^2}}} \mathrm{d}t \frac{X^2}{(X+\Omega)(X-\Omega-i0^+)}\frac{e^{-\frac{1}{K^2}(tX+\frac{X^2}{q^2}-2\mu-q^2)}}{\sqrt{X^2+q^4+2tq^2X-4q^2\mu}}\,, \tag{B.52}$$

Using $X \to x = X_- X$, the above integral becomes:

$$I_3 = \frac{-1}{(2\pi)^2}\int_0^1 \mathrm{d}x \int_{-1}^{-\sqrt{1-\frac{4\mu}{q^2}}} \mathrm{d}t\ \frac{X_- x^2}{(x+\frac{\Omega}{X_-})(x-\frac{\Omega}{X_-}-i0^+)}\frac{e^{-\frac{1}{K^2}(tX_x+\frac{X_-^2}{q^2}x^2-2\mu-q^2)}}{\sqrt{X_-^2x^2+q^4+2tq^2X_-x-4q^2\mu}}\,, \tag{B.53}$$

Thus the imaginary part of I_3 is given by:

$$\begin{aligned}\mathrm{Im}\{I_3\} &= \frac{-\pi}{(2\pi)^2}\int_0^1 \mathrm{d}x \int_{-1}^{-\sqrt{1-\frac{4\mu}{q^2}}} \mathrm{d}t\ \frac{X_- x^2\delta(x-\frac{\Omega}{X_-})}{(x+\frac{\Omega}{X_-})}\frac{e^{-\frac{1}{K^2}(tX_x+\frac{X_-^2}{q^2}x^2-2\mu-q^2)}}{\sqrt{X_-^2x^2+q^4+2tq^2X_-x-4q^2\mu}} \\ &= \frac{-\Omega}{8\pi}e^{-\frac{1}{K^2}(\frac{\Omega^2}{q^2}-2\mu-q^2)}\int_{-1}^{-\sqrt{1-\frac{4\mu}{q^2}}} \mathrm{d}t\ \frac{\theta\big(1-\frac{\Omega}{X_-(t)}\big)\,e^{-\frac{t\Omega}{K^2}}}{\sqrt{\Omega^2+q^4+2tq^2\Omega-4q^2\mu}}\,, \end{aligned} \tag{B.54}$$

The Heaviside function imposes the constraint $\frac{\Omega}{q^2} \leq -t - \sqrt{\frac{4\mu}{q^2} + t^2 - 1}$.

Putting together the imaginary parts of I_1, I_2 and I_3 (Eqs. (B.49,B.51,B.54)), we finally obtain:

$$\chi''_{\rm PH}(q \geq 2\sqrt{\mu}, \Omega > 0) = \frac{-\Omega\, e^{\frac{2\mu+q^2}{K^2} - \frac{\Omega^2}{q^2K^2}}}{2(2\pi)^2} \left[\int_{-\sqrt{1-\frac{4\mu}{q^2}}}^{1} + \int_{\mathrm{Max}\{-1, \frac{4\mu-q^2}{2\Omega} - \frac{\Omega}{2q^2}\}}^{-\sqrt{1-\frac{4\mu}{q^2}}} + \right.$$
$$\left. \theta(\frac{4\mu - q^2}{2\Omega} + \frac{\Omega}{2q^2}) \int_{\mathrm{Max}\{-1, \frac{4\mu-q^2}{2\Omega} - \frac{\Omega}{2q^2}\}}^{-\sqrt{1-\frac{4\mu}{q^2}}} \right] \frac{e^{-\frac{t\Omega}{K^2}}\, \mathrm{d}t}{\sqrt{\Omega^2 + q^4 + 2tq^2\Omega - 4q^2\mu}}\,. \tag{B.55}$$

The Heaviside function that accompanies the last integral imposes the constraint $(\frac{\Omega}{q^2} + \mathrm{Max}\{-1, \frac{4\mu-q^2}{2\Omega} - \frac{\Omega}{2q^2}\}) < 0$ as we are assuming $4\mu \leq q^2$.

$\mu = 0$

Since we have computed $\chi''_{\rm PH}(q, \Omega > 0)$ for $\mu > 0$ and a generic q, we can easily determine the $\mu = 0$ susceptibility $\chi''_{\rm PH}(q, \Omega > 0)$ by simply taking the limit $\mu \to 0$ (the zero chemical potential case). We find:

$$\chi''_{\rm PH}(q, \Omega > 0) = \frac{-\Omega}{2(2\pi)^2}\, e^{\frac{q^2}{K^2} - \frac{\Omega^2}{q^2K^2}} \int_{-1}^{1} \frac{e^{-\frac{t\Omega}{K^2}}\, \mathrm{d}t}{\sqrt{\Omega^2 + q^4 + 2tq^2\Omega}}\,. \tag{B.56}$$

Bibliography

[1] X.-G. Wen, *Quantum Field Theory of Many-body Systems: From the Origin of Sound to an Origin of Light and Electrons*, Oxford Graduate Texts (Oxford University Press, USA, 2004).

[2] N. Goldenfeld, *Lectures On Phase Transitions And The Renormalization Group*, Frontiers in Physics (Addison-Wesley Publishing, 1992).

[3] J. Cardy, *Scaling and Renormalization in Statistical Physics (Cambridge Lecture Notes in Physics)* (Cambridge University Press, 1996).

[4] H. Stanley, Reviews of Modern Physics **71**, S358 (1999).

[5] M. Fisher, Reviews of Modern Physics **70**, 653 (1998).

[6] K. Wilson and J. Kogut, Physics Reports **12**, 75 (1974).

[7] P. W. Anderson, Science (New York, N.Y.) **177**, 393 (1972).

[8] P. Clayton and P. Davies, eds., *The Re-Emergence of Emergence The Emergentist Hypothesis from Science to Religion* (Oxford University Press, 2006).

[9] S. Weinberg, *The Quantum Theory of Fields, Volume 2: Modern Applications* (Cambridge University Press, 2005).

[10] F. Wilczek, ed., *Fractional Statistics and Anyon Superconductivity*, Series on Directions in Condensed Matter Physics, Vol. 10 (World Scientific, 1990).

[11] S.-K. Ma, *Modern Theory of Critical Phenomena* (Westview Press, 2000).

[12] I. Herbut, *A Modern Approach to Critical Phenomena* (Cambridge University Press, 2010).

[13] T. Senthil, A. Vishwanath, L. Balents, S. Sachdev, and M. P. A. Fisher, Science (New York, N.Y.) **303**, 1490 (2004).

[14] S. Sachdev, *Quantum Phase Transitions*, 2nd ed. (Cambridge University Press, 2011).

[15] T. Senthil, L. Balents, S. Sachdev, A. Vishwanath, and M. P. A. Fisher, Physical Review B **70**, 1 (2004).

[16] X.-G. Wen, Physical Review B **89**, 035147 (2014).

[17] H. Bruus and K. Flensberg, *Many-Body Quantum Theory in Condensed Matter Physics, An Introduction*, Oxford Graduate Texts (Oxford University Press, 2004).

[18] G. D. Mahan, *Many-Particle Physics*, 3rd ed., Physics of Solids and Liquids (Springer, 2000).

[19] J. R. Schrieffer, *Theory of Superconductivity*, 3rd ed., Advanced Book Program (Westview Press, 1971).

[20] P.-G. de Gennes, *Superconductivity of Metals and Alloys*, Advanced Book Classics (Westview Press, 1999).

[21] J. Polchinski, "Effective Field Theory and the Fermi Surface," (1992), arXiv:9210046 [hep-th] .

[22] S. Hartmann, Studies in History and Philosophy of Science Part B: Studies in History and Philosophy of Modern Physics **32**, 267 (2001).

[23] C. Burgess, Annual Review of Nuclear and Particle Science **57**, 329 (2007).

[24] A. Auerbach, *Interacting Electrons and Quantum Magnetism*, Graduate Texts in Contemporary Physics (Springer, 1994).

[25] K. Wilson, Reviews of Modern Physics **47**, 773 (1975).

[26] S.-k. Ma, Rev. Mod. Phys. **45**, 589 (1973).

[27] T. Y. Cao, ed., *Conceptual Foundations of Quantum Field Theory* (Cambridge University Press, 2004).

[28] J. Polchinski, Nuclear Physics B **231**, 269 (1984).

[29] J. Zinn-Justin, *Phase Transitions and Renormalization Group*, Oxford Graduate Texts (Oxford University Press, 2013).

[30] M. Salmhofer, *Renormalization*, Theoretical and Mathematical Physics (Springer, 1999).

[31] J. Zinn-Justin, *Quantum Field Theory and Critical Phenomena (International Series of Monographs on Physics)*, 4th ed. (Oxford University Press, 2002).

[32] N. Nagaosa, *Quantum Field Theory In Condensed Matter Physics*, edited by S. Heusler, Theoretical and Mathematical Physics (Springer, 1999).

[33] A. Schwenk and J. Polonyi, eds., *Renormalization Group and Effective Field Theory Approaches to Many-Body Systems*, Lecture Notes in Physics, Vol. 852 (Springer, 2012).

[34] J. Klauder, Physical Review D **19**, 2349 (1979).

[35] L. S. Schulman, *Techniques and Applications of Path Integration* (Wiley, 1981).

[36] T. Hansson, V. Oganesyan, and S. Sondhi, "Superconductors are topologically ordered," (2004).

[37] T. H. Hansson, T. Kvorning, and V. P. Nair, "An Effective Field Theory for the Spinless p-wave Superconductor," (2013), arXiv:1310.8284 .

[38] J. Polchinski, Nuclear Physics B **422**, 617 (1994).

[39] M. E. Peskin and D. V. Schroeder, *An Introduction To Quantum Field Theory*, 1st ed., Frontiers in Physics (Westview Press, 1995).

[40] J. W. Negele and H. Orland, *Quantum Many-Particle Systems*, Advanced Books Classics (Westview Press, 1998).

[41] E. Fradkin, *Field Theories of Condensed Matter Physics*, 2nd ed. (Cambridge University Press, 2013).

[42] B. Delamotte, American Journal of Physics **72**, 170 (2004).

[43] D. J. Amit, *Field Theory; The Renormalization Group and Critical Phenomena*, 2nd ed. (World Scientific Publishing Company, 1993).

[44] A. M. Tsvelik, *Quantum Field Theory in Condensed Matter Physics*, 2nd ed. (Cambridge University Press, 2007).

[45] A. Altland and B. D. Simons, *Condensed Matter Field Theory*, 2nd ed. (Cambridge University Press, 2010).

[46] U. C. Täuber, Nuclear Physics B - Proceedings Supplements **228**, 7 (2012).

[47] C. Nayak and F. Wilczek, Nuclear Physics B **417**, 359 (1994).

[48] P. Kopietz, L. Bartosch, and F. Schutz, *Introduction to the Functional Renormalization Group* (Springer, 2010).

[49] W. Metzner, M. Salmhofer, C. Honerkamp, V. Meden, and K. Schonhammer, Reviews of Modern Physics **84**, 299 (2012).

[50] J. Berges, N. Tetradis, and C. Wetterich, Physics Reports **363**, 223 (2002).

[51] T. Machado and N. Dupuis, Physical Review E **82**, 041128 (2010).

[52] a. Rançon and N. Dupuis, Physical Review A **85**, 011602 (2012).

[53] R. Coldea, D. A. Tennant, A. M. Tsvelik, and Z. Tylczynski, Physical Review Letters **86**, 1335 (2001).

[54] R. Coldea, D. A. Tennant, and Z. Tylczynski, Physical Review B **68**, 1 (2003).

[55] S. Ghamari, C. Kallin, S.-S. Lee, and E. S. Sorensen, Physics in Canada / La Physique au Canada **68**, 4 (2012).

[56] O. A. Starykh and L. Balents, Physical Review Letters **98**, 2 (2007).

[57] I. Affleck, Journal of Physics: Condensed Matter **1**, 3047 (1989).

[58] I. Dzyaloshinsky, Journal of Physics and Chemistry of Solids **4**, 241 (1958).

[59] S. Ghamari, C. Kallin, S.-S. Lee, and E. S. Sorensen, Physical Review B **84**, 10 (2011).

[60] P. W. Anderson, Math. Res. Bull. **8**, 153 (1973).

[61] N. Elstner, R. R. P. Singh, and A. Young, Physical Review Letters **71**, 1629 (1993).

[62] N. Elstner, R. R. P. Singh, and A. P. Young, Journal of Applied Physics **75**, 5943 (1994).

[63] L. Capriotti, A. E. Trumper, and S. Sorella, Phys. Rev. Lett. **82**, 3899 (1999).

[64] S. White and A. Chernyshev, Physical Review Letters **99**, 127004 (2007).

[65] P. W. Anderson, *More and Different: Notes from a Thoughtful Curmudgeon* (World Scientific Publishing, 2011).

[66] L. Balents, Nature **464**, 199 (2010).

[67] C. Berthier, L. P. Levy, and G. Martinez, eds., *High Magnetic Fields*, Vol. Lecture Notes in Physics Volume 595 (Springer, 2002).

[68] C. Lacroix, P. Mendels, and F. Mila, eds., *Introduction to Frustrated Magnetism*, Series in Solid-State Sciences, Vol. 164 (Springer, 2011).

[69] T. Giamarchi, *Quantum Physics in One Dimension*, International Series of Monographs on Physics (Oxford University Press, 2003).

[70] P. A. Lee, Science (New York, N.Y.) **321**, 1306 (2008).

[71] D. S. Rokhsar and S. A. Kivelson, Physical Review **61**, 2376 (1988).

[72] R. Moessner and S. L. Sondhi, Physical Review Letters **86**, 1881 (2001).

[73] R. Moessner, S. Sondhi, and E. Fradkin, Physical Review B **65**, 024504 (2001).

[74] G. Misguich, D. Serban, and V. Pasquier, Physical Review Letters **89**, 137202 (2002).

[75] R. Moessner and K. S. Raman, "Quantum dimer models," (2008), arXiv:0809.3051 .

[76] M. Levin and X.-G. Wen, Physical Review B **67**, 245316 (2003).

[77] A. Kitaev, Annals of Physics **303**, 2 (2003).

[78] A. Kitaev, Annals of Physics **321**, 2 (2006).

[79] J. Chaloupka, G. Jackeli, and G. Khaliullin, Physical Review Letters **105**, 027204 (2010).

[80] E. K.-H. Lee, R. Schaffer, S. Bhattacharjee, and Y. B. Kim, Physical Review B **89**, 045117 (2014).

[81] I. Kimchi and A. Vishwanath, Physical Review B **89**, 014414 (2014).

[82] Y. Shimizu, K. Miyagawa, K. Kanoda, M. Maesato, and G. Saito, Physical Review Letters **91**, 107001 (2003).

[83] Y. Kurosaki, Y. Shimizu, K. Miyagawa, K. Kanoda, and G. Saito, Physical Review Letters **95**, 177001 (2005).

[84] T.-H. Han, J. S. Helton, S. Chu, D. G. Nocera, J. A. Rodriguez-Rivera, C. Broholm, and Y. S. Lee, Nature **492**, 406 (2012).

[85] S. Yan, D. a. Huse, and S. R. White, Science (New York, N.Y.) **332**, 1173 (2011).

[86] A. B. Harris, C. Kallin, and A. J. Berlinsky, Phys. Rev. B **45**, 2899 (1992).

[87] R. R. P. Singh, Physical Review B **76**, 180407 (2007).

[88] J. Alicea, O. I. Motrunich, M. Hermele, and M. P. A. Fisher, Physical Review B **72**, 1 (2005).

[89] J. Alicea, O. I. Motrunich, and M. P. A. Fisher, Physical Review B **73**, 1 (2006).

[90] G. Misguich, B. Bernu, C. Lhuillier, and C. Waldtmann, Physical Review Letters **81**, 1098 (1998).

[91] G. Misguich, C. Lhuillier, B. Bernu, and C. Waldtmann, Physical Review B **60**, 1064 (1999).

[92] T. Momoi, P. Sindzingre, and K. Kubo, Physical Review Letters **108**, 057206 (2012).

[93] R. V. Mishmash, J. R. Garrison, S. Bieri, and C. Xu, Physical Review Letters **111**, 157203 (2013).

[94] M. S. Block, D. N. Sheng, O. I. Motrunich, and M. P. A. Fisher, Physical Review Letters **106**, 1 (2011).

[95] R. Coldea, D. A. Tennant, R. A. Cowley, D. F. McMorrow, B. Dorner, and Z. Tylczynski, Journal of Physics: Condensed Matter **8**, 7473 (1996).

[96] R. Coldea, D. A. Tennant, R. Cowley, D. McMorrow, B. Dorner, and Z. Tylczynski, Physical Review Letters **79**, 151 (1997).

[97] R. Coldea, D. A. Tennant, R. A. Cowley, D. F. McMorrow, B. Dorner, and Z. Tylczynski, Journal of Magnetism and Magnetic Matreials **181**, 659 (1998).

[98] R. Coldea, D. A. Tennant, K. Habicht, P. Smeibidl, C. Wolters, and Z. Tylczynski, Physical Review Letters **88**, 1 (2002).

[99] Z. Weihong, R. McKenzie, and R. R. P. Singh, Physical Review B **59**, 14367 (1999).

[100] T. Pardini and R. R. P. Singh, Physical Review B **77**, 1 (2008).

[101] L. Faddeev and L. Takhtajan, Physics Letters A **85**, 375 (1981).

[102] L. D. Faddeev and L. A. Takhtadzhyan, Journal of Soviet Mathematics **24**, 241 (1984).

[103] V. E. Korepin, N. M. Bogoliubov, and A. G. Izergin, *Quantum Inverse Scattering Method and Correlation Functions*, Cambridge Monographs on Mathematical Physics (Cambridge University Press, 1993).

[104] M. Takahashi, *Thermodynamics of One-Dimensional Solvable Models* (Cambridge University Press, 1999).

[105] J.-S. Caux and R. Hagemans, Journal of Statistical Mechanics: Theory and Experiment **2006**, P12013 (2006).

[106] A. Weichselbaum and S. R. White, Physical Review B **84**, 1 (2011).

[107] C. H. Chung, J. B. Marston, and R. H. McKenzie, Journal of Physics: Condensed Matter **13**, 5159 (2001).

[108] S. Isakov, T. Senthil, and Y. Kim, Physical Review B **72**, 174417 (2005).

[109] M. Weng, D. N. Sheng, Z. Weng, and R. Bursill, Physical Review B **74**, 2 (2006).

[110] S. Yunoki and S. Sorella, Physical Review B **74**, 1 (2006).

[111] P. Hauke, T. Roscilde, V. Murg, J. Ignacio Cirac, and R. Schmied, New Journal of Physics **13**, 075017 (2011).

[112] D. Heidarian, S. Sorella, and F. Becca, Physical Review B **80**, 4 (2009).

[113] J. Reuther and R. Thomale, Physical Review B **83**, 024402 (2011).

[114] N. Read and S. Sachdev, Physical Review Letters **66**, 1773 (1991).

[115] S. Sachdev, Physical Review B **45**, 12377 (1992).

[116] S. Bhattacharjee, Physical Review B **84**, 104430 (2011).

[117] A. J. Beekman, D. Sadri, and J. Zaanen, New Journal of Physics **13**, 033004 (2011).

[118] M. Takahashi, Physical Review B **40**, 2494 (1989).

[119] M. Thesberg and E. S. Sø rensen, "A Quantum Fidelity Study of the Anisotropic Next-Nearest-Neighbour Triangular Lattice Heisenberg Model," (2014), arXiv:1409.1405 .

[120] M. Bocquet, F. H. L. Essler, A. M. Tsvelik, and A. O. Gogolin, Physical Review B **64**, 1 (2001).

[121] D. Dalidovich, R. Sknepnek, A. J. Berlinsky, J. Zhang, and C. Kallin, Physical Review B **73**, 184403 (2006).

[122] M. Veillette, A. James, and F. Essler, Physical Review B **72**, 134429 (2005).

[123] K. Harada, Physical Review B **86**, 184421 (2012).

[124] M. Thesberg and E. S. Sø rensen, Physical Review B **90**, 115117 (2014).

[125] M. Kohno, O. A. Starykh, and L. Balents, Nature Physics **3**, 790 (2007).

[126] S. Eggert, Phys. Rev. B **54**, R9612 (1996).

[127] Y. Frishman and J. Sonnenschein, *Non-Perturbative Field Theory: From Two Dimensional Conformal Field Theory to QCD in Four Dimensions*, Cambridge Monographs on Mathematical Physics (Cambridge University Press, 2010).

[128] A. E. B. Nielsen, J. Ignacio Cirac, and G. Sierra, Journal of Statistical Mechanics: Theory and Experiment **2011**, P11014 (2011).

[129] A. Tsvelik, Nuclear Physics B **612**, 479 (2001).

[130] E. F. Shender, Journal of Experimental and Theoretical Physics **56**, 178 (1982).

[131] J. Villain, R. Bidaux, J. Carton, and R. Conte, Journal of Physics France **41**, 1263 (1980).

[132] R. Bishop, P. Li, D. Farnell, and C. Campbell, Physical Review B **79**, 174405 (2009).

[133] I. Garate and I. Affleck, Physical Review B **81**, 144419 (2010).

[134] A. O. Gogolin, A. A. Nersesyan, and A. M. Tsvelik, *Bosonization and Strongly Correlated Systems*, 1st ed. (Cambridge University Press, 2004).

[135] S. Ghamari, S.-s. Lee, and C. Kallin, "RG Analysis on a Neck-Narrowing Lifshitz Transition in the Presence of Weak Short-Range Interactions in Two Dimensions," (2014), arXiv:1407.6732 .

[136] A. A. Gorkov, L. P. Dzyaloshinski, and A. E., *Methods of Quantum Field Theory in Statistical Physics* (Prentice Hall, 1964).

[137] M. A. Metlitski, D. F. Mross, S. Sachdev, and T. Senthil, "Are non-Fermi-liquids stable to Cooper pairing?" (2014), arXiv:1403.3694 .

[138] S. Sur and S.-S. Lee, "Quasi-Local Strange Metal," (2014), arXiv:1405.7357 .

[139] A. L. Fitzpatrick, S. Kachru, J. Kaplan, and S. Raghu, Physical Review B **88**, 125116 (2013).

[140] A. L. Fitzpatrick, S. Kachru, J. Kaplan, and S. Raghu, Physical Review B **89**, 165114 (2014).

[141] D. Dalidovich and S.-S. Lee, Physical Review B **88**, 245106 (2013).

[142] S. Sur and S.-S. Lee, Phys. Rev. B **90**, 045121 (2014).

[143] L. D. Landau, Sov. Phys. JETP , 101 (1957).

[144] L. D. Landau, Sov. Phys. JETP , 920 (1957).

[145] L. D. Landau, Sov. Phys. JETP , 70 (1959).

[146] C. M. Varma, Z. Nussinov, and W. van Saarloos, Physics Reports **361**, 267 (2002).

[147] R. Shankar, Physica A: Statistical Mechanics and its Applications **177**, 530 (1991).

[148] R. Shankar, Reviews of Modern Physics **66**, 129 (1994).

[149] G. Benfatto, G. Gallavotti, A. Procacci, B. Scoppola, D. Matematica, R. Tor, D. Fisica, R. La, and P. A. Moro, Communications in Mathematical Physics **171**, 93 (1994).

[150] Y. Huh and S. Sachdev, Physical Review B **78**, 064512 (2008).

[151] S.-S. Lee, Physical Review B **80**, 1 (2009).

[152] I. Mandal and S.-S. Lee, "UV/IR mixing in Non-Fermi Liquids," (2014), arXiv:1407.0033 .

[153] L. Van Hove, Phys. Rev. **89**, 1189 (1953).

[154] P. Kopietz and T. Busche, Physical Review B **64**, 155101 (2001).

[155] W. Metzner, C. Castellani, and C. Di Castro, Advances in Physics **47**, 317 (1998).

[156] S. Raghu, S. A. Kivelson, and D. J. Scalapino, Physical Review B **81**, 1 (2010).

[157] J. Luttinger, Physical Review **119**, 1153 (1960).

[158] A. V. Chubukov and D. L. Maslov, Physical Review B **81**, 245102 (2010).

[159] S. Maiti and A. V. Chubukov, AIP Conference Proceedings , 3 (2013).

[160] W. Kohn and J. Luttinger, Physical Review Letters **15**, 524 (1965).

[161] A. Chubukov, Physical Review B **48**, 1097 (1993).

[162] J. González, F. Guinea, and M. M. A. H. Vozmediano, Nuclear Physics B **485**, 694 (1997).

[163] I. M. Lifshitz, Sov. Phys. JETP **11**, 1130 (1960).

[164] I. M. Lifshitz, Journal of Experimental and Theoretical Physics **38**, 1569 (1960).

[165] Y. Yamaji, T. Misawa, and M. Imada, Journal of the Physics Society Japan **75**, 094719 (2006).

[166] M. Rodney, H. F. Song, S.-S. Lee, K. Le Hur, and E. S. Sorensen, Physical Review B **87**, 115132 (2013).

[167] V. Oganesyan, S. A. Kivelson, and E. Fradkin, Physical Review B **64**, 195109 (2001).

[168] M. A. Metlitski and S. Sachdev, Physical Review B **82**, 41 (2010).

[169] J. Hirsch and D. Scalapino, Physical Review Letters **56**, 2732 (1986).

[170] J. Hirsch, Physical Review B **31**, 4403 (1985).

[171] P. Lederer, G. Montambaux, and D. Poilblanc, Journal de Physique **48**, 1613 (1987).

[172] J. Reiss, D. Rohe, and W. Metzner, Phys. Rev. B **75**, 075110 (2007).

[173] A. Neumayr and W. Metzner, Physical Review B **67**, 035112 (2003).

[174] H. J. Schulz, Europhysics Letters (EPL) **4**, 609 (1987).

[175] C. Honerkamp, M. Salmhofer, and T. Rice, Eur. Phys. J. B **27**, 127 (2002).

[176] C. Honerkamp, M. Salmhofer, N. Furukawa, and T. M. Rice, Phys. Rev. B **63**, 035109 (2001).

[177] R. Hlubina, Phys. Rev. B **59**, 9600 (1999).

[178] D. Zanchi and H. Schulz, Physical Review B **61**, 13609 (2000).

[179] D. Zanchi and H. Schulz, Physical review. B, Condensed matter **54**, 9509 (1996).

[180] I. Khavkine, C.-H. Chung, V. Oganesyan, and H.-Y. Kee, Physical Review B **70**, 1 (2004).

[181] H. Yamase, V. Oganesyan, and W. Metzner, Physical Review B **72**, 035114 (2005).

[182] J. V. Alvarez, J. González, F. Guinea, and M. A. H. Vozmediano, Journal of the Physics Society Japan **67**, 1868 (1998).

[183] N. Furukawa, T. M. Rice, and M. Salmhofer, Physical Review Letters **81**, 3195 (1998).

[184] N. Furukawa, C. Honerkamp, M. Salmhofer, and T. M. Rice, Physica B: Condensed Matter **284-288**, 1571 (2000).

[185] J. González, Physical Review B **63**, 1 (2001).

[186] K. Le Hur and T. M. Rice, Annals of Physics **324**, 1452 (2009).

[187] R. Nandkishore, L. S. Levitov, and A. V. Chubukov, Nature Physics **8**, 158 (2012).

[188] A. Kapustin and I. Rothstein, "Effective Field Theory of the van Hove Singularity," (2012), (Unpublished).

[189] J. González, Phys. Rev. B **88**, 125434 (2013).

[190] D. Yudin, D. Hirschmeier, H. Hafermann, O. Eriksson, A. I. Lichtenstein, and M. I. Katsnelson, Phys. Rev. Lett. **112**, 070403 (2014).

[191] F. Haldane, Physical Review B **25**, 4925 (1982).

[192] K. Wilson and M. Fisher, Physical Review Letters **28**, 240 (1972).

[193] H. Kleinert and V. Schulte-Frohlinde, *Critical Properties of* Φ^4*-Theories* (World Scientific, 2001).

[194] T. Senthil and R. Shankar, Physical Review Letters **102**, 046406 (2009).

[195] S. El-Showk, M. Paulos, D. Poland, S. Rychkov, D. Simmons-Duffin, and A. Vichi, Phys. Rev. Lett. **112**, 141601 (2014).

[196] J. Polchinski, Nuclear Physics B **303**, 226 (1988).

[197] P. D. Francesco, P. Mathieu, and D. Senechal, *Conformal Field Theory* (Springer, 1997).

[198] A. B. Zamolodchikov, JETP Lett **43**, 730 (1986).

[199] J. L. Cardy, Physics Letters B **215**, 749 (1988).

[200] Z. Komargodski and A. Schwimmer, Journal of High Energy Physics **2011**, 99 (2011).

[201] H. Casini, M. Huerta, and R. C. Myers, Journal of High Energy Physics **2011**, 36 (2011).

[202] H. Casini and M. Huerta, Physical Review D **85**, 125016 (2012).

[203] T. Grover, Physical Review Letters **112**, 151601 (2014).

[204] S.-S. Lee, Journal of High Energy Physics **2014**, 76 (2014).

[205] S.-S. Lee, Nuclear Physics B **851**, 143 (2011).

[206] S.-S. Lee, Nuclear Physics B **832**, 567 (2010).

[207] A. O. Gogolin, A. A. Nersesyan, and A. M. Tsvelik, *Bosonization and Strongly Correlated Systems* (Cambridge University Press, 2004).

[208] E. Brezin and J. Zinn-Justin, eds., *Fields, strings and critical phenomena. Proceedings,49th Session of the Les Houches Summer School in Theoretical Physics, NATO Advanced Study Institute, Les Houches, France, June 28 - August 5, 1988* (Amsterdam, 1990) a chapter by Ian Affleck.

[209] D. G. Shelton, A. A. Nersesyan, and A. M. Tsvelik, Physical Review B **53**, 8521 (1996).

[210] S. Lukyanov, Nuclear Physics B **654**, 323 (2003).

[211] S. Lukyanov, Nuclear Physics B **522**, 533 (1998).

[212] L. D. Faddeev, International Journal of Modern Physics A **10**, 1845 (1995).

[213] L. D. Faddeev, "How Algebraic Bethe Ansatz works for integrable model," (1996), arXiv:9605187 [hep-th] .

[214] E. Witten, Communications in Mathematical Physics **92**, 455 (1984).

[215] D. Senechal, A.-M. Tremblay, and C. Bourbonnais, eds., *Theoretical Methods for Strongly Correlated Electrons* (Springer, 2003) a chapter by D. Senechal.

[216] I. Affleck and M. Oshikawa, Physical Review B **60**, 1038 (1999).

[217] J. Polchinski, *String Theory*, Cambridge Monographs on Mathematical Physics, Vol. 1 (Cambridge University Press, 2005).

Index